Characterisation of the novel melanoma associated Shc adaptor ShcD/RaLP

Thesis submitted for the degree of

Doctor of Philosophy

at the University of Leicester

by

Samrein B.M. Ahmed, MBBS

Department of Biochemistry

University of Leicester

2013

Declaration

The accompanying thesis submitted for the degree of Doctor of Philosophy entitled "Characterisation of the novel melanoma associated Shc adaptor ShcD/RaLP" is based on work conducted by the author in the Department of Biochemistry at the University of Leicester during the period September 2009 and April 2013. All of the work recorded in this thesis is original unless otherwise acknowledged inthe text or by references. None of the work has been submitted for another degree in this or any other university.

Signed

Date

Department of Biochemistry

University of Leicester

Lancaster Road

Leicester

LE1 9HN

Characterisation of the novel melanoma associated Shc adaptor ShcD/RaLP

Abstract

Samrein B.M. Ahmed

RaLP is a recently identified signalling adaptor protein found to be up-regulated in invasive melanoma. To characterise RaLP and investigate its cellular role, a polyclonal antibody was raised against RaLP and purified successfully; it was considered to be a good tool for RaLP characterisation. Moreover, stable cell lines that express either GFP-RaLP or FLAG-RaLP were generated. These cells showed a slightly higher increase in the percentage of G1 cells when compared to the parental counterparts using FACS analysis, and increased levels of p21/cip, a marker of G1 arrest. The underlying mechanism for the increased level of p21/cip remains unclear, but this may contribute to enhanced melanoma migration or survival induced by RaLP.

The subcellular localisation of RaLP, as revealed by fluorescence microscopy and subcellular fractionation, was not restricted to the cytoplasm and cell membrane as has been reported previously, but a proportion of the protein was found to be present in the nucleus and mitochondria. Herein we show for the first time that RaLP shuttles between the nucleus and cytoplasm, and that the RaLP-CH2 domain has a critical role in RaLP export from the nucleus. Analysis of deletion and point mutants revealed that the sequence ^{83}LCTLIPRM^{90} represents a functional nuclear export signal within the CH2 domain. Moreover, we have demonstrated that RaLP accumulates in the nucleus upon oxidative stress. Preliminary experiments showed that RaLP associates with the DNA and might play a role in gene transcription. Moreover, using mass spectrometry we were able to identify a phosphorylation site at Thr156/159 within the CH2 domain that is induced upon oxidative stress, while Ser132 was phosphorylated in unstressed conditions as well. These phosphorylation events may play a role in nuclear localisation or function of RaLP. Further support of a role for RaLP in the nucleus and mitochondria was provided by analysis of protein complexes containing GFP-RaLP by mass spectrometry. Proteins identified included a nuclear pore complex protein, importin-β, transcriptional regulators, and mitochondrial proteins, in addition to the receptor tyrosine kinases Ret and TrkC.

In a previous study, the invasion suppressor Nischarin was identified as an interacting partner with the CH2 domain of RaLP using a yeast two-hybrid library screen. Here we confirm that RaLP co-immunoprecipitates with Nischarin when overexpressed in cells or when present at endogenous levels. Mapping the RaLP-CH2 domain for the sequence required for Nischarin binding revealed that the first 93 amino acids are required for RaLP/Nischarin interaction, while interaction is greatly reduced upon deletion of the first 24 amino acids. Interestingly, Nischarin was also identified by mass spectrometry as part of a complex precipitated by GFP-RaLP from N1E-115 cells. Confocal microscopy provided additional evidence of co-localisation within melanoma cells. While we were unable to observe any effect of the RaLP/Nischarin association on the LIMK/cofilin pathway, very preliminary evidence suggested that RaLP might relieve suppression of Erk activation induced by Nischarin. Taken together, our results point to diverse roles for RaLP in cellular signalling and migration.

Acknowledgements

Above all, I would like to express my sincere thanks and gratitude to my supervisor Dr Sally Prigent for suggesting the project, for her constructive ideas, for her generosity with her time and continual guidance and help she so willingly offered.

I am so grateful to Dr. Sue Shackleton and Prof. Catrin Pritchard for their invaluable advice and encouragement during the committee meetings.

In addition, I would like to acknowledge Dr. Kees Straatman for his patience and kind assistance with the computerized microscopy techniques. My thanks go to Dr Raj Patel for his invaluable ideas and information during the lab meetings that I really benefited from them.

I am grateful to Dr. Andrew Bottrill and Shairbanu Ashra for their kind helps in the mass spectrometry work. I would also like to thank Dr. Macip Salvador for his generous help in showing me how to analyse the flow cytometry data. Thank you to all my colleagues in lab 2/38 for their kind helps and support: Eva, Dalhee and Juhan. And I am also thankful to Lab/42 members for being kind neighbours, when I needed to use their chemicals or equipments from their lab. I am thankful to all the members of the Biochemistry department who have helped in providing advice, reagents and equipments.

My work would not have been possible without my husband, Mohamed, understanding and unrelenting support. I am eternally thankful for all the encouragement he provided. My especial thanks to my mother and father for their support and help. Finally, I would like to express my love to my little boys, Ahmed and Omer, for being such good boys during my PhD that really gave me time to finish this work!

List of Contents:

List of tables:

List of Figures

Chapter 1-General Introduction

Chapter 3- Tools Generation

Chapter 4- RaLP in the nucleus

Chapter 5- Characterisation of the Stable cell lines

Chapter 6- RaLP and Nischarin

Chapter 7 Discussion and conclusion

Abbreviations:

Akt	Protein kinase B
ALK	Anaplastic lymphoma kinase
APS	Ammonium persulfate
AP2 complex	Assembly protein complex2
ATP	Adenosine triphosphate
Bad	Bcl2 antagonist of cell death
BDNF	Brain derived neurotrophic factor
bp	Base pair
BSA	Bovine serum albumin
cDNA	Complementary deoxy ribonucleic acid
CH	Collagen homology domain
ChIP	Chromatin immunoprecipitation
^{o}C	Celsius
C-terminus	Carboxy-terminus
DMEM	Dubblecco's modifies eagle medium
DMSO	Dimethyl sulphoxide
DNA	Deoxyribonucleotides
dNTP	Deoxy nucleotide triphosphate
DTT	Dithiothreitol
EDTA	Ethylenediaminetetraacetic acid
EEA1	Early endosome antigen1
EGTA	Ethylene glycol tetraacetic acid
EGF	Epidermal growth factor
EGFR	Epidermal growth factor receptor
ErBb2	Human epidermal growth factor receptor 2 (HER2/neu)
EpiSCS	Epiblast stem cells
Eph B	Ephrin B receptor
ERK	Extracellular signal-regulated kinase
ESC	Embryonic stem cells
FAK	Focal adhesion kinase
FBS	Foetal bovine serum

x g	G-force / relative centrifocal force (RCF)
Gab1	Grb2-associated binding protein
GFP	Green fluorescent protein
GPCR	G-protein coupled receptor
GST	Glutathione *S*-transferase
GTP	Guanine triphosphate
Grb2	Growth factor receptor-bound protein2
dH_2O	Distilled water
H_2O_2	Hydrogen peroxide
HEK 293	Human embryonic Kidney 293 cells
Hela cells	Immortal cervical carcinoma cells
hr	Hour
HRP	Horseradish peroxidase
HSP70	Heat shock protein 70
IGF	Insulin growth factor
IGF1R	Insulin-like growth factor 1 receptor
IPTG	Isopropyl β-D-thiogalactopyranoside
IQGAP1	Ras GTPase-activating-like protein
IRAS	Imidazoline receptor anti-sera/Nischarin
IRS4	Insulin receptor substrate 4
JNK	C-Jun N-terminal kinases
LB	Luria-Bertani
LIMK	Lim-domain actin binding kinase
LMB	Leptomycine B
MAPK	Mitogen- activated kinase pathway
MEK	MAP/ERK kinase
Met	Mesenchymal-epithelial transition factor (HGF receptor)
MIF	Macrophage migration inhibitory factor
min	Minute
MLCK	Myosin light chain kinase
Mpl	Myeloproliferative leukemia protein
mRNA	Messenger ribonucleic acid
Musk	Muscle specific kinase

NAD	Nicotinamide adenine dinucleotide
NADH	NAD+ hydrogen (H)
NCAM	Neural cell adhesion molecule
Nedd8	Neural precursor cell expressed developmentally down-regulated protein 8
NIH3T3	Mouse fibroblast cells
N-terminal	Amino-terminal
OD	Optic density
O/N	Over night
PAK	P21-activated kinase
PBS	Phosphate buffered saline
PBST	Phosphate buffered saline Tween
PCR	Polymerase chain reaction
PI3K	Phosphoinositide 3-kinase
PI3P	Phosphatidyl inositol-3 phosphate
PKC	Protein kinase C
pH	Percentage hydrogen
PIP2	Phosphatidylinositol(3,4) biphosphate
PIP3	Phosphatidylinositol(3,4,5)-triphosphate
PLCγ	Phospholipase C gamma
PC-PLC	Phosphatidylcholine-Selective phospholipase
PMSF	Phenylmethylsulfonyl fluoride
PTB	Phosphorylated binding domain
PTEN	Phosphatase and tensin homolog
PTP-PEST	Protein tyrosine phosphatase contains PEST
PX	Phox domain
RaLP	Rai-like protein
RaLPΔCH2	Truncated version of RaLP lacks N-terminal CH2
RaLPΔSH2	Truncated version of RaLP lacks C-terminal SH2
Ran	Ras-related nuclear protein
Ret	Rearranged during transfection
RGP	Radial growth phase
RNA	Ribonucleic acid

Rnase	Ribonuclease enzyme
ROS	Reactive oxygen species
rpm	Revolutions per minute
RT	Room temperature
RTK	Receptor tyrosine kinase
RT-PCR	Reverse transcription-polymerase chain reaction
RVLM	Rostral ventrolateral medulla
SDS	Sodium dodecylsulphate
SDS-PAGE	Sodium dodecyl sulphate polyacrylamide gel electrophoresis
Ser/S	Serine
Sec	Seconds
SH2	Src homology 2
Shc	Src homology and collagen
SHIP	SH2 domain containing inositol 5-phosphatase
SMAD3	Mothers against decapentaplegic homolog 3
SNX2	Sorting nexin2
Sos	Son of sevenless
Src	Proto-oncogene tyrosine-protein kinase Src
STAT/Stat	Signal transducer and activator of transcription
TEMD	N,N,N’N’-tetramethylethylene diamine
Thr/T	Threonine
TGF-β	Transforming growth factor-beta
Trk	Nerve growth factor receptor
Tyr/Y	Tyrosine
UV	Ultra-Violet light
V	Volt
VEGF	Vascular endothelial growth factor
VGP	Vertical growth phase

Chapter 1

General Introduction

1.1 Introduction:

Signal transduction is essential for translating the extracellular events into appropriate biological responses. For this reason the intracellular networks need to be tightly regulated. Adaptor proteins are one of the factors for maintaining the intracellular homeostasis; any disturbance in regulation of adaptor proteins may lead to a disease condition or in some cases may trigger cancer formation. One of the most studied adaptor protein families is the Src homology and Collagen (Shc) family that is implicated in both physiological and disease conditions. The Shc family of docking proteins is an essential element in signalling cascades mediated by different extracellular signals, such as growth factors, cytokines and integrins (Ravichandran, 2001). Shc proteins generally exert their action via activating mitogen activated protein kinases (MAPK) as well as phosphoinositide-3-kinase/ Akt signalling pathways.

Adaptor proteins facilitate protein-protein interactions, which are responsible for intracellular signal propagation as well as organization. The Shc family consists of a group of adaptor proteins, which are evolutionary related by sharing some of their functional and structural features (Fagiani et al., 2007). The distinctive structural feature of Shc proteins is that they comprise an amino terminal phosphotyrosine binding (PTB) domain, a linker collagen homology 1 (CH1) domain and a carboxy terminal Src homology 2 (SH2) domain. An additional amino terminal collagen homology region (CH2) exists in the longest Shc protein transcripts (Figure 1.1) (Fagiani et al., 2007).
The Shc family consists of four members encoded by four distinct genes, which are Shc/Shc1/ShcA, Sli/Shc2/ShcB, Rai/Shc3/ShcC and RaLP/Shc4/ShcD (Figure 1.1). Broadly, Shc proteins contribute in mediating several intracellular signalling cascades; they are implicated in cell proliferation, cell differentiation, cell survival and migration. In addition, their role in angiogenesis and tumourgenesis has been determined. The ShcA protein is widely expressed in human tissue (Pelicci et al., 1992).

1.2 Functional diversity of the Shc family:

Shc family members propagate signal transduction to yield different biological events. Many factors contribute to the functional diversity of Shc proteins: multiple domains

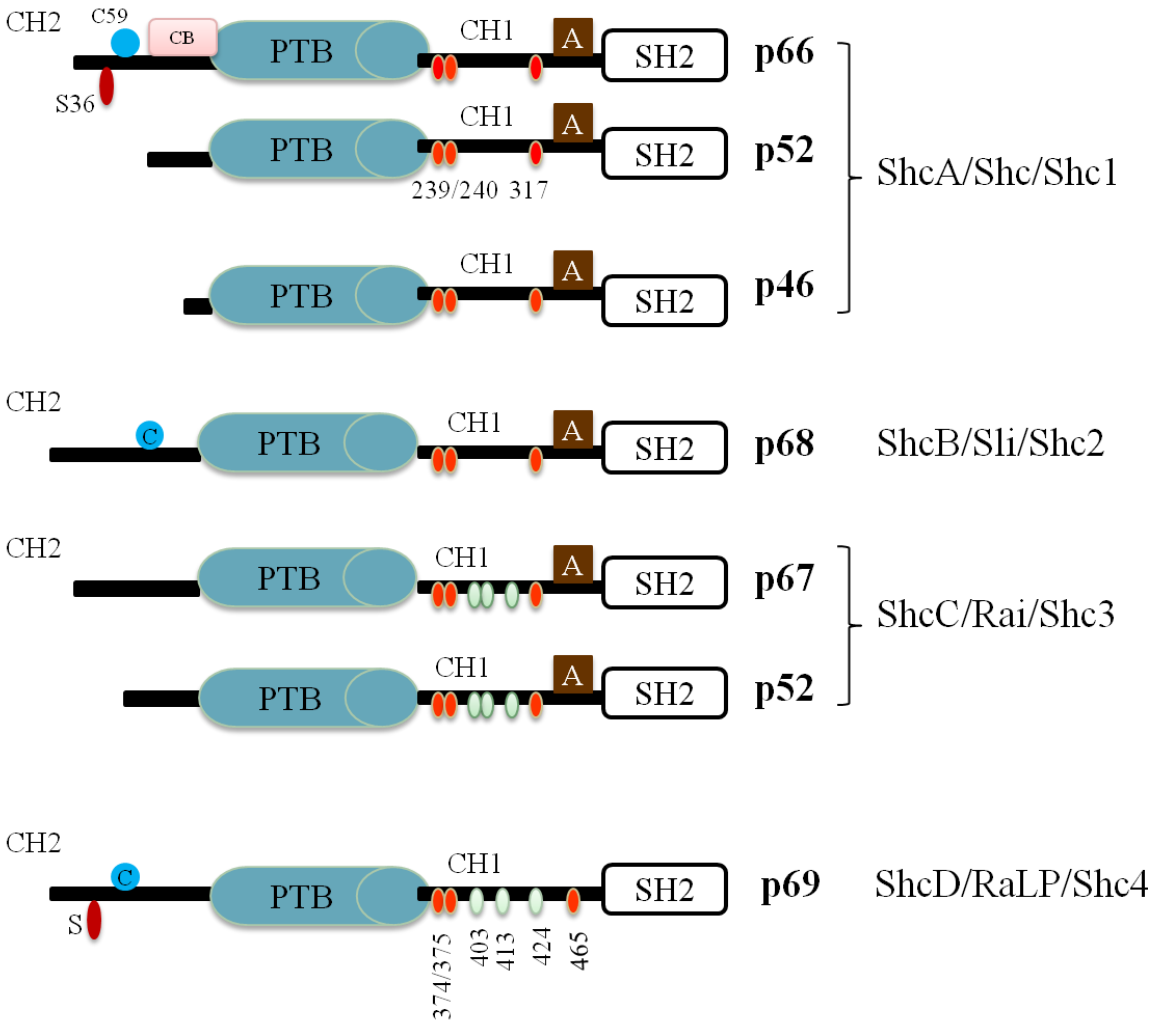

Figure 1.1 Schematic representation of the structural modularity of the Shc family of proteins. Shc proteins share the same structural hallmark with highly conserved PTB and SH2 domains, and poorly conserved CH2 and CH1 domains. Three conserved tyrosine phosphorylation sites in the CH1 domain (orange). Additional tyrosine phophorylation residues (non conserved) in the same CH1 domain (green), in ShcC and ShcD/RaLP. While Ser36 in the the p66ShcA-CH2 domain (red) is responsible for the oxidative-stress response function. RaLP-CH2 also contains a putative serine site for phosphorylation. A cysteine (C) residue in the p66ShcA-CH2 domain is involved in oligomerisation; it is present in ShcB and ShcD/RaLP (blue). Cytochrome c (CB) binding site is only present in the p66ShcA but not other Shc proteins (pink). An Adaptin binding motif (A) is present in all Shc proteins except ShcD/RaLP (brown). Adapted from Wills and Jones 2012.

offer Shc proteins the ability to bind different signalling proteins; their gene product might give more than one transcript, each having a particular role, Shc proteins possess various serine, threonine and tyrosine residues that can potentially be phosphoryated, and finally structural properties of Shc proteins assist their relocation to different intracellular organelles. All the above factors grant Shc family members a capacity to regulate various signalling cascades in the different intracellular compartments.

1.2.1 Shc proteins domains:

Despite Shc adaptor proteins lacking intrinsic enzymatic activity, they are equipped with different domains (CH2, PTB, CH1 and SH2) that are defined by distinctive amino acids motifs and sequences that help the Shc proteins to convey, organize and amplify the signals received.

1.2.1.1 Phosphotyrosine binding domains:

Shc proteins are the only adaptor proteins that possess both a PTB (phosphotyrosine binding) domain as well as a SH2 (Src homology 2) domain (Ravichandran, 2001). PTB and SH2 domains are the most conserved regions among Shc family members (Figure 1.1) (Fagiani et al., 2007); they bind to phosphotyrosine motifs allowing Shc proteins to be recruited to activated receptors, for example, receptor tyrosine kinases (RTKs), antigen receptors, G-protein coupled receptors and cytokine receptors (Ravichandran, 2001). The Shc phosphotyrosine binding domains also enable Shc proteins to interact with cytosolic tyrosine kinases (McGlade et al., 1992).The Shc-PTB domain binds the phosphorylated tyrosine present in the motif NPXpY while the SH2 domain preferentially interacts with phosphorylated tyrosine contained in a pYXXΦ context, where Φ represents a hydrophobic amino acid (Ravichandran, 2001).

The combination of SH2 and PTB domains enables Shc to switch between signalling pathways; it was shown that the SH2 domain is specifically needed in cell proliferation while the PTB domain is important in cell migration (Collins et al., 1999).

Site directed mutagenesis revealed that R175 in p52ShcA or R285 in p66ShcA, in the tyrosine binding pocket of the PTB domain, is pivotal for Shc anchoring to certain tyrosine phosphorylated proteins (Zhou et al., 1995; Luschning et al., 2000).

In addition to the role of the Shc-PTB domain in binding phosphotyrosine residues, the PTB domain also contributes to localising Shc to the cytosolic side of the plasma membrane via its interaction with plasma membrane phospholipids (Ravichandran, 2001 and Smith et al., 2006). NMR studies have further shown that the residues that are responsible for binding the membranous phospholipids are distinct from the phosphotyrosine binding residues (Ravichandran et al., 1997). This implies that recruitment of ShcA to the inner membrane does not always require activation of the upstream receptors. Notably, mutation of Met46 to Pro in the p52ShcA-PTB domain abrogated Shc's ability to activate c-Src, which subsequently diminished Stat-induced p21/cip upregulation (Sato et al., 2002).

The PTB domain of p52ShcA contains a potential phosphorylated Ser29 residue in the RHGSFVNK motif that has a role in Shc's interaction with the tyrosine phosphatase (PTP-PEST), which plays a role as a safety valve to hinder the flow of ligand-induced signalling via its association with ShcA (Faisal et al., 2002).

Although tyrosine phosphorylation is a requirement for Shc PTB and SH2 domains coupling to other proteins, it was reported that the PTB domain binds PTP-PEST as well as IQGAP independent of tyrosine phosphorylation (Faisal et al., 2002; Smith et al., 2010). Additionally, ShcA associates with Ran-GTPase via the former's SH2 domain and the interaction does not require tyrosine phosphorylation of the latter (George et al., 2009). As a consequence, Shc-SH2 domain initiates Shc nuclear translocation without binding to tyrosine phosphorylated sites.

1.2.1.2 Proline and Glycine rich domains:

Collagen homology regions include the CH1 as well as the CH2 domains. The CH1 domain links the PTB and SH2 regions while the CH2 is located at the extreme N-terminal region of the Shc proteins (Figure 1.1). They were designated by these names (CH1 and CH2) since they showed 50% homology to human α1 collagen, which is rich in glycine and proline. The Shc proteins' collagen homology regions also possess a frequent and conserved GXX motif, where X is generally lysine or proline (Pelicci et al., 1992). Importantly, the CH2 domain does not exist in the shorter isoforms of Shc family members it is only present in p66ShcA, p68ShcB, p67ShcC and p69ShcD/RaLP. The proline and glycine stretches enable the collagen homology domains to act as docking sites for proteins containing SH3 domains (Ravichandran, 2001). Both CH1

and CH2 domains represent the least conserved regions among Shc family members (Jones et al., 2007).

Shc proteins can be phosphorylated by tyrosine kinases on certain conserved tyrosine residues, which are housed within the CH1 region (Figure 1.1) (Collins et al., 1999). The phosphorylated tyrosine residues, in the CH1 domain, represent binding sites for many proteins, the best characterised of these is Grb2. Grb2 recruits Sos that activates the Ras/MAPK signalling pathway (Ravichandran et al., 1995). ShcC and ShcD/RaLP were reported to have additional potential tyrosine phosphorylation sites in the CH1 domain (Jones et al., 2007), which might contribute to activate unique signal transduction pathways (Figure 1.1).

The ShcA-CH1 region also contains the Adaptin interacting motif (amino acids 346-355) that contributes to Shc's ability to associate with endosomes (Okabayashi et al., 1996). Unlike the CH1 domain, the CH2 region is likely to be phosphorylated on serine and threonine residues (Ravichandran, 2001). One of the most studied examples is the serine 36 in the p66ShcA-CH2 that plays a pronounced role in the oxidative-stress response that is mediated by p66ShcA (Migliaccio et al., 1999) (Figure 1.1). The p66ShcA also houses a cytochrome c interacting region at the carboxy terminal of the CH2 domain (Giorgio et al., 2005) (Figure 1.1). In addition, the p66ShcA-CH2 domain contains cysteine 59 that is responsible for the protein dimerisation (Figure 1.1); it was suggested to have an effect on p66ShcA-mediated stress response (Gertz et al., 2008). An interesting observation was made by Khanday et al. 2006 regarding the inhibitory effect of the p66ShcA-CH2 domain on the p66ShcA/Ras signalling. Under oxidative stress conditions, p66ShcA was found to dissociate Sos1 from Grb2-SH3 by the former's CH2 domain, subsequently this results in mediating Sos1-eps8 association that leads to activation of Rac1 rather than Ras (Khanday et al., 2006). Furthermore, cytoskeletal reorganisation was reported to mediate Erk activation via p52ShcA or p46Shc phosphorylation but not by p66ShcA. This was attributed to the fact that the p66ShcA-CH2 sequence has an inhibitory effect on the Erk phosphorylation mediated by cytoskeletal reorganisation (Faisal et al., 2004).

It is apparent that the domains of Shc proteins orchestrate protein-protein interactions that lead to perfectly regulated downstream pathways.

1.2.2 The expression profiles of Shc proteins and their isoforms:

The Shc family consists of at least seven identified proteins arising from four different genes; this is attributed to the alternative use of the initiation codons and mRNA splicing (Jones et al., 2007). The presence of the Shc protein isoforms provides the Shc family with a range of functions. Shc scaffolds show distinct expression patterns that facilitate conveying messages in different cellular settings.

The ShcA protein is present in the intracellular compartment in three isoforms p46, p52 and p66ShcA (Figure 1.1), each of which has an implication in certain intracellular pathways. The three isoforms arise from two mRNAs derived from the Shc gene, which encode p66ShcA and p46/p52ShcA (Okada et al., 1997; Ravichandran, 2001).

Although all ShcA isoforms are derived from the same gene, p66ShcA has an extension of 110 amino acids at its amino-teminus. This extension has provided p66ShcA with a distinct role from the two shorter isoforms (p46ShcA; p52ShcA). p46ShcA and p52ShcA are involved in cell cycle progression and cell differentiation (Wary et al., 1996; Stevenson et al., 1999), whereas p66ShcA plays a role in apoptosis in response to oxidative stress (Migliaccio et al., 1999). Unlike the shorter Shc isoforms, p66ShcA restrains Ras activation (Ma et al., 2010). In contrast to p46 and p52 ShcA, p66ShcA expression is absent in human haemopoietic cells (Pelicci et al., 1992).

The ShcA protein was proved to be ubiquitously expressed in all tissues except the adult mature brain. Unlike ShcA, ShcB, ShcC and ShcD demonstrated abundant expression in the brain (Nakamura et al., 1998; Jones et al., 2007). ShcB and ShcC with its two isoforms (p67, p52) were determined to be involved in neuronal cell development and survival, while ShcB's main function is linked to the peripheral nervous system rather than the central nervous system (Sakai et al., 2000). The dominancy of ShcC function in brain signalling originated from the fact that it has a higher affinity for NGF and BDNF receptors than ShcB (Nakamura et al., 1998). Opposite to ShcC, ShcB is present in retina, heart and vascular endothelial cells (Ratcliffe et al., 2002) while ShcC showed a unique expression in lymphocytes that is not shown by ShcB (Savino et al., 2009).

Recently, the new Shc family member RaLP/ShcD was shown to be expressed in brain, neuronal derived tissues e.g. melanocytes, and skeletal muscle in adult mice (Jones et al., 2007; Fagiani et al., 2007). The reported role of RaLP/ShcD is in triggering melanoma invasion, maturation of the neuromuscular junction and it was shown to contribute to mouse embryonic development (Fagiani et al., 2007; Jones et al., 2007; Turco et al., 2012). Despite of the reported intracellular roles for RaLP, the exact molecular mechanisms by which RaLP achieves these functions are still unclear.

An interesting example of the switch in expression between Shc adaptor proteins to satisfy cellular needs was described by Conti et al. 2001. Implementing two-colour FACS enabled them to show that ShcC expression is limited to the postmitotic neuronal cells while ShcA is mainly available in neuronal progenitors. ShcA expression was initially required to facilitate progenitor cell proliferation, which was then replaced by ShcC that assisted in neuronal cell maturation by mediating cell differentiation as well as survival. Accordingly, it was suggested that modifying ShcA and ShcC expression during the development of the brain acts as a crucial event for determining neuronal cells proliferation and differentiation (Conti et al., 2001).

1.2.3 Shc protein localisation:

The extracellular events influence the internal environment of the cell to elicit specific responses. There are certain proteins that sense the extracellular signals and transmit them to mediate the relevant intracellular cascades. Shc members assist in transmitting signals through different ways; one of them is by inducing relocation into different subcellular compartments. As Shc proteins were originally characterised as adaptors coupling receptor tyrosine kinases to downstream signalling pathways, it was thought that Shc members are cytoplasmic proteins; however recent reports have shown Shc proteins in different intracellular compartments.

p52ShcA and p46ShcA are mainly distributed in the cytoplasm; however, upon their tyrosine-phosphorylation they translocate to the membrane where they convey the extracellular signals to the intracellular environment (Sato et al., 2000). In addition, the Shc-PTB domain contributes to the membrane localisation of Shc (Ravichandran et al., 1997). Since p66ShcA plays a role in reactive oxygen species metabolism its mitochondrial translocation has been analysed (Nemoto et al., 2006).

Moreover, the p46ShcA isoform was also shown to translocate into the mitochondrial matrix by means a mitochondrial target sequence that is present in its PTB domain (Ventura et al., 2004).

Interestingly, nuclear localisation of p46ShcA was reported in both hepatocytes and hepatic carcinoma cells (Yoshida et al., 2004). Since Shc isoforms lack the classical nuclear localisation signal (NLS), it was thought they translocate to the nucleus through a NLS-independent mechanism. Only the shorter isoforms (p46ShcA and p52ShcA) of ShcA were shown to coimmunoprecipitate with the overexpressed Ran-GTPase, which is a key component of the nuclear transport machinery. The association of ShcA/Ran is enhanced by serum stimulation after the cells were deprived from growth factors (George et al., 2009). Using FRET, direct interaction between the two proteins in the nucleus was clearly observed, and it was suggested that Ran mediates ShcA nuclear import. The fact that Ran is upregulated in cancer cells (Xia et al., 2008) led the researchers to assume that Shc nuclear translocation might contribute to the oncogenic effect of Ran. Moreover, their interactome data indicated some nuclear proteins that might associate with ShcA highlighting its role in the nucleus (George et al., 2009).

In a different context, subcellular fractionation revealed the presence of tyrosine phosphorylated Shc, Grb2, Sos and active EGFR in the endosomes in response to EGF treatment (Guglielmo et al., 1994). In unstimulated cells, ShcA was shown to reside on the rough endoplasmic reticulum mainly within the perinuclear cisternae, while treatment with EGF stimulated the redistribution of Shc to the membrane region as well as to endosomes (Lotti et al., 1996). AP2 has a well-studied role in clathrin-dependent endocytosis (Collin et al., 2002). Shc interacts with AP2 (Okabayashi et al., 1996) mediating EGFR internalisation into early endosomes, upon subjecting the cells to epidermal growth factor (EGF) (Oksvold et al., 2000; Sakaguchi et al., 2001).

Nerve growth factor (NGF) treatment prompted ShcA translocation to the cytoskeleton and the membranous regions, as well as triggering ShcA-actin interaction (Thomas et al., 1995). ShcA association with the cytoskeleton was later confirmed by Smith et al 2010. In EGF-treated metastatic bladder cancer cells and a skin carcinoma cell line, immunostaining for Shc and IQGAP1, a cytoskeletal-associated protein, demonstrated recruitment of the two proteins to the membrane ruffles as well as to the lamellipodia (Smith et al., 2010). Depleted levels of ShcA negatively affect the formation of motility

structures and result in failure of IQGAP1 recruitment to the membranous region and to lamellipodia (Smith et al., 2010). Alternatively, protein kinase C-δ (PKCδ) was found to regulate Shc translocation to the cytoskeleton and mitochondria in H_2O_2-treated cardiomyocytes (Guo et al., 2010).

Interestingly, stimulation of $\alpha_6\,\beta_4$ integrins, which are part of hemidesmosomes structure (Jones et al., 1991), with laminin resulted in p52ShcA recruitment that in turn resulted in p52ShcA phosphorylation (Mainiero et al., 1995). Hemidesmosomes are key elements in epithelial cell-basement membrane adhesion (Borradori and Sonnenberg, 1999); $\alpha_6\,\beta_4$ integrin is part of their composition (Jones et al., 1991). Accordingly, this has delineated a new insight in ShcA localisation in the intracellular compartment, which might also indicate ShcA function in cell-basement membrane adhesion.

In conclusion, Shc adaptor proteins respond to various stimuli by altering their intracellular distribution to relay messages, activating different downstream pathways dictated by the cellular needs.

1.3 The role of the Shc family in different intracellular signalling cascades

The fact that the Shc family comprises different proteins provides the Shc family diversity in its function. They have been shown to be involved in cell proliferation, differentiation, migration, oxidative stress response and survival (Figure 1.2). It was originally thought that Shc protein action was restricted to transducing signals from upstream receptors such as RTKs, cytokine receptors as well as integrins, but many recent reports have revealed different aspects of Shc signalling.

1.3.1 Shc and cell proliferation:

In mouse fibroblasts, activated EGF receptor interacts with ShcA and results in tyrosine phosphorylation of ShcA on 239/240 and 317, which in turn binds growth factor receptor-bound protein 2 (Grb2) (Figure 1.2). The Shc/Grb2 complex recruits son of sevenless (Sos), which is a guanine nucleotide exchange factor of Ras. Activation of Ras induces the Raf/MAPK pathway which subsequently leads to upregulation of c-fos that drives mitogenesis (Figure 1.2) (Collins et al., 1999).

The role of Shc in cell proliferation is not confined to MAPK activation; it was shown that Shc can exert its mitogenic effect through inducing c-Myc expression (McGlade et al., 1992). In response to EGF stimulation, phosphorylation of ShcA at 239 and 240 tyrosine residues have been shown to induce c-Myc-mediated cell proliferation (Gotoh et al., 1997).

In addition, Shc plays a role in integrin (α5β1, α1β1 and αvβ3)-mediated proliferation (Barberis et al., 2000). Caveolin, a membrane scaffold protein, recruits the Src kinase family member (Fyn) promoting its interaction with integrin. Fyn undergoes a conformational alteration, due to its interaction with integrin, which allows its SH3 domain to interact with ShcA leading to MAPK activation (Barberis et al., 2000) (Figure 1.2).

Conversely, dephosphorylation of ShcA via its binding to SHIP phosphatase is implicated in Ras/MAPK downregulation, which suppressed haemopoietic cell proliferation (Lioubin et al., 1996). The association of ShcA with SHIP was investigated further by Marchetto et al 1996. Upon stimulating haemopoietic cells with colony stimulating factor 1 receptors, ShcA as well as SHIP are recruited to the activated receptors (Marchetto et al., 1999). SHIP binds ShcA-PTB domain (Marchetto et al., 1999) and subsequently interferes with the latter's ability to recruit Grb2; thereby it inversely affects the Ras/MAPK signalling pathway. Moreover, in B lymphocytes signalling Shc phosphorylation is adversely affected by PTP-PEST binding that might interfere with the mitogenic outcome (Faisal et al., 2002).

1.3.2 The role of Shc in cell survival and oxidative stress:

1.3.2.1 The impact of Shc on mediating survival signal:

On the basis of signalling pathway crosstalk, Shc can activate the PI3K/Akt pathway via the MAPK pathway, thereby, it can promote cell survival (Ravichandran, 2001) (Figure 1.2). In addition, Shc was reported to interact with Grb2-associated binding protein 1 (Gab1), which is known to activate the PI3K/Akt pathway (Gu et al., 2003). Furthermore, the role of ShcB and ShcC in promoting cell survival through inducing PI3K/Akt pathway in certain subsets of neurons has been discussed by Skai and coworkers (Skai et al., 2000).

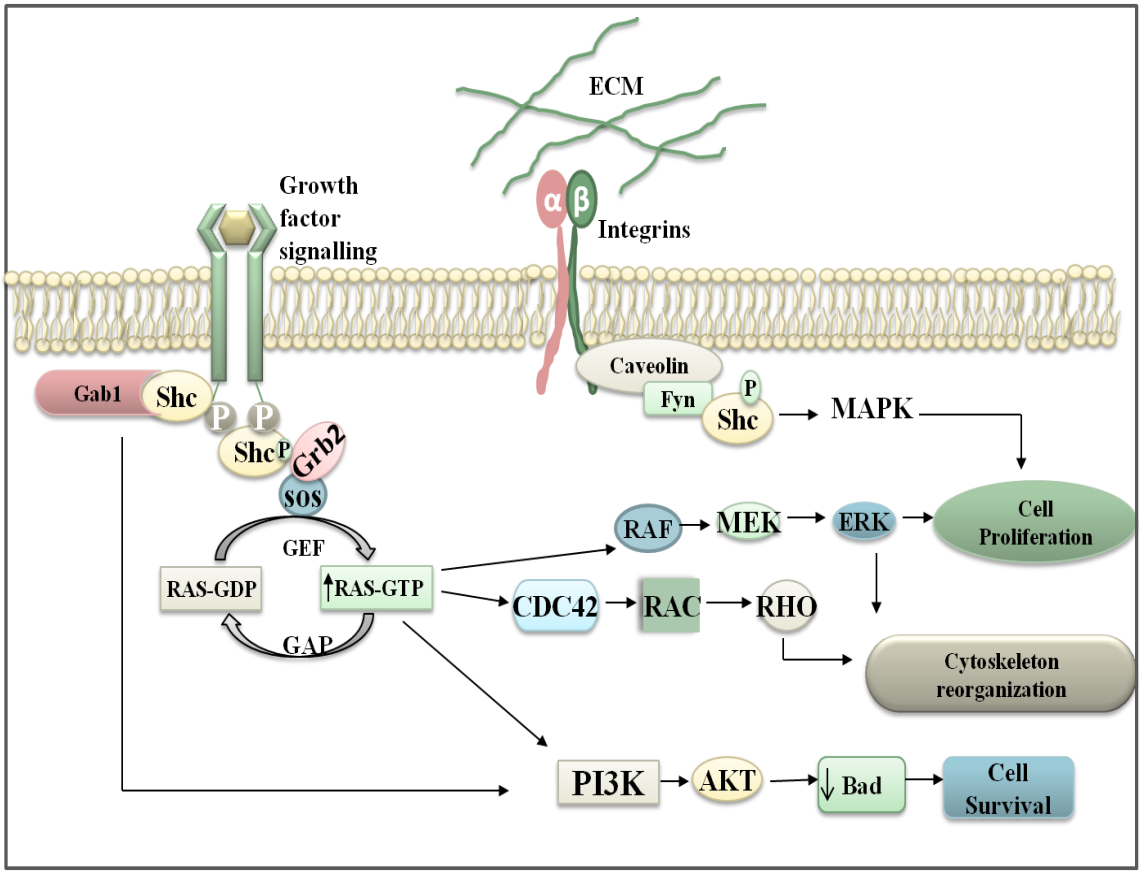

Figure 1.2 Shc acts as a bridge connecting the extracellular signal and the different intracellular signalling pathways. Shc is recruited by activated cell surface receptors or integrins. Phosphorylation of Shc can either occur by receptor tyrosine kinases (EGFR) or cytosolic tyrosine kinases (Fyn, a protein of the Src family). Phosphorylated Shc can then interact with Grb2, leading to the activation of different pathways such as the MAPK, PI3K/Akt and RhoA pathways via activation of Ras. Therefore, Shc proteins trigger different intracellular cascades resulting in various cellular responses (adapted from Zhu and Parada, 2002).

On the other hand, upon cell exposure to oxidative stress, p66ShcA becomes phosphorylated on its Ser36 residue leading to activation of a p53-independent pathway, which in turn induces apoptosis (Migliaccio et al., 1999).

ShcC is primarily expressed in neuronal cells while its expression in the remaining body tissues is limited (O'Bryan et al., 1996), therefore its function was studied in the neuronal context. ShcC is upregulated by high grade astrocytomas; it was found to be tyrosine phosphorylated by Ret tyrosine kinase. The ShcC/Ret association was revealed to play a role in survival of astrocytoma through triggering the PI3K/Akt signalling pathway (Magrassi et al., 2005). In a different study, ShcC has been shown to mediate prosurvival signals by both Ret-dependent and independent pathways, since a relative increase in the phospho-Akt levels was observed downstream of unstimulated and stimulated Ret receptors. In addition overexpression of ShcC provided PC12 cells with resistance to the death signal generated from serum starvation (Pelicci et al., 2002). Surprisingly, opposite to the anti-apoptotic function in neurons, ShcC impaired the survival signal of the T and B lymphocytes. Although ShcC as a pro-apoptotic factor, participates in modulating the balance between lymphocyte proliferation and survival, its overexpression might result in immunological-related diseases (Savino et al., 2008).

Independent of the role of p66ShcA in oxidative stress-induced apoptosis, p66ShcA was found to initiate anoikis, apoptosis due to loss of integrin contact with the cell exterior (Frisch and Francis, 1994), when the cells were forced to grow in suspension (Ma et al., 2007). In contrast to the impact of p66ShcA in oxidative stress-induced apoptosis (Galimov, 2010), ShcC plays a role in protecting the neuronal cells from death following oxidation or hypoxic insults, via induction of the PI3K/Akt signalling cascade (Troglio et al., 2004). In haemopoietic cells, ShcA induces a survival signal in early developing B cells that facilitates B cell development (Giles et al., 2009).

1.3.2.2 Shc as a key regulator in promoting oxidative stress response:

Shc proteins are commonly involved in transmitting signals from upstream receptors to downstream effectors. P66ShcA has shown an interesting role in mediating the stress response. P66ShcA-/- knockout mice displayed a 30% increase in life span and less susceptibility to oxidative stress than the wild type counterparts (Migliaccio et al., 1999), which highlighted a new role of ShcA in the stress response and aging.

Migliaccio et al were first to demonstrate the contribution of p66ShcA in signal transduction pathways involved in response to reactive oxyegen species (ROS). In addition, the study exposed the crucial role of Ser36 phosphorylation of p66ShcA in induction of the oxidative stress response. Interestingly, p66ShcA was revealed to upregulate p21/cip levels in response to oxidative stress which was suggested to be independent of p53 (Migliaccio et al., 1999).

Moreover, p66ShcA was revealed to contribute to neuronal death in Alzheimer's disease in response to amyloid β (Aβ)-peptide due to oxidative stress. p66ShcA influenced the production of the ROS in the intracellular compartment and particularly in the mitochondria, which induced Aβ-mediated cell death. This function of p66ShcA was clearly related to its phosphorylation at Ser36, which is partially dependent on JNK activation (Smith et al., 2004). In the same study, p66ShcA phosphorylation was found to elevate ROS levels by negatively regulating the transcription of ROS-scavenging enzymes such as Mn superoxide dismutase (MnSOD) and catalase, mainly through intervening with phosphorylation of forkhead proteins (Smith et al., 2004; Lebiedzinska et al., 2010) (Figure 1.3). Strikingly, p66ShcA was reported to act as one of the downstream effectors of p53 and upregulation of p66ShcA by p53 was observed upon UV treatment (Figure 1.3). Thorough experiments have shown that p66ShcA has a key role in p53-mediated ROS elevation and apoptosis (Trinei et al., 2002).

In a different context, constitutively active Rac1 induces ROS production partially via mediating p66ShcA phosphorylation at Ser54 and Thr386, through p38MAPK and JNK stress kinases. The phosphorylation of p66ShcA protected the protein from being degraded by reducing its ubiqutination. This study provided a new mechanism for regulating the Shc protein (Khanday et al., 2006). Likewise, p66ShcA and Rac1 association was investigated in the context of endothelial cells; their interaction was induced upon VEGFR activation. The interaction was found to induce ROS production that triggers capillary branch formation suggesting a contribution of p66ShcA to VEGF-mediated angiogenic responses in the endothelial cells (Oshikawa et al., 2012) (Figure 1.3). Indeed, p66ShcA has been shown to be a key regulator in oxidative stress conditions; these events do not always result in cell death but they might also yield different responses that are linked to angiogenic-linked diseases such as atherosclerosis and diabetes (Graiani et al., 2005; Camici et al., 2008).

Some experimental evidence demonstrated a role for p66ShcA in oxidative-stress induced apoptosis, but the exact mechanism was not clear until a study was conducted by Orsini et al. 2004. Treatment of mouse embryo fibroblast cells (MEFs) with staurosporine, a proapoptotic agent that induces cytochrome c release and activation of caspase-3, resulted in diminished levels of cleaved caspase-3 in p66ShcA-/- cells when compared with wild type MEFs. The proapoptotic function of p66ShcA was proposed to be due to changes in of mitochondrial transmembrane potential leading to cytochrome c release to the cytoplasm, which in turn results in apoptosis. The apoptotic role of p66ShcA was shown to be repressed by mitochondrial HSP70, which forms a complex with the former in non-oxidative stress conditions (Orsini et al., 2004).

Liver cells obtained from wild type (wt) mice as well as p66ShcA knockout mice were treated with CCl4, a chemical responsible for ROS generation. The mitochondria were then isolated and tested for the level of ROS by spectrofluorimetry technique. The wt cells exhibited an elevation in ROS level proportionate to an increase in the fluorescence of 2', 7' –dichlorofluorescin diacetate (H_2DCFDA), a compound that fluoresces in response to oxidation by ROS, while it persisted unaltered in the p66ShcA-/- cells (Giorgio et al., 2005). Further studies were conducted to reveal the mechanism underlying the role of p66ShcA in mitochondrial ROS production. p66ShcA was found to interact physically with the reduced cytochrome c, which leads to oxidation of the latter and ROS production (Giorgio et al., 2005)) (Figure 1.3).

A novel mechanism of how p66ShcA regulates the cellular ROS was illustrated by Kumar et al (Kumar et al., 2009). In endothelial cells p66ShcA potentiates ROS production via constraining the expression of Kruppel like factor-2 (KLF2), which was proved to induce the expression of the ROS scavenging enzyme, catalase (Dekker et al., 2006; Kumar et al., 2009). In UV and H_2O_2 treated melanoma cells, p66ShcA's function in inducing ROS production was found to be abrogated by the secreted protein, melanoma inhibitory activity (MIA) (Kasuno et al., 2007).

p66ShcA ablation in MEFs resulted in less ATP generation and reduced oxygen consumption by the mitochondria, which consequently resulted in decline in ROS levels, while an elevation in lactate level was observed (Nemoto et al., 2006).

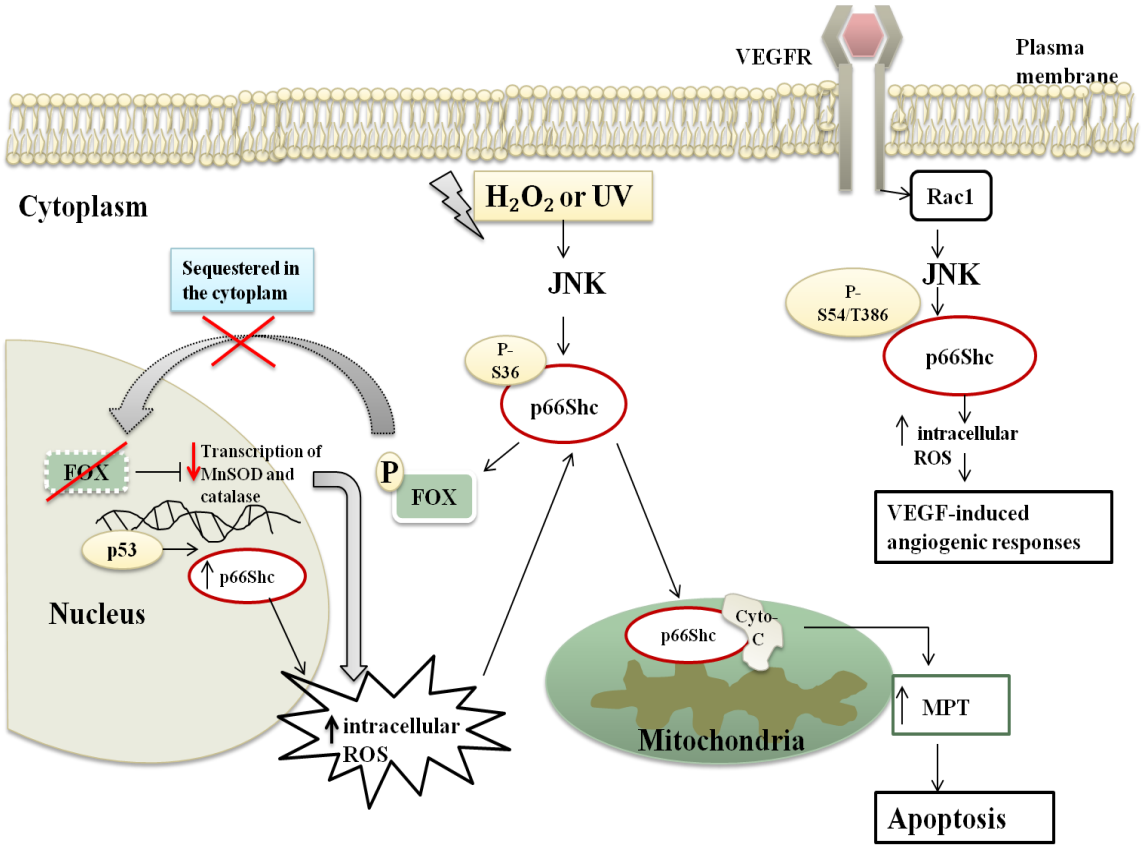

Figure 1.3 p66ShcA has a key role in the oxidative stress response. p66ShcA is phosphorylated on Ser36 via activation of stress kinases such as JNK, by exposing cells to oxidative stress agents e.g. H_2O_2 and UV. This results in translocation of a fraction of p66ShcA into the mitochondrial intermembrane space where it binds physically with cytochrome c (Cyto-c) resulting in mitochondrial permeability transition (MPT). Release of cytochrome c results in apoptosome formation initiating the apoptotic process. p66ShcA is also responsible for phosphorylation of the transcription factor FOX via an unknown mechanism (a member of forkhead protein family) causing the sequestration of the latter in the cytoplasm; thereby inhibiting the transcription of scavenging enzymes such as catalase and MnSOD. Upon VEGF stimulation in endothelial cells, p66ShcA is phosphorylated on Ser54 as well as Thr286 as a response to Rac1 activation. As a consequence, the produced intracellular reactive oxygen species (ROS) initiate the VEGF- mediated angiogenic response.

For the p66ShcA-/- MEF cells to meet their energy requirements they used an alternative pathway, aerobic glycolysis that generates ATP by converting pyruvate into lactate. The loss of p66Shc-/- also reduced the degree of regeneration of NADH from NAD. This study provided mechanistic evidence into the role of p66ShcA mechanistic in regulating the intracellular reactive oxygen species, as well as in the aging process (Nemoto et al., 2006). Interestingly, p66ShcA acts as a downstream effector for p53-induced apoptosis following oxidative stress (Trinie et al., 2002). In contrast, Apurinic/apyrimidinic endonuclease 1 (APE-1), a multifunctional protein that plays a role in DNA repair and in regulating the intracellular ROS (Tell et al., 2009), dephosphorylates p66ShcA via inhibition of PKC (Lee et al., 2011).

1.3.3 The role of Shc family in cellular migration and metastasis

In addition to the role of Shc in cell proliferation and survival, it is also implicated in cell motility. It acts as a regulatory molecule in directing an intracellular pathway either to proliferation or migration. This is found to be performed through alternative use of its phospho-tyrosine binding domains (PTB and SH2). The PTB domain has been shown to drive the cell towards haptotactic (directional) movement while the SH2 domain was found to be involved in cell cycle progression (Collins et al., 1999).

PTEN is known to be a negative regulator at the Akt pathway, which is involved in cell survival, by converting PIP3 to PIP2. It was reported that 35% of melanoma cell lines downregulate PTEN. Interestingly, a novel function of PTEN was shown in downregulation of focal adhesion kinase (FAK) and ShcA by directly dephosphorylating their modified active forms. Based on this finding when PTEN is depleted, ShcA and FAK will be active in promoting tumour development, migration and invasiveness (Gu et al., 1999; Pasini et al., 2009). In a study by Schneider et al, the role of PTEN in migration of renal cancer cells was analysed. It was found that PTEN expression is related to less metastatatic tumours due to dephosphorylation of ShcA, while FAK phosphorylation remained unchanged (Schneider et al., 2010).

Moreover, ShcD/RaLP has been found to be overexpressed in invasive melanoma, inducing both Ras-dependent and independent migratory pathways (Fagiani et al., 2007). p66ShcA was found upregulated in breast cancer accompanied by nodal invasion that is independent of Ras activation, thereby suggesting a role of ShcA in breast cancer metastasis (Jackson et al., 2000).

In a different study, mutant forms of the Met oncoprotein, that associated only with PLCγ, p85 subunit of PI3K, Grb2 or ShcA, were generated. This enabled to define the contribution of individual pathways downstream of Met receptor tyrosine kinase to be evaluated. Unlike other tested adaptor proteins (PLCγ and p85 subunit of PI3K), ShcA or Grb2 were able to induce lung metastasis in nude mice (Fixman et al., 1996; Saucier et al., 2002). An additional experiment on epithelial cells demonstrated the role of ShcA/Met signalling on epithelial cells scattering, which is a crucial aspect of cell metastasis (Saucier et al., 2002).

In contrast to studies implicating various Shc proteins in cell migration, p66ShcA overexpression in Lewis lung carcinoma provided the cells with striking resistance to migration. This function was found to be due to the inhibiting effect of p66ShcA on Ras activation (Ma et al., 2010). Furthermore, p46/p52ShcA interact with α5β1 integrin, the fibronectin (FN) receptor, and significantly modulates the association of extra cellular matrix to integrins that leads to acceleration of MCF-7 breast epithelial cell spreading on FN. Ectopic expression of p52ShcA in MCF-7 cells augmented the adhesion rate to fibronectin; thereby negatively affecting cell motility. Interestingly, using Boyden chambers to explore the role of ShcA in the same system revealed that ShcA expression has an impact on promoting cell motility, in particular upon EGF or IGF-1 treatments; when investigated using FN-coated inserts (Mauro et al., 1999). The association of ShcA with α5β1 has revealed another aspect of Shc regulation to cell motility and adhesion.

In breast tumour cells that express activated ErbB2, treatment with TGF-β results in a striking increase in cell motility in comparison to cells expressing mutant inactive ErbB2 cells. This finding pinpointed the possibility of synergism between ErbB2 and TGF-β pathways. The ShcA protein showed a central role in the cooperation between ErbB-2 and TGF-β pathways. In the same cell system, ShcA expression was proved to be crucial for TGF-β- induced focal adhesion turnover that is indispensable for ErbB2 expressing cells motility. Dominant negative p52ShcA (ShcA/3F), which lacks the three tyrosine residues (Y239/240 and Y317) essential for ShcA signalling, impaired TGF-β-mediated cell migration and invasion; this effect was ascertained to be independent of Shc-Grb2 association (Northey et al., 2008).

1.3.4 Shc as a key element in cell differentiation:

For the cells to gain a specialized function, some molecular modification should occur to facilitate the differentiation process. Shc proteins are needed for particular types of cells to be more specialized such as haemopoietic or neuronal cells.

In a haemopoietic cell line, the adaptor protein ShcA acts as a mediator of c-Mpl (a cytokine receptor) induced differentiation in response to thrombopoietin (TPO). Although, the tyrosine phosphorylation of ShcA was a consequence of this stimulation it did not result in Ras/MAPK activation. The PTB domain of ShcA was proved to be the key factor in this molecular event (Hill et al., 1996). An additional implication for ShcA protein in haemopoiesis was revealed; ShcA tyrosine phosphorylation was detected to be a crucial element for B cells transition from pre-pro B cell to pro-B cell, which leads to more mature and differentiated B cell formation (Giles et al., 2009).

Thomas et al delineated the role of ShcA in PC12 cells by testing the impact of the PTB and the SH2 domains of ShcA in transducing the signal downstream of the nerve growth factor (NGF) receptor, TrkA. Upon stimulating PC12 cells with NGF, ShcA was recruited to the activated TrkA receptor via its PTB domain; resulting in phosphorylation of ShcA on tyrosine 239/240. This interaction was proved to be important for NGF-mediated neurite extension in PC12 cells (Thomas et al., 1997). The ShcA involvement in PC12 differentiation was studied further by Hinsby et al., 2004. By utilizing a coculture method where PC12 were seeded on a monolayer of fibroblasts that either expressed, or did not express the neuronal cell adhesion molecule (NCAM), NCAM was found to form a complex with the focal adhesion kinase (FAK) and Fyn tyrosine kinase, which then results in ShcA phosphorylation. ShcA phosphorylation and Grb2 association was revealed to have a central role in NCAM-mediated neurite outgrowth (Hinsby et al., 2004).

Ectopic expression of ShcC in neural progenitor, as well as in post-mitotic cells, not only resulted in an increase in survival, but also showed neurite elongation, a feature of neuronal differentiation (Conti et al., 2001). A thorough examination of the molecular mechanisms by which ShcC provokes these biological events revealed that ShcC controls the PI3K-Akt-Bad prosurvival pathway as well as ERK pathway. In the same context ShcC was found to induce Bad phosphorylation (Conti et al., 2001); thereby the latter is sequestered by 14-3-3 initiating an anti-apoptotic signal (Zha et al., 1996).

1.3.5 Shc proteins are involved in oncogenic events:

Initially ShcA protein oncogenicity was deduced by the fact it is able to transform mouse fibroblast cells. The expression of ShcA ectopically in NIH3T3 fibroblasts provided the cells with the ability to form colonies on soft agar, as well as the ability to form tumours when injected into nude mice (Pelicci et al., 1992). In contrast to the transforming function of ShcA in NIH3T3 cells, overexpression of ShcA was not sufficient to grant breast cancer cells a profound transforming advantage (Mauro et al., 1999). Additionally, tyrosine phosphorylation of ShcA plays an important role in morphological transformation of rat fibroblasts (Fr3T3) upon coupling to the Met oncoprotein receptor (Fixman et al., 1996; Saucier et al., 2002). In the same cellular context, ShcA/Met association facilitated the growth of rat fibroblast cells in soft agar that indicated the ability of ShcA to encourage anchorage-independent growth (Saucier et al., 2002).

An in vivo experiment has demonstrated the role of ShcA protein in ErbB2 mammary epithelial cell induced-tumourgenesis. The expression of ShcA in mammary epithelial cells is central for the ErbB2-mediated transition from hyperplasia to invasive cancerous cells (Ursini et al., 2008). Another interesting function for ShcA in mammary tumour progression is in prompting tumour angiogenesis. In mammary tumour cells that expressed functionally active ErbB2, overexpression of mutant ShcA (ShcA/3F), which lacks the three tyrosine residues (Y239/240 and Y317), strikingly affected the ability of ErbB2-transformed cells to secrete vascular endothelial growth factor (VEGF) (Ursini et al., 2008). Further understanding of ShcA-mediated cell transformation was shown in Met expressing rat fibroblasts. The expression of Met prompted ShcA phosphorylation along with Grb2 recruitment, unlike the mutated Met (Y489F) that failed to transform Fr3T3 cells due to its inability to form a complex with ShcA and Grb2 (Fixman et al., 1996).

Interestingly, Middle T antigen (PymT), a component of polyomavirus, is responsible for hemangioma formation (blood vessel tumours that originate from the lining endothelial cells) in neonatal mice. A PymT mutant variant that was unable to recruit ShcA failed to transform endothelial cells. Subsequently, the PymT-mediated endothelial transformation phenomenon was found to be through formation of Shc/Grb2/Gab1 complex that mainly initiates the PI3K as well as Ras/MAPK pathways (Ong et al., 2001).

ShcC protein was found to be overexpressed and highly phosphorylated in high grade astrocytomas (Magrassi et al., 2005), as well as being present at high levels in higher grade neuroblastomas (Miyake et al., 2009). Soft agar assays showed that ShcC mediates anchorage-independent growth in human neuroblastoma cells (TNB1). Moreover, injecting TNB1/ShcC-/- cells subcutaneously into athymic mice resulted in small size tumours when compared with cells expressing ShcC, which implicates ShcC in neuroblastoma progression (Miyake et al., 2009). The oncogenic effect of ShcC in neuroblastoma cells was correlated partially to the formation of the ShcC/ALK complex that is mainly dependent on the pronounced phosphorylation of ShcC (Miyake et al., 2002).

Another in vivo evidence of a role for Shc proteins in tumourgenesis was determined by Fagiani et al. Injection of metastatic melanoma cells expressing high levels of RaLP into nude mice resulted information of larger tumours, compared with cells in which the levels of RaLP had been depleted (Fagiani et al., 2007).

1.3.6 Cardiovascular role of Shc:

Abrogation of the three ShcA isoforms (p46ShcA, p52ShcA, and p66ShcA) was proved to produce embryonic lethality at day 11.5 due to cardiovascular defects (Lai and Pawoson, 2000). The ShcA protein was shown to transduce a signal from tyrosine kinase receptors as well as from G-protein coupled receptors (Ptasznik et al., 1995). Subsequently, it was proposed by Graiani et al that of p66ShcA has an impact in G protein-coupled angiotensin receptor signalling. In Ang II treated cardiomyocytes, deletion of p66ShcA abrogated the cardiac hypertrophy-induced by Ang II (Graiani et al., 2005).

Cardiovascular side effects that resulted from tyrosine kinase inhibitors such as trastuzumab, which targets ErbB2, and imatinib an inhibitor for platelet-derived growth factor receptor, has highlighted the role of tyrosine kinase receptors; in normal adult heart networks (Vanderlaan et al., 2011). The molecular role of ShcA in postnatal cardiomyocytes was discussed by Vandarlaan et al. The transmission of signal from tyrosine kinases by ShcA PTB and SH2 domains was found to be necessary for normal myocardial function. In the absence of p46ShcA and p52ShcA but not p66ShcA, the myocardium experienced a disturbance in the extracellular matrix; this was reflected by

normal contractility of the cardiomyocytes, while the global heart contractility was clearly affected (Vanderlaan et al., 2011).

A comprehensive study was conducted to study the role of the PTB and SH2 domains of ShcA, as well as the CH1 phosphotyrosine sites in the developing heart. 48% of embryos that were deficient of functional Shc PTB died by day 11.5, while the remaining embryos experienced malformations in the cardiac trabeculae, enlarged hearts and irregularity in the heart beats. In addition the role of ShcA in the integrity of the developing heart was proved to be independent of the SH2 domain or the CH1 phosphotyrosine sites (Hardy et al., 2007).

1.4 Shc protein regulation:

1.4.1 Modulating Shc expression at the transcriptional level:

Proteins expression can be regulated at the transcriptional, translational levels or through regulation on protein stability in order to elicit distinct responses to cope with the cellular needs. The mechanisms underlying Shc protein regulation have not been studied thoroughly, only a few papers describe the regulation of the longevity associated protein, p66ShcA.

Transfection of a p66ShcA promoter reporter construct into cell lines that lacked endogenous p66ShcA expression resulted in normal promoter activity. This led to the suggestion that the promoter might possibly be regulated by epigenetic factors (Ventura et al., 2002). To further investigate this possibility, 32D haempoietic cells that lack p66ShcA expression, were treated with the histone deacetylase inhibitor (TSA), or demethylating agent (5-aza-dc), which resulted in p66ShcA expression at both mRNA and protein levels. Histone deacetylases are usually recruited to methylation sites in a promoter (Nan et al., 1998). Moreover, analysis of the p66ShcA promoter in cell lines that express high levels of p66ShcA revealed an unmethylated promoter (Ventura et al., 2002). Taking into consideration that histone deacetylases are implicated in transcriptional repression of methylated promoters, this work indicates that p66ShcA expression is modulated at the transcriptional level by methylation (Ventura et al., 2002).

In addition, elevated levels of homocysteine an amino-acid used in methionine biosynthesis, which is linked to vascular endothelial dysfunction have been proposed to to be due to modulation of p66ShcA expression. Since homocysteine is involved in cellular methylation, it was hypothesised that it regulates p66ShcA promoter methylation, thereby modulating p66ShcA expression. Using bisulfite sequencing of genomic DNA from an endothelial cell line, methylated CPG dinucleotides were identified in the p66ShcA promoter, which were hypomethylated by homocysteine treatment. As a consequence of p66ShcA expression in response to homocysteine treatment, reactive oxygen species were elevated in endothelial cells (Kim et al., 2011).

1.4.2 Shc proteins are post-translationally modified:

1.4.2.1 Shc protein phosphorylation:

The phosphorylation of Shc proteins plays a key role in the activation of intracellular cascades. p52ShcA was shown to be phosphorylated at three tyrosine residues in the CH1 domain (Tyr239/240; Tyr317) that were later shown to be conserved in the other Shc family members (Ravichandran, 2001; Jones et al., 2007). The tyrosine phosphorylation in the CH1 region is implicated in relaying the signal from the activated tyrosine kinase receptors, or cytoplasmic tyrosine kinases to the downstream effectors; (McGlade et al., 1992; Faisal et al., 2004). These events usually occur via Grb2 recruitment to the tyrosine phosphorylated ShcA, together with the associated Sos leading to Ras/MAPK signalling pathway activation (Hallberg et al., 1998). Parallel to that, phosphorylated Y239/240 were found to be involved in c-Myc induction rather than activating the MAPK cascade (Gotoh et al., 1997).

The Shc proteins contain different serine and threonine residues that can be phosphorylated. Phosphorylation of p66ShcA at Ser36 was found to have a role in the oxidative stress response (Migliaccio et al., 1999). Additionally, oxidative stress was reported to induce p66ShcA phosphorylation at Ser54 in the CH2 domain as well as at Thr386 in the CH1 domain (Figure 1.4) (Khanday et al., 2005).

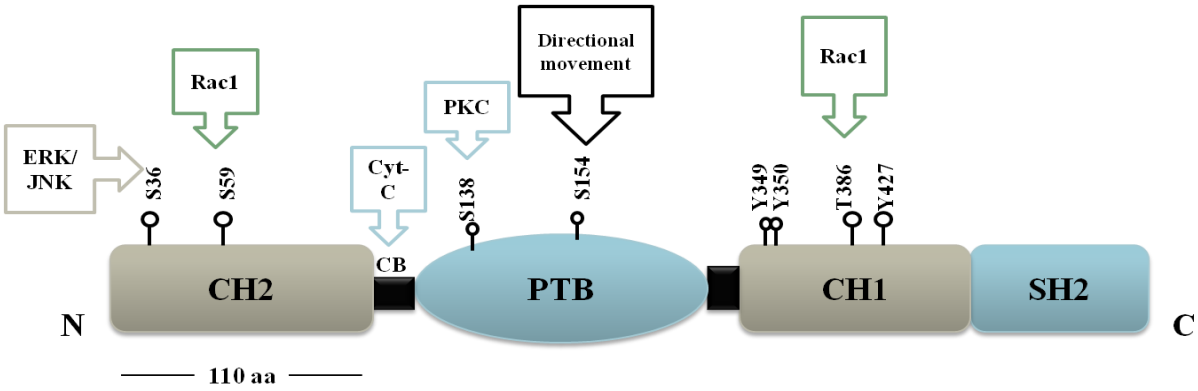

Figure 1.4 Schematic representation illustrates the phosphorylation sites on p66ShcA. There are three tyrosine phosphorylation sites and a threonine phosphorylation residue in the CH1 domain. There is one serine phosphorylation site on (Serine 138) the PTB domain as well as two serine phosphorylation sites in the amino terminal CH2 domain. p66ShcA has a unique cytochrome c binding region (CB). Ser36, S59, S138 and T386 are involved in oxidative stress response while S154 has a role in the directional movement of pancreatic cells. Phosphorylation of tyrosine residues in the CH1 are invoved in MAPK activation. (Adapted from Rajendran et al., 2010).

Osmotic shock and insulin treatment induced serine phosphorylation of p66ShcA, while p52ShcA becomes phosphorylated on serine and tyrosine in response to osmotic shock (Kao et al., 1997). The decrease in electrophoretic mobility of the p66ShcA protein was proved to be MEK-dependent, but independent of ERK (Kao et al., 1997). Although p66ShcA becomes serine/threonine phosphorylated upon EGF treatment, it unexpectedly impairs ERK activation in response to EGF stimulation (Okada et al., 1997). Faisal and coworkers studied ShcA phosphorylation upon 12-O-tetradecanoylphorbol-13-acetate (TPA) treatment, which is a PKC inducer (Faisal et al., 2002). TPA treatment resulted in phosphorylation of p66ShcA at Ser36, Ser138 and Thr29 while it induced phosphorylation of p52ShcA at Ser29.

The phosphorylation at Ser29 of p52ShcA as well as at Ser138 of p66ShcA mediates ShcA/PTP-PEST association; PTP-PEST is responsible for ShcA dephosphorylation following insulin stimulation (Faisal et al., 2002). Phosphorylation of p66ShcA at Ser36 is not only restricted to the oxidative stress response, it was also found to have a function in cardiomyocyte networks (Obreztchikova et al., 2006).
Unpredictably, ShcC was found to be dephosphorylated on Serine/Threonine residues subsequent to H_2O_2 or $CoCl_2$ treatments, the latter being a stimulator of hypoxia (Troglio et al., 2004). Interestingly, unlike other reports that addressed the role of Shc serine and threonine residue phosphorylation in the stress response, Ser154 (in the PTB domain) was reported to be responsible for haptotactic movement of pancreatic cancer cells (Figure 1.4) (Collins et al., 1999).

In summary, serine/threonine phosphorylation of the ShcA protein is mediated by different stimuli such as H_2O_2, UV, Taxol, endothelin-1, Thrombin, nor-epinephrine and PKC inducers such as TPA and PMA (Yang et al., 2000; Migliaccio et al., 1999; Chahdi et al., 2010; Faisal et al., 2002; Obreztchikova et al., 2006; Lee et al., 2011). Additionally, tyrosine phosphorylation of ShcA protein was reported to be essential for transducing signals from the upstream tyrosine kinases to the downstream effectors.

1.4.2.2 Ubiquitination affects Shc protein stability:

p66ShcA was found to be regulated at the protein level, and its level is elevated in progressive types of prostate cancer, ovarian cancer, breast cancer, which are steroid

hormone-sensitive tumours (Alam et al., 2009). It was therefore suggested that steroid hormones can affect p66ShcA expression. A 5α-dihydrotesterone (DHT)-treated prostate cancer cell line, as well as an estrogen-treated ovarian cancer cell line showed elevated levels of p66ShcA when compared with untreated controls. Furthermore, treatment with MG132 (a proteosome inhibitor) caused increased levels of p66ShcA protein. Ubiquitinated p66ShcA was clearly reduced after DHT treatment; similar to the effect induced by MG132 treatment (Kumar et al., 2011). It has previously been shown that, the stability of p66ShcA is also induced by a p53-dependent mechanism under oxidative stress (Trinei et al., 2002); however Kumar et al rather observed no alteration in p53 levels in their system.

P66ShcA phosphorylation on Ser54 and Thr386 by Rac1 under oxidative stress conditions induced the protein stability by deubiquitination (Khanday et al., 2006).

1.4.2.3 A novel way for Shc regulation at the protein level:

Interestingly, a recent report has described a ubiquitin-like modification that occurs on ShcA protein in T cells. Neddylation of ShcA by NEDD8 was shown to be essential for Grb2 and ZAP70 recruitment that are responsible for propagating signals for normal proliferation, cytokine production and differentiation via ERK activation (Jin et al., 2013). Mass spectrometry has revealed that neddylation occurs on lysine 3 of p52ShcA; mutating lysine 3 to arginine failed to elicit ERK activation. In contrast to the reported role of ubiquitin in ShcA protein stabilisation, the recent neddylation report has only defined the impact of the modification of ShcA on protein interactions and subsequent signalling, rather than protein stability (Jin et al., 2013).

1.5 RaLP /ShcD/Shc4

1.5.1 General introduction

Rai-like protein (RaLP) is the latest identified member of Shc family of adaptor proteins, and its mechanisms of action, as well as its exact function remain obscure.

TBLASTn analysis of *Homo sapiens* and *Mus musculus* genomes with sequences of previously identified Shc family members (ShcA/Shc, ShcB/Sli and ShcC/Rai) from

various organisms resulted in the identification of the RaLP gene (Fagiani et al., 2007). Structurally, RaLP has the same domain structure as the other Shc proteins that is CH2-PTB-CH1-SH2 (Figure 1.1) (Fagiani et al., 2007; Jones et al., 2007).

RaLP has been shown to be predominantly a cytosolic protein based on immunofluorescence microscopy. This finding was further confirmed by performing cell fractionation, which revealed the predominant existence of RaLP in the cytosolic fraction, while a small amount was found in the membrane fraction (Fagiani et al., 2007). In addition, RaLP localisation in the post synaptic membrane in the neuromuscular junction (NMJ) together with muscle specific kinase (MUSK) receptor was determined by Jones and colleagues (Jones et al., 2007). RaLP is found to be expressed as a 69 kDa protein, but its sequence contains other potential initiation codons suggesting shorter forms may exist. It has been shown that RaLP is physiologically expressed in the adult mouse brain, skeletal muscle, it is expressed in early murine embryonic developing tissues and in the melanocytes (Jones et al., 2007).

1.5.2 RaLP structural differences in comparison to other Shc family proteins:

Although RaLP shares sequence similarity to other Shc adaptor proteins, it has some unique structural differences. The residues in the ShcA-PTB, which are crucial for binding to acidic phospholipids and contribute to the distribution of Shc at the inner side of the cell membrane, are partially absent in RaLP (Fagiani et al., 2007). The significance of this observation has not yet been addressed. The assembly protein complex 2 (AP2) interacting site which is important for surface receptor endocytosis (Okabayashi et al., 1996), is present in other Shc family members but absent in RaLP (Figure 1.1) (Jones et al., 2007). The C59 residue, that is involved in dimerisation of p66ShcA, is also present in the newly identified member, suggesting that oligmerisation of RaLP may regulate its function (Figure 1.1).

The three tyrosine phosphorylation sites within the CH1 domain of Shc responsible for ERK activation are conserved in RaLP, as in other Shc proteins. Interestingly, it has been reported that RaLP/ShcD possesses an additional tyrosine residue (Y424) in the CH1 domain that can be phosphorylated by protein tyrosine kinases, and it represents an extra site for Grb2-SH2 recruitment that is not present in other Shc family members (Jones et al, 2007).

Furthermore, the phosphorylated serine residue Ser36 in the CH2 domain of p66ShcA, which is responsible for the proapoptotic function, is absent in RaLP (Fagiani et al, 2007). Instead RaLP has Ser37, Ser76 and Thr142 residues as putative targets for phosphorylation by various kinases (Fagiani et al., 2007).

1.5.3 Insights into the role of RaLP in the intracellular compartment:

1.5.3.1 RaLP functions as an oncogene in mediating melanoma invasion:

Adopting in situ hybridization (ISH) on a set of tissue microarrays (TMA), obtained from different normal human and tumour tissues, Fagiani and coworkers were able to report that RaLP was upregulated in invasive melanoma, a tumour of the melanocytes. More precisely, RaLP was found to be overexpressed in vertical growth phase and metastatic melanoma (Figure 1.5), while it was expressed at low levels in benign dysplastic nevi and radial growth phase melanoma. In addition, experiments by Fagiani et al revealed RaLP expression in non-melanoma tumours such as gliomas, neuroblastoma and neuroectodermal tumours, which all share the same neuronal origin (Fagiani et al., 2007).

Tumour cells exploit different cellular mechanisms to satisfy their needs. Malignant melanoma overexpresses RaLP to acquire a more invasive and migratory potential, which allows them to metastasise to distal organs (Figure 1.5). The fact that RaLP expression is a prerequisite for melanoma cell migration was approached using a transwell assay, comparing both metastatic melanoma cells that expressed RaLP against their counterparts in which RaLP was silenced. Melanoma cells were allowed to migrate from serum-free medium towards serum-containing medium. Serum-mediated motility was almost abrogated in RaLP-silenced metastatic melanoma cells.

RaLP can be phosphorylated upon epidermal growth factor receptor (EGFR) and insulin like growth factor -1 receptor (IGF-1R) activation in melanoma cells (Fagiani et al., 2007) (Figure 1.6). Both EGF and IGF-1 receptor kinases play a crucial role in melanoma cell growth, survival and migration, mainly through mediating the mitogen activated kinase (MAPK) pathway (Neudauer et al., 2003; Fagiani et al., 2007).

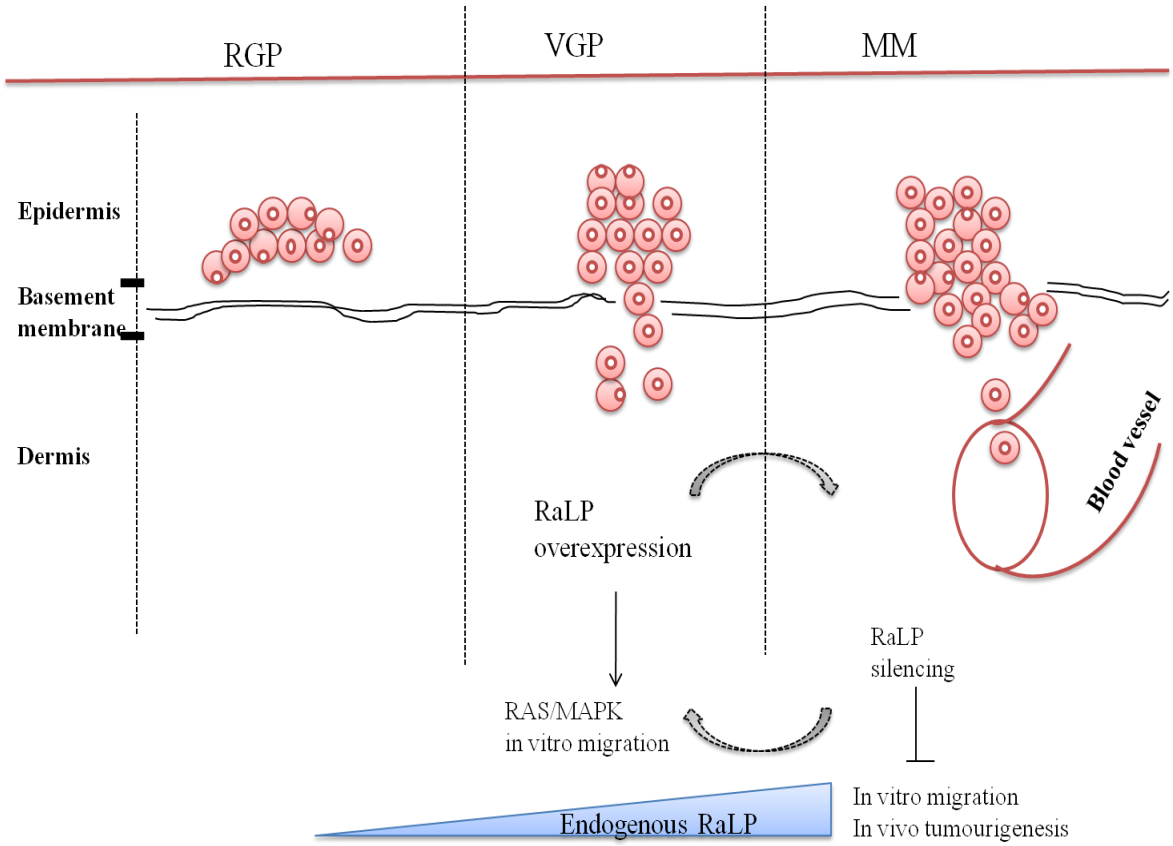

Figure 1.5 RaLP and its role in transition from radial growth phase (RGP) melanoma to vertical growth phase (VGP). Melanoma cells upregulate RaLP to acquire a more invasive phenotype to metastasize and to invade the basement membrane. Radial growth phase melanoma cells have lower levels of RaLP than invasive melanoma (Fagiani et al., 2007; Pasini et al., 2009). RGP: radial growth phase, VGP: vertical growth phase and MM: metastatic melanoma.

Consequently, researchers aimed to link the impact of RaLP in migration and MAPK activation. Surprisingly, the basal levels of MAPK activation were not affected upon silencing RaLP, therefore it was concluded that RaLP may affect cell motility through activation of MAPK-dependent and independent pathways (Fagiani et al., 2007).

1.5.3.2 RaLP acts as a substrate to different receptors:

A SPOT peptide array approach was employed to find binding partners for different PTB domains, from various adaptors, using a human library of NPXY motifs. All the PTB domains were tagged to GST at the N-terminus and their binding specificities investigated against arrays of NPXY peptides. RaLP-PTB domain was found to interact with TrKB/C, Met, Ret, IGF1R, ErbB2/4, VEGFR3, and unlike other Shc proteins, the RaLP-PTB domain was found to bind muscle specific kinase receptor (MUSK). Using the immunoprecipitation technique, the interaction between Myc-tagged RaLP-PTB and ERBb2, Ret and MUSK was verified (Smith et al., 2006) (Figure 1.6).

The expression of RaLP in mouse skeletal muscle prompted Jones et al to further study the RaLP and MUSK association. Despite confirming the RaLP and MUSK interaction by coimmunoprecipitation of exogenously expressed proteins, as well as performing GST pull downs, they were unable to coprecipitate endogenously expressed RaLP and MUSK from C2C12 myoblast cell extracts. The RaLP-PTB domain interacts with a phosphorylated juxtamembrane motif of muscle specific kinase (MUSK), and allows the early assembly of acetylcholine receptors, which has a role in their phosphorylation and hence signal transmission at the neuromuscular junction (Jones et al, 2007) (Figure 1.6).

A group of researchers in China had executed yeast two hybrid assays and coimmunoprecipitation experiments to verify the RaLP and TrkB receptor interaction that has been determined previously by the SPOT peptide arrays. They showed that RaLP association with TrkB relies on the PTB or/and the SH2 domains. TrkB phosphorylation in response to the brain derived neurotrophic factor (BDNF) resulted in recruitment of RaLP and its phosphorylation on the CH1 domain. RaLP phosphorylation was determined to be required for BDNF-mediated MAPK signalling (You et al., 2010) (Figure 1.6).

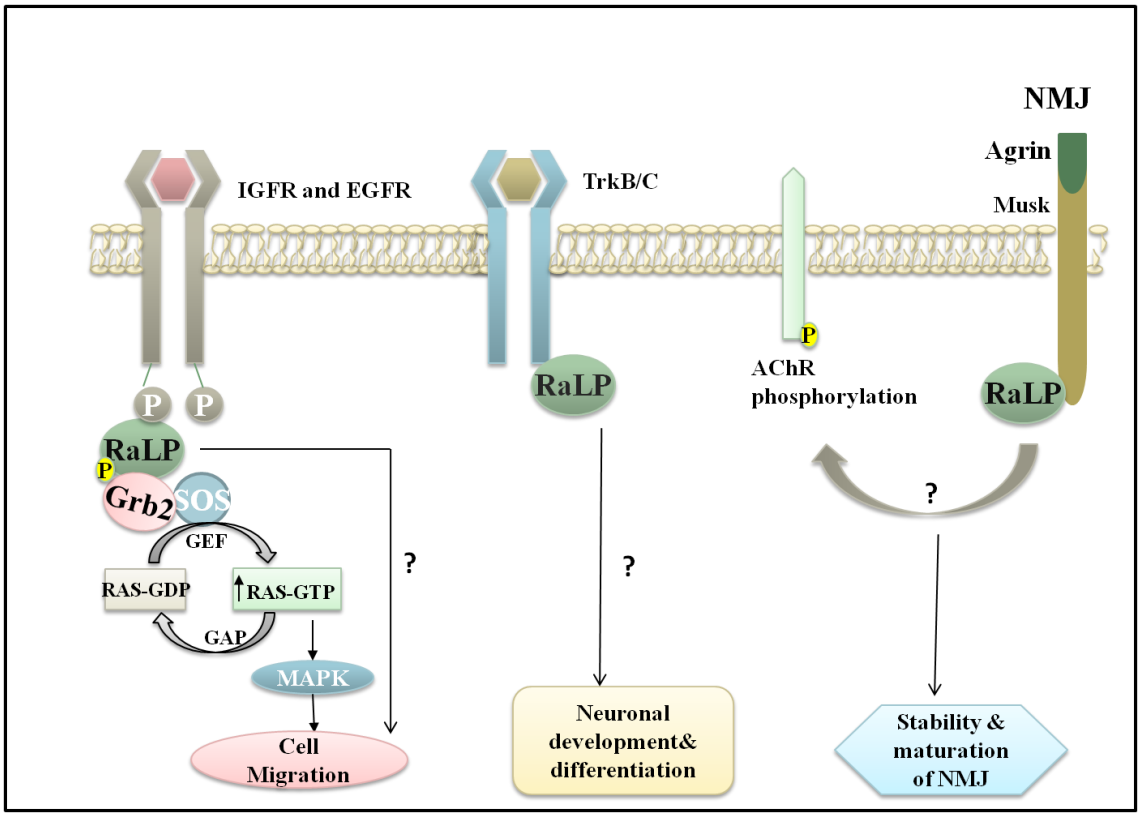

Figure 1.6 Diagrammatic representation summarizes the role of RaLP as a substrate to different tyrosine kinase receptors. RaLP acts downstream of the epidermal growth factor (EGF) and insulin like growth factor (IGF) receptors thereby it induces cell migration via both MAPK dependent and independent pathways. Moreover, the association of RaLP with neurotrophic receptors (TrkB/C) was reported and the interaction was suggested to be involved in neuronal development and differentiation. In contrast to the other Shc members, RaLP interacts with muscle specific kinase receptor (MUSK) at the neuromuscular junction (NMJ) resulting in formation of clusters of acetylcholine receptors (AChR) that play a role in the stability and maturation of the neuromuscular junction.

1.5.3.3 RaLP expression pattern in the mouse embryo and its possible role in embryonic stem cells:

Immunohistochemical studies revealed the expression of RaLP in developing mouse embryo. RaLP was present in the nervous system and both in the endochondral and intramembranous bones, whereas it was notably absent in immature chondrocytes. Additionally RaLP expression was observed in all kinds of contractile tissues such as cardiac, smooth and skeletal muscles. Intriguingly, RaLP demonstrated a broad expression in differentiated epithelia within various developing organs, it was found in skin, lung, kidney and digestive tract epithelia (Harley et al., 2010).

In an attempt to investigate the definite role of RaLP in the developing embryo, Turco et al generated a RaLP-/- knock out mouse, and the embryonic stem cells derived from this mouse were employed for studying RaLP's role in this context. During the early steps of embryo development, embryonic stem cells (ESC) differentiate to epiblast stem cells (EpiSCS), this process involves different gene expression modulations, and importantly Oct4, Sox2 and Nanog are required (Niwa et al., 2000; Chambers et al., 2007; Masui et al., 2007). Oct4 expression is crucial for self-renewal, differentiation and cell survival events in the embryonic stem cells (Niwa et al., 2000). Exploiting flow cytometry revealed that RaLP-/- ES cells have a delay in the differentiation process, and experienced a higher death rate. Lower levels of Oct4 were observed when compared with their controls during the transition of the cells to EpiSC. Therefore, it was inferred that absence of RaLP has led to prolongation of the transition time between ESC and EpiSC, and this might involve Oct4 downregulation (Turco et al., 2012). Despite their findings nothing has been reported regarding the changes due to lack of RaLP in the RaLP knock out mouse.

1.6 Summary and Aims:

1.6.1 Summary:

The Shc family of adaptor proteins contribute in different convoluted intracellular cascades. Their structural modularity, different gene products, and phosphorylation have equipped Shc proteins with the ability to propagate the intracellular signals. RaLP/ShcD is the newly identified member of the Shc family and its function is not yet well characterised. Therefore, we aimed to contribute in characterising the melanoma associated Shc adaptor, RaLP/ShcD. Though RaLP shares the structural hallmarks with the other Shc family proteins, it does not necessarily have identical functions to other Shc proteins. In fact there is increasing evidence that the Shc family members can have overlapping but distinct functions. To this end, we aimed to study the role of the newly identified Shc member, RaLP/ShcD, beyond the traditional role of Shc proteins in stimulating the Ras/MAPK cascade.

1.6.2 General aims:

Initially, it was aimed to produce a polyclonal antibody against RaLP, as well as to generate a cell line that stably expresses RaLP to facilitate RaLP characterisation. By generating a cell line in which the whole cell population overexpresses RaLP, it enables us to compare the morphological and molecular alterations in comparison to the wild type counterpart.

In preliminary studies, a fraction of GFP-RaLP was observed to be present in the nuclei of transfected melanoma cells that prompted us to study the RaLP nuclear cytoplasmic shuttling phenomenon. In addition we aimed to investigate the underlying conditions that promote RaLP nuclear translocation.

As RaLP's role in migration has been described previously, Yeast two-hybrid screens were conducted by a previous student to identify RaLP interacting partners that facilitate its role in cell migration. A negative regulator to cell motility, Nischarin was found to interact with RaLP-CH2 domain. Given the reported role of Nischarin in invasion suppression, it was aimed to explore this interaction further to determine if it has any relevance to melanoma migration.

Since at least one of the roles of the RaLP adaptor is to assemble signalling complexes, it is likely that identification of proteins in these complexes will hold the key of its functions. While Yeast two-hybrid library screens are useful in this regard, they also have their limitations. We therefore sought to isolate RaLP from transfected, and identify associated proteins by mass spectrometry.

Chapter 2

Materials &Methods

2.1 Materials:

2.1.1 General chemicals and reagents:

All the general chemicals and reagents that were used in the buffer preparations were provided from Fischer Scientific, Sigma or Melford. Reagents that were used for culture of mammalian cell lines were supplied by Gibco.

2.1.2 Cell lines:

518.A2, DAUV cell lines are primary cell lines obtained from human metastatic melanomas. They were kindly provided by Dr. Mike Browning (Infection, Immunity and Inflammation Department, University of Leicester). HEK 293 cells were a gift from Dr. Terry Herbert (University of Leicester, UK).

2.1.3 Plasmids:

GFP, FLAG, mCherry and GST tagged RaLP constructs were generated by the Protex facility (Biochemistry Department, University of Leicester). All the tags were present at the amino terminus of the RaLP sequence. The sequences of the constructs were verified by DNA sequencing by the PNACL facility (University of Leicester). All the constructs for the reporter assays were provided kindly by Prof. A. Sharrocks (University of Manchester, UK). The GFP-Nischarin expression vector was a generous gift from S. Alahari (Rockefeller University, New York). Myc-hIRAS was kindly provided by W. Hong (Institute of Molecular and Cell biology, Singapore). pGEM-T cloning vector was purchased from Promega with the pGEMT®-T Easy Vector kit (A1360). FLAG-p21 was kindly gifted by M. Hung (University of Texas, USA).

2.1.4 Imaging materials:

Hoechst 33342 (Thermo scientific; 62249), Mitotracker dye (Invitrogen; MP07510), and Propidium iodide (Sigma; p4864).

2.1.5 Antibodies:

2.1.5.1 Primary Antibodies:

Anti-Vinculin antibody was kindly provided by Bipin Patel (Biochemistry Department, University of Leiceter), while other used antibodies are listed in Table 2.1.

Primary antibody	Type	Dilution in W.B	Amount used for I.P	Blocking buffer W.B	Company	Cat. No
GFP	mouse	1:1000-1:2000	3µg	milk	Sigma	G6539-2ML
FLAG	mouse	1:1000	3µg	milk	Sigma	F1804
Shc4	mouse	1:1000	_	milk	abcam	Ab57808
Nischarin	mouse	1:1000	4-5µg	milk	BD-Pharmingen	558262
H1(AE-4)	mouse	1:1000	_	milk	Santa-Cruz	sc-8030
GAPDH	mouse	1:10,000	_	milk	Millipore	MAB374
LaminA/C	goat	1:1000	_	milk	Santa Cruz	sc-6215
Tubulin	mouse	1:1000	_	milk	Sigma	T5168
ATP50	mouse	1:1000	_	milk	abcam	Ab58684
p21	mouse	1:1000	_	milk	BD-Pharmingen	556431
CyclinD1	mouse	1:1000	_	milk	Santa-Cruz	sc-8396
p53 (ab28)	mouse	1:1000	_	milk	abcam	PAb1801
p44/42	rabbit	1:1000	_	milk	Cell signalling	9102
P-p44/42	rabbit	1:1000	_	milk	Cell signalling	9101
LIMK	rabbit	1:1000	_	BSA	Cell signalling	3842
pLIMK1(T508) /LIMK2(T505)	rabbit	1:1000	_	BSA	Cell signalling	3841
pCofilin(77G2)	rabbit	1:1000	_	BSA	Cell signaling	3313
Nup107	rabbit	1:1000	_	milk	GeneTex	GTX116664
TIF-1β	rabbit	1:1000	3µg	milk	Proteintech	15202-1-AP
p115	rabbit	1:1000	2.5µg	milk	GeneTex	GTX115114
Shc PG-797	mouse	1:1000	_	milk	Santa cruz	Sc-967
IgG	mouse	_	3-4µg	_	Sigma	18765-10MG
Flotilin-2	Rabbit	_	3µg	_	Sigma	1805
PKTAG (cont)	mouse	_	5µg	_	Serotec	MCA1360

Table 2.1: Primary antibodies that were used in western blotting (W.B) and immunoprecipitation (I.P) techniques.

2.1.5.2 Secondary antibodies:

Name	Dilution	Application	Company	Catalogue No
Anti-mouse IgG	1:10,000	W.B	Jackson Immunoresearch	115-035-146
Anti-Rabbit IgG	1:10,000	W.B	Jackson Immunoresearch	111-035-144
Anti-Goat	1:10,000	W.B	Jackson Immunoresearch	305-036-003
Anti-Rabbit Alexafluor594	1:1000	I.F	Invitrogen molecular probe	A11012
Anti-Rabbit Alexafluor488	1:1000	I.F	Invitrogen molecular probe	A11001
Anti-Mouse Alexafluor594	1:1000	I.F	Invitrogen molecular probe	A11005

Table 2.2: Secondary antibodies that were used in western blotting (W.B) or immunofluorescence (I.F) techniques.

2.1.6 Protein and DNA size markers:

2.1.6.1 DNA ladders:

1 Kb Plus DNA ladder was purchased from Invitrogen (10787-018).

2.1.6.2 Protein molecular weight markers:

Prestained molecular weight markers were supplied from Sigma (SDS7B2; 180-26.6 kDa), Precision Plus Protein standards from BIO-RAD (161-0373; 250-10 kDa) or PageRuler Prestained Protein Ladder from Thermo Scientific (26616; 170-10 kDa), while the unstained marker was from Sigma (SDS7; 66-14 kDa).

2.2 Methods

2.2.1 General buffers:

Luria-Bertani Broth (LB): 5 g NaCl, 5 g Bacto-tryptone and 2.5 g Bacto-yeast in 500 ml dH_2O.

LB agar plates: 5 g NaCl, 5 g Bacto-tryptone, 2.5 g Bacto-yeast, 7.5 g agar and 500 ml dH_2O, the mixture was autoclaved and allowed to cool <60ºC; this was followed by addition of 50 µg/ml Kanamycin or Ampicillin.

X-gal plates: 40 µl of X-gal (20 mg/ml) and 4 µl of IPTG (200 mg/ml) were spread on Ampicillin/LB agar plates, containing appropriate antibiotic. The plates were left to dry for 4 hrs before plating the bacteria.

2x $Ca^{2+}Mn^{2+}$ solution: 40 mM $NaOAc.3H_2O$, 100 mM $CaCl_2.2H_2O$ and 70 mM $MnCl_2.4H_2O$ pH 5.5.

Tris-EDTA (TE): 10 mM Tris, 1 mM EDTA; pH 7.4.

50x TAE: 40 mM Tris-base, 50 mM EDTA pH 8.0, 5.72% v/v glacial acetic acid.

10x phosphate buffered saline PBS (pH 7.4): 80 g of NaCl, 2.0 g of KCl, 14.4 g of Na_2HPO_4 and 2.4 g of KH_2PO_4 in 1 L dH_2O.

PBST: 1x PBS, 0.1% (v/v) Tween 20.

Blocking buffer for western blotting (WB): 5% (w/v) BSA or skimmed milk in PBST.

Antibody dilution buffer in WB: 5% (w/v) BSA or skimmed milk in PBST with the recommended amount of either the primary antibody or the secondary antibody.

Chemiluminescence buffer: 0.198 mM p-Coumaric acid, 1.25 mM Luminol-5-aminodihydrol-1,4-phthalazinedione (diluted from stocks prepared in DMSO) in 10 ml of 100 mM Tris-HCl pH 8.5, and 0.03% v/v of 30% H_2O_2 was added just before use .

Triton lysis buffer (TLB): 50 mM Tris, 150 mM NaCl, 5 mM EGTA, 25 mM Benzamidine, 1% Triton-X100 and just before use 1 mM PMSF (phenylmethylsulfonyl fluoride), 1 mM Na_3VO_4, 50 mM NaF as well as protease inhibitor cocktail (1/100) (Sigma) were added.

HiLO buffer: 50 mM Tris pH 7.4, 0.825 M NaCl, 1% v/v NP-40. Just before use add 1 mM PMSF, 1 mM Na_3VO_4, 50 mM NaF as well as protease inhibitor cocktail (1/100) were added.

3x SDS-PAGE Sample buffer: 0.15 M Tris-HCl pH 6.8, 6% SDS, 30% Glycerol, 0.2 mg Bromophenol blue, in 20 ml of dH_2O.

Coomassie stain: 45% (v/v) MetOH, 10% v/v glacial acetic acid, 1.25 gm coomassie brilliant blue-R250.

Destain solution: 25% v/v MetOH, 7% acetic acid.

1 M Sodium phosphate buffer (pH 8.0) (100 ml): 93.2 ml of 1 M Na_2HPO_4 (14.2 g in 100 ml dH_2O), 6.8 ml 1 M NaH_2PO_4 (12 g in 100 ml dH_2O).

2x YT medium (pH 7.0): 8 gm Bactotryptone, 5 gm Bacto-yeast and 2.5 gm NaCl in 500 ml dH_2O.

2.2.2 General molecular biology techniques:

2.2.2.1 Generating chemically competent bacteria:

One colony of DH5α grown on an LB plate free of antibiotics was picked to inoculate 10 ml of 2xYT medium. The bacteria were left to grow overnight at 37ºC in the shaking incubator at 250 rpm. 2 ml of the cultured bacteria were added to 200 ml prewarmed 2xYT. The bacteria were left to grow for ~2 hrs until the OD_{600} reached 0.2, thereafter; 4 mls of 1 M $MgCl_2$ was added to a final concentration of 20 mM. After 45 min $MgCl_2$ treatment, the OD_{600} was between 0.45 and 0.55 and the bacterial culture was divided

into 4 (x 50 ml) prechilled falcon tubes. The bacteria were left on ice for 2 hrs and then pelleted at 3,000 rpm for 5 min at 4ºC. The supernatant was discarded and each pellet was resuspended in 25 ml prechilled 1x $Ca^{2+}Mn^{2+}$ solution. The suspensions were kept on ice for 45 min then pelleted again; pellets were combined in 5 ml of 15% Glycerol containing $Ca^{2+}Mn^{2+}$ buffer (2 ml sterile dH_2O, 3 mls of sterile 50% glycerol and 5 ml of 2x $Ca^{2+}Mn^{2+}$ solution). Bacteria were aliquoted into prechilled sterile eppendorf tubes, snap frozen in liquid nitrogen, and then stored at -80ºC. The buffers in this experiment should all be sterile and prechilled.

2.2.2.2 DH5α transformation:

1 µl of the DNA was incubated with 50 µl of gently thawed competent DH5α on ice for 30 min. The bacteria were heat shocked by incubation at 37ºC for 5 min, which was then followed by 2 min incubation on ice. 500 µl of LB was added to the bacteria/DNA mixture and the bacteria were left to recover for 1 hr at 37ºC in the shaking incubator. 250-500 µl of the culture was plated on an LB agar plate containing the appropriate antibiotic and the bacteria were left to grow overnight at 37ºC.

2.2.2.3 Plasmid DNA preparations:

2.2.2.3 (i) Plasmid DNA isolation using Miniprep kit from QIAGEN:

A bacterial pellet that was obtained from 3 ml of overnight culture of E.Coli containing the desired plasmid, was resuspended in 250 µl of P1 buffer (50 mM Tris HCl pH 8.0, 10 mM EDTA, 100 µg/ml RNase A). After the bacterial pellet was resuspended properly, 250 µl of P2 buffer (200 mM NaOH, 1% SDS) was added and the tube was inverted 4-6 times. 350 µl of buffer N3 (3.0 M KOAc, pH 5.5) was added to the mixture and mixed thoroughly by inverting the tube 4-6 times. The suspension was centrifuged for 10 min at 13,000 rpm. The supernatant was then applied to the QIAprep spin column and centrifuged for 1 min. The column was washed initially with 0.5 ml of PB buffer (5 M GuHCl; 30% isopropanol) followed by additional wash with 0.75 ml PE buffer (75% EtOH, 25 mM NaCl, 5 mM Tris-HCl, pH 7.5). Spinning for an extra minute was performed to get rid of any residual buffer. The spin column was then placed in a fresh eppendorf tube and 50 µl of buffer EB (10 mM Tris·Cl, pH 8-8.5) was

added to elute the DNA. After 1 min incubation at room temperature the spin column was centrifuged for 1 min to collect the isolated plasmid DNA.

2.2.2.3 (ii) Plasmid DNA extraction for minipreps using the alkaline lysis method:

The bacterial pellet, from 3 ml overnight grown bacterial culture, was resuspended in 100 µl of ice-cold solution I (50 mM glucose, 25 mM Tris.Cl (pH 8.0), 10 mM EDTA), this was followed by vortexing until no bacterial clumps remained. 200 µl of fresh solution II (0.2 M of NaOH, 1% SDS) was added to the bacterial suspension and the tube was inverted 10 times. The resulting suspension was mixed with 350 µl of prechilled solution III (60 ml of 5 M KOAc, 11.5 ml glacial acetic acid, 28.5 ml dH_2O) by inverting the tube 10 times. The mixture was incubated on ice for 5 min; the insoluble fraction was pelleted by centrifuging the tube at 12,000 rpm for 5 min at 4ºC. The supernatant was placed into a fresh sterile tube and an equal volume of phenol:chloroform solution (Sigma) was added to remove the protein impurities. The mixture was spun at 12,000 rpm for 5 min at 4ºC to separate the organic and the aqueous layers. The upper aqueous layer was transferred into a fresh tube, while the lower organic layer was discarded. The plasmid DNA was precipitated from the aqueous fraction by adding two volumes of 70% EtOH, which was left to stand for 2 min at RT. The DNA was pelleted at 12,000 rpm for 5 min at 4ºC and it was then washed with 1 ml EtOH. The pellet was left to dry at RT for 10 min after discarding the EtOH. Finally, the pellet was dissolved in 50µl of 1xTE and any residual RNA was hydrolysed by adding DNase-free RNase (0.2 mg/ml).

2.2.2.3 (iii) Large culture preparation and large scale plasmid DNA preparation using QIAGen maxi-prep Kit :

One single bacterial colony was left to grow in 5 ml of antibiotic selective LB medium. 1 ml of overnight culture was used to inoculate 500 ml of antibiotic selective LB culture medium and then left to grow overnight at 225 rpm in the shaking incubator at 37ºC. The grown bacteria were then pelleted at 6,000 rpm for 15 min at 4ºC, using a sorvall centrifuge. The resulting pellet was resuspended in 10 ml of ice-cold buffer P1 (50 mM Tris-Cl, pH 8.0, 10 mM EDTA, 100 µg/mL RNase A).

After no bacterial clumps remained, the bacteria were lysed by mixing the suspension with buffer P2 (200 mM NaOH, 1% SDS) followed by inverting the tube 6 times and the mixture was incubated at RT for 5 min. 10ml of prechilled buffer P3 (3.0 M potassium acetate; pH 5.5) was then mixed with the lysed bacteria by inverting the tube 6 times, which was then followed by incubation on ice for 20 min. The fluffy precipitate formed was separated from the soluble fraction by centrifuging at 13,000 rpm for 30 min at 4ºC. To remove any traces of the insoluble material, the supernatant was spun again at 13,000 rpm for 15 min at 4ºC. The resin in the column was equilibrated with 10 ml of buffer QBT (750 mM NaCl, 50 mM MOPS, pH 7.0, 15% isopropanol, 0.15% Triton x-100) then the supernatant was added to the column. The column containing bound DNA was washed twice with 30 ml of buffer QC (1.0 M NaCl, 50 mM MOPS pH 7.0, 15% isopropanol). The DNA was eluted by adding 15ml of the elution buffer QF (1.25 M NaCl, 50 mM Tris-HCl pH 8.5, 15% isopropanol) and then the DNA was precipitated by adding 10.5 ml of isopropanol. After mixing, the plasmid DNA was pelleted at 15,000 rpm for 30 min at 4ºC. The pellet was rinsed with 70% EtOH and the centrifugation was repeated for 10 min. After discarding the EtOH, the pellet was left to dry for ~10 min and then dissolved by 500 µl of sterile 1x TE. Purified plasmid DNA was kept at -20ºC for long term storage. A sample of the DNA was run on a 1% agarose gel to test for the DNA quality. The amount of the DNA in the DNA prep was quantified by measuring the OD_{260} using BIO-RAD Smart spec™ 3000.

2.2.3 DNA separation by agarose gel electrophoresis:

Agarose gels were prepared by dissolving 1-2% (w/v) agarose in 1x Tris-acetate-EDTA (TAE) buffer. Before the gel set 0.5 µg/ml of ethidium bromide was added to visualise the DNA. The DNA sample was made denser by adding DNA loading dye (10 mM Tris-HCl pH 7.6, 0.15 % orange G, 60 % glycerol and 60 mM EDTA) in a ratio of 5:1. The DNA marker was separated along with the DNA samples at 120 volts. The DNA was then visualised by a UV transilluminator.

2.2.4 Semiquantitative reverse transcription-polymerase chain reaction (RT-PCR):

2.2.4.1 Total RNA isolation:

A 10 cm dish of cells ~90% confluent was lysed with 2 ml of TRI ® Reagent (Sigma) for 5 min at RT to extract RNA, DNA and protein. 1 ml was then transferred to a fresh tube and 0.2 ml chloroform (Sigma) was added, vortexed briefly and incubated at RT for 12 min to denature the proteins. The extract was centrifuged at 12,000 x g at 4ºC for 15 min to separate the aqueous soluble phase from the organic phase; rich in protein, and the middle layer containing the DNA. The upper layer was added to a fresh tube and remaining sample was discarded. The RNA was then precipitated by adding 0.5 ml isopropanol (Sigma) for 8 min at RT, followed by centrifugation at 12,000 x g for 10 min at 4ºC. The supernatant was removed and the pellet was rinsed with 70% ethanol and the previous centrifugation conditions were repeated for 5 min. The ethanol was discarded and the pellet was left to air-dry for 5-10 min and then solubilised with RNase-free water at 55-60ºC for 10-15 min, followed by storage at -80ºC. The RNA concentration was measured at OD_{260} using the conversion factor OD_{260} of 1 = 40 µg/ml.

2.2.4.2 Converting the mRNA to cDNA using RevertAid™ Minus First Strand cDNA Synthesis Kit (Fermentas):

The poly(A)$^+$ mRNA was primed by adding 1 µl of oligo (dT) primer to 2 µg of the total RNA and the volume was adjusted to 12 µl by DEPC-treated water. The solution was mixed gently, centrifuged briefly and incubated at 70ºC for 5 min. This was followed by chilling the mixture on ice and spinning it briefly again. RNA degradation was prevented by adding 1 µl (20 units) of Ribolock ™ Ribonuclease inhibitor, and 4 µl of 5 x reaction buffer and 2 µl of 10 mM dNTP were added; the mixture was then incubated at 37ºC for 5 min. To convert the mRNA to cDNA, 200 units of the reverse transcriptase enzyme was added to the mixture, which was then incubated at 42ºC for 60 min. The reaction was stopped by heating at 70ºC for 10 min and the mixture was then chilled on ice. The cDNA samples were diluted by addition of 80 µl DEPC-treated H_2O followed by storing samples at -80ºC.

2.2.4.3 Amplifying the resulted cDNA by the polymerase chain reaction PCR:

The cDNA in 5 µl cDNA mixture was amplified by adding 1x Reaction buffer, 1 µM forward and reverse oligonucleotide primers (Table 2.3), and 1.25 units of Taq polymerase in a final volume of 30 µl. The following PCR parameters were used:

94ºC (Initial denaturation step) for 2 min
94ºC for 1min
65ºC (annealing) for 2 min } x35 cycles
72ºC (elongation) for 2 min
72ºC for 10 min

Name of the primer	Primer sequence (5´-3´)
RaLP(PCR)F	TCC AAG TGC AGC AGT GTA TAT
RaLP(PCR)R	TTT GTT GGA ATG CAA AAG TGC
Actin-β (PCR)F	CAA CCG TGA AAA GAT GAC
Actin-β (PCR)R	CCA GAC AGC ACT GTG TTG

Table 2.3: Shows both forward (F) and reverse (R) primers for both RaLP and β-actin for the purpose of amplification by polymerase chain reaction (PCR).

2.2.5 Introducing mutations into the RaLP sequence using QuikChange® Site-Directed Mutagenesis Kit (Stratagene):

The muatgenesis reaction (50 µl) was set as follows; 50 ng of the double stranded template, 125 ng of both mutated forward and reverse primers-containing desired mutation (Table 2.4, 2.5 and 2.6), 1x reaction buffer (diluted from 10x stock), 1.25 mM dNTPs, and the total reaction volume was made up to 50 µl with adding sterile dH_2O. Finally, 1 µl (2.5 U/µl) pfu polymerase was added. The reaction was incubated in the thermocycler using the following parameters:

95ºC (denaturation) for 30 sec
95ºC for 30 sec
55ºC (primers annealing) for 1 min } x18 cycles
68ºC for 7 min

The methylated template DNA was digested by treating the mutagenesis reaction with 1 µl of the Dpn1 endonuclease for 1 hr at 37ºC. The mutagenesis product was transformed into XL1-blue super competent bacteria according to the protocol supplied with the kit. A miniculture was set up from one colony of the transformed bacteria, and plasmid DNA extracted using a miniprep kit (QIAGEN). The presence of the introduced mutation was confirmed by sending the DNA for sequencing (PNACL).

Primer Name	Primer sequence 5´-3´
RaLP	**F** CGCTAAAGATCTCGAGAACGCGGCCAGGACAGC
	R CGCTAAAGCTTTCATTTGTTGGAATGCAAAAG
RaLPp69#2	**F** ATGCTGCACAGGGC
	R CGCTAAAGCTTTCATTTGTTGGAATGCAAAAG
Del1	**F** GGTAGCTCCGGAGGCTCGGT
	R CGCTAAAGCTTTCATTTGTTGGAATGCAAAAG
Del2	**F** TCGCAGGAGAGCCCCACCCCA
	R CGCTAAAGCTTTCATTTGTTGGAATGCAAAAG
RaLPp59	**F** ATGAAGCTGGCCAA
	R CGCTAAAGCTTTCATTTGTTGGAATGCAAAAG
RaLPp49/ΔCH2	**F** CGCTAAGATCTCACTTTCTACAGCACCTGTTG
	R CGCTAAAGCTTTCATTTGTTGGAATGCAAAAG
RaLPΔSH2	**F** CGCTAAAGATCTCGAGAACGCGGCCAGGACAGC
	R CGTCAAAGCTTTTAGCTCCACAGCTGCTGCTTAATG

Table 2.4: Forward 5´-3´ (F) and the reverse primers 3´-5´(R) that were used to generate RaLP truncated versions to study RaLP nuclear localisation.

Template	Name and the sequence primer 5´-3´
Wt RaLP (FL)	**L83G-F** GAGAGCCCCACCCCAGGGTGCACCTTGATCCCC
	L83G-R GGGGATCAAGGTGCACCCTGGGGTGGG GCTCTC
Wt RaLP (FL)	**I87G-F** CCA CTG TGC ACC TTG GGC CCCCGC ATG GCA AGC
	I87G-R GCT TGC CAT GCG GGG GCC CAA GGT GCA CAG TGG
RaLP I87G	**L86G-MUTF** ACC CCA CTG TGC ACC GGG GGC CCC CGC ATG GC
	L86G-MUTR GCC ATG CGG GGG CCC CCG GTG CAC AGT GGG GT
RaLP I87G	**M90G-MUTF** ACC TTG GGC CCC CGC GGG GCA AGC ATG AAG CTG
	M90G-MUTR CAG CTT CAT GCT TGC CCC GCG GGG GCC CAA GGT

Table 2.5: Forward (F) and reverse (R) primers that were used to introduce point mutations into the RaLP predicted export sequence (ILCTLIPRM) to test for the functional nuclear export signal (NES).

Template	Name and the sequence (5´-3´) of the forward primer
Wt RaLP p59	RaLP-K238G-F GCA AAT GGA GCC ATT AAA GGG CGA AAG CCT CCA G
	RaLP-K238G-R CTG GAG GCT TTC GCC CTT TAA TGG CTC CAT TTG C
RaLPp59 K238G	RaLP-K237G-F GCA AAT GGA GCC ATT GGA GGG CGA AAG CCT CCA G
	RaLP-K237G-R CTG GAG GCT TTC GCC CTC CAA TGG CTC CAT TTG C
RaLPp59 K238/K237G	R239G-F GCA AAT GGA GCC ATT GGA GGG GGA AAG CCT CCA G
	R239G-R CTG GAG GCT TTC CCC CTC CAA TGG CTC CAT TTG C
RaLPp59 K238/K237/R239G	RaLP-K240G-F GCC ATT GGA GGG GGA GGG CCT CCA GTT GAG TTC
	RaLP-K240G-R GAA CTC AAC TGG AGG CCC TCC CCC TCC AAT GGC

Table 2.6: Forward (F) and reverse (R) primers that were used to introduce mutations into KKRK amino acid motif (237-240) in GFP-RaLPp59 sequence to test for the functional nuclear localisation signal (NLS).

2.2.6 Cloning RaLP full length sequence into pCMV-GAL vector:

2.2.6.1 Polymerase chain reaction to amplify RaLP:

To clone RaLP into the pCMV-GAL vector, it was decided to introduce the Sal1 restriction site at the 5´ and Xba1 restriction site at the 3´ of the RaLP sequence, for this PCR was employed. The primer annealing temperature was first optimized for RaLP amplification by PCR using a temperature gradient (48, 52, 56, 60 or 65ºC). To amplify RaLP, the PCR reaction was set by adding 100 ng template DNA, 1 µM of each forward and reverse primers (Table 2.7), 200 µM dNTPs, 1x reaction buffer, 1.25 units of the pfu polymerase (Fermentas; EP0501) and the reaction volume made up with sterile dH_2O to 30 µl.

Name of the primer	Primer sequence 5´-3´
RaLP FL-F	GCTACGCGTCGACCTATGCGAGAACGCGGCCAGGAC
RaLP FL-R	GCTATCTAGATCATTTGTTGGAATGCAAAAGTGC

Table 2.7: Primers used to amplify RaLP for cloning into pCMV-GAL vector.

PCR parameters were as follows:

94ºC for double stranded DNA denaturation for 2 min

94ºC for 1 min
(48-56)ºC (annealing) for 1 min
72ºC (elongation) for 2 min
} X 35 cycles

72ºC for 7 min

The PCR products along with DNA marker were resolved on an agarose gel that contained 0.5 µg/ml ethidium Bromide. The resulting product was then extracted from the gel using a gel extraction kit from QIAGEN.

2.2.6.2 Cloning RaLP into pCMV-GAL vector:

The PCR product of RaLP was initially cloned into a linearised pGEM-T vector with thymidine-overhangs that facilitates PCR product ligation after adenine incorporation using Taq polymerase. The pGEM-T Easy Vector System from Promega (TM042) was employed to achieve this. The recombinants were selected as white colonies growing on X-gal plates. The insert was digested from the vector by a double digest reaction using Sal1 and Xba1 restriction enzymes (New England Biolabs) and the digested product was then extracted from an agarose gel using a QIAGEN kit for gel extraction. The pCMV-GAL4 vector was linearised using Sal1 and Xba1, followed by gel purification. A sample of purified vector and PCR product were analysed on an agarose gel to estimate the concentration so as to optimise vector: insert ratio. The vector and the insert were added at a ratio of 1:3 and the ligation was performed at 16ºC overnight using T4 DNA ligase (New England Biolabs; M0202S) along with its reaction buffer that contained ATP.

2.2.7 Luciferase reporter assay:

HEK 293 cells were transfected with pG5LUC, pRL-TK and pCMV-GAL4-RaLP, pGAL4-VP16 or pCMV-GAL4. After 24 hrs, the cells were lysed as described in the Promega kit protocol for Dual-luciferase Reporter assays (E1910). The luminescence that resulted from Firefly and Renilla Luciferase enzymes was measured using VICTOR^{TM} X5 Multilabel Plate Reader (PerkinElmer; 2030).

2.2.8 Cell culture techniques

2.2.8.1 Cell line maintenance:

The cells were maintained in Dulbecco Modified Eagle's medium DMEM (Gibco; 61965) supplemented with 10% Foetal bovine serum (Gibco; 10270), and penicillin (100 U/ml) / streptomycin (100 µg/ml) antibiotic mixture (Gibco; 15140). The cells were left to grow in a humidified incubator provided with 5% CO_2. The cells were dissociated from the dish when they reached 90-100% confluence using 1x Trypsin/ EDTA (Gibco; 15400). All the mammalian cell culturing was performed under aseptic conditions.

2.2.8.2 Freezing and thawing of cultured cells:

A stock of the mammalian cell lines was always maintained via freezing the cells using the cryogenic preservation protocol. The cells were grown into either a 10 cm dish or 75 cm^2 flask until they reached 90-100 % confluence. The cells were detached from the surface by adding 1 ml of 1x trypsin/ EDTA to cover cells, then trypsin/ EDTA was removed. The cells were then kept in a 37°C incubator for 2-5 min according to the cell line. The detached cells were then resuspended in 2 mls FBS and transferred to a sterile universal tube. 2 mls of filter steriled freezing medium (20% DMSO in a normal DMEM with 10% FBS) was added in a drop wise manner. The mixture was then placed in labelled cryogenic vials. The tubes were kept for 1-2 days wrapped in cotton wool in an insulated polystyrene box at -80°C, then transferred to liquid Nitrogen for long term storage.

When a cell line was needed, cells were thawed by incubating the frozen cryogenic vial in a 37°C water bath. After 2 min, the thawed cells were added to 10 mls of medium and spun at 1100 rpm for 5 min in a bench top centrifuge. The cell pellet was finally resuspended in 1 ml of DMEM medium and added to a sterile culture plate containing fresh medium and left to grow.

2.2.8.3 Generation of stable cell lines:

HEK 293 were first tested for their sensitivity to neomycin (G418), and 1 mg/ml was found to be sufficient to kill all the cells. The cells were transfected with FLAG-RaLP, FLAG-RaLPΔCH2 or GFP-RaLP constructs that carry the neomycin resistance gene. The transfected cells were then selected by applying 1 mg/ml neomycin (G418). The colonies which were able to withstand G418 treatment were harvested using cloning discs from Sigma and they were grown under the selective conditions for several few passages. The surviving clones were tested for their expression of the desired protein using western blotting and immunoprecipitation techniques. The generated stable cell lines were maintained in a selective DMEM (containing 400 µg/ml G418) to ensure that the exogenous protein expression was maintained. The clones of HEK 293 cells that express FLAG-RaLP were designated as F1 and F4, and ΔCH2/2 for cells expressing FLAG-RaLPΔCH2, while GFP-RaLP expressing clone was called G5.

2.2.9 SDS-PAGE gel related techniques

The samples were prepared by adding 3x SDS sample buffer to a final concentration of 1.5x and dithiothreitol (DTT) was added to a final concentration of 100 mM. The samples were boiled for 5-10 min at 100ºC and then loaded on to appropriate SDS-PAGE gel (Table 2.8). The proteins in the cell lysates were then resolved along with a prestained protein molecular weight standard marker by running at a voltage of 150 V. The percentage of the acrylamide in the gel was decided according to the protein molecular weight (Table 2.8).

%Gel / Reagent	Resolving gel					3% (stacking)
	6%	8%	10%	12.5%	15%	
30% acrylamide	4 ml	5.34 ml	6.67 ml	8 ml	10 ml	1 ml
Tris (pH) 8.8	7.5 ml	7.5 ml	7.5 ml	7.5 ml	7.5 ml	Tris (pH 6.8) 1.2 ml
APS (10%)	150 µl	150 µl	150 µl	150 µl	150 µl	200 µl
SDS (10%)	100 µl	100 µl	100 µl	100 µl	100 µl	100 µl
TEMED	24 µl	24 µl	24 µl	24 µl	24 µl	15 µl
dH_2O	8.3 ml	6.9 ml	5.6 ml	4.2 ml	2.2 ml	7.6 ml

Table 2.8: Summarizes the composition of the different percentageSDS-PAGE gels.

2. 2.9.1 Protein gel staining:

The expressed and purified fusion proteins were all tested by running the samples on an SDS-PAGE gel followed staining for 1 hr with coomassie stain (section 2.2.1). To remove any residual stain from the gel, several incubations with destain solution (section 2.2.1) were performed.

2.2.9.2 Western blotting technique:

The SDS-PAGE gel was soaked in transfer buffer (29.1 gm Tris base, 14.6 gm Glycine, 1 L MeOH, 9.375 of 20% SDS and 4 L dH_2O) for 10 min. The proteins were then transferred to a nitrocellulose membrane (Whatman), using a BioRad semi-dry transfer apparatus at 22 V for 90 min. The membrane was then rinsed with dH_2O and blocked either with 5% milk or BSA in PBST for 1 hr at RT or O/N at 4ºC. After diluting the primary antibody (Table 2.1), in its dilution buffer, it was incubated with the blocked membrane O/N at 4ºC. The next day, the membrane was washed four times with agitation using PBST buffer. The secondary antibody coupled to HRP (Table 2.2) was added to a fresh dilution buffer and then incubated with the membrane for 1 hr at RT. Any unbound antibody was removed by applying four washes with wash buffer, allowing 5-10 min for each wash.

2.2.10 Enhanced Chemiluminescence (ECL):

The antibody bound to proteins on the membrane was visualised using Chemiluminescence buffer for 1 min. The membrane was then wrapped in Saran Wrap and exposed to X-ray film and the latter developed by the X-ray developing machine.

2.2.11 Reprobing the Nitrocellulose membrane:

To reprobe the membrane with a different antibody, the membrane was stripped using a stripping buffer (62.5 mM Tris-Cl, 2% SDS, freshly supplemented with 0.7% β-mercaptoethanol; pH 6.7) at 55ºC for 1 hour. The membrane was then washed 3 times with PBST, each wash for 5 min accompanied by agitation. The membrane was blocked again and then the same above steps were repeated.

2.2.12 Immunoprecipitation

2.2.12.1 Protein G-sepharose beads

The cells from a 10 cm dish, that was 90-100% confluent, were washed twice with prechilled PBS. 1 ml of Triton lysis buffer was then added to the cells and incubated with the cells for 5 min on ice to solubilise the phospholipid membranes. The cell lysates were then spun down at 14,000 rpm for 5 min at 4ºC to get rid of the insoluble materials. A 20 µl slurry of protein G-sepharose 4B Fast Flow beads (Sigma; P3296), was incubated with 2-5 µg of the desired antibody for 2 hrs on ice, then supernatant from cell lysate was added. The mixture was left overnight with rotation in the cold room. The next day, the mixture of cell lysate and the beads mixture was centrifuged briefly using the bench top microcentrifuge to pellet the beads. The supernatant was discarded and the beads were washed 4 times with ice cold 0.1% Triton-X100 in 1x PBS. The bound proteins were then dissociated using 80 µl of 2x SDS-PAGE sample buffer with 100 mM DTT and then boiled for 5-10 min at 100ºC.

2.2.12.2 GFP-trap for isolation of RaLP interacting partners, or testing RaLP phosphorylation status upon H_2O_2 treatment

2.2.12.2 (i) Preparing GFP-trap beads:

50 µl slurry of GFP-Trap-A (ChromoTek; 250) beads was transferred into a fresh tube and the beads were washed 3x with 500 µl dilution buffer (10 mM Tris-Cl pH 7.5, 150 mM NaCl, 0.5 mM EDTA, 1 mM PMSF and 1/100 protease inhibitors cocktail, the last two were added just before use). In between each wash, the beads were spun down at 2,700 x g for 2 min at 4ºC.

2.2.12.2 (ii) Cell lysate preparation:

The cells, which were obtained from ten 90-100 % confluent 10 cm dishes, were washed twice with prechilled 1x PBS. Each 10 cm dish of cells was lysed using 1 ml of ice cold HiLO buffer. The cells, with HiLO buffer, were incubated on ice for at least 1 min before the cells were scraped off the surface of the dish. The cell lysates from the

all dishes were combined in one tube and sonicated 3 times for 15 sec, with a 15 sec interval between rounds of sonication. The sonicated sample was spun at 13,000 rpm for 20 min at 4ºC, using an SS34 rota. A 25G needle was used to aspirate the clear lysate avoiding both the lipid-like upper and the precipitated bottom layers. To obtain as clear lysates as possible a subsequent round (or more) of spinning was performed for 10 min using the same conditions. The clear cell lysate (~ 10 ml) that was obtained from 10x 10 cm dishes was incubated with equilibrated beads with gentle shaking at 4ºC for 2 hrs. Beads were spun down at 2,000 x g for 2 min at 4ºC and the supernatant was discarded. The non-specific binding proteins were removed by washing the beads twice with the wash buffer (10 mM Tris-Cl pH 7.5, 500 mM NaCl, 0.5 mM EDTA and containing freshly added PMSF to 1 mM, 1x protease inhibitors cocktail). The GFP-trap was resuspended in 60 µl 2x SDS-PAGE sample buffer contained 100 mM DTT. The proteins in the samples were resolved on a 6% SDS-PAGE gel. The proteins were then stained for 1 hr using Instant blue coomassie from Expedeon. Finally, the gel was gently rinsed with dH_2O (milliQ). The stained bands on the gel were excised and digested by trypsin. The samples were analysed using LC MS/MS mass spectrometry and orbitrap to detect phosphorylation on GFP-RaLP and to identify any associated proteins (PNACL, University of Leicester).

2.2.13 Sub cellular fractionation and related methods:

2.2.13.1 Nuclear cytoplasmic fractionation:

DAUV, 518.A2 melanoma cells, and FLAG-RaLP expressing cells obtained from a 10 cm dish. The cell pellet was lysed with 400 µl of prechilled hypotonic buffer (10 mM HEPES pH 7.8, 25 mM β-glycerolphosphate, 25 mM $MgCl_2$, 0.1 mM Na_3VO_4, 0.5 mM EDTA and 1% protease inhibitors) and the nuclear membrane was disrupted by addition of 10% NP40 (to a final concentration of 0.6%). Thereafter, the separation of the nuclear fraction was performed by spinning the cell lysates at 13,000 x g for 30 sec at 4ºC. The nuclear proteins were released by adding 50 µl of high salt extraction buffer (50 mM HEPES pH 7.8, 50 mM KCl, 300 mM NaCl, 0.1 mM EDTA, 1mM DTT, 10% glycerol, 0.2 mM NaF, 0.2 mM Na_3VO_4, 1% protease inhibitor cocktail). Both the cytoplasmic and the nuclear fractions were employed in western blotting and immunoprecipitation experiments.

2.2.13.2 RaLP- DNA association:

2.2.13.2 (i) Crude method:

The nuclear fraction was separated from the cytoplasmic fraction as described above. The extraction of the DNA associated proteins was achieved following a protocol adapted from Dittmann et al., 2005. Briefly, the nuclear fraction obtained from HEK 293 cells that stably express FLAG-RaLP was treated with 1% formaldehyde. The nuclei were disrupted by sonication, and the DNA-protein complexes were separated from the insoluble nuclear material by centrifugation at 13,000 x g for 5 min at 4ºC. The supernatant was incubated with two volumes of isopropyl alcohol to precipitate the DNA O/N at 4˚C. The DNA and its associated proteins were then electrophoresed on an SDS-PAGE gel and western blotting was performed to identify proteins associated with precipitated DNA.

2.2.13.2 (ii) Chromatin extraction:

After the nuclear pellet was obtained from the DAUV cells following the stated protocol, it was washed twice with PBS followed by two washes with the chromatin extraction buffer with no nuclease (10 mM Tris-HCl pH 7.5, 1 mM $CaCl_2$, 1.5 mM $MgCl_2$, 0.25 M sucrose) supplemented with 1 µl Okadaic acid. The washed nuclear pellet was then digested by adding 200 µl of the chromatin extraction buffer along with nuclease (0.008 units/µl) at 30°C for 15 min. The soluble chromatin fraction was obtained after centrifugation at 20,000 x g for 10 min at 4°C. The soluble chromatin fraction was then incubated with immobilised anti-RaLP antibody overnight at 4°C.

2.2.13.3 Mitochondrial fractionation (Ventura et al., 2003):

A 10 cm dish of 90-100% confluent cells was washed twice with prechilled 1x PBS. The cells were scraped off the surface in 1 ml PBS and pelleted at 1200 x g for 10 min at 4ºC. The pelleted cells were then resuspended in 5 volumes of MT buffer (10 mM Tris/MOPS pH 7.4, 1 mM EGTA, 250 mM sucrose, 1 mM PMSF, 1mM Na_3VO_4 and 1:200 protease inhibitors cocktail). The resuspended cells were mechanically broken by applying 40-50 hand stokes from a Dounce homogeniser and the disrupted cells were

then transferred to a fresh eppendorf tube. The nuclei, debris and insoluble materials were pelleted twice for 5 min at 800 x g. The supernatant was transferred to a fresh tube and the mitochondrial fraction was isolated from the cytoplasmic fraction at 8,000 x g for 10 min at 4ºC. The mitochondrial pellet was washed once and then lysed with 2x SDS-PAGE sample buffer containing 100 mM DTT.

2.2.14 Cell imaging

2.2.14.1 Coverslips preparation:

Glass coverslips of 22 µm thickness were initially rinsed with distilled water in a glass beaker. They were then incubated with 1 M HCl for 30 min and then followed by thorough rinse with dH_2O. The acid-treated coverslips were sterilized by the addition of absolute EtOH for 30 min to overnight. The coverslips were dried on a piece of clean blue roll, thereafter; the dried coverslips were placed in a clean glass beaker and hence baked at 240ºC for 4 hours. After the coverslips were sterile and cold, they were placed in a sterile 10 cm plate.

2.2.14.2 General method for Immunofluorescence staining:

The cells were seeded on sterile acid treated cover slips. After 24 hrs, the cells were washed briefly with PBS and fixed with 3.7% formaldehyde for 20 min at RT. Any residual formaldehyde was removed by 3 washes with PBS. Cell permeabilisation was then performed by adding 0.1% Triton-x100 in PBS for 10 min and the cells were then saturated with 3% BSA in PBS. The primary antibody (Table 2.9) in dilution buffer (3% BSA in PBS) was then added for 1 hr at RT. The cells were then rinsed thoroughly with PBS three times. The secondary antibody (Table 2.2) was then added for 1 hr at RT and the cover slips washed 3 times with PBS. The nuclei were then stained with Hoechst 33342 (1 µg/ml) for 5-10 min. Three washes with PBS were applied to get rid of any unbound material and the coverslips were mounted using a 90% glycerol buffer containing anti-bleaching agent 0.5% w/v N-propyl gallate in 20 mM Tris pH 8.0. The coverslips were sealed with clear nail varnish and the cells were visualised using a Nikon microscope and 100x 1.4 N.A oil objective. Openlab software and Volocity software were employed for image acquisition.

Name	Dilution in I.F	Company	Catalogue No
Anti-RaLP (TB2/4333)	1:50-1:1000	(custom made by Cambridge Biochemicals)	_
Anti-FLAG	1:500	Sigma	F1804
Anti-MYC	1:500	Invitrogen	R951-25

Table 2.9 Primary antibodies used in immunfluorescence (I.F) experiments.

2.2.14.3 RaLP and Nischarin colocalisation:

518.A2 melanoma cells were seeded on coverslips and cells were co-transfected with FLAG-RaLP and GFP-Niscahrin or transfected with individual FLAG-RaLP or GFP-Nischarin (see section 2.2.20.1) . The cells were fixed with 3.7% formaldehyde and permeabilized with 0.1% Triton-X100, followed by addition anti-FLAG antibody for 1 hr. Alexafluor 495 (red) was used to visualise FLAG-RaLP and the nuclei were stained with Hoechst 33342. The cells were visualised by Leica TCS SP5 Laser Scanning Confocal Microscopy using x63/ 1.4-0.6 N.A oil immersion objective. The overlay was performed using Leica software LAS-AF-Lite 2.6.0 or ImageJ.

2.2.14.4 Mitochondrial staining:

The mitochondria of the cells that were grown on coverslips were stained by adding prewarmed (37ºC) staining solution (175 nM Mitotracker dye in growth medium) for 15 min at 37ºC. The cells were then washed twice with prewarmed PBS; this was followed by fixing the cells with 3.7% prewarmed formaldehyde for 15 min at 37ºC. Three washes with prewarmed PBS were applied and then the cells were permeabilised with ice-cold acetone for 5 min at -20ºC. After that the desired protein was stained and visualised as described previously.

2.2.15 Quantifying the cytoplasmic:nuclear (C: N) ratio using ScanR for:

2.2.15 (i) GFP-RaLPp59 wild type (wt) and its mutants to study RaLP nuclear localisation signal (NLS):

518.A2 melanoma cells were transfected with GFP-RaLPp59 wt along with the constructs that carry mutations of the KKRK motif. The screening was done on ~300 fixed green cells for each transfected construct using an Olympus microscope, 10x N.A 0.4 objective and Scanˆ R acquisition software (version 2.2.0.8). The results were further analysed using the Scan^R analysis software version 1.2.0.4 with background subtraction, gated for nuclear size, nuclear and cytoplasmic intensities, and the intensity in green channel measured. The gating was performed based on the FITC stain to select for green cells, Hoechst intensity was used to select for the nuclei, and 30 pixels was selected around the nuclei to represent the cytoplasm. The cytoplasmic mean intensity to the nuclear mean intensity ratio was calculated employing Scanˆ R analysis software. The experiment was performed 3 times and standard error of mean was calculated to show the variation in the ratios in each sample.

2.2.15 (ii) FLAG-p21 in GFP or GFP-RaLP expressing cells to study RaLP expression on cytoplasmic p21:

N1E115 neuroblastoma cells were transfected with FLAG-p21 and with GFP or GFP-RaLP constructs. The cells were then immunostained with ani-FLAG antibody as has been described earlier in 2.2.16.1. The screening was performed on the fixed cells using Scanˆ R acquisition software (version 2.2.0.8) as in 2.2.17 (i). Generally, the same gating and analysis were used except in this case red channel intensity was measured for both the nuclei and the cytoplasm.

2.2.16 Quantifying the nuclear distribution of GFP-RaLP wild type (wt) and its mutants to determine the nuclear export signal (NES):

518.A2 melanoma cells were transfected with GFP tagged RaLP, RaLPp69#2, RaLPp59, RaLPp49, RaLPL83G, RaLP I87G, RaLP L86/I87G or RaLP M90/I87G. The nuclear distribution of RaLP and the mutants was determined following certain

inclusion criteria. Only the transfected green cells were counted, the nuclei should not be distorted and the nuclear intensity of the expressed GFP tagged protein should either be similar to the cytoplasmic intensity or more. The percentage of the green cells that showed green nuclei following the stated criteria was calculated from the total number of the counted green cells. Three independent experiments were conducted and 50-100 cells per sample were counted. Standard error of mean was calculated to show the variation in the percentage in each sample.

2.2.17 Flow cytometry (FACs):

Cells growing at 50-60% confluence were washed briefly with PBS. The cells were collected by scraping them off the surface using a cells scraper and then pelleted at 1100 rpm for 5 min. The cell pellet was fixed with ice cold 70% ethanol that was added drop wise, while the cells were gently vortexed. The cells were incubated on ice for 30 min or more while preparing the other samples. 2-3 washes were performed to get rid of the remaining ethanol and then each cell pellet was resuspended in 400-500 µl of ice cold 20 µg/ml propidium iodide (P.I) in PBS containing 100 µg/ml RNase in PBS. The suspension was covered with foil and kept in a dark cold place overnight. The cell cycle profile of the samples was tested using a BDIS flow cytometer.

2.2.18 Cell treatments:

2.2.18.1 LMB treatment:

518.A2 melanoma cells, which were seeded on coverslips, were either transfected with GFP-RaLP or untransfected. The cells were treated with Leptomycin B (1 µg/ml) for 3 hrs and the cells were fixed with 3.7% formaldehyde as described previously. In the case of testing the effect of LMB on the endogenous RaLP the cells were treated for 8 or 24 hrs.

2.2.18.2 H_2O_2 treatment:

FLAG-RaLP expressing HEK 293 (F4) cells or 518.A2 were grown in 10 cm plates until the cells were 90-100% confluent. The cells were cultured under normal conditions

and then either stimulated with 5 mM H_2O_2 for 1 hr, 2 hrs or 4 hrs or left unstimulated. The medium was collected along with the cells, and the cells were pelleted at 1100 rpm for 5 min and medium was removed. The cells were fractionated into nuclear and cytoplasmic fractions.

2.2.19 Wound migration assays:

The cells were cultured in a 6 well plate until they reached 80% confluence; the cells were transfected as described earlier. After 24 hrs, the wounds were performed to the confluent monolayer of the cultured cells. The cells washed once with PBS, and then phenol red free medium containing Glutamine was added. The wound imaging was carried out using a Nikon fluorescence microscope and 10x objective. The images were taken every 20 min for 24 hrs employing Nikon NIS-elements software. The data were analysed by ImageJ software (Macro created by Dr Kees Straatman, University of Leicester).

2.2.20 DNA/siRNA transfection into mammalian cells:

2.2.20.1 DNA transfection:

The transfections were performed using ExGen 500 (Fermentas) following the manufacturer's protocol. Briefly, the cells were cultured to a density of 50-80%. The DNA was initially diluted in 150 mM NaCl, which was then followed by adding ExGen 500, and the ratio between the DNA amount to ExGen 500 volume is 1:3 (e.g. for a well in 6 wells plate 3 µg (DNA): 9.87 µl (EXGen 500). The amount of DNA/ExGen 500: NaCl should be 10% of the volume of the medium. The cells were incubated with the transfection mixture for 24-48 hours in the normal culture conditions to express the desired protein.

2.2.20.2 siRNA transfection:

The cells were seeded in a 24 wells plate until they reached 70% confluence. The cells were then transfected with 5, 10 or 15 nM siRNA using Turbofect transfection reagent (Fermentas). Initially, the siRNA was diluted in serum free medium followed by adding

the transfection reagent, according to the manufacturer's guide lines. After 24 hrs the transfections were repeated and the cells were incubated for an additional 48 hrs.

2.2.21 Antibody production and purification

2.2.21.1 Antibody production:

2.2.21.1 (i) Small scale HIS-$CH1_f$ expression and purification:

The expression of the HIS-$CH1_f$ region (RaLP amino acids 386-468) was performed on a small scale to test for the optimum conditions to express the fusion protein in BL21/DE3 bacteria.

One colony of the HIS-$CH1_f$ transformed BL21 bacteria was picked to inoculate 5 ml of LB culture with 50 µg/ml kanamycin, and left to grow for 16 hrs at 37ºC in the shaking incubator. A new culture of 10 ml LB, 10 mM $ZnCl_2$ and 200 µl of the overnight grown BL21 bacteria was incubated at 30ºC for 1 hr. 1 ml of the culture was placed into each of two fresh eppendorf tubes. 0.2 mM of Isopropyl β-D-thiogalactopyranoside (IPTG) was used to induce the fusion protein expression in the remaining 8 mls. 2 mls of the IPTG-treated culture was collected as described earlier after 1, 2, 4 and 6 hrs after the induction. The bacteria were pelleted at 12,000 rpm at 4ºC and the pellets were kept at -80ºC. One set of the bacterial pellets from each time points was boiled in 2x SB containing 100 mM DTT, while each bacterial pellet from the second set was resuspended in 200 µl resuspension buffer (1x PBS, 1 mM PMSF and 1:60 protease inhibitor). The five resuspended bacterial pellets were sonicated 3 times, each time for 15 sec with 15 sec intervals. For further lysing, 10% Triton-x100 was added to final concentration of 1% to each sonicated sample for 1 hr with agitation at 4ºC. The soluble and the insoluble fractions were separated by spinning the lysed bacteria at 14,000 rpm for 10 min. Both soluble and insoluble fractions were denatured by addition of 200 µl of 2x sample buffer containing 100 mM DTT followed by boiling. Samples were resolved on a 15% SDS-PAGE gel, which was then stained with coomassie stain.

2.2.21.1 (ii) Large scale HIS-$CH1_f$ protein expression:

Initially, 5 ml of LB (with the selective antibiotics) was inoculated with a colony of HIS-CH1 transformed BL21/DE3 bacteria and bacteria were left to grow at 37˚C for

6 hrs in the shaking incubator. The grown bacteria were left to further replicate in a total volume of 20 mls LB O/N at 37ºC. The overnight culture was inoculated into 1 L of LB (with the selective antibiotic), and the fusion protein expression was induced by adding 0.2 mM IPTG for 4 hrs at 30˚C. The bacteria were then pelleted at 6,000 rpm for 15 min in a centrifuge at 4˚C. The supernatant was discarded and the pellet was kept at -80˚C until it was needed.

2.2.21.1 (iii) Purification of HIS-CH1$_f$ using a Ni-column:

Equilibration of beads and large Scale protein purification via extraction of insoluble fusion protein from the inclusion bodies:

Initially, 1 ml of chelating sepharose beads was first washed with 1x PBS, and then the beads were charged with 5 ml of 1 M $NiCl_2$ for 2-16 hrs at room temperature. The beads were then washed twice with dH_2O, which was followed by 2 washes with the equilibration buffer (50 mM Na_2HPO_4 pH 8.0, 0.5 M NaCl and 8 M urea). The bacteria were spun down each time at 3,500 rpm for 3 min.

The bacterial pellet was thawed and gently resuspended in a lysis buffer without denaturants (50 mM Na_2HPO_4 pH 8.0, 0.3 M NaCl, 1 mM PMSF and protease inhibitors cocktail). The proteins were released out of the bacteria by sonication 3 times for 20 sec, with 20 sec interval. The sonicated mixture was then spun for 15 min at 14,000 rpm at 4˚C. The inclusion bodies were resuspended thoroughly in 20 ml of lysis buffer with denaturants (50 mM Na_2HPO_4 pH 8.0, 0.3 M NaCl, 1 mM PMSF, protease inhibitor cocktail and 6 M GuHCl) and incubated at 30˚C for 30 min in the shaking incubator. This was followed by spinning down the mixture at 14,000 rpm for 15 min in a cold centrifuge. The supernatant was left to tumble with the equilibrated beads overnight at 4˚C. The beads and the bound proteins were applied to a fresh column and all the nonspecific unbound proteins were removed by three times washing with the wash buffer (8 M urea, 20 mM Tris pH 7.5, 0.5 M NaCl). To further wash out all the contaminants two more washes were applied using the same wash buffer containing 10 mM imidazole. The interactions between the HIS tag and the Nickel ions (Ni^{2+}) were broken by an elution buffer containing high concentration of imidazole (8 M urea, 20 mM Tris pH 7.5, 100 mM NaCl and 250 mM imidazole). The eluted fractions were resolved on an SDS-PAGE gel. The combined fractions were dialysed against elution

buffer with 10 mM imidazole to remove the imidazole using dialysis tubing of molecular weight cut off 3 kDa.

2.2.21.1 (iv) Removal of contaminating proteins:

The dialysed protein was applied again to a column containing regenerated $NiCl_2$-charged beads with a capacity of 20 mg/ml and the fusion protein was left to bind the beads overnight at 4ºC. Washing of the column and protein elution were performed using a BioRad fraction collector that facilitated the collection of 1 ml fractions every 2 min using an imidazole gradient that ranged between 10-500 mM. The elution fractions were tested for their protein content by resolving them on an SDS-PAGE gel and afterwards the gel was stained with coomassie staining solution. The accurate protein concentration was estimated using BCA protein assay with a BSA standard curve. 2 mg/ml was sent to Cambridge Biochemicals for the Antibody production.

2.2.21.2 Antibody Purification:

2.2.21.2 (i) Expression and Purification of the GST-CH1 fusion protein:

One colony of GST-CH1 (RaLP amino acids 349-523) transformed BL21/DE3 was picked to inoculate 10 ml of LB medium with 50 µg/ml kanamycin and the bacteria was left to grow overnight in a shaking incubator at 37ºC. 10 ml of overnight culture was inoculated into in a large culture of 500 ml LB/kanamycin and grown at 37ºC until the $O.D\lambda_{600}$ reached 0.6. The protein expression was then induced by adding 0.2 mM IPTG to the large culture and the bacteria were left to grow overnight with shaking at 30ºC. The next day, the bacterial pellet from 1 ml culture was dissolved using SDS sample buffer and analysed on an SDS-PAGE gel to confirm the induction of the fusion protein. After confirming the successful fusion protein expression, the bacterial cells that were grown in the large culture were pelleted at 6,000 rpm for 15 min at 4ºC. The pellet was resuspended in prechilled resuspension buffer (1x PBS buffer, 1 mM PMSF, and 1:100 protease inhibitor cocktail). The resuspended bacterial cells were broken by applying pressure 3 times using a French Press. To solubilise proteins, 0.1% Triton-x100 was added and the mixture was incubated with tumbling in the cold room for 1 hr. The suspension was then spun at 10,000 rpm (ss34 rota) at for 20 min at 4ºC. 0.5 ml of the

glutathione sepharose beads (GE- Healthcare; 17-0756-01) were washed four times with 5 ml washing buffer (1x PBS, 1 mM PMSF and 1:100 protease inhibitor cocktail), then supernatant containing GST-CH1 was added with tumbling O/N. The next day, the pelleted beads were washed 5 times with the wash buffer (1x PBS, 1 mM PMSF and 0.1% Triton-x100). The 500 µl beads with its associated proteins were then placed in a 10 ml column and the GST-CH1 fusion protein was eluted with 5 ml of the elution buffer (100 mM HEPES pH 8.0 and 50 mM reduced glutathione (Sigma; G-4251), in the cold room. The 10 collected fractions (500 µl each) were tested for their protein content by running 20 µl from each fraction on a 12.5% SDS-PAGE gel.
Elution fractions containing GST-CH1 protein were combined and dialysed twice against 2 L of dialysis buffer (0.2 M $NaHCO_3$, 0.5 M NaCl pH 8.3) so that the buffer would be compatible for binding to the NHS-activated beads.

2.2.21.2 (ii) Coupling the purified GST-CH1 to the NHS-activated beads:

2 ml of NHS-activated beads was washed 2 times with dH_2O and this was followed by twelve washes using 15 ml of ice cold 1 mM HCl (pH 8.5). Thereafter, the dialysed GST-CH1 was incubated with the washed beads tumbling overnight in the cold room. Beads were then pelleted at 2,000 rpm for 2 min at 4ºC and the supernatant was removed. The beads with the coupled protein were then incubated with ice cold blocking buffer (0.5 M ethanolamine, 0.5 M NaCl pH 8.3) for 2 hrs at 4ºC. To remove all the unwanted proteins the beads with the immobilised fusion protein were washed 3 times with alkaline washing buffer (0.1 M Tris-HCl pH 8.5) which was then followed by 3 washes with acidic washing buffer (0.1 M NaOAc and 0.5 M NaCl pH 4.5), and this was repeated 5 times. To test the efficiency of the coupling procedure, 20 µl from the fusion protein supernatant was taken before and after the incubation with the NHS-activated beads for analysis by SDS-PAGE.

2.2.21.2 (iii) Purifying the rabbit anti-serum using the generated affinity chromatography column:

The coupled beads were washed once with 50 mM Glycine pH 2.2 buffer and this was followed by two washes with 100 mM sodium phosphate buffer (pH 8.0). After that, 4 mls of the harvested bleed from rabbit 4443 was incubated with the coupled NHS-

activated beads and tumbled in the cold room for 4 hrs. The beads were pelleted at 2,000 rpm for 2 min and the supernatant was then removed. The beads were placed in a column and three washes with 100 mM Sodium phosphate buffer (pH 8.0) were applied, 15 ml each. The last 3 ml was collected in three fresh eppendorf tubes, 1 ml each. The antibody bound to the column was then eluted by 15 mls of Glycine pH 2.2 and 1 ml fractions were collected. The 15 collected elution fractions were neutralised by adding 100 µl of 1 M Na_2HPO_4. The protein concentration in all the elution fractions along with last collected washes (pre elution) was measured at OD_{280}. The elution fraction that contained the maximum protein concentration was dialysed against 1x PBS and then aliquoted followed by storage at -20ºC.

Chapter 3

Tools Generation

3.1 Introduction:

Upregulation of RaLP in invasive melanoma has been reported to play a role in mediating cell migration by both MAP kinase dependent and independent pathways (Fagiani et al., 2007). The exact molecular mechanism by which RaLP induces migration remains undetermined. Furthermore, RaLP was found to be abundantly expressed in neuronal derived cells and skeletal muscle, which might suggest its role in neuronal development and neuromuscular junction maturation (You et al., 2010; Jones et al., 2007). Despite all this work on RaLP, there is no compelling evidence of how exactly RaLP leads to these suggested biological events.

Structurally, RaLP possesses at its amino-terminal region multiple methionine residues, which might act as alternative initiation codons (Figure 3.1). Different isoforms of RaLP may therefore exist, which may have different cellular functions. ShcA, a member from the same family as RaLP has three well characterised isoforms that provide ShcA with diversity in its function. In order to study the function of RaLP and its cellular distribution, it was necessary to generate appropriate tools. The first aim was to produce a polyclonal antibody that recognises RaLP.

The Shc family members all possess highly conserved PTB and SH2 domains (Figure 3.1) and poorly conserved CH1 and CH2 domains (Figure 3.1). We chose to raise an antibody against the least conserved region on the CH1 domain (amino acids 386 to 468) to minimise the cross-reactivity with the other Shc proteins. In addition the CH1 domain exists in all the possible naturally occurring shorter isoforms of RaLP, whereas the N-terminal CH2 domain is either partially or completely lost in the shorter RaLP translation products.

In order to elucidate the cellular role of RaLP it was decided to generate stable cell lines overexpressing RaLP, so that their properties could be compared to cells expressing low levels of the protein.

3.2 Aims of this chapter:

In this chapter the production, purification and characterisation of a polyclonal antibody recognising RaLP are described. The establishment and characterisation of stable cell lines expressing RaLP are also reported.

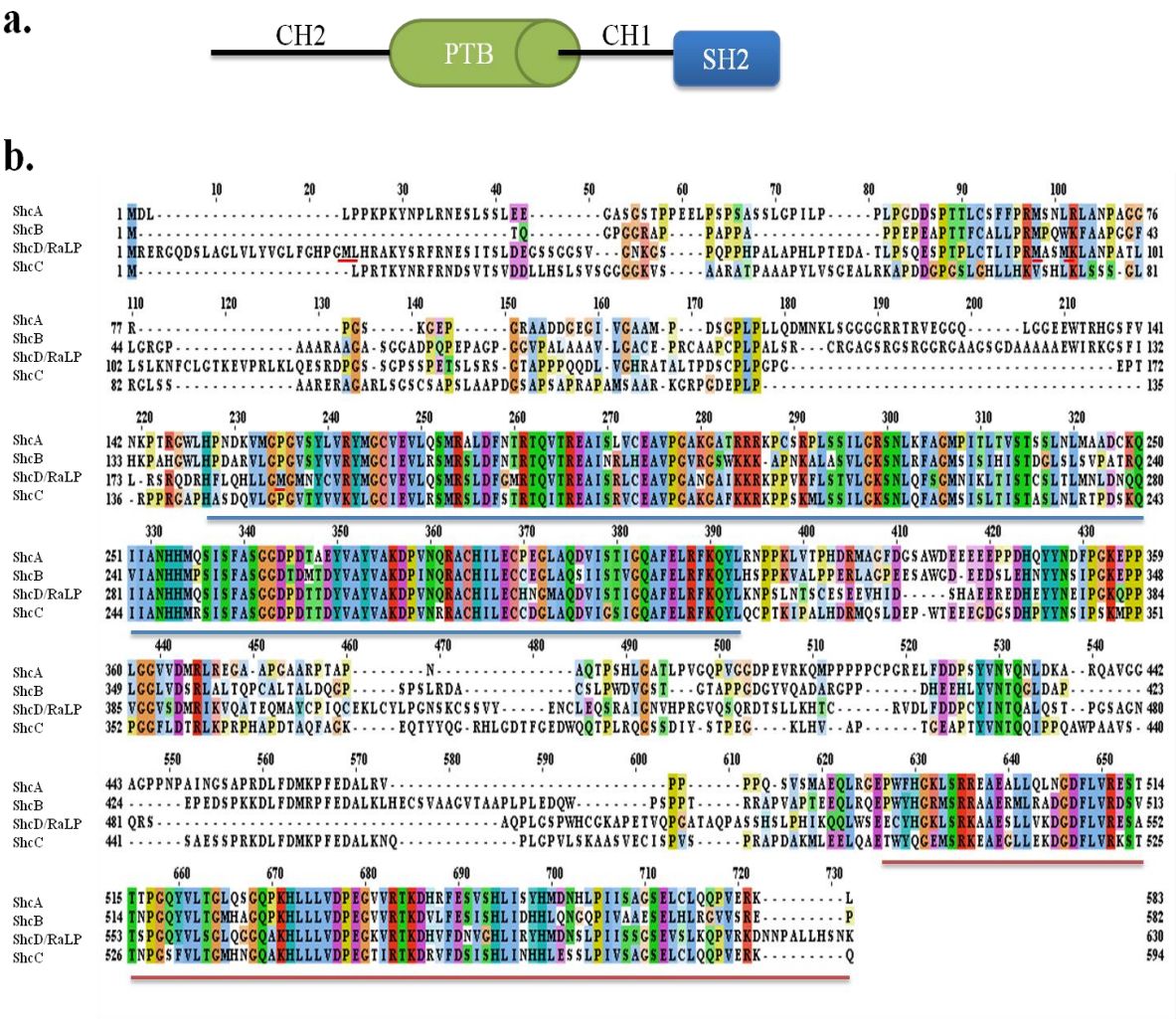

Figure 3.1 Alignment of human RaLP amino acid sequence with those of other Shc proteins. (a) Schematic representation demonstrates different RaLP domains. (b) Alignment of RaLP with the different Shc family members: p66ShcA, ShcB and p67ShcC using T-Coffee multiple alignment programme and Jalview software; 2012. The blue and the red lines are showing the PTB and the SH2 domains, respectively. The highest degree of homology is shown by the SH2 and the PTB domains. Uniprot identifiers for the aligned proteins are as follows, RaLP: Q6S5L8; ShcA: P29353; ShcB: P98077; ShcC: Q92529. CH1: Collagen homology 1 domain; CH2: Collagen homology 2 domain; PTB: Phosphotyrosine binding domain; SH2: Src homology 2 domain.

3.3 Results:

3.3.1 Generating RaLP stably expressing cell line:

One of the ways to characterise a protein is to generate a stable cell line that overexpresses the protein. Thus the generated cell line can be compared with the parental counterparts for any signalling alterations or morphological changes due to the overexpressed protein. HEK 293 cells were transfected with constructs that carry the neomycin resistant gene and encode FLAG-RaLP, GFP-RaLP or FLAG-RaLPΔCH2, which lacks the amino-terminal CH2 domain. The cells that survived in the presence of neomycin (G418) were tested for their expression of FLAG-RaLP, GFP-RaLP or FLAG-RaLPΔCH2 by western blotting (Figure 3.2a, b and c). Further confirmation of FLAG-RaLP and GFP-RaLP expression was achieved by performing immunoprecipitation experiments using anti-FLAG or anti-GFP antibodies (Figure 3.2d and e). Two clones were generated that express FLAG-RaLP (F1and F4), one clone that expresses GFP-RaLP (G5) and two clones that express FLAG-RaLPΔCH2 (CH2/2 and CH2/3). These were used in subsequent experiments.

3.3.2 Antibody production:

3.3.2.1 The expression and the solubility of the HIS-CH1 fragment (HIS-$CH1_f$):

It was important to determine the solubility of the HIS-$CH1_f$ (amino acids 386 to 468), in order to decide the conditions under which the protein needs to be extracted and purified. After the expression of HIS-$CH1_f$ was optimised, it was revealed that 4 hrs of induction by IPTG at 30ºC using BL21/DE3 bacterial strain was optimal for the HIS-$CH1_f$ expression (Figure 3.3a). Bacteria were lysed by sonication followed by addition of non-ionic detergent. The insoluble (Figure 3.3b) and soluble (Figure 3.3c) fractions were separated by centrifuging the bacteria at 14,000 rpm for 10 min. Since the 14 kDa fusion protein was present in the insoluble fraction (Figure 3.3b), its extraction and purification was subsequently performed under denaturing conditions.

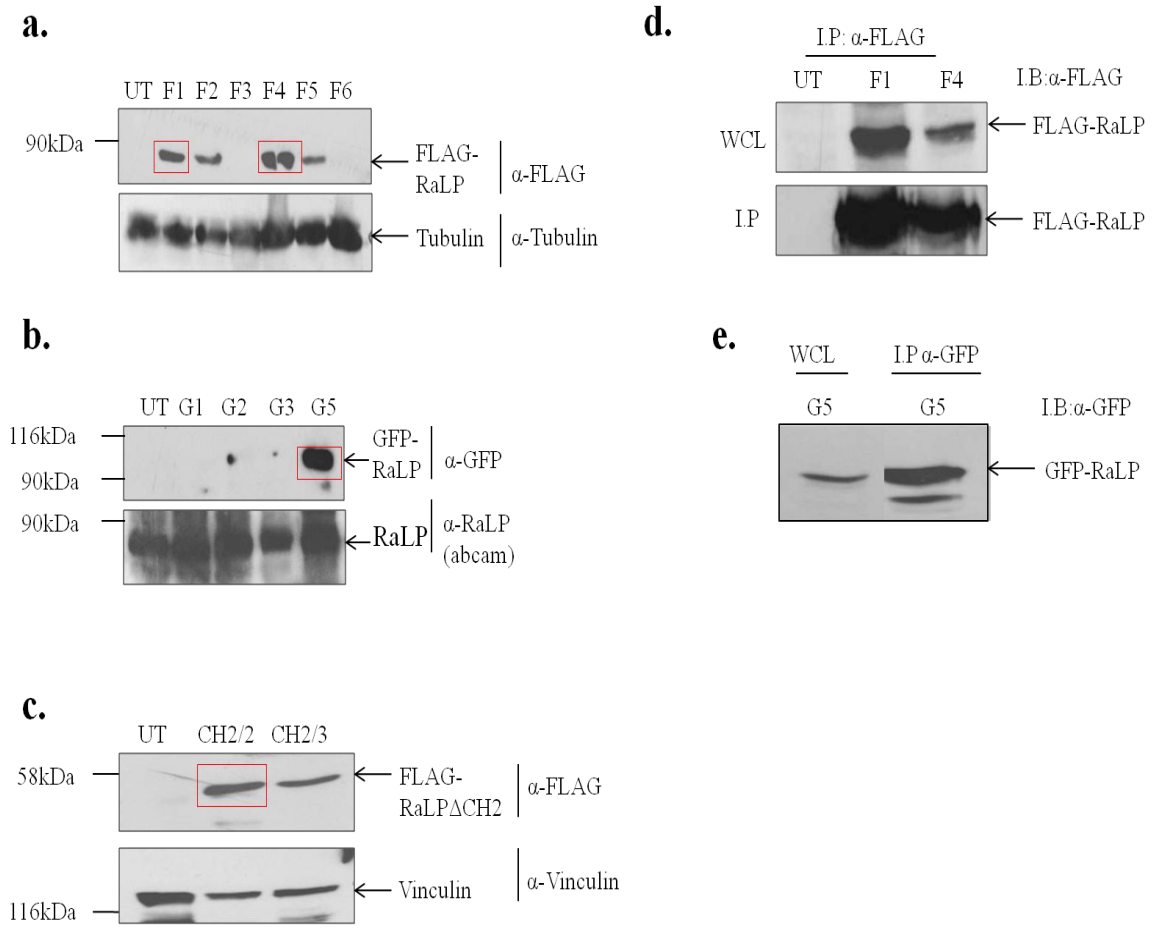

Figure 3.2 Generation of stable cell lines that express RaLP: HEK 293 cells were transfected either with FLAG-RaLP or GFP-RaLP or FLAG-RaLPΔCH2 constructs that carry the neomycin (G418) resistant gene. The transfected cells were then selected by applying G418 at 1 mg/ml. The colonies that survived in G418 were harvested by cloning discs and left to grow until they reached 100% confluence in 6 wells plates in culture medium containing G418. The whole cell lysates were then tested for their exogenous protein expression by western blotting with α-FLAG antibody (a and c) or α-GFP (b). Immunoprecipitation of FLAG-RaLP from F1 and F4 cells (d) or GFP-RaLP from G5 cells (e) was also performed followed by western blotting with α-FLAG (d) or α-GFP (e) antibodies. UT: Untransfected; WCL: Whole cell lysate. The red boxes represent the clones that were employed for further experiments in the subsequent chapters.

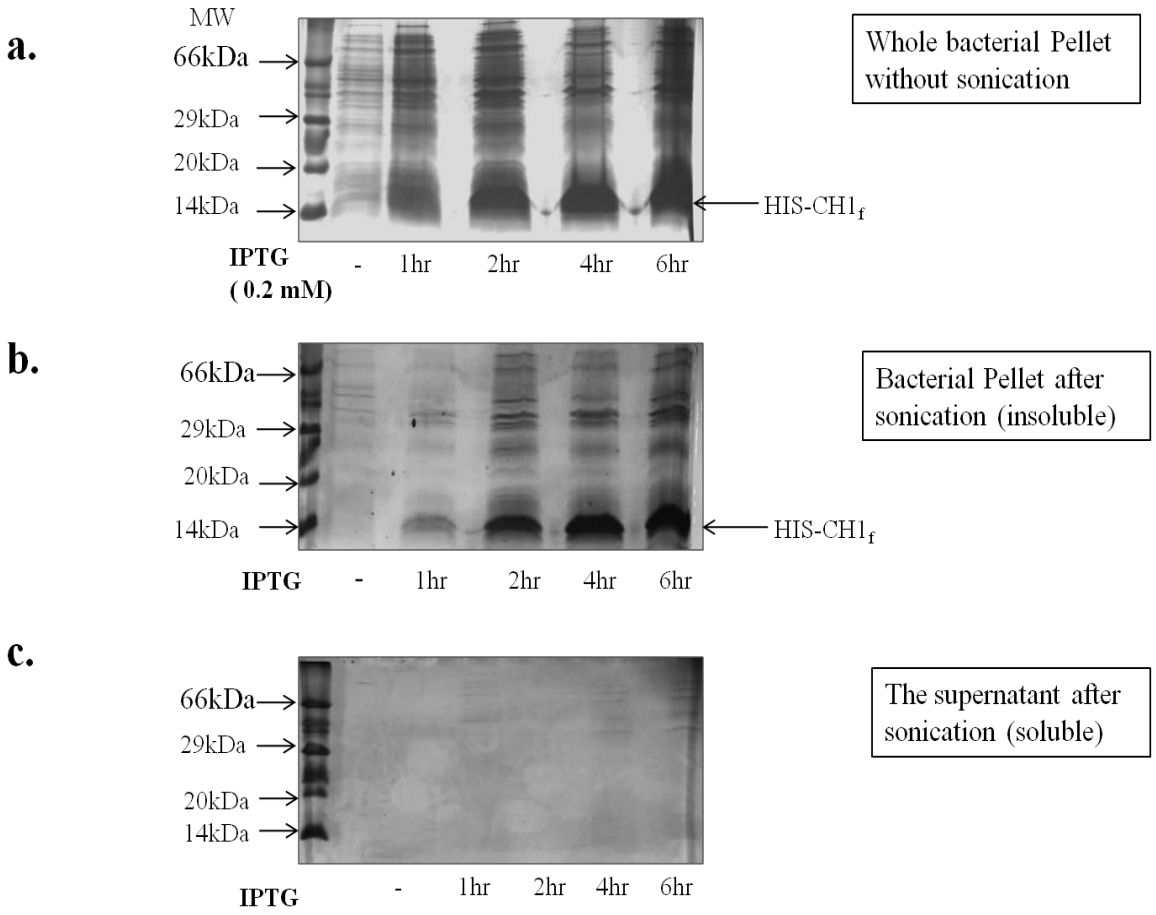

Figure 3.3 Expression of recombinant HIS-CH1$_f$ by BL21/DE3. The HIS-CH1$_f$ construct was transformed into BL21/DE3 bacteria; the expression of HIS-CH1$_f$ protein (~14 kDa) was induced by 0.2 mM IPTG at 30˚C for different subsequent periods. Total bacterial pellets were analysed by SDS-PAGE (a), or pellets were sonicated, centrifuged and insoluble (b) and soluble (c) fractions were analysed.

3.3.2.2 HIS-CH1$_f$ purification by Ni-NTA affinity chromatography:

Since the HIS-CH1$_f$ protein contains a HIS tag, Ni-NTA metal affinity chromatography was used to purify HIS-CH1$_f$. After the fusion protein was expressed in a large scale and extracted from inclusion body using denaturing conditions, the fusion protein was applied to chelating agarose beads coupled to Ni^{2+}. The HIS tagged CH1$_f$ was then eluted by the addition of imidazole that is able to compete with the HIS tag to bind Ni^{2+} and subsequently release HIS-CH1$_f$. The eluted HIS-CH1$_f$ yielded a band of 14 kDa the expected molecular size with little contamination (data not shown). For further purification, the HIS-CH1$_f$ fusion protein was dialysed to remove the imidazole, which was then followed by applying the fusion protein to chelating agarose beads coupled to Ni^{2+}. This time the elution was performed by applying a gradient of imidazole ranged between 10 to 500 mM. Fractions 10-17 were pooled as they contained the highest concentration of the HIS-CH1$_f$ protein (~14 kDa), as well as a lesser degree of contamination was observed in comparison to the first attempt of purification (Figure 3.4). The protein concentration was then estimated by BCA assay using a BSA standard curve. 2 mg of HIS-CH1$_f$ was sent to Cambridge Research Biochemicals where two rabbits were immunised with the denatured fusion protein (HIS-CH1$_f$) and the immunosera, which were at 2 week intervals, were sent to us for testing.

3.2.2.3 Testing immunosera from the two rabbits using western blotting:

The test bleeds from the two rabbits (4442 and 4443) were tested for their immunreactivities against cell lysates obtained from HEK 293 cells stably overexpressing GFP-RaLP (G5 clone) (Figure 3.5a and c) and HEK 293 cells (Figure 3.5b and d) by using western blot analysis. Although, the test bleeds (TB2-TB4) from 4442 rabbit showed immunoreactivity towards a 100 kDa band in the G5 lysates, no band was detected by the pre-immune serum from the same rabbit (Figure 3.5a). This 100 kDa band was confirmed to be GFP-RaLP by reprobing TB2 strip with anti-GFP antibody (Figure 3.5a). The test bleeds from rabbit 4443 (TB1-TB4) demonstrated immunoreactivity against a band of 100 kDa that was proved to be GFP-RaLP by immunoblotting TB2 strip with anti-GFP antibody (Figure 3.5c). Moreover, the test bleeds (TB2-TB4) from rabbit 4443 recognised an intense band at about 70 kDa in G5 lysates (Figure 3.5c) that was not detected by 4442 test bleeds.

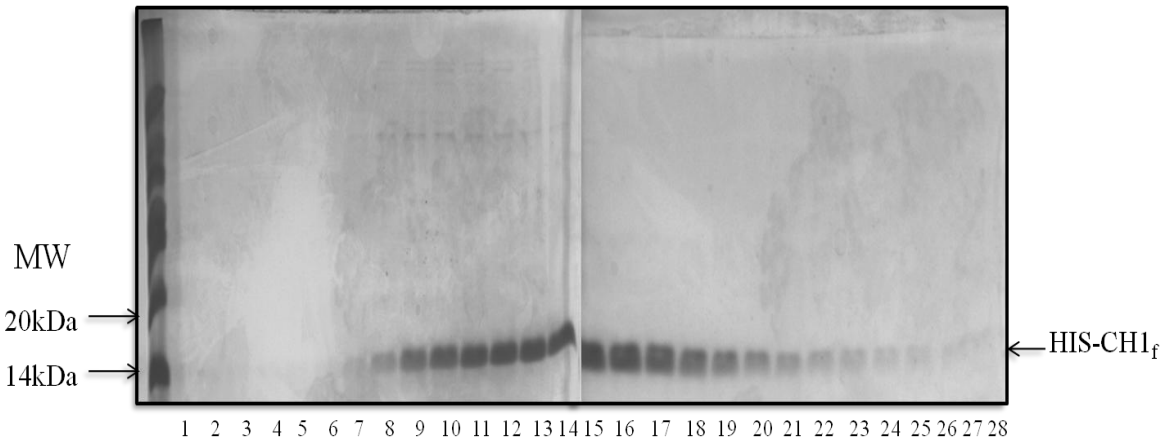

Figure 3.4 HIS-CH1$_f$ fusion protein purification by Ni-NTA affinity chromatography. HIS-CH1$_f$ (386-468 aa) was extracted from BL21/DE3 bacterial cells under denaturing conditions, and applied to a Nickel column. The fusion protein was then eluted by imidazole gradient ranging from 10 mM to 500 mM and 44 fractions were collected, in the figure only 28 fractions are shown, the rest showed no protein bands. 10 µl of each fraction was run on 15% SDS-PAGE gels, which were then stained with coomassie-blue stain. A protein of approximately 14 kDa represents the HIS-CH1$_f$ fusion protein.

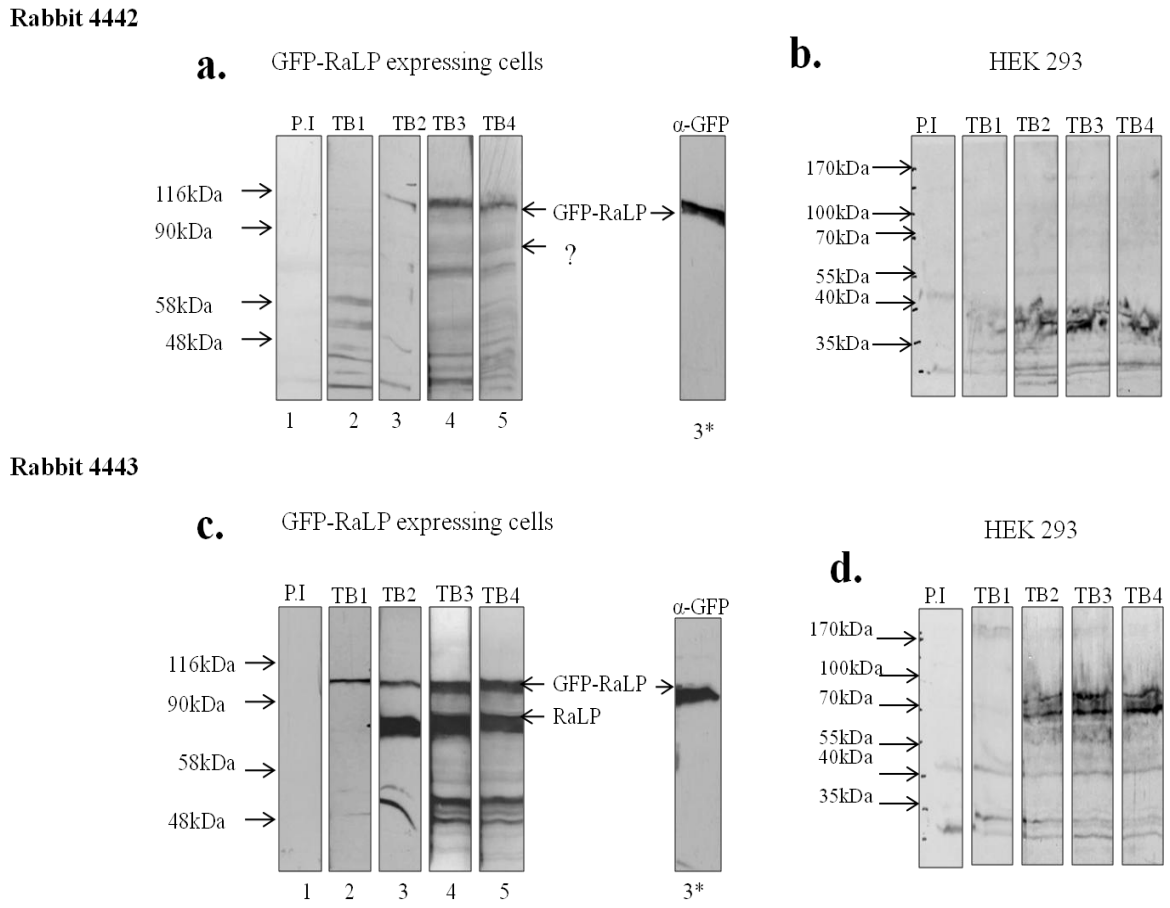

Figure 3.5 Examining the rabbit test bleeds that were raised against the HIS-(RaLP) CH1$_f$ by western blotting. Two rabbits were immunised with the denatured HIS-CH1$_f$ protein (4442, 4443). The pre-immune serum (P.I) along with four subsequent test bleeds (TB1-TB4) were tested against cell extract obtained from HEK 293 cells that stably express GFP-RaLP. It is noteworthy to mention that HEK 293 possibly expresses RaLP endogenously (~70 kDa). The cell extract was resolved on an 8% SDS-PAGE gel, the proteins were then transferred onto nitrocellulose membranes followed by immunoblotting with the four different test bleeds (from each rabbit), using a 1:1000 dilution. The nitrocellulose strip (3) that had been probed with test bleed 2 from each rabbit was stripped and reprobed with anti-GFP antibody (3*).

It appeared later that the intense band at about 70 kDa is actually two bands in untransfected HEK 293 lysates (Figure 3.5d); these bands may correspond to endogenous RaLP protein. The same samples were incubated with pre-immune serum from 4443 rabbit but no reactivity was detected (Figure 3.5d). In conclusion, the test bleeds from rabbit 4443 displayed better immunoreactivities than 4442 test bleeds against the recombinant RaLP and possibly the endogenous RaLP.

3.3.2.4 Rabbit 4443 test bleeds were tested against DAUV extracts:

Since the test bleeds from 4443 rabbit demonstrated better immunoreactivity than the 4442 test bleeds, it was thought to further test 4443 test bleeds against untransfected or GFP-RaLP transfected DAUV cells. The test bleeds but not the pre-immune serum, from the same rabbit, detected two bands of about 70 kDa that are consistent with the expected molecular weight of RaLP (Figure 3.6). Furthermore, the test bleeds detected a band of approximately 100 kDa in the GFP-RaLP expressing cells that was not present in the untransfected cells lysates or in the blot performed with pre-immune serum (Figure 3.6). Therefore, it was concluded that the test bleeds from rabbit 4443 show a specific reactivity towards the recombinant RaLP and possibly they detect the endogenous protein in melanoma cells.

3.3.2.5 Testing the immunosera by immunocytochemistry using DAUV melanoma cells:

The test bleeds from the two rabbits were used to explore the intracellular distribution of RaLP by immunocytochemistry. The 4442 rabbit test bleeds showed a pattern of staining that is similar to the pre-immune serum from the same rabbit (Figure 3.7a). In contrast to 4442 test bleeds, the 4443 test bleeds (TB2-TB4) displayed unique staining that is unlike the pre-immune serum. Anti-RaLP (4443) antibody staining showed the presence of protein in the cytoplasm and the nucleus (Figure 3.7b). In addition we observed a tortuous and branched distribution of RaLP at the perinuclear region which could possibly be the mitochondria (Figure 3.7b). The staining by the Alexafluor 594 coupled secondary antibody did not show any staining, which confirms the specificity of the staining with the test bleeds (Figure 3.7c). In conclusion, the 4443 test bleeds (2-4) showed nuclear and cytoplasmic staining in addition to a unique network staining at the perinuclear region that is different from the pre-immune serum from the same rabbit.

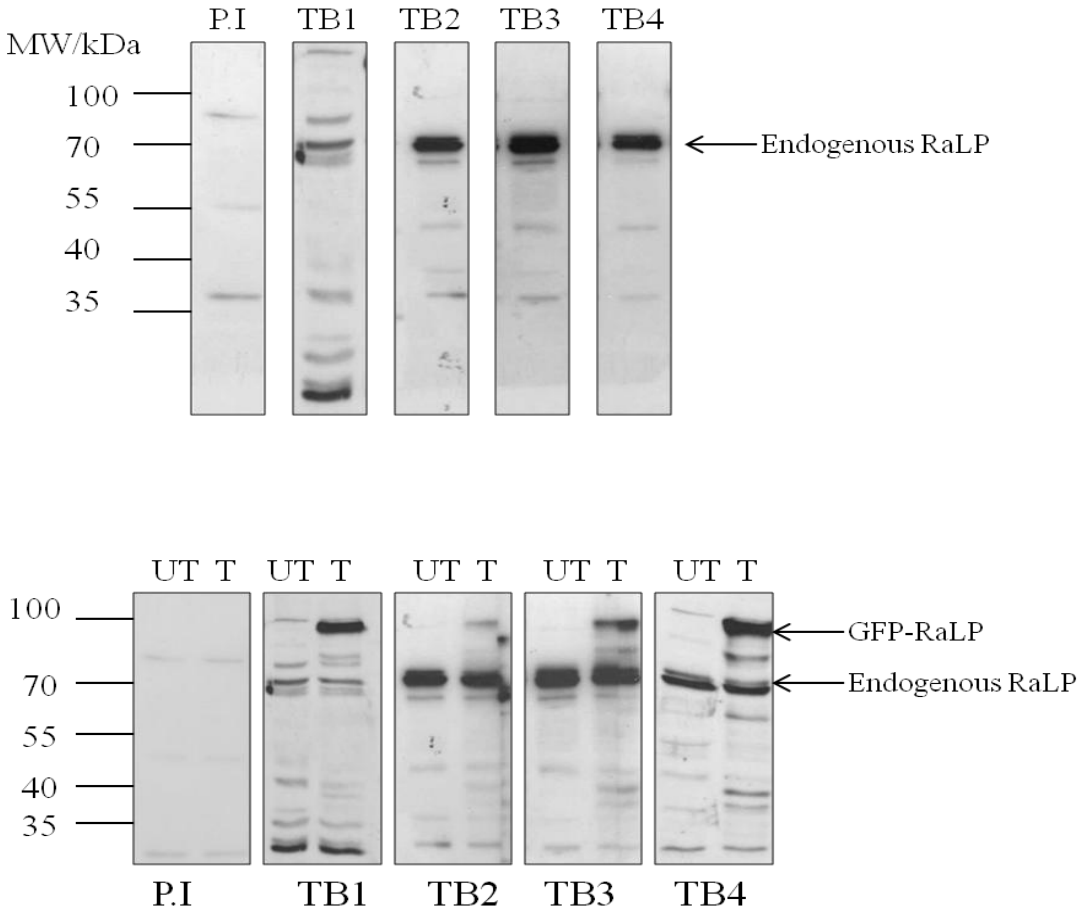

Figure 3.6 Testing the anti-sera against DAUV melanoma cell lysates: DAUV melanoma cells were either untransfected (UT) or transfected (T) with GFP-RaLP. After 24 hrs, the cells were lysed with Triton lysis buffer. The cell lysates were then resolved on an 8% SDS-PAGE gel. After transferring the protein onto a nitocellulose membrane, immunoblotting was performed using the test bleeds, obtained from 4443 rabbit (TB1-TB4) at a dilution 1:1000. In addition, the obtained extracts were tested using the pre-immune serum from the same rabbit (P.I). Top panel represents the untransfected and the bottom panel represents untransfected and transfected DAUV extracts immunoblotted with the different test bleeds along with the pre-immune serum from rabbit 4443.

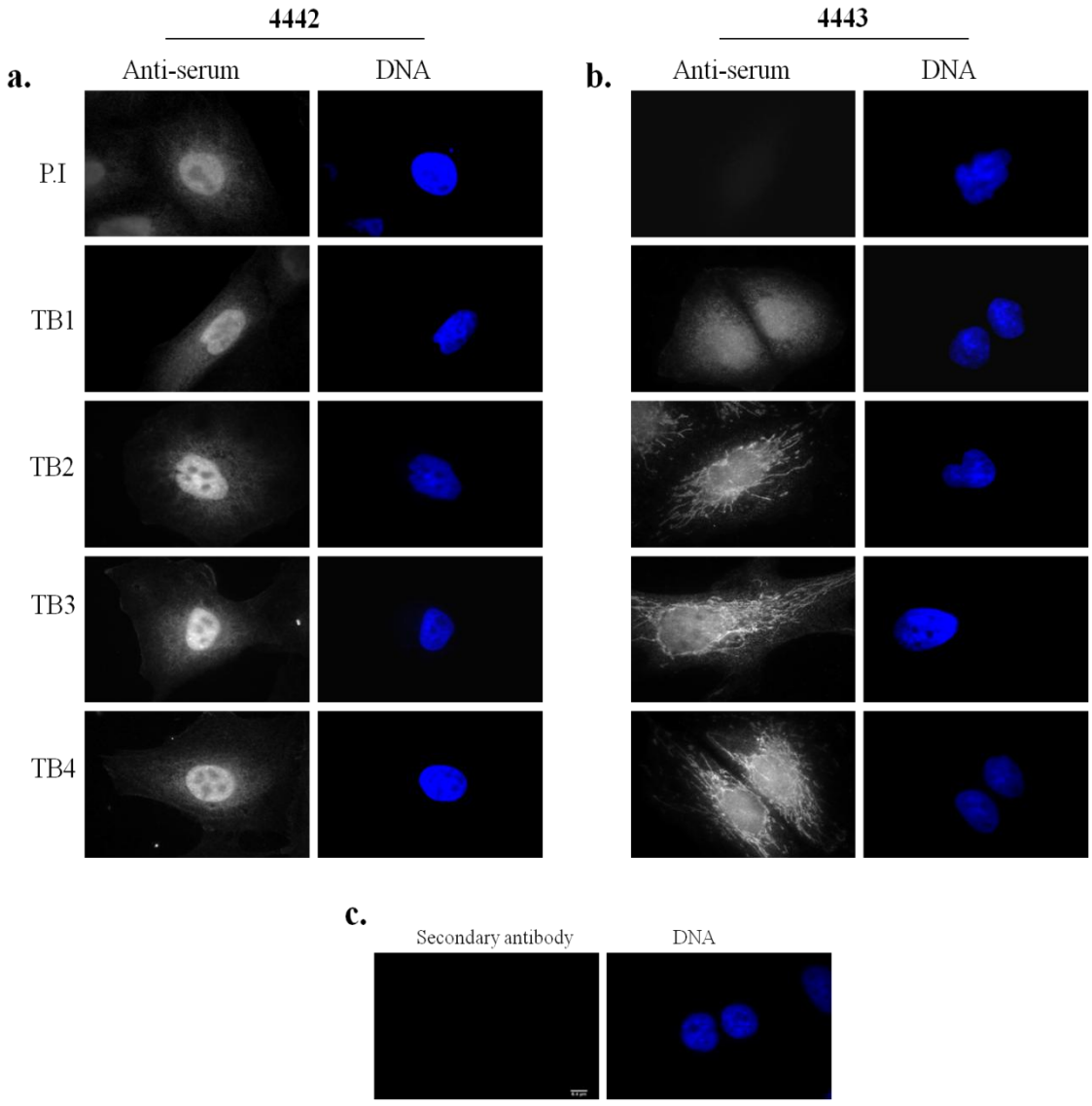

Figure 3.7 The antisera from the two rabbits were tested by immunocytochemistry. DAUV melanoma cells were seeded on coverslips overnight. The cells were then fixed with formaldehyde and permeabilised with 0.1% Triton-x100. Immunostaining was performed using the antisera raised against RaLP, obtained from 4442 (a) and 4443 rabbits (b). All the test bleeds were tested (TB1-TB4) along with the pre-immune serum from the corresponding rabbit at 1:100 dilution. Bound antibody was detected using Alexafluor 594 conjugated secondary antibody. Additionally, a set of cells was only stained with the Alexafluor 594 coupled secondary antibody (c). The coverslips were then mounted and sealed. The cells were visualised using a Nikon fluorescence microscope using 100x 1.4 N.A oil immersion objective. Scale bar 6.4 µm.

3.3.2.6 Antibody purification:

The serum from rabbit 4443 that was immunised with HIS-$CH1_f$ proved to recognise a band consistent to the predicted molecular weight of RaLP and also detected the exogenous protein. Despite this, there were two minor concerns about the produced antibody (1) it proved difficult to knock down the endogenous RaLP and (2) the anti-RaLP antibody was detecting a band in both extracts of pancreatic cancer and human colon cancer cell lines, which were shown by a previous student not to express RaLP at the mRNA level (data not shown). Based on these observations, it was suggested that the anti- HIS antibody present in the anti-serum cross reacts with a protein of the same size as RaLP masking the real band of the latter. As a consequence, it was decided to purify the anti-serum (4443) by generating an affinity chromatography column. This was initially achieved by inducing the expression of GST-CH1 (amino acids 349 to 523) fusion protein in BL21/DE3 bacteria (Figure 3.8a), which was then purified using glutathione sepharose beads (Figure 3.8b). The purified fusion protein was bound covalently to NHS-activated sepharose beads, which were used as an affinity column to purify the antibody (Figure 3.8c). The outcome of eluting the purified antibody from the affinity column by low pH Glycine buffer is shown in Figure 3.9a and b.

3.3.2.7 Testing the antibody (4443) after purification by western blotting and immunocytochemistry:

The purified antibody was tested for its ability to recognise transfected GFP-RaLP and endogenous protein in DAUV extracts by western blotting. Multiple bands at 70, 58 and 40 kDa levels were detected which might represent different splicing variants of RaLP or different translation products (Figure 3.10a). To compare the immunostaining pattern of the purified antibody with the unpurified antibody, the immunocytochemistry was repeated. The same pattern of staining was observed with both purified and non-purified antibody in DAUV cells (Figure 3.10b). It was deduced that the antibody purification was successful since it yielded cleaner blots, although; there is no major difference between the immunostaining observed with antibody 4443 after and before purification.

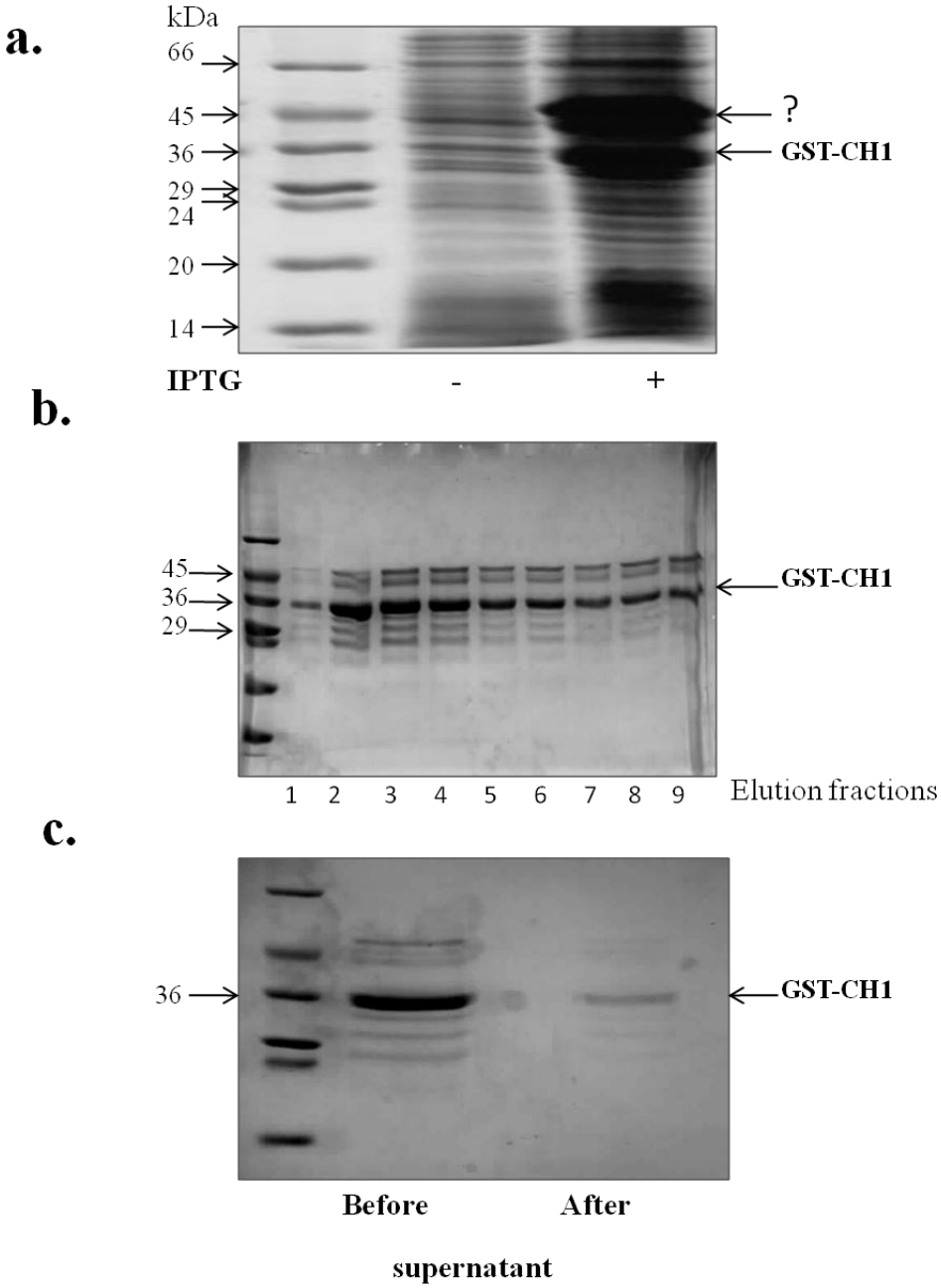

Figure 3.8 Generation of an affinity chromatography column to purify anti-RaLP antibody (4443). (a) GST-CH1 construct was transformed into BL21/DE3 bacteria and the expression of GST-CH1 fusion protein (~36 kDa) was induced by adding 0.2 mM IPTG at 30˚C O/N. (b) GST-CH1 fusion protein was purified using glutathione sepharose beads. The fusion protein was eluted by adding 50 mM reduced glutathione and 10 µl of each eluted fraction was analysed by SDS-PAGE and coomassie staining; only 9 elution fractions are shown. (c) Fractions containing the eluted protein were dialysed and covalently coupled to the NHS-activated beads. The efficiency of the coupling of the fusion protein to the beads was tested by analysing the amount of protein in the supernatant before and after incubation with the NHS-activated beads.

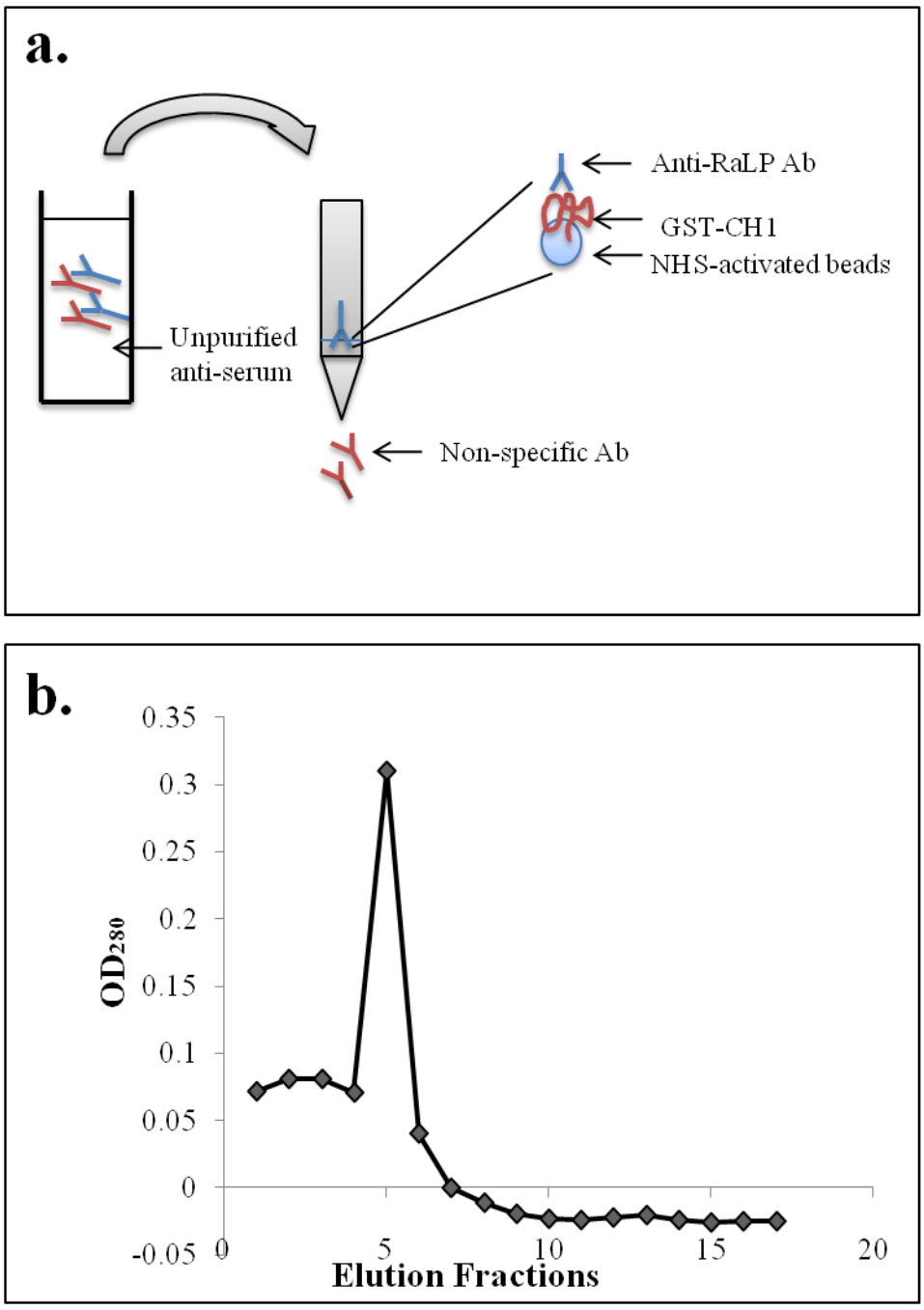

Figure 3.9 The antibody purification by affinity chromatography. (a) 4 ml of the harvested bleed was applied to the NHS-activated beads coupled to GST-CH1, followed by extensive washing. (b) The antibody against the CH1 fragment was eluted with 50 mM Glycine (pH 2.2) and the protein concentration in the elution fractions was measured at OD_{280}. The first two readings demonstrate the washes before the elution buffer was applied. Fraction five was retained for further analysis.

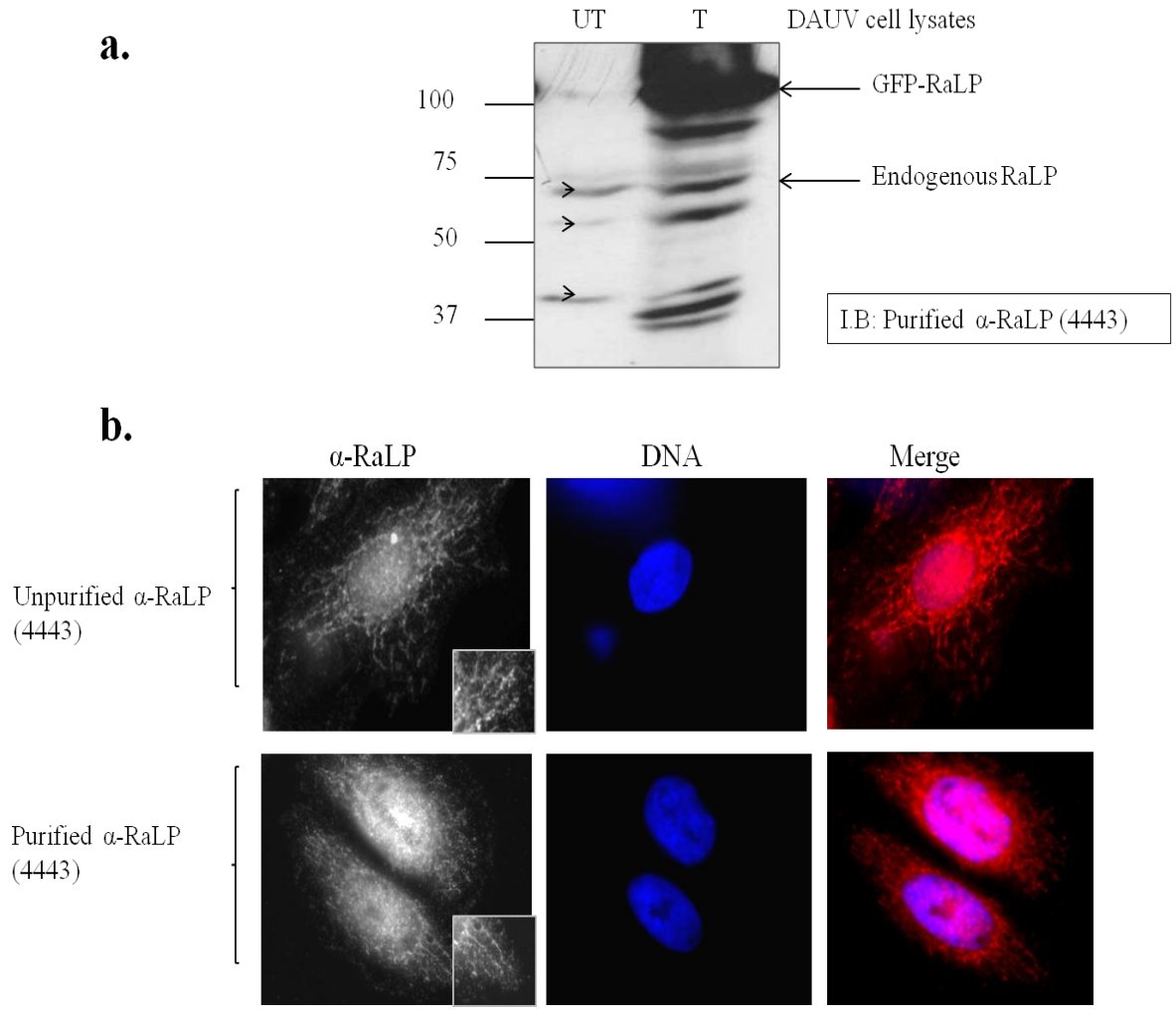

Figure 3.10 Testing the antibody after its purification. (a) HEK 293 cells were either untransfected (UT) or transfected (T) with GFP-RaLP and the cells were then lysed. The extracts were resolved on an 8% SDS-PAGE gel followed by immunoblotting with purified anti-RaLP antibody (4443). The arrows indicate the possible RaLP forms. (b) DAUV Melanoma cells were seeded on cover slips and the cells were then fixed with 3.7% formaldehyde. The immunostaining was performed with anti-RaLP antibody (1:100 before purification and 1:50 after purification). The cells were visualised using a Nikon fluorescence microscope and 100x 1.4 N.A oil immersion oil objectives.

3.3.2.8 Validation the specificity of the produced antibody (4443):

To confirm the specificity of the produced antibody, the endogenous RaLP was knocked down using small interference RNA (siRNA). The oligonucleotide sequence was published by Fagiani et al., 2007 previously. In RaLP siRNA transfected DAUV and HEK 293 cells, two bands at around 70 kDa showed a significant knock down (Figure 3. 11a and b), while in DAUV cell lysates a band just below 48 kDa displayed a slight knock down as well (Figure 3.11b) when the cells were transfected with RaLP siRNA.
These data indicated that RaLP was knocked down by siRNA in DAUV melanoma cells and HEK 293 cells (Figure 3.11c and d). From these data, it was inferred that the generated antibody showed specificity towards the endogenous RaLP.
Additionally, in order to verify the validity of our antibody, semi-quantitative RT-PCR was repeated to test whether RaLP does exist in pancreatic cancer and human cancer cell lines at the mRNA level. To achieve this semi-quantitative RT-PCR was carried out using primers that were generated to span the intron-exon borders therefore would give a different sized product if contaminating genomic DNA was present (Figure 3.12). In contrary to what has been observed previously, both pancreatic cancer (BxPC-3) and colon cancer (HCT-116) cell lines expressed RaLP mRNA, which indicated that the produced antibody recognises a band that might represent endogenous RaLP in these cell lines.

3.3.2.9 Immunoprecipitation of RaLP with polyclonal antibody 4443:

The ability of the generated antibody to pull down the native protein was tested by performing immunoprecipitation. DAUV cells were lysed under mild conditions using a non-ioninic detergent, the cell lysates were clarified then either incubated with α-RaLP (4443) or α-RaLP (abcam) that was raised against the full length protein. Immunoblotting with α-RaLP (4443) detected a band at about 70 kDa in immunoprecipitates performed with both antibodies (Figure 3.13a). This provides clear evidence that the two antibodies are able to recognise the native protein, which can be detected by α-RaLP (4443) on western blotting. On the other hand, the antibody from abcam was able to immunoprecipitate an additional protein of 90 kDa in addition to the 70 kDa band corresponding to RaLP (Figure 3.13a).

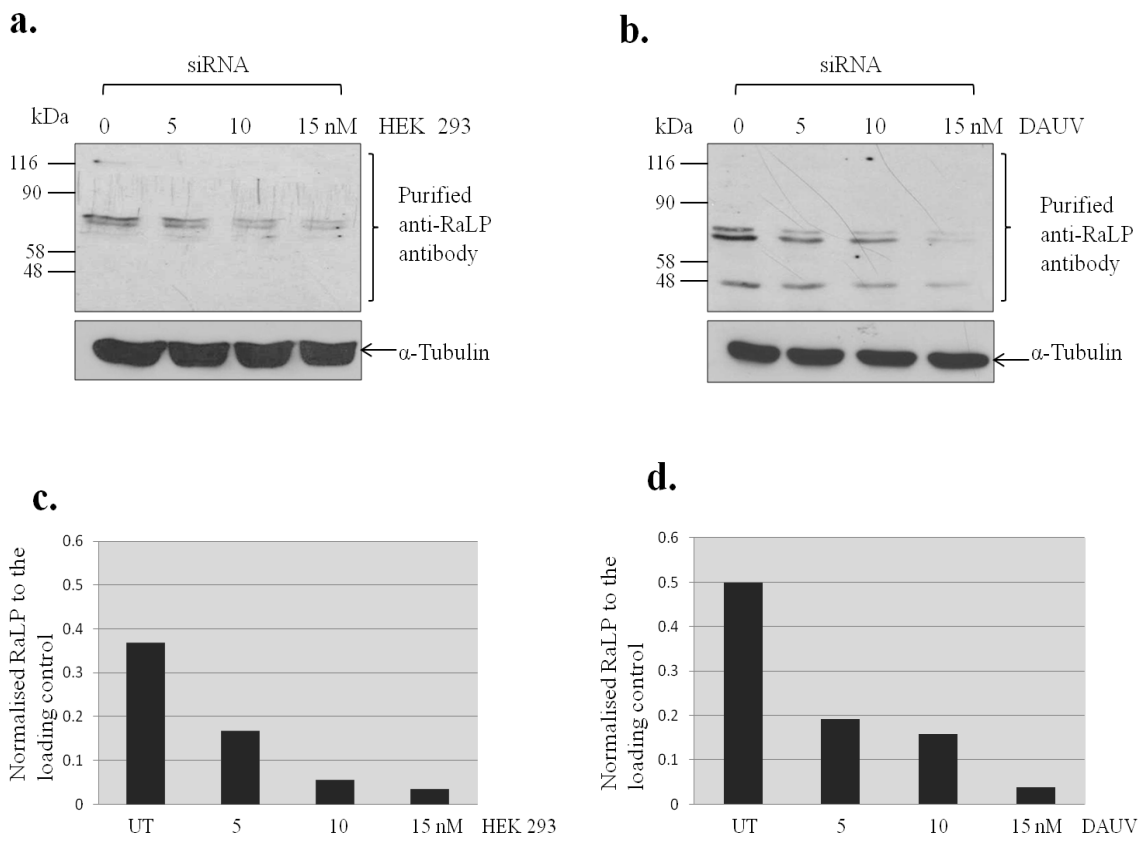

Figure 3.11 Verifying anti-RaLP (4443) antibody specificity by siRNA knockdown. (a) HEK 293 and (b) DAUV melanoma cell lines were transfected with RaLP siRNA for 72 hr using Turbofect transfection reagent at different concentrations (5, 10 and 15 nM) and immunoblotting was then performed with α-RaLP (4443). Expression levels of RaLP were normalised to α-Tubulin and the results presented graphically (c and d).

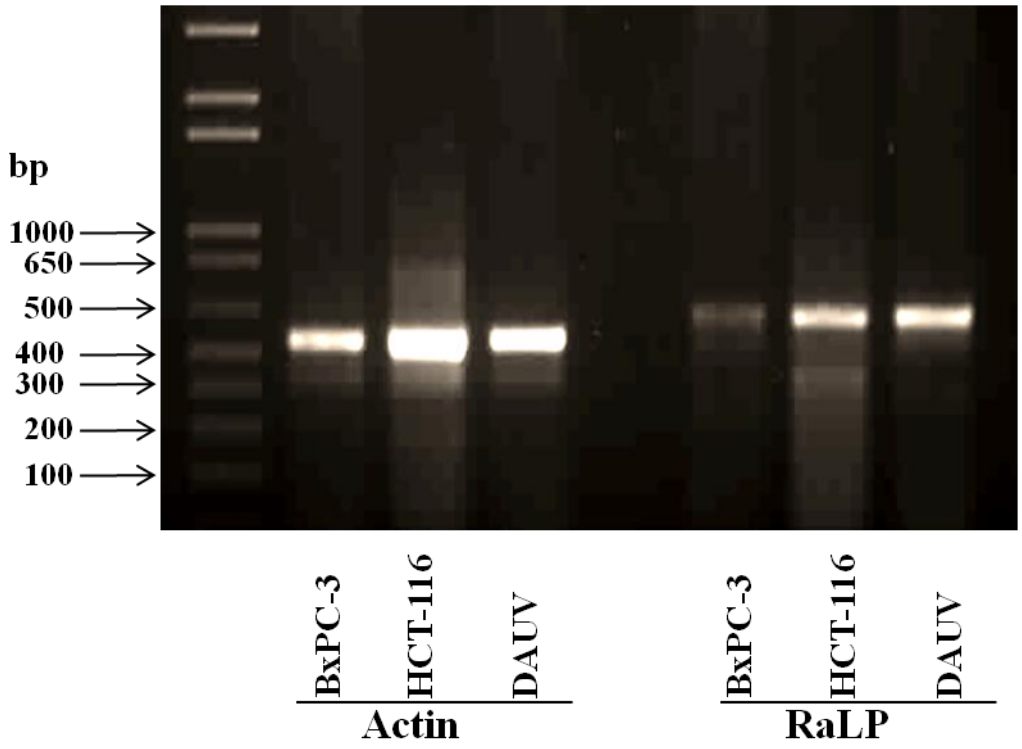

Figure 3.12 Expression of RaLP in pancreatic cancer, colon cancer and melanoma cell lines at mRNA level. Semi-quantitative RT-PCR was carried out by isolating the total RNA from pancreatic cancer (BXPC-3), human colon cancer (HCT-116) and DAUV melanoma cell lines. The RNA was converted to cDNA by using RevertAid™ H Minus First Strand cDNA Synthesis Kit. The cDNA was then amplified by performing a PCR reaction using either actin primers (control) or RaLP primers.

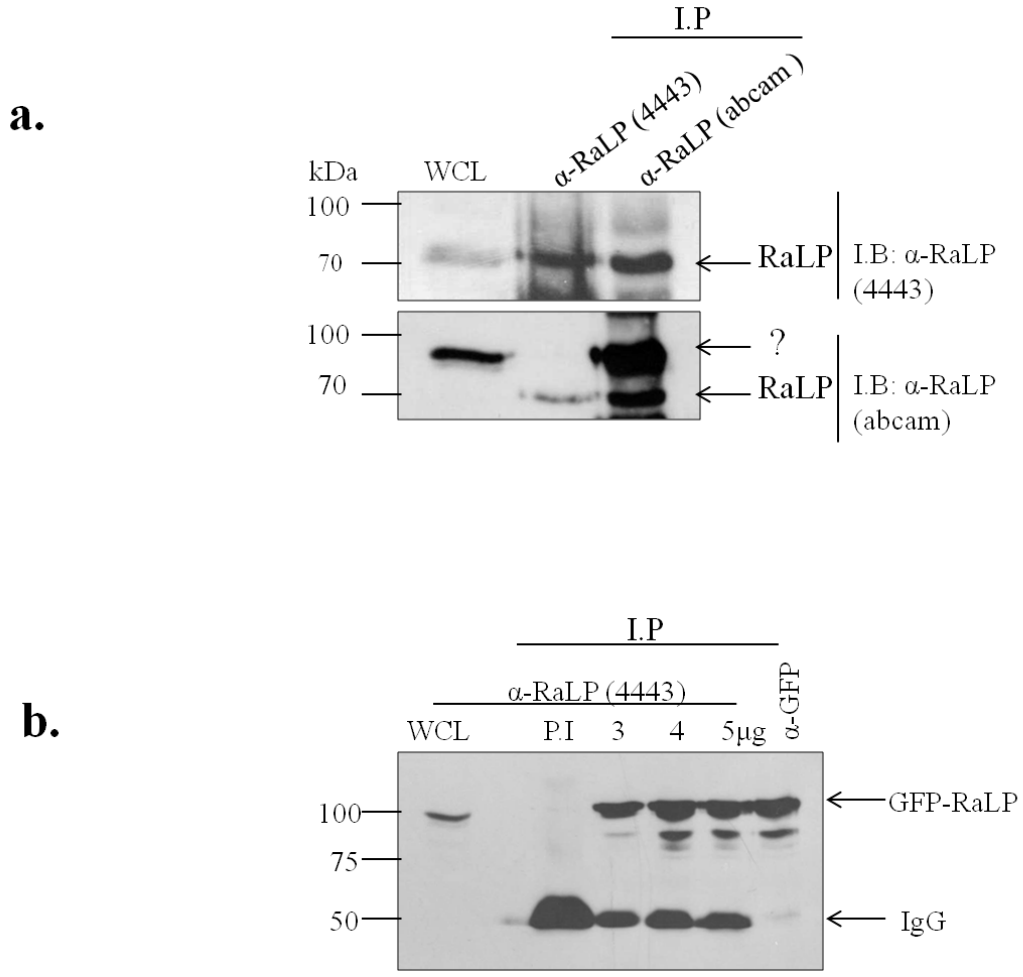

Figure 3.13 Anti-RaLP (4443) antibody recognises the native RaLP using immunoprecipitation. (a) DAUV melanoma cells were lysed and the cells lysate was incubated with immobilised anti-RaLP (4443) or anti-RaLP (abcam) overnight. The unbound protein was washed away and the bound proteins were denatured by SDS sample buffer and were then resolved on a 6% SDS-PAGE gel. Immunoblotting was performed with either α-RaLP (4443) (top) or the abcam commercial α-RaLP (bottom). (b) GFP-RaLP was immunoprecipitated from G5 extract using either preimmune serum 4443 (P.I), different concentrations of the purified anti-RaLP (4443) or anti-GFP antibodies and immunoblotting was performed using anti-RaLP antibody (4443) (1:1000). WCL: whole cells lysate.

The immunoblotting with α-RaLP (abcam) revealed a 70 kDa band in the immunoprecipitates performed with both antibodies, and a 90 kDa band in the whole cell lysate (WCL) and in abcam antibody immunoprecipitates but not in α-RaLP (4443) immunoprecipitate (Figure 3.13a). From this experiment, it was concluded that α-RaLP (4443) immunoprecipitates a protein of about 70 kDa, which is consistent with the expected molecular weight of RaLP. Regarding α-RaLP (abcam), it immunoprecipitated a band corresponding to RaLP's molecular size, and a higher band of 90 kDa, which could either be a form of RaLP with post-translational modification, or it is a cross reactivity towards another protein. The fact that this band was not recognised by 4443 suggests that it may be another protein.

Another immunoprecipitation experiment was conducted to test whether α-RaLP (4443) is able to immunoprecipitate the recombinant RaLP. Different amounts of the purified antibody (3, 4 and 5 µg) were used to immunoprecipitate GFP-RaLP from GFP-RaLP expressing cells (G5) lysates and precipitated protein was identified with anti-RaLP antibody 4443 (Figure 3.13b). The antibody successfully precipitated a band of 100 kDa, which was proved to be GFP-RaLP since the anti-GFP antibody precipitated the same sized band (Figure 3.13b). The pre immune-serum failed to pull down the same band (Figure 3.13b), which confirmed the specificity of α-RaLP antibody (4443).

3.3.2.10 RaLP expression is not restricted to melanoma cells:

RaLP was reported to have limited expression patterns in living tissues, therefore; we were interested to explore RaLP expression in different cell lines using our purified antibody (Figure 3.14). Our data showed that RaLP is broadly expressed in human colon cancer (HCT-116), neuroblastoma (N1E-115), human embryonic kidney cells (HEK 293) and at lower levels in pancreatic cancer (BXPC-3) in addition to melanoma cells (518, DAUV and A375P) (Figure 3.14). According to these findings, RaLP expression was revealed not to be restricted to melanoma and neuronal cells, but is also found in human colon cancer cells and at low levels in the human pancreatic cancer cells.

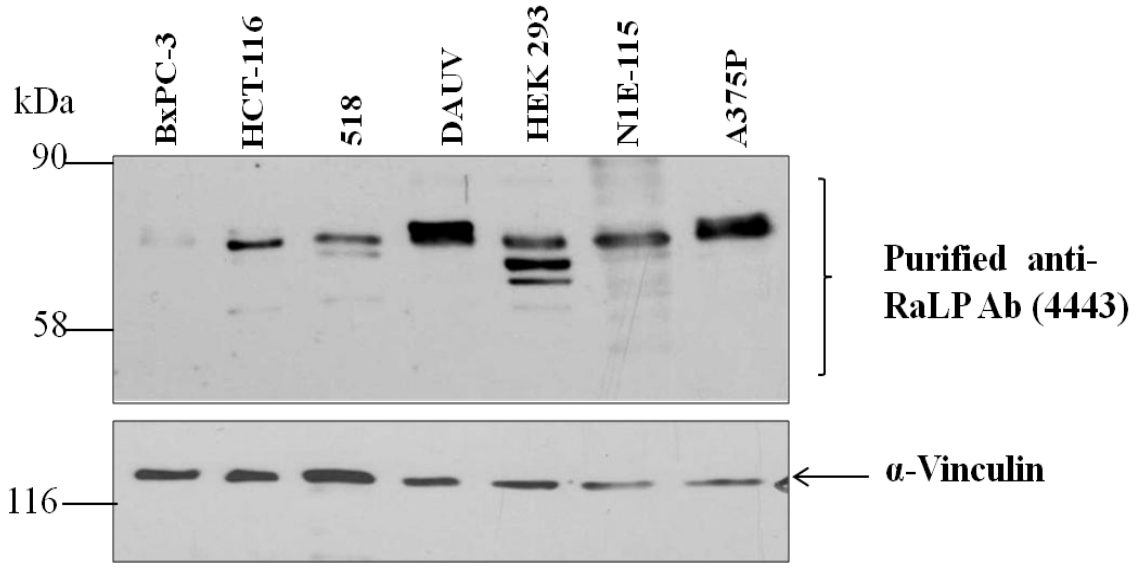

Figure 3.14 Western blotting to test RaLP protein expression in various cell lines using different anti-RaLP antibodies. Cell extracts were obtained from different cell lines; pancreatic cancer (BXPC-3), human colon cancer (HCT-116), 518 and DAUV metastatic melanomas (primary cell lines), human embryonic kidney cells (HEK 293), mouse neuroblastoma (N1E-115) cells and commercially available non-metastatic melanoma cells (A375P). The extracts were resolved on a 6% SDS-PAGE gel, followed by immunoblotting, which was performed using the purified anti-RaLP (4443) or anti-Vinculin antibodies, all at 1:1000 dilution.

3.3.2.11 RaLP is present in the mitochondria:

As has been shown previously the immunostaining with α-RaLP (4443) showed a unique network of staining at the perinuclear region, that looked like mitochondrial staining.

To determine whether RaLP localises with the mitochondria, cells were simultaneously stained with Red-mitotracker which stains the mitochondria. An apparent overlap between RaLP and the mitochondria was observed in DAUV melanoma cells (Figure 3.15) and in 518 melanoma cells (Figure 3.16). Neither the Alexafluor 488 nor the preimmune serum staining demonstrated colocalisation with mitochondria in 518 cells (Figure 3.16). To study this phenomenon further, mitochondria were fractionated from 518 melanoma cells, and mitochondrial and cytoplasmic fractions analysed by western blotting. The purity of the mitochondrial fraction was confirmed by western blotting with an anti-ATP50 antibody and blotting with anti-Vinculin antibody was used to confirm the lack of cytoplasmic contamination of the mitochondrial fraction. Immunoblotting with α-RaLP (4443) showed 34% of cytoplasmic RaLP exists in the mitochondria (Figure 3.17a). It was crucial for us to determine whether the exogenous protein behaved similarly. Therefore, mitochondria were fractionated from the cytosol of HEK 293 cells stably expressing FLAG-RaLP. Immunoblotting analysis with anti-FLAG antibody confirmed the existence of FLAG-RaLP in the mitochondrial fraction (Figure 3.17b).

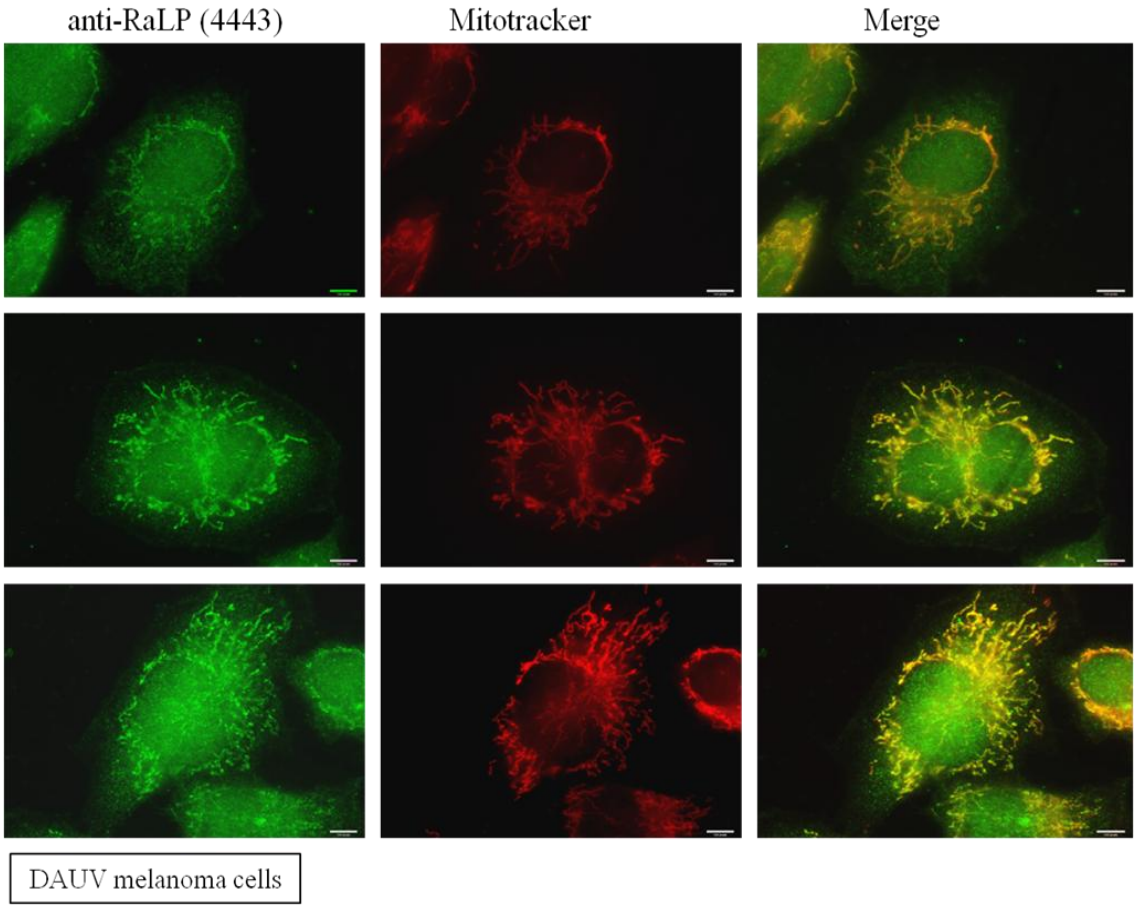

Figure 3.15 Expression of RaLP in mitochondria in DAUV melanoma cells. DAUV cells that were grown on coverslips overnight, then stained with MitoTracker (Invitrogen) followed by formaldehyde fixation at 37˚C for 15 min. The cells were then stained for endogenous RaLP by using anti-RaLP antibody (4443) and Alexa fluor 488 coupled goat anti-rabbit antibody. The cells were visualised by Nikon fluorescence microscopy, using 100x 1.4 oil immersion objective and the merged image was created by Openlab software. Scale bar 6.4 μm.

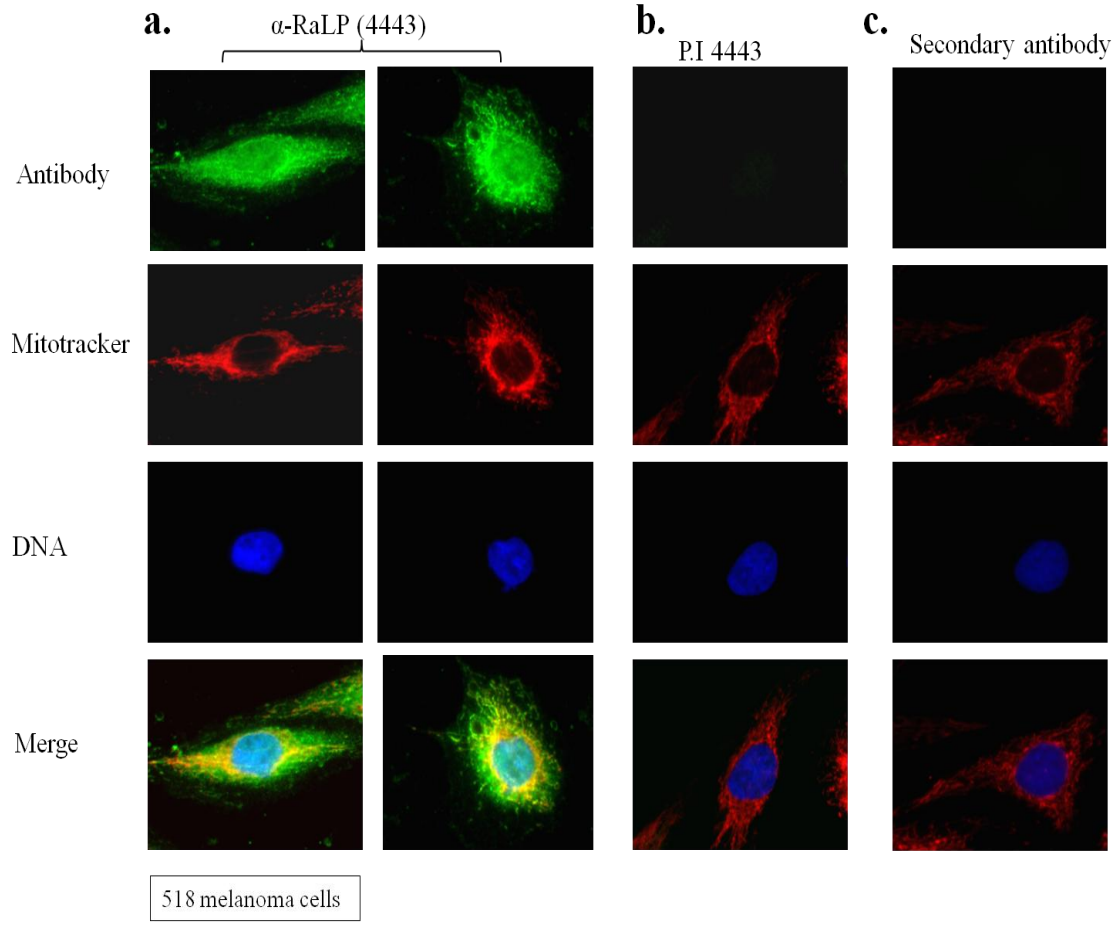

Figure 3.16 Localisation of RaLP in mitochondria of 518 melanoma cells. 518 melanoma cells were grown on coverslips overnight, then stained with MitoTracker (Red) followed by formaldehyde fixation at 37˚C for 15 min. The cells were then stained for endogenous RaLP by using anti-RaLP antibody (4443) (a) or pre-immune serum (P.I) 4443 (b), followed by detection with Alexa fluor 488 conjugated goat anti-rabbit secondary antibody (green). (c) A subset of cells was only stained with secondary antibody. The nuclei were stained using Hoechst 33342 at 1 µg/ml final concentration (blue). The cells were then visualised using a Nikon fluorescence microscope, using 100x 1.4 N.A oil immersion objective. The image acquisition was perfomed by Volocity software, while the merged image was created by ImageJ software.

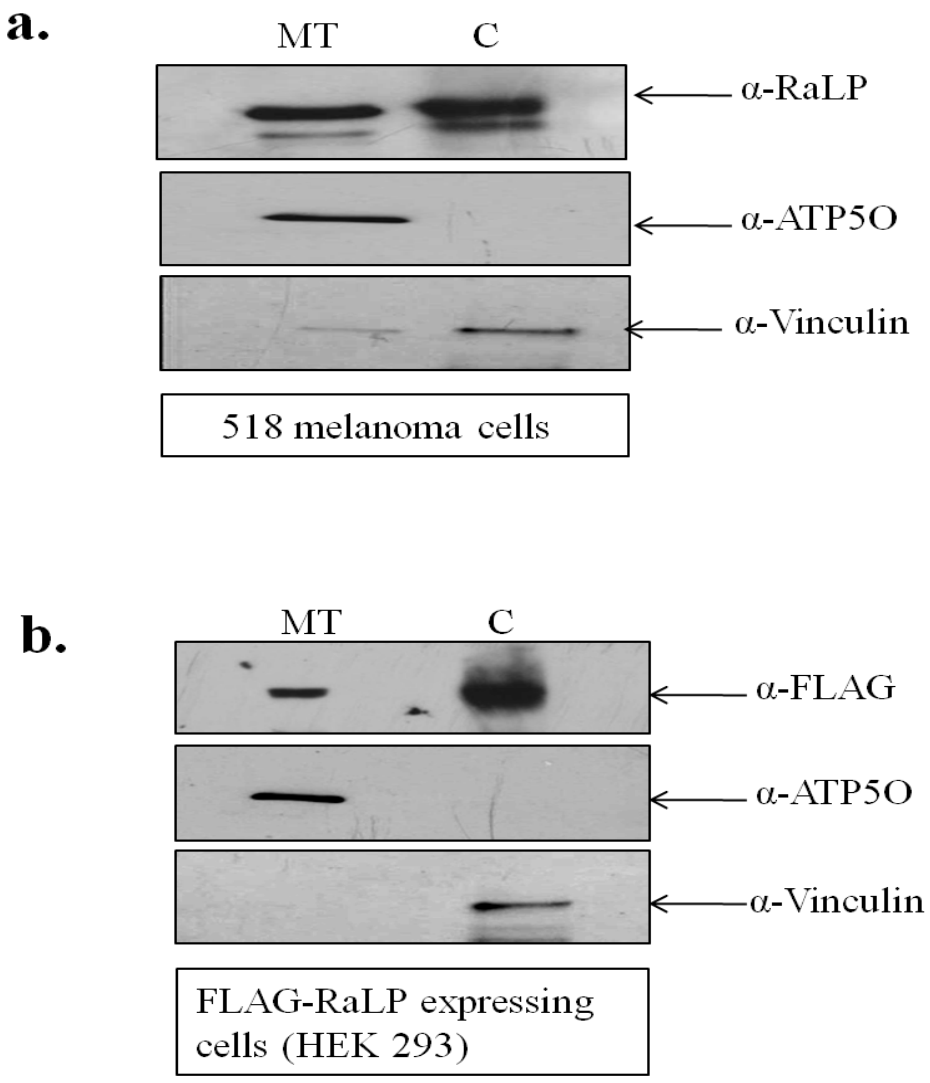

Figure 3.17 RaLP is present in mitochondrial fractions of 518 and FLAG-RaLP expressing cells. The cells obtained from a 10 cm culture plate were pelleted and then treated with MT buffer (methods chapter). The cells were then broken mechanically using a Dounce homoginizer. After separating the nuclei and the cell debris with a low speed spin, the mitochondria were isolated by spinning the cytoplasm at 8,000 x g for 10 min at 4ºC. The mitochondrial pellet was dissolved in SDS-PAGE sample buffer and resolved on an 8 % SDS-PAGE gel along with the cytoplasmic fraction. The purity of the mitochodrial fraction was confirmed by immunoblotting with an antibody against the mitochondrial marker (ATP50) antibody, and the purity of the cytoplasmic fraction was verified using an anti-Vinculin antibody. Endogenous RaLP was detected by anti-RaLP (4443) in the case of 518 melanoma cells (a), while FLAG-RaLP was detected by anti-FLAG in the case of FLAG-RaLP expressing cells (b).

3.4 Discussion:

From the presented data in this chapter, we were able to generate stable cell lines that overexpress RaLP, which in turn provided a tool for RaLP characterisation. Additionally, an anti-RaLP polyclonal antibody was raised against a RaLP-CH1 domain fragment, the least conserved region among Shc proteins. The anti-serum from rabbit 4443 proved to exhibit a specific immunoreactivity against the recombinant RaLP as well as detecting two bands of ~ 70 kD that corresponds to the molecular size for RaLP as described by Fagiani and Jones, in tranfected HEK 293 and different melanoma cell lines. The two bands that were detected by the produced antibody were knocked down by RaLP siRNA designed by Fagiani and co-workers (Fagiani et al., 2007). This has further confirmed the specificity of the antibody (4443) against the endogenous protein. More knock down experiments are needed, including control siRNA, to ascertain the specificity of the RaLP siRNA knock down. The purified antibody showed more or less the same pattern of bands on western blotting as the unpurified rabbit serum, although the bands were sharper with the purified antibody. The purified serum 4443 also produced a similar pattern of staining in immunocytochemistry as the unperified serum. The antibody was able to recognise the native protein, which might represent an advantage for this antibody in testing interacting partners for RaLP.

In comparison between the produced antibody (4443) and anti-RaLP antibody from abcam, the 4443 detects a band consistent with the reported molecular weight of RaLP, while the abcam antibody showed an additional stronger band of higher molecular weight. The 4443 antibody was raised against a fragment of RaLP-CH1, whereas abcam antibody was raised against the full length RaLP protein. Thus, each antibody might recognise different epitopes on RaLP. These data might indicate two possibilities, either the abcam antibody recognises a form of RaLP that is post-translationally modified or it detects a non specific band. In summary, the generated antibody 4443 represents a good tool to investigate the exact biological role of RaLP in the intracellular compartment.

ShcA is the most studied Shc protein; it has three isoforms that provide it with multiplicity in its function (Kisielow et al., 2002). Interestingly, the presence of more than one band on western blotting and the observed pattern of staining by the generated

antibody supported the possibility of naturally occurring isoforms of RaLP. Each RaLP isoform might have a preference for distribution in a distinct intracellular compartment thus contributing to functional divergence. To investigate this further, the presence of alternative splicing variants could be explored at the mRNA level by designing special primers that detect the different predicted RNA products of the RaLP gene. Alternatively, as more commercial antibodies become available we should look in a number of cell lines to see which bands are consistently present, and subsequent knock down with siRNA may help to identify the alternative splicing products of RaLP.

According to our data, RaLP demonstrated a broader expression among different cell lines than it was reported previously by Fagiani and Jones. RaLP has also been found to be expressed in melanoma cells and neuronal cells, which is consistent with previous reports. In disagreement with other researchers, RaLP showed existence in human colon cancer cell line (HCT-116), human embryonic kidney cells (HEK 293) and a low expression was observed in pancreatic cancer cell line (BxPC-3). Intriguingly, RaLP has appeared to have different forms in the examined cell lines, which might indicate the occurrence of post-translational modification or a presence of different splicing variants to RaLP or alternative translation products.

Moreover, the anti-RaLP antibody shows an interesting mitochondrial staining that is consistent with ShcA distribution. This may possibly be due to the presence of the conserved sequence GCVEVLQSM in RaLP-PTB domain, which has been reported to be responsible for the mitochondrial translocation of p46ShcA that is absent in ShcB and C (Ventura et al., 2004). p66Shc, an isoform of ShcA, was found to reside in the mitochondria to execute its function in reactive-oxygen-species (ROS) metabolism via its association with cytochrome c (Giorgio et al., 2005). Adding to that, p66ShcA also potentiates the mitochondrial-apoptotic pathway following its dissociation from an inhibitory protein complex, including HSP70 (Orsini et al., 2004). Although this presents clear evidence that mitochondrial localisation is not a novel observation for Shc proteins, the need to knock down the endogenous protein to confirm the specificity of the anti-RaLP staining still remains.

In summary, tools were successfully generated to assist the characterisation of the recently identified protein, RaLP. The possibility of RaLP naturally occurring isoforms was supported to an extent by the multiple bands observed on western blotting by the generated antibody. Although, for the first time our data presented compelling evidence of RaLP localisation to the mitochondria, the role of RaLP in the mitochondria needs to be investigated further.

Chapter 4

RaLP in the Nucleus

4.1 Introduction:

RaLP has the same structural features as the other Shc proteins (CH2-PTB-CH1-SH2), however; it possesses an extreme amino terminal CH2 domain that might contribute to novel functions of RaLP, since it is the least conserved domain among Shc proteins. RaLP is a downstream substrate of different receptor tyrosine kinases e.g. EGFR, IGFR (Fagiani et al., 2007) and unlike other Shc proteins, RaLP binds MUSK (Jones et al., 2007). In addition a role in neuronal development and differentiation has been proposed (You et al., 2010). RaLP like other Shc adaptors resides mainly in the cytoplasm to propagate signal from the upstream receptors to the intracellular compartment.

The response of cells to different growth stimuli and different stresses can influence the intracellular redistribution of Shc proteins and other proteins. p52ShcA and p46ShcA, ShcA isoforms, are mainly distributed in the cytoplasm, however; upon their phosphorylation they can translocate to the membrane where they transduce extracellular signals to the intracellular environment (Sato et al., 2000). Since p66ShcA plays a role in reactive oxygen species metabolism its mitochondrial translocation has been analysed (Nemoto et al., 2006). Interestingly, nuclear localisation of p46ShcA was reported in both hepatocytes and hepatic cell carcinoma cells (Yoshida et al., 2004). In addition p46ShcA was shown to bind overexpressed Ran-GTPase, which led to the nuclear translocation of p46ShcA (George et al., 2009).

The conventional nuclear cytoplasmic transport is determined by a nuclear localisation signal that is rich in the basic amino acids Lysine (K) and Arginine (R) that provides a protein with a license to be recognised by importin system components resulting in translocation of the complex to the nucleus (Kutay et al., 1997) (Figure 4.1). Classical protein export requires a nuclear export signal (NES) that is commonly rich in leucine and similar hydrophobic residues (Fornerod et al., 1997; Kosugi et al., 2008) (Figure 4.1). This NES is recognisable by the chromosomal maintenance region (CRM) export system, which was found to be efficiently paralysed by the anti-fungal agent, leptomycin B (Kudo et al., 1999).

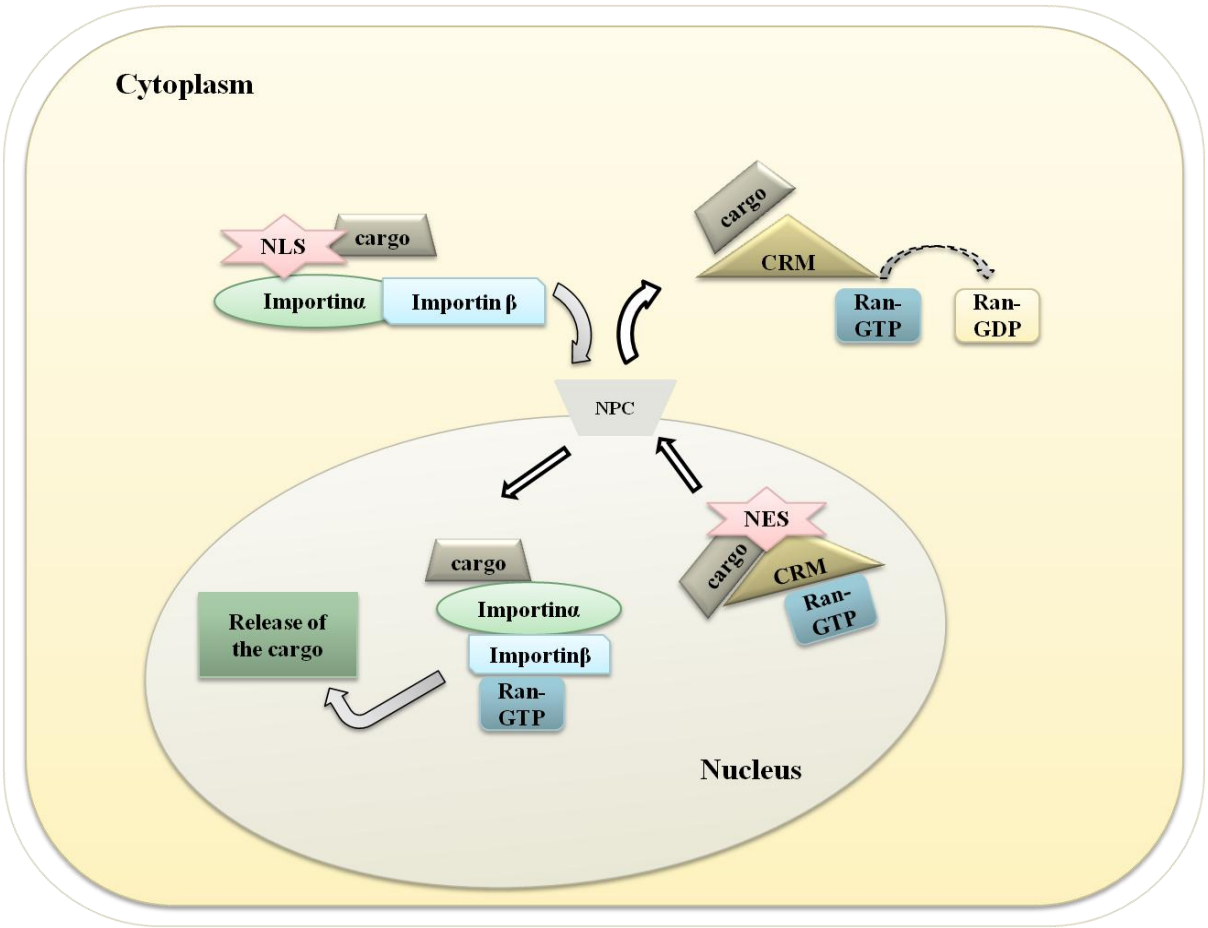

Figure 4.1 Nuclear transport in mammalian cells. A cargo protein in the cytoplasm is assembled with importins α and β via the cargo protein nuclear localisation signal (NLS). The complex then docks at the nuclear pore complex (NPC) followed by its translocation into the nucleus. Binding of Ran-GTP causes a conformational change that releases the cargo. The export of the cargo protein is accomplished by the CRM nuclear export receptor, which detects a nuclear export signal (NES) on the cargo protein. After the translocation of the complex to the cytoplasm it disassembles, using energy form of GTP hydrolysis.

4.2 Aims of this chapter:

The exact role of RaLP and how it induces migration is yet unknown and it needs clarification, therefore we aimed to study RaLP distribution in the intracellular compartment, because protein localisation can provide an indication of its function.
In the previous chapter anti-RaLP (4443) antibody showed some staining in the nucleus, which prompted us to investigate the dynamic movement of RaLP to the nucleus.
We aimed to identify whether RaLP has a functional NES and NLS, by generating deletion and point mutations in RaLP that might interfere with normal cellular distribution. We also aimed to investigate the underlying conditions that influence RaLP nuclear translocation. Since RaLP was observed in the nucleus, we sought to determine whether RaLP can associate with DNA.

4.3 Results:

4.3.1 RaLP is present in the nuclear compartment:

Although the role of Shc proteins is best characterised in the cytoplasm, recent reports have suggested that some Shc proteins are present in the mitochondria and nucleus (Orsini et al., 2004; Yoshida et al., 2004; George et al., 2009). In order to determine the subcellular distribution of RaLP, GFP-RaLP was ectopically expressed in 518.A2 melanoma cells, and the cells were fixed and visualised by confocal microscopy (Figure 4.2). GFP-RaLP was found to exist mainly in the cytoplamic compartment, consistent with the findings of Fagiani et al., 2007. Interestingly, nuclear localisation of RaLP was observed in a small proportion (25.6% ± 0.42) of the cells (Figure 4.2a). In order to support the microscopy data, we wished to confirm the nuclear localisation of RaLP using nuclear cytoplasmic fractionation. DAUV melanoma cells were fractionated using hypotonic cell lysis, and equivalent amounts of nuclear and cytoplasmic extracts were analysed by immunoblotting. A small fraction of endogenous RaLP was detected in the nuclear fraction using the anti-RaLP antibody, corresponding to approximately 17 % of total RaLP protein (Figure 4.2b). Blotting with anti-GAPDH and anti-Histone H1 antibodies was performed to confirm the purity of cytoplasmic and nuclear fractions (Figure 4.2b). These preliminary experiments indicated the presence of RaLP in the nuclear compartment.

a.

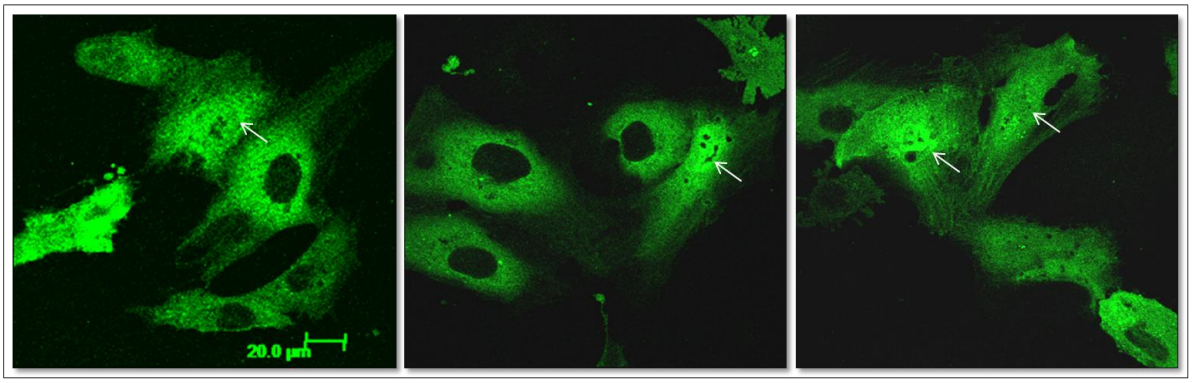

b.

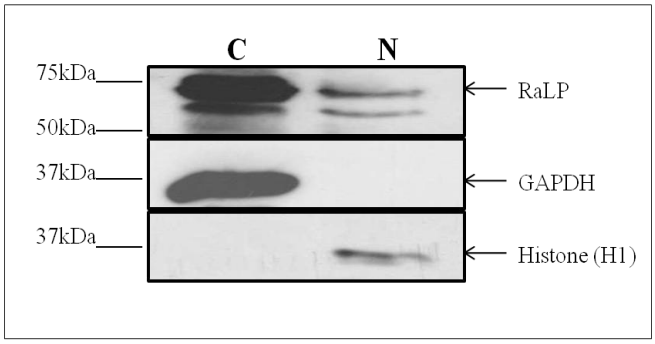

Figure 4.2 RaLP does exist in the nuclear fraction of the melanoma cells. (a) 518.A2 melanoma cells were transfected with GFP-RaLP for 24 hrs. Localisation of GFP-RaLP was determined in fixed cells by laser confocal microscopy using a 63x oil immersion objective. Scale bars represent 20 µm. White arrows indicate GFP-RaLP in the nucleus. (b) DAUV melanoma cells were fractionated into nuclear and cytoplasmic fractions. The nuclear proteins were released by adding high salt extraction buffer. Both the cytoplasmic (C) and the nuclear (N) fractions were analysed by western blotting using α-RaLP, α-GAPDH or α-Histone (H1) antibodies.

4.3.2 Leptomycin B resulted in RaLP nuclear sequestration:

Having confirmed that a proportion of RaLP resides in the nucleus, it was hypothesised that RaLP may shuttle between the cytoplasm and the nucleus, and have an as yet uncharacterised role in the nucleus. Proteins that shuttle between the nucleus and cytoplasm usually exit the nucleus using the chromosomal region maintenance (CRM) nuclear export system, and their presence within the nucleus can be induced using a specific inhibitor of this export system, leptomycin B (LMB) (Kudo et al., 1999). To determine whether RaLP accumulates in the nucleus when CRM dependent export is inhibited, 518.A2 melanoma cells, DAUV melanoma cells and NIH3T3 cells transiently expressing GFP-RaLP, GFP protein or GFP-Nischarin were treated with LMB (1 µg/ml) for 2 hours. Interestingly, after LMB treatment GFP-RaLP showed a striking accumulation in the nucleus compared to the untreated cells, unlike the subcellular distribution of GFP protein and GFP-Nischarin which did not change with the addition of LMB (Figure 4.3b).

Time lapse live cell imaging revealed that this accumulation occurs within 30 minutes (Figure 4.4). Based on this observation, it was assumed that RaLP possesses a nuclear export signal that failed to be recognised by the paralysed CRM export system in the presence of LMB, resulting in its accumulation in the nucleus.

To ensure that this was not an artefact due to overexpression, endogenous RaLP subcellular distribution in 518.A2 melanoma cells was assessed using a rabbit polyclonal anti-RaLP antibody raised against the CH1 domain of RaLP described in chapter 3, in the presence and absence of LMB (Figure 4.5).

Consistent with previous findings, RaLP showed a predominant cytoplasmic distribution, while a small fraction was present in the nuclear compartment. LMB-treated cells exhibited accumulation of endogenous RaLP in the nucleus (Figure 4.5). We conclude that the melanoma associated Shc adaptor, RaLP, might be able to translocate to the nucleus, and its export depends on the CRM export system.

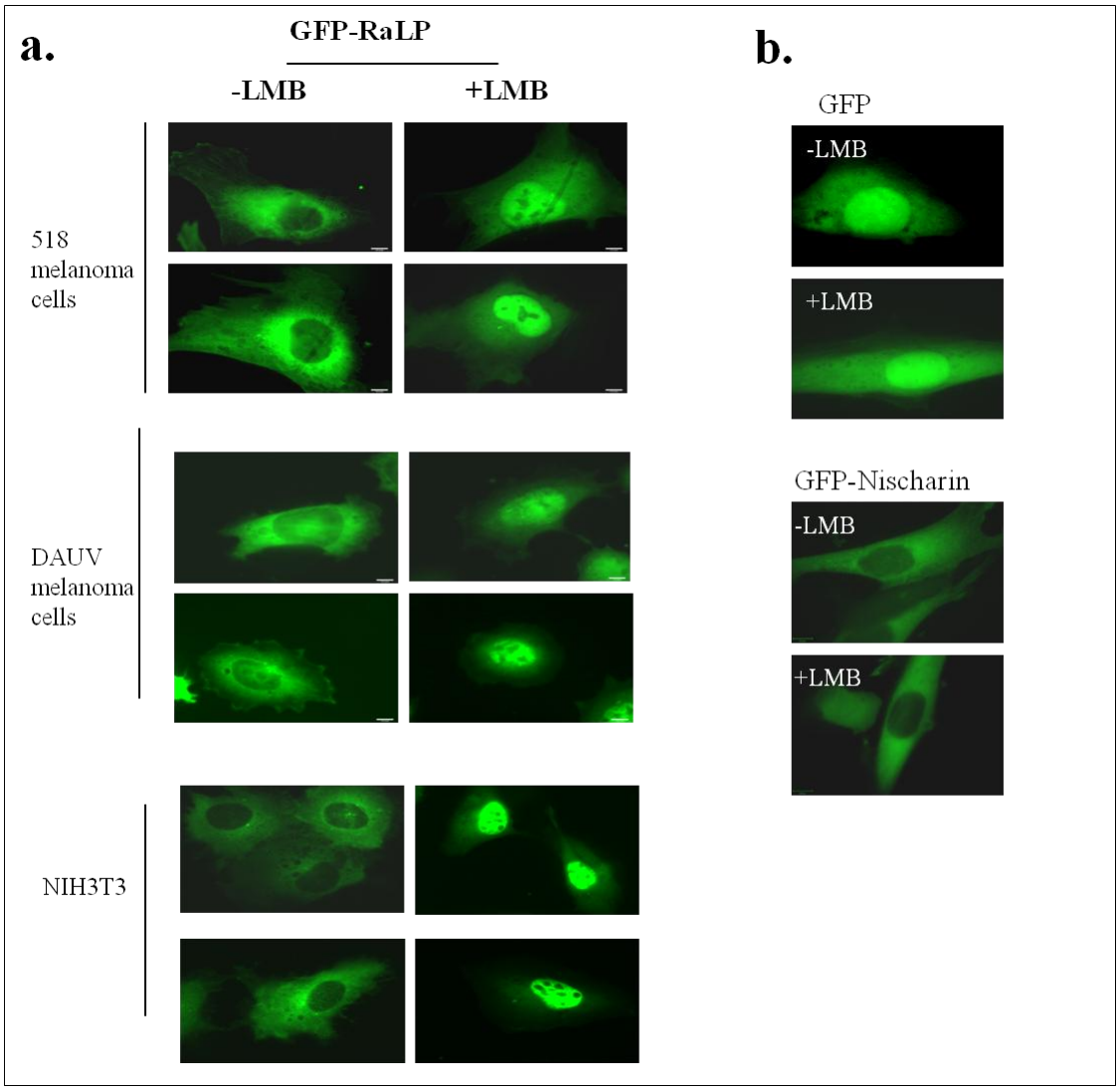

Figure 4.3 Leptomycin B induced sequestration of GFP-RaLP in the nuclei of different cell lines. (a) 518.A2 melanoma cells, DAUV melanoma cells and NIH3T3 cells were transfected with GFP tagged full length RaLP. The cells were then subjected to 1 µg/ml leptomycin B (LMB) for 2 hrs. The fixed cells were then visualised. (b) 518.A2 melanoma cells were transfected with either GFP or GFP-Nischarin. And after 24 hrs the cells were treated with 1 µg/ml leptomycin B (LMB) for 2 hrs. The fixed cells in A and B were then visualised using a Nikon fluorescence microscope and 100x N.A 1.4 oil immersion objective. Scale bars represent 6.4 µm.

a.

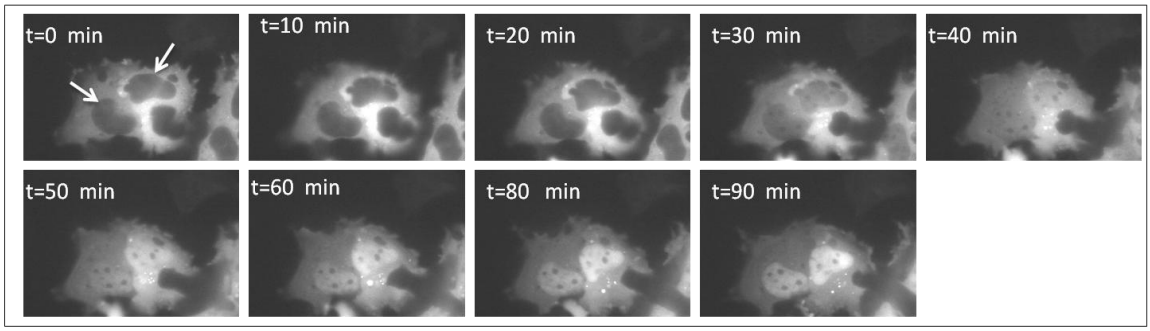

b.

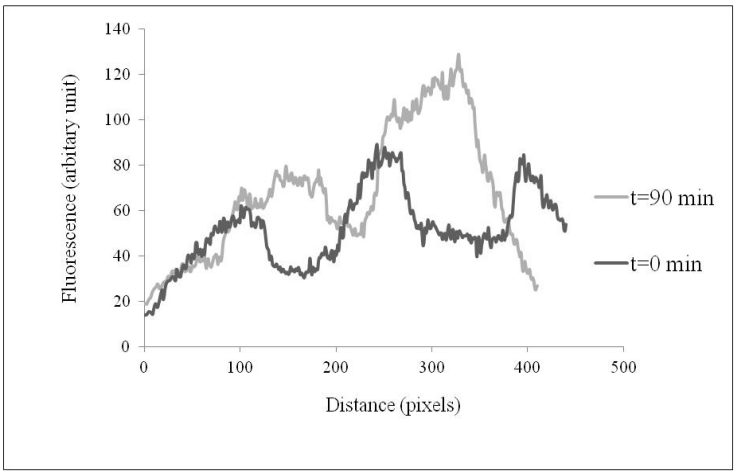

Figure 4.4 LMB sequestered GFP-RaLP in the nucleus in live DAUV melanoma cells. (a) DAUV melanoma cells that were seeded on coverslips were transiently transfected with GFP-RaLP. The cells on the coverslip were placed in a closed perfusion chamber (POC chamber system) that allowed us to perfuse medium with 1 µg/ml LMB. The live cells were imaged every 5 min for 90 min using Cellˆ R software. (b) Analysis of the Gray value that is indicative of the fluorescence signal was performed using ImageJ software. The analysis included the two indicated cells in the t=0 field and it was performed at time 0 (t=0) when the LMB was applied as well as at t=90 min time point, after 90 min of LMB treatment; see the attached CD for the video.

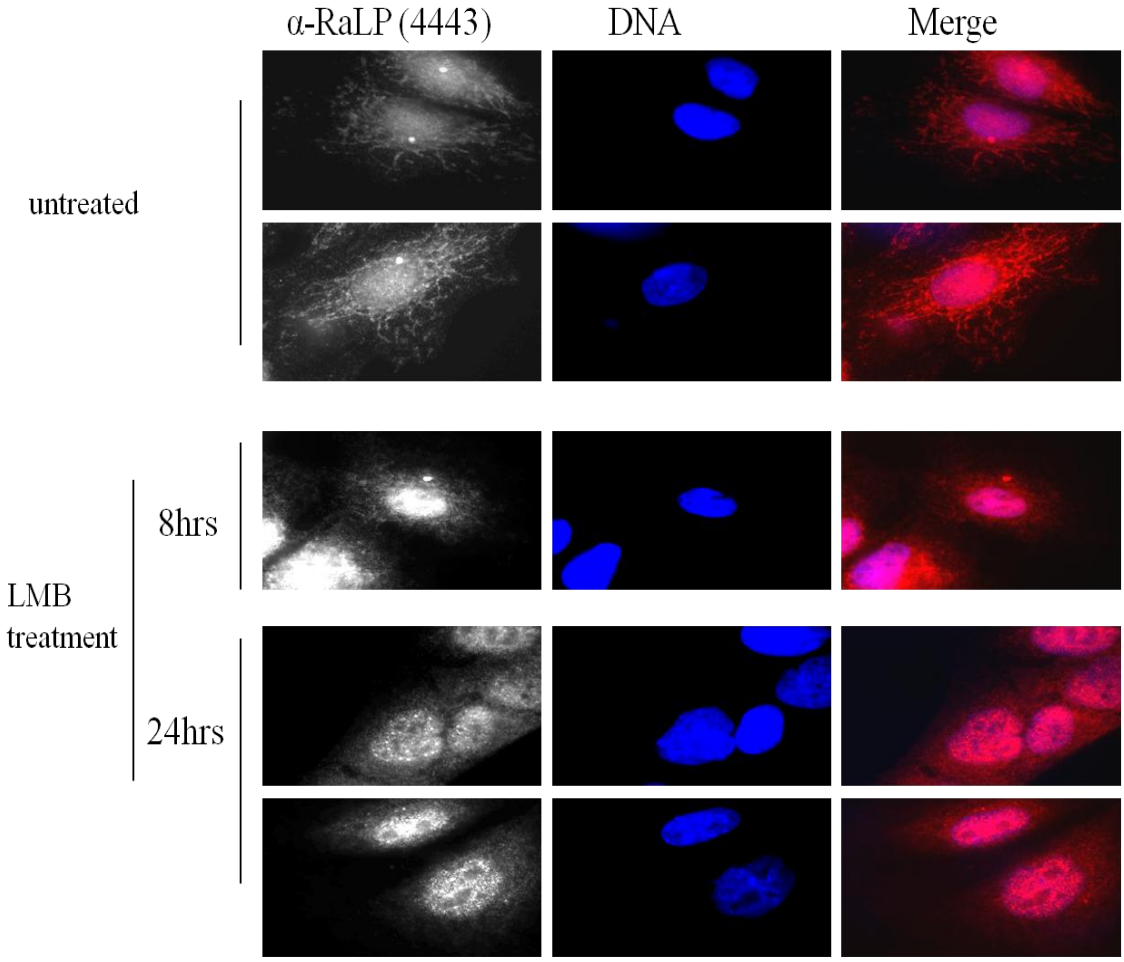

Figure 4.5 Treatment with LMB resulted in accumulation of endogenous RaLP in 518.A2 melanoma cell nuclei. 518.A2 melanoma cells were either untreated or treated with LMB for 8 or 24 hrs. Immunostaining of fixed, permeabilised cells was performed using anti-RaLP antibody (4443). Cells were visualised by fluorescence microscopy using a 100x oil immersion objective.

4.3.3 The CH2 domain of RaLP is crucial for its cytoplasmic localisation:

Having demonstrated that RaLP can shuttle between the nucleus and cytoplasm we sought to determine which domain in RaLP is responsible for its nuclear and cytoplasmic localisations. mCherry-RaLP truncations were generated as indicated in Figure 4.6a, lacking either the SH2 domain (mCherry-RaLPΔSH2) or CH2 domain (mCherry-RaLPΔCH2) and were transfected into DAUV melanoma cells along with a construct encoding the full length protein (mCherry-RaLP). To ensure that the mCherry tag or the DAUV cells did not influence the localisation, and that the localisation was not dependent on cell type, GFP tagged truncations (RaLPΔSH2 and RaLPΔCH2) were transfected into 518.A2 melanoma cells along with GFP-RaLP (full length). Strikingly, the tagged RaLPΔCH2 showed a predominant nuclear distribution in both DAUV and 518.A2 melanoma cells while mCherry-RaLP, GFP-RaLP, mCherry-RaLPΔSH2 and GFP-RaLPΔSH2 were mainly present in the cytoplasm (Figure 4.b and c). This led us to conclude the CH2 domain of RaLP plays an essential role in nuclear exclusion through the CRM export system.

4.3.4 Identification of the RaLP Nuclear Export Signal (NES):

Since the CH2 domain of RaLP was essential for cytoplasmic location, it was assumed that this must house a nuclear export signal (NES) that contains hydrophobic residues recognised by the CRM export system. In order to identify the RaLP-NES, various deletion mutants were generated systematically lacking increasing numbers of amino acids from the N-terminus (Figure 4.7a and b). Of these truncations, p69#2RaLP (24-630), p59RaLP (93-630) and p49RaLP (188-630) correspond to the p69#2, p59 and p49 isoforms reported by Jones et al., 2007, that represent alternative translation products of RaLP, and may be naturally occurring variants. The generated mutations were all tested for their molecular size using western blotting analysis that revealed the expected sizes for the mutants (Figure 4.7c). All cells expressing RaLPΔCH2 (188-630), or p59RaLP (93-630) showed striking nuclear localisation of the proteins in 100% of cells as shown in Figure 4.8b. The truncated RaLP forms p69#2 (24-630), Del1 (44-630) and Del2 (76-630) were primarily in the cytoplasm (Figure 4.8).

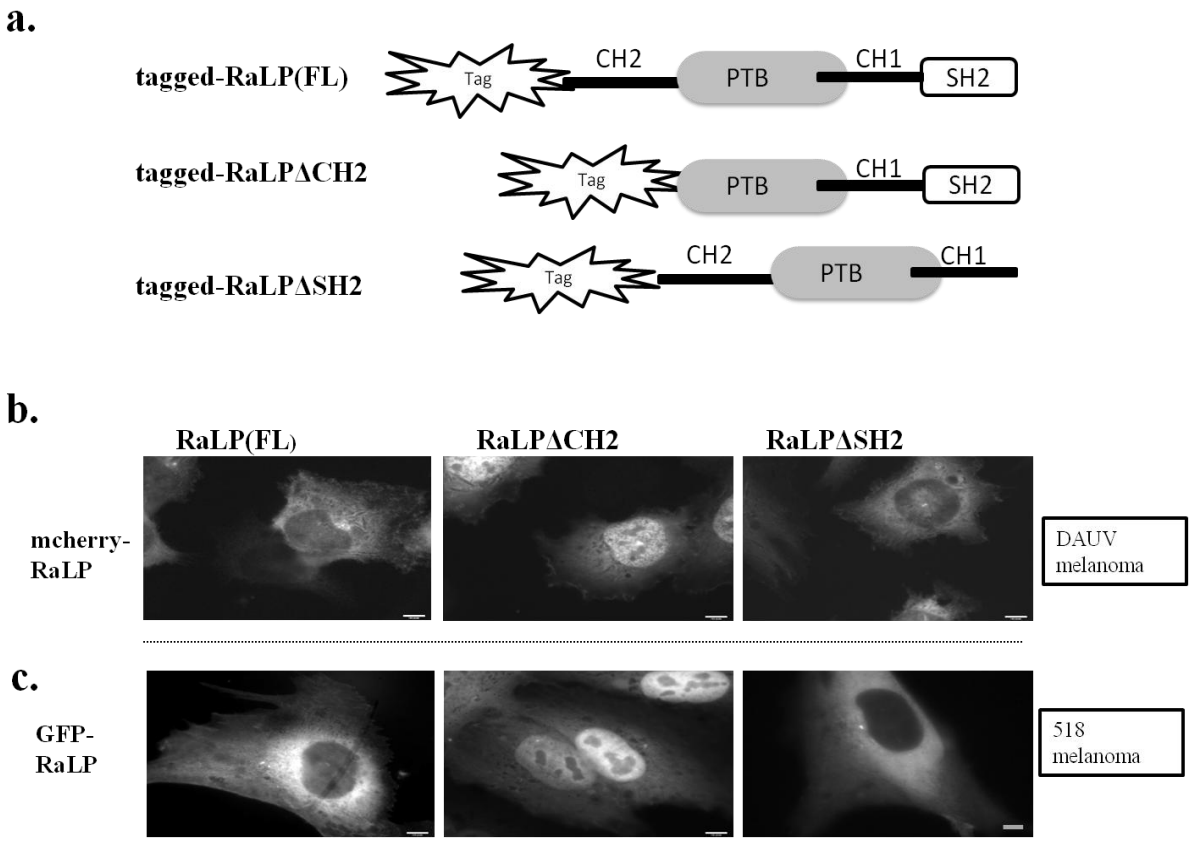

Figure 4.6 The CH2 domain of RaLP plays a role in its cytoplasmic localisation. (a) Schematic representation of RaLP domains and the truncations that were designed, RaLP full length (FL) and its truncations were tagged to mCherry at the amino terminus of RaLP. (b) DAUV melanoma cells were transiently transfected with mCherry tagged RaLP (FL), RaLP ΔCH2 that lacks the CH2 domain, or RaLPΔSH2 that lacks the SH2 domain. The cells were fixed with 3.7% formaldehyde for 20 min and visualised using a Nikon fluorescence microscope, using a 100x1.3 oil immersion objective. Scale bar 6.4μm (c) 518.A2 melanoma cells were transiently transfected with GFP tagged either RaLP (FL), RaLP ΔCH2 or RaLPΔSH2. The cells were fixed and visualised as mentioned in (b). Scale bar 6.4 μm.

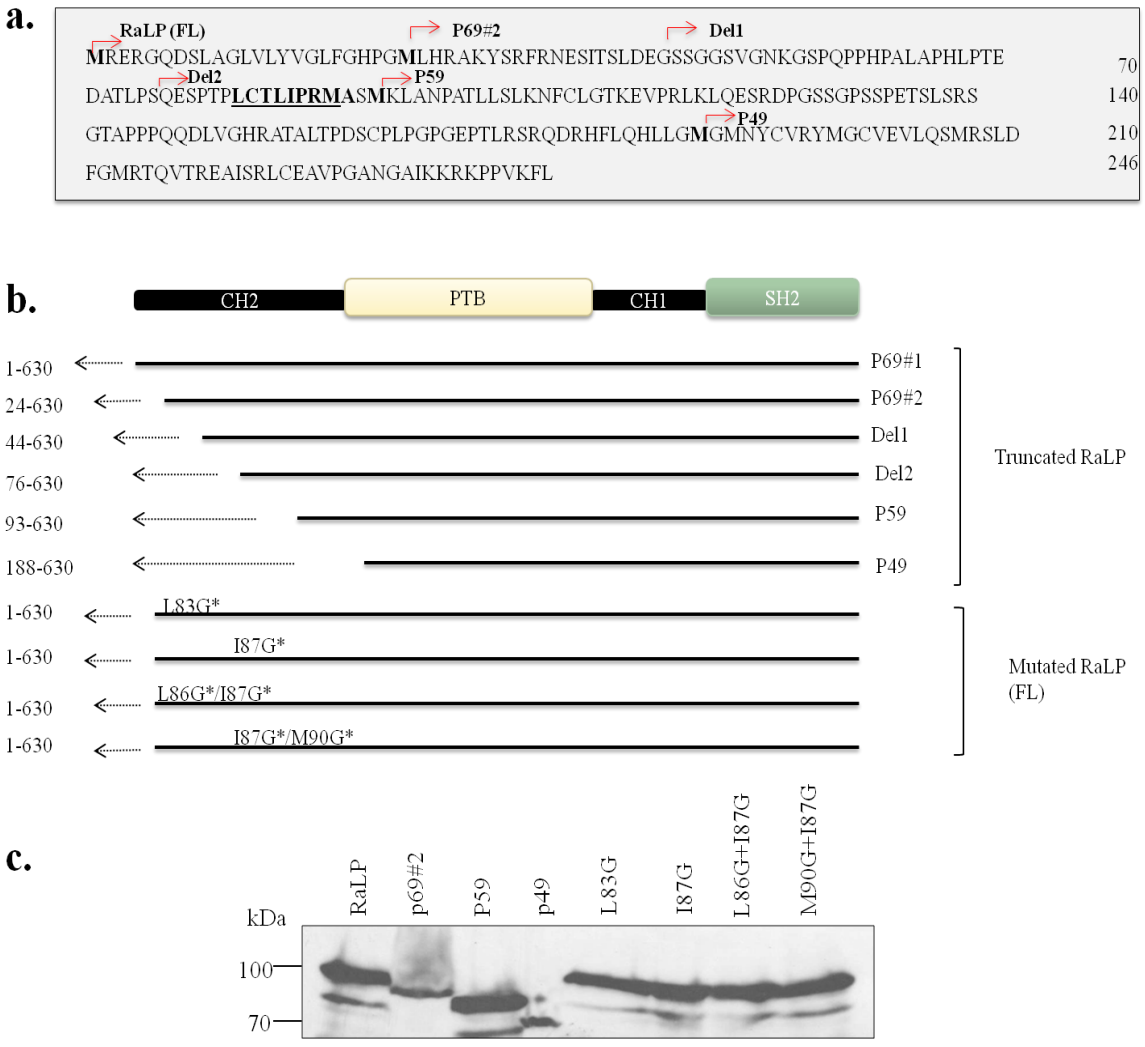

Figure 4.7 RaLP mutations for nuclear export signal (NES) identification. (a) Amino acid sequence of RaLP CH2 domain (1-188) and part of the phosphotyrosine binding domain (PTB) 189-246. The underlined sequence is the predicted NES and the red arrows indicate the start of the generated truncated versions (p69#2, Del1, Del2, p59 and p49). (b) Schematic representation of the RaLP structural domains and the generated mutants for NES identification. (c) HEK 293 cells were transiently transfected with the GFP tagged full length RaLP (FL) or with its mutants followed by cell lysis. Immunoblotting analysis was then performed using α-GFP at 1:1000.

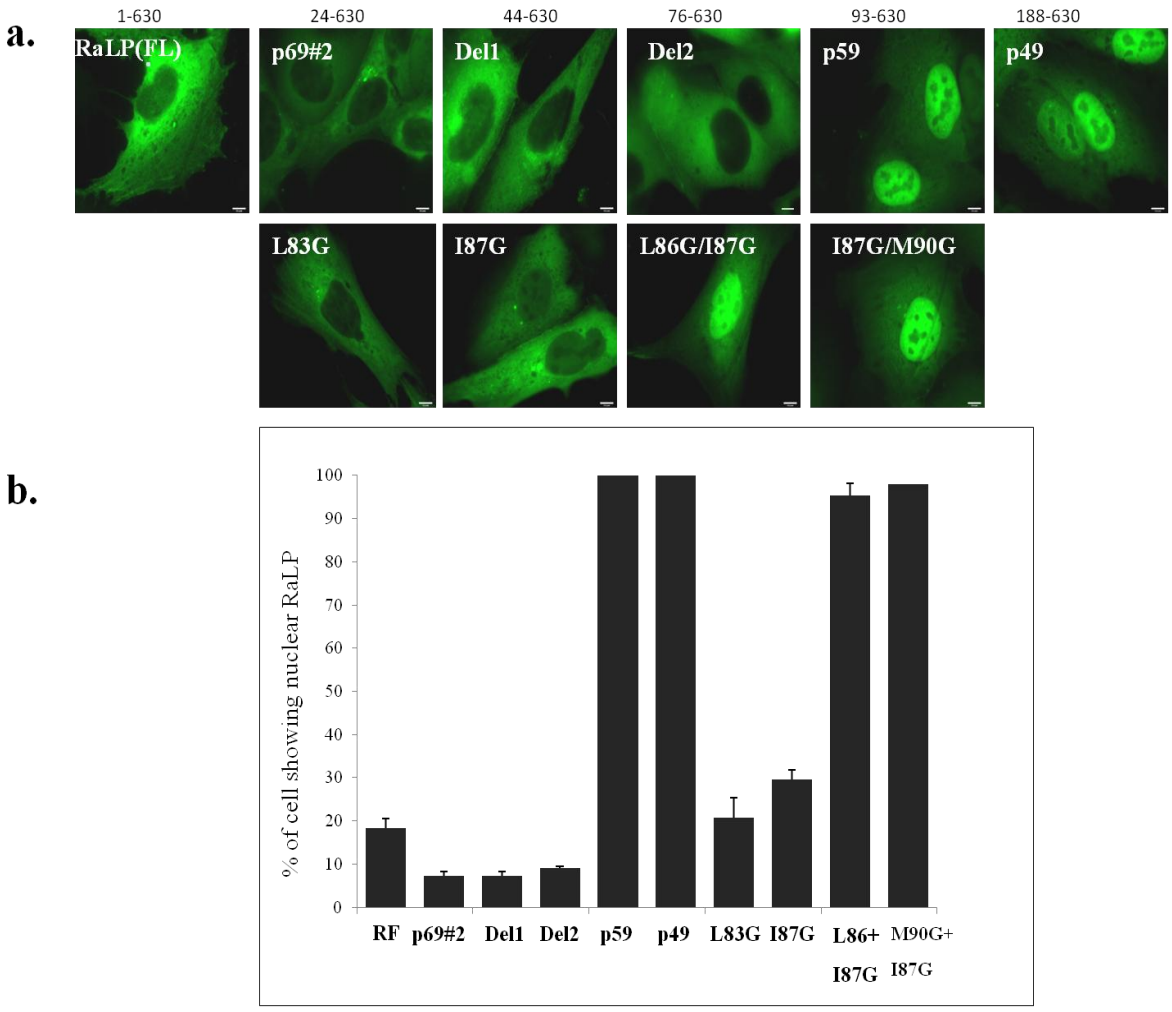

Figure 4.8 Identification of the RaLP Nuclear Export Signal (NES). (a) Subcellular localisation of N-terminal truncated and mutated RaLP transcripts. 518.A2 melanoma cells were transiently transfected with either N-terminal GFP-tagged truncated or mutated RaLP versions. The cells were then fixed and visualised by Nikon fluorescence microscopy using 100 x 1.4 oil immersion objective. Scale bar 6.4 µM. (b) GFP-RaLP full length (RF) along with its truncated mutatnts were transiently transfected into 518.A2 melanoma cells. The cells were fixed with formaldehyde and the % of nuclear RaLP was calculated following certain criteria. Only the transfected green cells were counted, the nuclei should not be distorted and the nuclear intensity of the expressed GFP tagged protein should either be similar to the cytoplasmic intensity or more. The percentage of the green cells that showed green nuclei following the stated criteria was calculated from the total number of the counted green cells. Three independent experiments were conducted and 100 cells per sample were counted. Error bars represent standard errors of mean.

Therefore, it was deduced the region including amino acids 76-93 contained the functional NES of RaLP. Exploiting a newly designed NES identification system by Kosugi et al. 2008, we identified the sequence from amino acids 83-93 (LCTLIPRMASM), as a possible NES (Figure 4.7a). To confirm that this region contains the NES, substitution point mutations were introduced to exchange L83 or I87 of RaLP for glycine. Both point mutant proteins were mainly present in the cytoplasm while I87GRaLP showed 12% increase in nuclear localisation than the L83GRaLP when both were compared with non mutated RaLP (Figure 4.8a and b). Additional mutations were introduced using I87GRaLP as a template to produce L86G/I87GRaLP or I87G/M90GRaLP. Introducing a second mutation led to defective nuclear export, and hence accumulation of the double mutated L86G/I87GRaLP and I87G/M90GRaLP in the nucleus of 98% and 95 % of the transfected cells, respectively (Figure 4.8). In conclusion L86, I87 and M90 present within the predicted nuclear export sequence, are all important for nuclear export of RaLP.

4.3.5 Test to determine whether L86G/I87GRaLP or I87G/M90GRaLP possesses any residual nuclear export activity:

518.A2 melanoma cells that expressed all GFP tagged RaLP mutants shown in Figure 3.7c were either treated or untreated with LMB. Treatment with LMB resulted in significant nuclear accumulation of RaLP (1-630 aa), p69#2 (24-630 aa), Del1 (44-630 aa), Del2 (76-630 aa), L83GRaLP and I87GRaLP while no significant change in the nuclear localisation of p59 (93-630 aa), p49 (188-630 aa), L86G/I87GRaLP and I87G/M90GRaLP occurred upon LMB treatment (Figure 4.9). Thus, the identified nuclear export region from 83 to 90 (LCTLIPRM) plays a major role in RaLP nuclear export.

4.3.6 Does RaLP utilise a classical nuclear localisation signal (NLS) to translocate to the Nucleus?

Having identified the region of RaLP required for nuclear export it was of interest to explore the mechanism that mediates RaLP nuclear localisation. Different mechanisms have been reported whereby proteins can be imported into the nucleus.

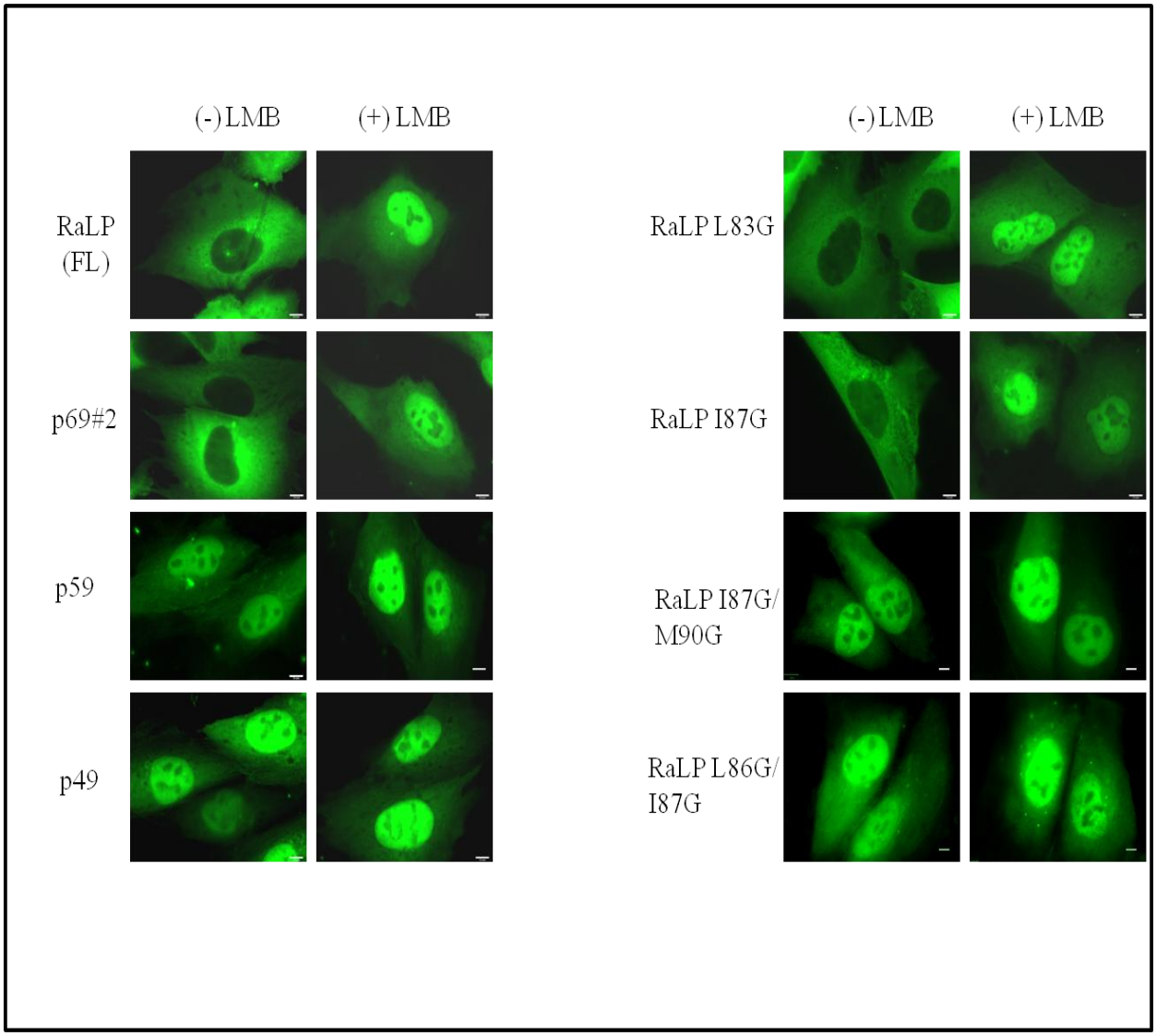

Figure 4.9 Testing the residual activity of the nuclear export signal in the mutated versions of RaLP. 518.A2 melanoma cells were transiently transfected with GFP tagged full length RaLP or with its mutants (p69#2, p59, p49, RaLPL83G, RaLPI87G, RaLP I87G/M90G and RaLP L86G/I87G). The cells were treated with 1 µg/ml LMB or left untreated for 2 hrs at 37°C. The fixed cells were then visualised using a Nikon fluorescence microscope and 100x N.A oil immersion objective. Scale bars represent 6.4 µm.

These include diffusion of proteins smaller than approximately 60 kDa, use of nuclear localisation signals (NLS) rich in lysine (K) and arginine (R) residues (Liang and Clarck, 1999), phosphorylation dependent nuclear import signals (Chuderland et al., 2008) or formation of complexes with other proteins facilitating import into the nucleus (George et al., 2009). Close observation of the RaLP sequence revealed a KKRK motif (amino acids 237-240) in the PTB domain of RaLP that could possibly act as a monopartite NLS (Figure 4.10a). In addition, using cNLS mapper, an NLS prediction programme, yielded GAIKKRKPPVKF (234-245 aa) as a predicted RaLP monopartite NLS with score of 5.5 that indicates protein existence in both cytoplasmic and nuclear compartments (Kousgi et al., 2009). We assumed that if the KKRK motif was required for nuclear import, then mutation of one or more of these basic residues would result in a cytoplasmic accumulation of GFP tagged p59RaLP (93-630 aa), which in its wild type form shows a predominant nuclear localisation. Mutants in which one, two, three or all of the basic residues (K237, K238, R239 and K240) in the putative NLS were replaced by glycine were analysed for their localisation and western blotting analysis revealed the expected molecular size for the generated mutants (Figure 4.10b). No dramatic change in cytoplasmic translocation of GFP-p59RaLP was observed in any of the mutants (Figure 4.10c and d), although careful quantification using Olympus Scan ^ R software revealed a 24 % ($p=0.07$) increase in cytoplasmic/nuclear ratio in the mutant in which all four basic residues had been replaced, as compared to the wild-type protein (Figure 4.10d). We conclude that although the basic KKRK motif at amino acids 237-240 may contribute to nuclear import of RaLP, clearly other mechanisms exist to facilitate this process.

4.3.7 Oxidative stress promotes RaLP nuclear translocation:

Reactive oxygen species (ROS) are known to play a significant role in carcinogenesis (Klaunig et al., 2010). ROS can contribute to changes in protein phosphorylation events that can alter the subcellular localisation of target proteins thereby influencing their function (Wang and Jin, 2010). We therefore investigated whether ROS affect RaLP distribution in the cell. Moreover, RaLP is a known substrate to epidermal growth factor receptor (EGFR), which was proved to translocate to the nucleus upon subjecting keratinocytes to 5 mM H_2O_2 for 60 minutes (Xu et al., 2009).

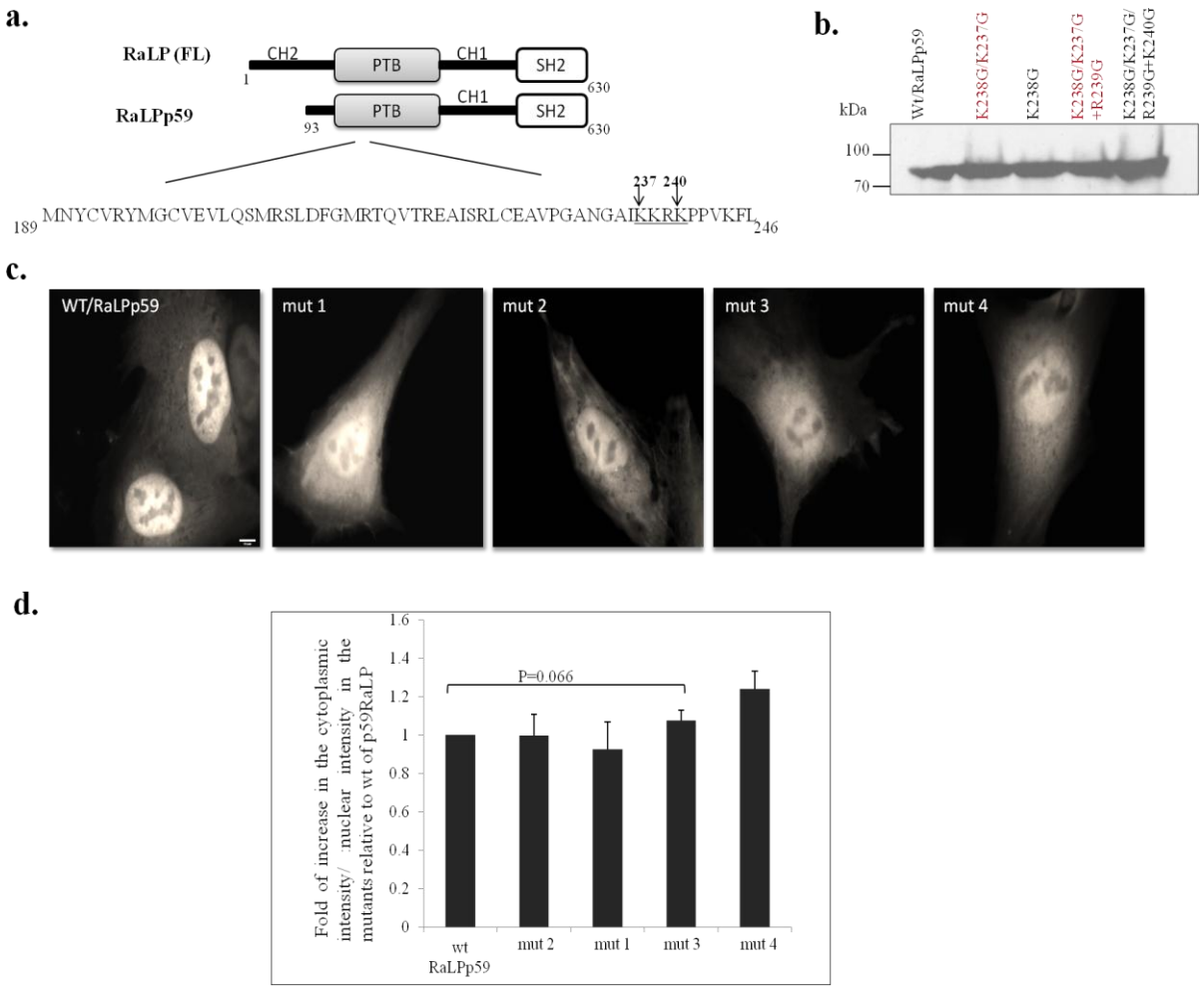

Figure 4.10 Investigating the role of a putative nuclear localisation sequence in RaLP localisation. (a) Diagrammatic representation shows p59RaLP and the position of a possible NLS (KKRK) within the PTB domain. Mutants were generated in which positively charged residues within this motif were substituted for glycine. (b) HEK 293 cells were transiently transfected with GFP-tagged p59RaLP or with its mutated versions K238G (mut1) , K238G/K237G (mut 2), K238G/K237G/R239G (mut 3) and K238G/K237G/R239G/K240G (mut 4). Western blotting analysis was then performed using α-GFP (c). The 518.A2 melanoma cells were transfected with GFP-RaLPp59 or with its mutants. The cells were then fixed and visualised using a Nikon fluorescence microscope and a x 100 oil immersion objective. Scale bar represents 6.4 μm. (d) GFP-tagged RaLPp59 wild type (wt) along with its mutants were transiently transfected into 518.A2 melanoma cells followed by fixing of cells. The ratio of the cytoplasmic mean intensity to the nuclear mean intensity of the green signal for RaLPp59 wt and each of its mutants was calculated by ScanR analysis software. The values were all related to the RaLPp59 (wt) to determine the folds-change. Three independent experiments were carried out and results are represented graphically. Error bars represent standard error of mean.

FLAG-RaLP was immunoprecipitated from the nuclear and cytoplasmic fractions of FLAG-RaLP expressing cells (F4) with or without treatment with 5 mM H_2O_2 (Figure 4.11a and b). Upon oxidative stress there was a 2.5 fold increase in RaLP in the nucleus after 1 hr ($p<0.05$; N=3). To confirm that endogenous RaLP responds similarly to oxidative stress, the experiment was repeated using 518.A2 melanoma cells. In this case the immunoprecipitation step was omitted, and nuclear and cytoplasmic extracts were analysed directly by immunoblotting (Figure 4.11c and d). Similar results were obtained, with a 13 fold increase in nuclear RaLP being observed after 1 hr treatment with 5 mM H_2O_2 ($p<0.05$; N=3). Our data revealed that a fraction of RaLP does exist in the nucleus and it increases upon subjecting the cells to oxidative stress.

In an attempt to mimic the in vivo conditions, 518.A2 melanoma cells that expressed GFP-RaLP were either stressed with 100 µM H_2O_2 for 3 or 6 hrs, deprived from serum or left unstressed. RaLP nuclear translocation was assessed using fluorescence microscopy and Scanˆ R software; the experiment was executed three times independently. Although, subjecting cells to 100 µM H_2O_2 for 6 hrs resulted in an elevation in the nuclear RaLP, unlike the cells that were deprived from serum, the p value (0.24) suggested a lack of the statistical significance of this observation (Figure 4.12). Taken together, these data confirmed the phenomenon of RaLP nuclear translocation upon oxidative stress, however; the nuclear translocation of RaLP was less significant at low H_2O_2 concentration. This need to be studied further using the same H_2O_2 concentration for longer time points.

4.3.8 RaLP is found in complexes with DNA:

Since the DNA is the main nuclear component, it was suggested that RaLP could possibly associate with the DNA. This was tested by isolating DNA and associated proteins from HEK 293 cells that stably express FLAG-RaLP (F4 cells). The precipitated DNA, with associated cross-linked proteins was dissolved in SDS-PAGE sample buffer, and western blotting was performed to detect the presence of RaLP. FLAG-RaLP was found to be associated with the DNA fraction using an anti-FLAG antibody (Figure 4.13a). An additional experiment was executed to determine the endogenous RaLP association with the DNA. DAUV melanoma cells were fractionated into cytoplasmic and nuclear fractions.

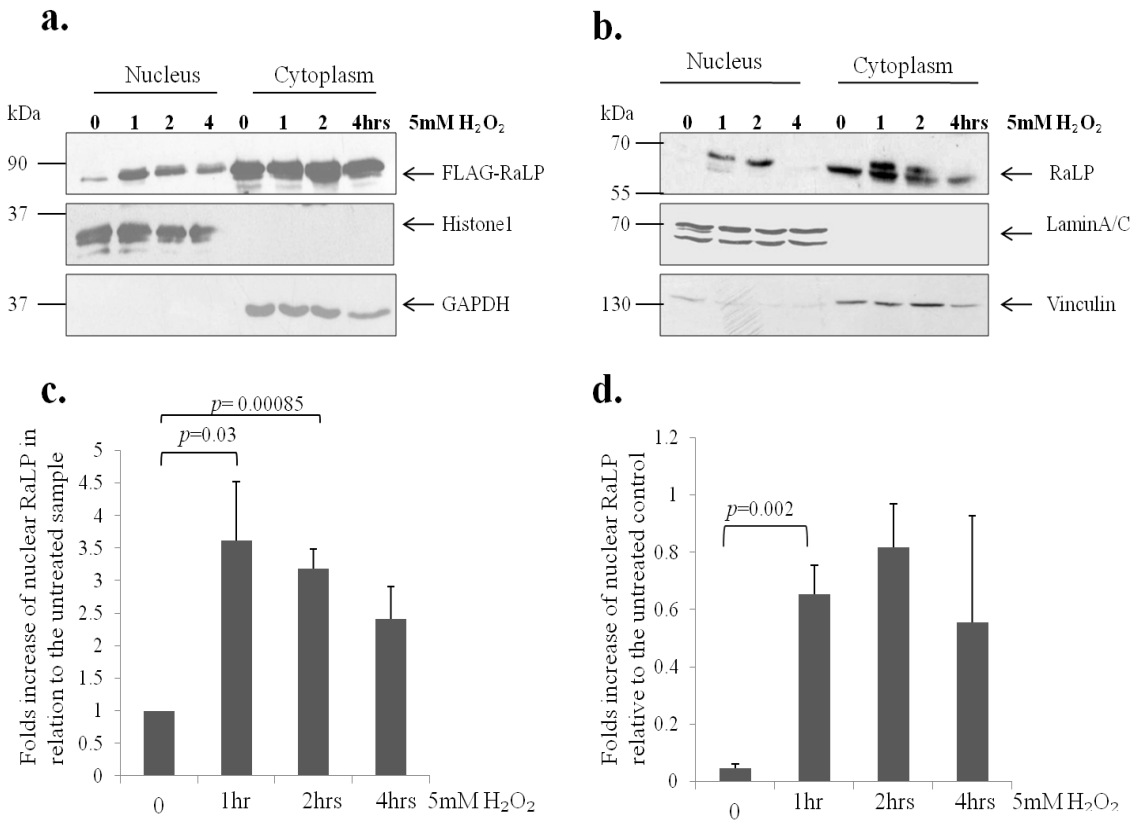

Figure 4.11 Hydrogen peroxide treatment promotes RaLP nuclear translocation. (a) F4 cells that stably express FLAG-RaLP were either subjected to 5 mM H_2O_2 for 1, 2 or 4 hrs, or left untreated. Subcellular fractionation was performed to obtain nuclear and cytoplasmic fractions from which FLAG-RaLP was immunoprecipitated using anti-FLAG antibody. Immunoblotting was then performed using anti-FLAG antibody. Samples of the nuclear and cytoplasmic fractions used for the immunoprecipitation were analysed by western blotting with anti-Histone H1, or anti-GAPDH antibodies. Data from three independent experiments was quantified and the results are presented graphically (b). Error bars represent standard error of the mean. (c) 518.A2 melanoma cells were either untreated or treated with 5 mM H_2O_2 for 1, 2 or 4 hrs. The cells were then fractionated into nuclear and cytoplasmic fractions. The fractions were analysed by SDS-PAGE and western blotting using anti-RaLP, anti-LaminA/C or anti-Vinculin antibodies. Data from three independent experiments was quantified and the results are presented graphically (d).

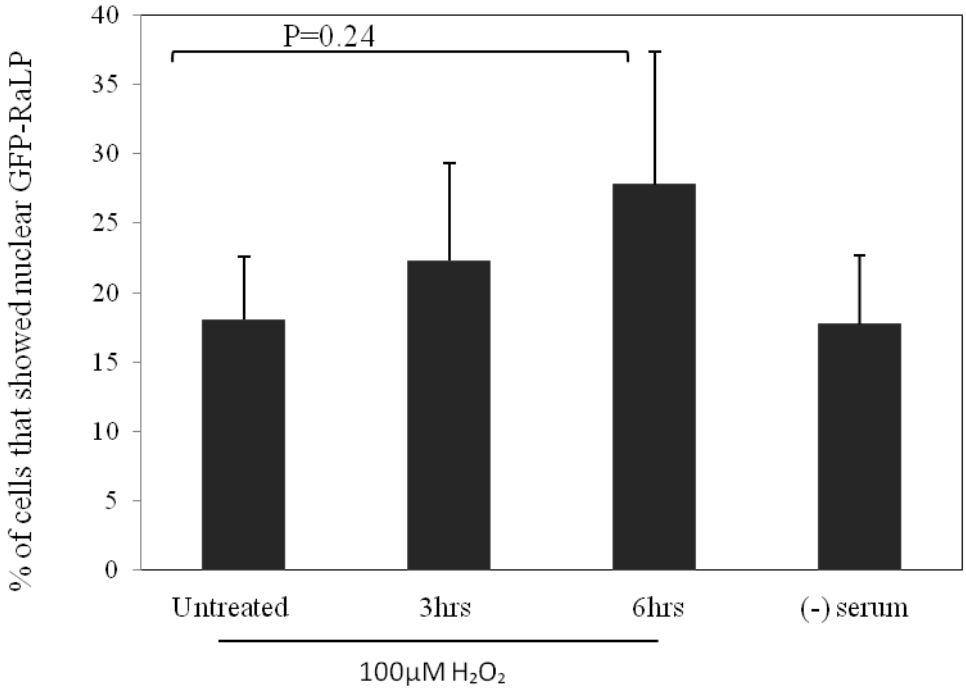

Figure 4.12 The effect of hydrogen peroxide at low concentration on GFP-RaLP localisation in melanoma cells. 518.A2 melanoma cells were transiently transfected with GFP-RaLP and after 24 hrs the cells were stressed using 100 µM H_2O_2 for 3/6 hrs, or deprived from serum for 6 hrs or left unstressed. The cells were then fixed and the % of the cells that showed nuclear GFP-RaLP was calculated using ScanR software. Three independent experiments were carried out and the data presented graphically. Error bars represent standard error of mean.

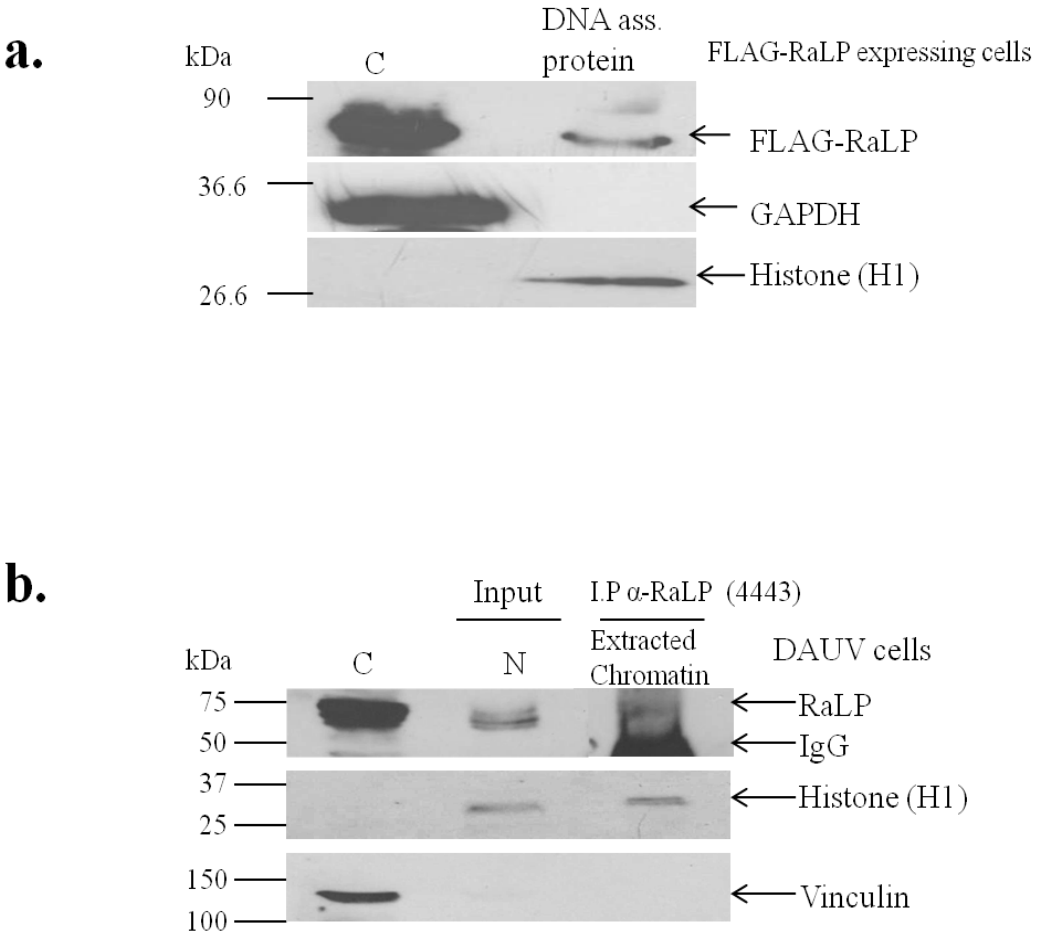

Figure 4.13 RaLP and the DNA association. (a) A method to determine RaLP and DNA association in HEK 293 cells that stably express FLAG-RaLP. HEK 293 cells that stably express FLAG-RaLP were initially fractionated into cytoplasmic and nuclear fractions. The nuclear proteins were cross linked to the DNA by using formaldehyde. The DNA was isolated from the nuclear fraction and the DNA associated proteins were analysed by SDS-PAGE and western blotting using antibodies against FLAG (to detect the tagged RaLP), GAPDH or Histone H1. Cytoplasmic extract (C) was analysed for comparison. (b) DAUV melanoma cells from two confluent 10 cm dishes were fractionated into cytoplasmic (C) and nuclear (N) fractions. The nuclear pellet of one of the dishes was used for chromatin extraction. The extracted chromatin was then incubated at 4°C with the immobilised anti-RaLP antibody (4443). Immunoblotting

analysis was then carried on using anti-RaLP antibody, anti-Histone (H1) and anti-Vinculin antibody.
The chromatin was extracted from the nuclear pellet using chromatin extraction buffer supplemented with Micrococcal nuclease (see the Materials and Method part). The extracted chromatin was then incubated with immobilised α-RaLP (4443). Immunoblotting analysis with α-RaLP (4443) revealed a faint band in the anti-RaLP immunoprecipitates, which indicated the association of endogenous RaLP with the chromatin. Successful fractionation and chromatin extraction was indicated by the existence of Histone (H1) in the nuclear fraction and the extracted chromatin while Vinculin was only seen in the cytoplasmic fraction (Figure 4.13b). This experiment was conducted twice; therefore it does need repetition including immunoprecipitation with a control antibody to prove the band we are observing in α-RaLP immunoprecipitates is specific. Accordingly, it was demonstrated that RaLP does exist in the nucleus and might form complexes with the DNA, either directly or by association with other proteins.

4.3.9 The potential role of RaLP in gene regulation:

We have demonstrated that RaLP shuttles between the cytoplasm and the nucleus, and that nuclear RaLP is increased upon oxidative stress. In addition, preliminary evidence suggests that RaLP can associate with the DNA, either directly or indirectly via interactions with other proteins. These results tempted us to speculate that RaLP could have a role in promoting gene transcription. To investigate this further, a reporter assay was employed in which the firefly luciferase gene is placed under the control of a promoter containing multiple GAL4 binding sites. Control plasmids were already available but we needed to generate a construct encoding RaLP fused to the GAL4 DNA binding domain. Initially, it was decided to amplify the RaLP coding sequence from another plasmid to generate appropriate cloning sites. The amplification conditions were optimised by varying the annealing temperature as indicated in Figure 3.14a. The band obtained using an annealing temperature of 56ºC was excised, DNA extracted and cloned into the pGEM-T vector, which was designed for cloning PCR products (Figure 4.14b). The insert was excised with Xba1 and Sal1, and the pCMV-GAL4 vector was digested with the same enzymes (Figure 4.14c).

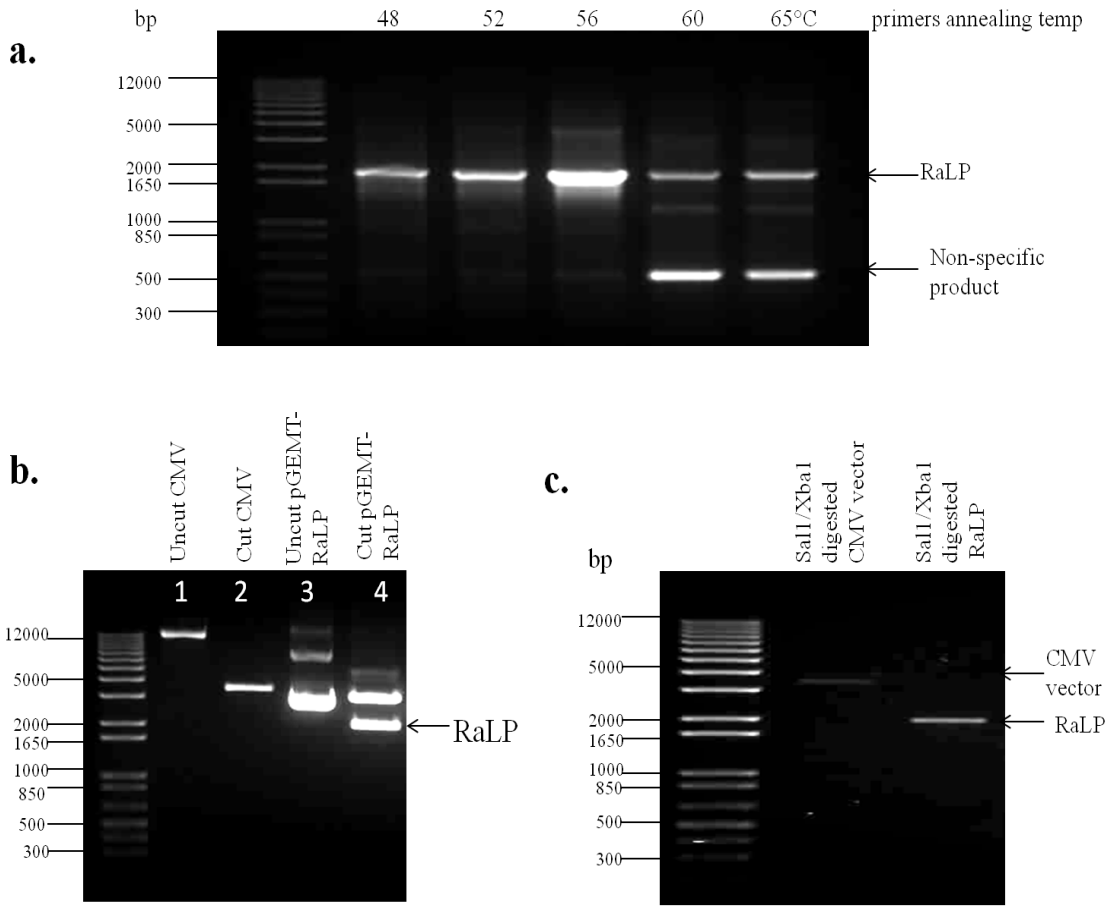

Figure 4.14 Preparation of RaLP cDNA and pCMV-GAL vector for cloning. (a) Amplification of RaLP by polymerase chain reaction (PCR). RaLP cDNA was amplified from the FLAG-RaLP vector. The primers for RaLP amplification were designed to contain Sal1 and Xba1 restriction sites. The PCR reaction was performed at different primer annealing temperatures. (b) Cloning RaLP into pGEM-T vector. RaLP was cloned in pGEM-T vector following the stated protocol by the manufacturers and the plasmid (pGEM-T-RaLP) was isolated from a white colony grown on selective X-gal containing plates. The uncut pGEM-T vector in lane 3 was double digested with Sal1 and Xba1 restriction enzymes as shown in (lane 4). Uncut pCMV-GAL4 vector (CMV) in lane 1 was double digested with Sal1 and Xba1 (lane 2). The digested pCMV-GAL4 and RaLP insert (lane 4 ~2000bp) were excised from the gel and the DNA was extracted using DNA extraction kit from QIAGEN and the result of the DNA yield is demonstrated in (c).

The extracted fragment corresponding to RaLP was cloned into the gel purified pCMV-GAL4 vector using a ratio of 3:1. Successful insertion (clone 2) was confirmed by restriction digestion of resultant plasmids with Sal1 and Xba1 to give bands corresponding to the cut vector (~3000 bp) and the insert (~1800 bp) (Figure 4.15). The sequence of the cloned pCMV-GAL4-RaLP was then confirmed by DNA sequencing.

Having constructed the GAL4-RaLP vector, reporter assays were carried out. Introduction of a mammalian expression vector encoding the GAL4 DNA binding domain (pCMV-GAL4) into HEK 293 cells has no effect on activation on the GAL4-driven luciferase reporter (Figure 4.16). However when the cDNA encoding the transcriptional transactivation domain of VP16, is cloned downstream of the GAL4 DNA binding domain, expression of the GAL4 fusion protein induces reporter expression (Figure 4.16). When the GAL4-RaLP construct was introduced into HEK 293 cells, together with the Firefly luciferase reporter, the GAL4-RaLP fusion protein was seen to significantly activate the reporter to same extent as the positive control GAL4-VP16, showing significant difference in reporter activity compared to the GAL4 binding domain on its own ($p<0.05$) (Figure 4.16). Overall these results suggest that nuclear RaLP has the potential to induce gene expression.

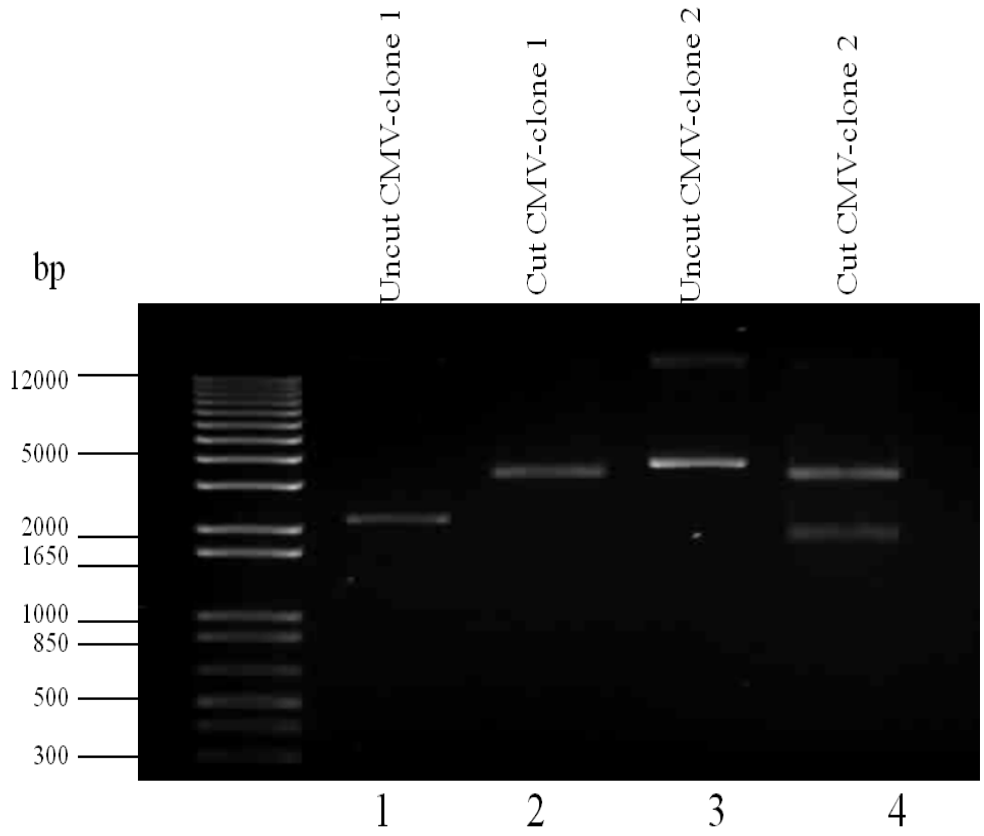

Figure 4.15 RaLP cloning into pCMV-GAL4 vector. A ligation reaction was set up using the digested RaLP, and pCMV-GAL4 vector in a ratio of 3:1. The following day, 2 µl of the ligation reaction was transformed into chemically competent DH5α bacteria. Plasmid was isolated from two individual colonies (lane 1 and 3). Double digestion was performed using Sal1 and Xba1 restriction enzymes and the result of digestion is shown in (lane 2 and 4).

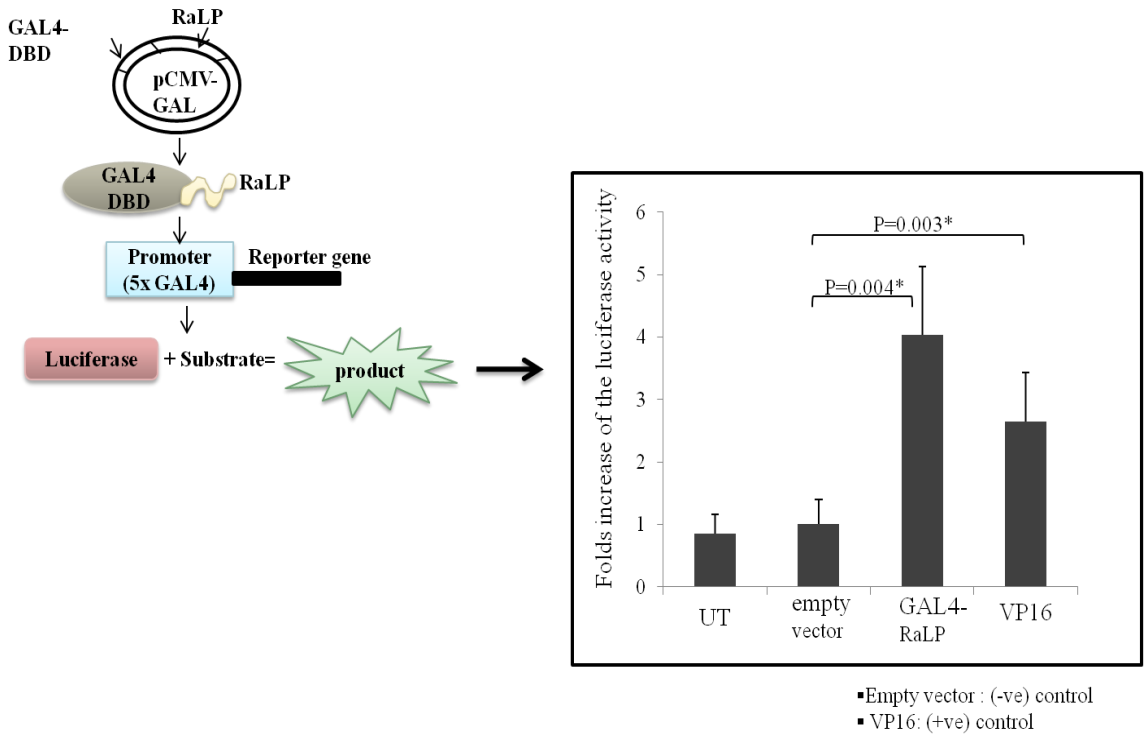

Figure 4.16 RaLP fused to the GAL4 DNA binding domain promotes transcription of a GAL4 dependent luciferase reporter. RaLP was cloned into pCMV-GAL4 vector, downstream of the GAL4 DNA binding domain (GAL4-RaLP). The ability of RaLP to induce gene transcription was determined using a GAL4 reporter plasmid, pG5LUC, in which the Firefly luciferase gene is driven by five GAL4 binding sites. For comparison the pCMV-GAL4 vector without insert, encoding the GAL4 DNA binding domain alone was used. As a positive control a construct encoding GAL4 DNA binding domain fused to the VP16 transactivation domain was used (GAL4-VP16). Transfection efficiency was normalised by Renilla luciferase activity, expressed from a separate plasmid (pRL-TK). Luciferase activity was measured in transfected and untransfected (UT) cells using a Dual Reporter assay. Luciferase activity is presented relative to that obtained from cells expressing the un-fused GAL4 DNA binding domain. Results represent the mean of three experiments, each performed in duplicate. Error bars represent standard error of mean. Calculated P values are indicated. *indicates $p<0.05$

4.3 Discussion:

Herein for the first time we found that the melanoma associated Shc adaptor RaLP shuttles between the cytoplasm and the nucleus. p52ShcA and p46ShcA members from Shc family were shown before to form a complex with Ran-GTPase and translocate to the nucleus in immortalized T-lymphocytes cells (George et al., 2009). In addition, immunohistochemical and western blot analysis revealed the presence of p46Shc in the nuclei of hepatic cancer cells as well as in normal gastric mucosa and cancer (Yoshida et al., 2004; Yukimasa et al., 2005). Consistent with the observation that RaLP can undergo nucleocytoplasmic shuttling, other adaptors like downstream of tyrosine kinase1 (DOK1) have been determined to shuttle between the nucleus and the cytoplasm and this shuttling relies on the state of tyrosine phosphorylation of DOK1 (Niu et al., 2006). The SH2B1 adaptor that is a normal cytoplasmic resident was shown to locate to the nucleus to mediate neurite growth in response to nerve growth factor stimulation in PC12 cells (Maures et al., 2010).

Treatment of cells expressing exogenous and endogenous RaLP with LMB, a cytotoxic drug known to paralyse CRM receptor, resulted in nuclear sequestration of RaLP. To further investigate this finding, mutation of the hydrophobic residues at L86, I87 and M90 within the LCTLIRPM motif revealed striking accumulation of RaLP in the nucleus. CRM export receptor recognises motifs that are rich in hydrophobic amino acids in the cargo protein, which then facilitates the cargo protein nuclear export. Taken together, it was deduced that RaLP nuclear export is mediated by CRM export receptor.

Different isoforms of Shc family members are known to be present different intracellular compartments, serving different roles, and hence provide the Shc family with functional diversity. It was suggested before that RaLP might exist as different versions (Jones et al., 2007) due to the presence of potential alternative initiation codons at its amino-terminus. When the full length RaLP is expressed in HEK 293 cells forms corresponding to the p59 and p49 proteins were observed (Jones et al., 2007). Moreover, investigating the RaLP expression profile in different parts of the brain using anti-RaLP antibody (produced by Jones and et al., 2007) revealed a band of ~75kDa as well as a band of ~58kDa in the cerebellum lysates (Jones et al., 2007). Based on this observation, it was postulated that RaLP shorter isoforms might naturally exist and have

different subcellular localisations. Interestingly, GFP tagged p49 and p59 forms of RaLP were predominantly present in the nucleus that suggesting that if these shorter isoforms exist naturally, they will be nuclear proteins. In addition a band of ~60 kDa was seen on western blot analysis of DAUV and HEK 293 lysates in addition to a band at ~70 kDa with anti-RaLP antibody (4443), which might suggest that the p59 isoform exists naturally in DAUV melanoma and HEK 293 cell lines. Although, this observation has suggested the presence of RaLP shorter isoforms, further experimental work is required to prove the real existence of RaLP shorter versions.

In an attempt to explore the nuclear localisation mechanism of RaLP, a motif rich of basic amino acids was revealed in the RaLP-PTB domain (KKRK) that could represent a nuclear localisation signal (NLS). Mutating the predicted NLS mislocated a small portion of GFP-p59, which is mainly present in the nucleus, to the cytoplasm suggesting a partial impact of this region on RaLP nuclear translocation. RaLP nuclear transport might be independent of the predicted NLS as other proteins such as β-catenin has been shown to translocate to the nucleus without relying on the ordinary NLS, or importin-dependent nuclear import mechanism (Fagotto et al., 1998).

On the other hand, our data showed that RaLP accumulates in the nucleus when the cells are exposed to oxidative stress. Notably, in previous reports cells treated with agents that induce DNA damage e.g. IR, UV, cisplatin and H_2O_2, resulted in EGFR translocation to the nucleus. A role in the DNA repair process was suggested based on EGFR association with DNA-dependent protein kinase (DNAPK) (Xu et al., 2009; Liccarddi et al., 2011). Phosphorylation of EGFR on tyrosine 1148 and 1173 is required for UV-mediated nuclear translocation of EGFR, and interestingly these phosphotyrosine residues bind the adaptor protein ShcA, which might suggest a role of Shc in EGFR nuclear translocation (Xu et al., 2009). Since RaLP is a known downstream adaptor to the EGFR and our data showed RaLP nuclear translocation in response to H_2O_2 treatment, we proposed that either RaLP becomes phosphorylated by EGFR, or could possibly form a complex with EGFR, which in turn facilitates RaLP translocation to the nucleus. RaLP and EGFR association in the nuclear fraction after different stimuli needs to be determined. In addition it is of interest to investigate whether RaLP nuclear translocation in response to oxidative stress promotes an apoptotic or anti-apoptotic signal. Alternatively, RaLP nuclear import might occur in response to some signal allowing RaLP phosphorylation that might be required to yield

an appropriate transport signal resulting in redistribution of RaLP in the cell. It was shown previously that stimulating cells with 12-O-tetradecanoylphorbol-13-acetate (TPA) phosphorylates an SPS motif on ERK, which lacks the canonical NLS, facilitating its nuclear transport (Chuderland et al., 2008).

Treating 518.A2 melanoma cells as well as FLAG-RaLP expressing human embryonic kidney cells with 5 mM of H_2O_2 for 1 hr resulted in RaLP nuclear translocation. A point might be raised, whether the 5 mM H_2O_2 might perturb the active nuclear transport machinery and subsequently this might affect our interpretation of RaLP nuclear localisation. A study by Kodiha and et al showed that 1 hr treatment with 10 mM H_2O_2 was shown to be optimal to mislocalise a fraction of NLS-GFP to the cytoplasm while at lower concentrations of hydrogen peroxide NLS-GFP persisted in the nuclei (Kodiha et al., 2004). Based on that, it was deduced that the H_2O_2 < 10 mM had not affected the nuclear transport components, which suggests that RaLP nuclear transport might be facilitated by the ordinary nuclear transport mechanisms at 5 mM H_2O_2 concentration.

Examination of the CH1 domain of RaLP reveals six cysteine residues and two histidine residues that are conserved between mouse and human RaLP, but completely absent from other Shc proteins. Such cysteine and histidine rich regions often represent zinc binding regions that are common in proteins that associate with the DNA (Bulyk et al., 2001). Accordingly, it was thought to study RaLP association with the DNA in a crude test by isolating DNA associated proteins from HEK 293 cells that stably express FLAG-RaLP. In addition RaLP was immunoprecipitated from the chromatin fraction of DAUV cells providing preliminary evidence that RaLP may associate with chromatin. This result still requires more confirmation by employing more techniques for instance; DNase footprinting, gel shift assay, or ChIP on chip assay that may provide the DNA sequence with which RaLP associates. Oxidative stress might possibly attenuate or strengthen RaLP association with DNA; or translocation of RaLP to the nucleus in response to oxidative stress may have a role independent of DNA association, this will indeed require more investigation.

Our results present a possible role of RaLP in gene transcription; however, it is not clear whether RaLP transactivates a specific DNA sequence directly or indirectly via its

association with a transcription complex. On the other hand, RaLP possesses two domains that are rich in proline residues, and such regions in other proteins have been determined to play role in transcription, for instance the PXXP motif was reported to contribute in the transcriptional role of the p63 protein (Helton et al., 2008). Interesting enough, RaLP has the same motif in the amino-terminal CH2 domain.

Although our preliminary reporter assays raise the interesting idea that RaLP might assist in gene transcription, we still should include more controls to test whether an insertion of a control DNA upstream of GAL4-DBD produces the same result as RaLP.

The fact that RaLP is present in both the cytoplasmic and the nuclear compartments provides RaLP potential diversity in its function, a lot of work needs to be carried out in order to explore and characterise the exact role of the novel melanoma associated adaptor RaLP/ShcD in the nucleus.

Chapter 5

Stable cell lines Characterisation

5.1 Introduction and the targets of the chapter:

One of the approaches to study a newly identified protein is to generate a stable cell line that allows an exogenous piece of DNA to integrate with the genome and provide a stable expression of the exogenous protein. Thus, by comparing the generated stable cell lines with the parental counterparts, it may be possible to pinpoint the difference between the two cell lines due to the expression of the exogenous protein. As well, the stable expression of a protein allows us to avoid the toxic effect that results from the transfection reagents. Furthermore, stable expression of a protein provides an advantage that the whole cell population expresses the exogenous protein, which makes it more reliable for comparison with the parental counterparts.

As described in chapter 4, RaLP undergoes nuclear translocation in response to oxidative stress. This prompted us to investigate the effect of the oxidative stress on RaLP phosphorylation status that might play a role in RaLP nuclear translocation or explain the role of RaLP in the nucleus. The p66ShcA-CH2 domain houses a serine residue, Ser36, which gets phosphorylated upon exposure to ultraviolet light and H_2O_2 (Migliaccio et al., 1999; Le et al., 2001). Likewise, RaLP possesses a CH2 domain that contains potential serine and threonine phosphorylation sites, which might represent possible substrates for certain kinases according to the GPS 2.1 phophorylation prediction programme (Figure 5.1). In order to determine whether H_2O_2 induces phosphorylation of RaLP at specific sites, immunoprecipitation of GFP-RaLP from GFP-RaLP stably-transfected cell line was performed together with mass spectrometry to identify phosphopeptides.

As the exact molecular mechanism by which RaLP contributes in the intracellular signalling cascades is not yet known, it was thought that by performing immunoprecipitation experiments it would be possible to identify potential interacting partners for RaLP by utilising the GFP-RaLP stably expressing cell line, the GFP-trap technology and mass spectrometry.

Shc proteins have been shown before to have various contributions to the biological machinery of the cell. ShcA isoforms play a role in cell cycle progression, cell differentiation and p66ShcA was determined to have a crucial impact on reactive oxygen species metabolism (Giorgio et al., 2005).

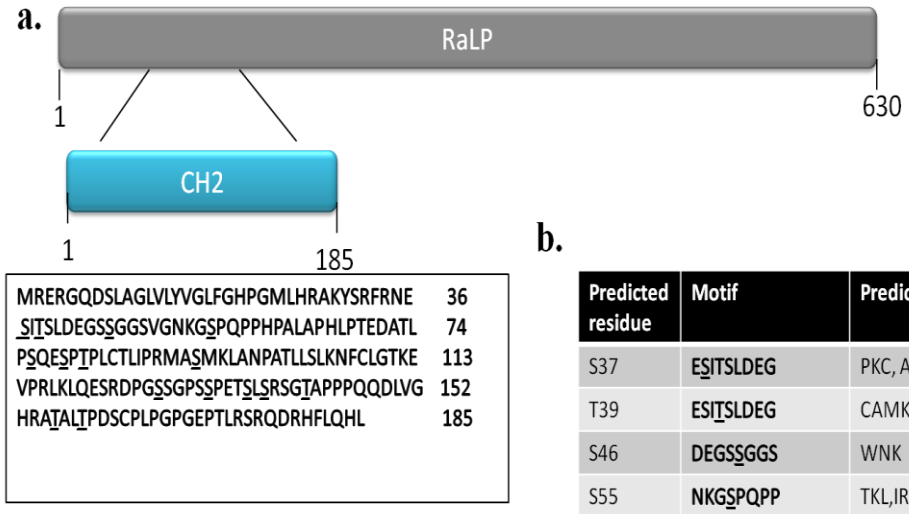

b.

Predicted residue	Motif	Predicted kinase/s
S37	**ESITSLDEG**	PKC, AKT1/2,PKA
T39	**ESITSLDEG**	CAMK,PDK
S46	**DEGSSGGS**	WNK
S55	**NKGSPQPP**	TKL,IRAK,p38
S76	**TLPSQESPT**	ERK,ATM,PIKK
S79	**SQESPTPLC**	ERK,JNK,p38,CDKs
T81	**ESPTPLCTLI**	CDK5
S92	**RMASMKLA**	SGK
S127	**DPGSSGPSSP**	IKK,GRK,BARK
S132	**GPSSPETSLS**	ERK,p38,JNK,DYRK,CDKs,PKR,FRAP,PIKK
S136	**PETSLSRSGT**	ILK
S138	**TSLSRSGTAP**	AKT
T142	**RSGTAPPPQ**	RSK,MAPKAPK,DMPK,CAMK
T156	**HRATALTPD**	GARK
T159	**TALTPDSCP**	ERK,p38,JNK,CDKs,PKB,MAP2K1

Figure 5.1 Potential phosphorylated serines and threonines in the CH2 domain of RaLP. (a) Schematic representations showing the sequence of the CH2 domain of RaLP (1-185aa) and the predicted sites of phosphorylation of Serine (S) and Threonine resides (T) using the GPS 2.1 phosphorylation prediction programme. (b) Table shows the predicted S and T residues and the motifs contained within the CH2 domain. In addition a summary of the kinases that might phosphorylate the predicted residues are indicated. The kinases were selected by choosing a high threshold setting of 1 or more from the cutoff score. PKC: protein kinase C; AKT1/2 or PKB: protein kinase B; PKA: protein kinase A; CAMK: Ca2+/Calmodulin-dependent protein kinase; PDK: pyruvate dehydrogenase kinase; WNK: lysine deficient protein kinase; TKL: tyrosine kinase-like; IRAK: Interleukin-1 receptor-associated kinase; p38: a mitogen activated protein kinase; ERK: extracellular signal regulated kinase; JNK: c-Jun N-terminal kinase; CDKs: Cyclin dependent kinase; SGK: Serine/threonine-protein kinase; IKK: Inhibitor of KappaB Kinase; GRK: G Protein-Coupled Receptor Kinase; BARK: Beta-Adrenergic Receptor Kinase; DYRK: Dual Specificity Tyrosine Phosphorylation Regulated Kinase; PKR: Protein kinase RNA-activated; FRAP: FKBP12-rapamycin-associated protein or mTOR; PIKK:Phosphatidylinositol 3-kinase-related kinases; ILK: integrin-linked kinase; RSK:ribosomal S6 kinase; MAPKAPK: MAP kinase-activated protein kinase; DMPK: dystrophia myotonica-protein kinase; MAP2K1: Dual specificity mitogen-activated protein kinase kinase 1.

On the other hand, Sli (ShcB) and Rai (ShcC) were determined to play a role in neuronal survival and differentiation (Sakai et al., 2000; Miyake et al., 2009). Therefore, it was of interest to utilise the stable cell lines to attempt to establish a cellular role for RaLP.

5.2 Results:

5.2.1 Mass spectrometry analysis to identify RaLP phosphorylation and RaLP interacting partners:

5.2.1.1 Immunoprecipitation of GFP-RaLP and its associated proteins from G5 lysates using GFP-trap

Phosphorylation is not only crucial for intracellular signal propagation and regulation but can also play a role in protein import into the nucleus. In this regard, we planned to screen for RaLP phosphorylation motifs to understand the mechanisms of RaLP nuclear- cytoplasmic shuttling as well as its phosphorylation status in response to stress. GFP-RaLP was pulled down by GFP-trap from cell extracts, which were obtained from H_2O_2 treated and untreated GFP-RaLP stably expressing cells (G5) (Figure 5.2). Untreated HEK 293 cell extracts were also incubated with the GFP-trap to serve as a negative control to determine the specificity of the GFP-RaLP associated proteins (Figure 5.2). The GFP-RaLP bands (~100 kDa) from both H_2O_2 treated or untreated cells were excised and digested with trypsin and analysed with LTQ-Orbitrap mass spectrometry. Interestingly, the phosphopeptide analysis of RaLP by mass spectrometry highlighted a phosphorylated Thr156 or Thr159 (HRA<u>T</u>AL<u>T</u>PDS) within the RaLP-CH2 domain (1-185 amino acids) in hydrogen peroxide treated cells when compared with untreated counterparts (Table 5.1a). Furthermore, RaLP was found to be phosphorylated with or without hydrogen peroxide treatment on Ser132 (SGPS<u>S</u>PET) housed in the CH2 domain and on Ser510 or Ser511 (QPA<u>SS</u>HSLP) included in the CH1 domain of RaLP (Table 5.1a). It is worth to mention that the coverage sequence was 67% for GFP-RaLP obtained from both H_2O_2 treated and untreated cells, therefore more phosphorylated residues would have been detected if the coverage perecentage is higher (Table 5.1b). An alignment of the amino-terminal of different human Shc proteins (RaLP/ShcD, ShcA, ShcB and ShcC) revealed that all the detected phosphorylated motifs on the CH2 and the CH1 domains of RaLP are not conserved on the other Shc family members (Figure 5.3; Figure 3.1).

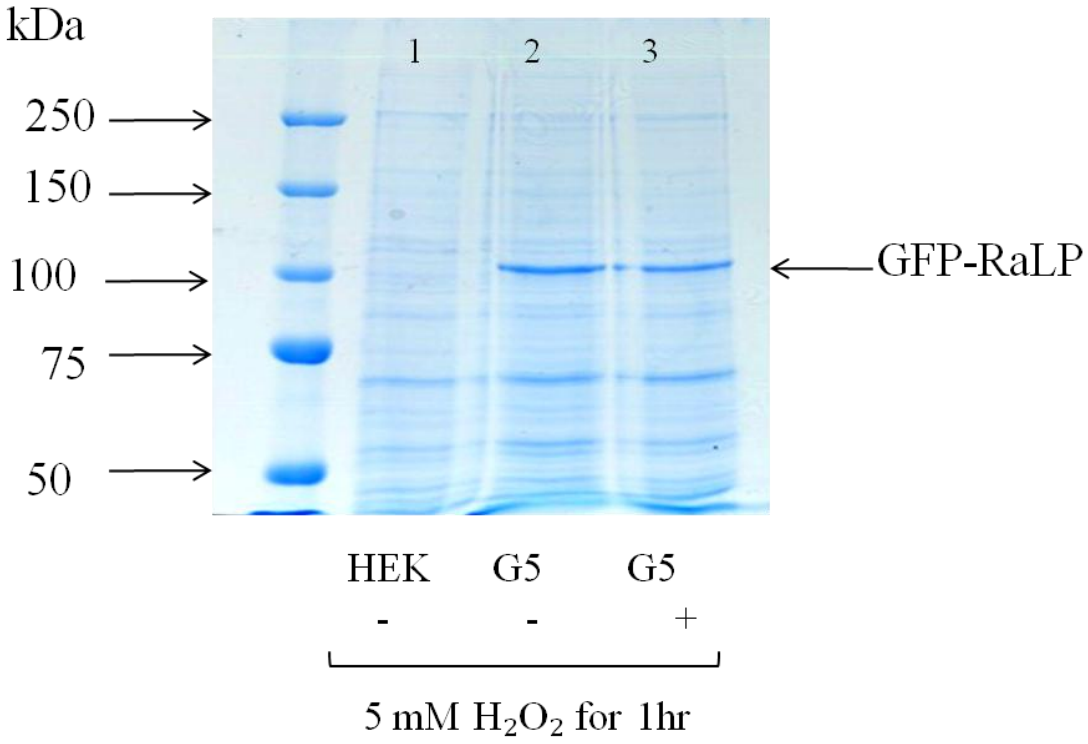

Figure 5.2 Investigating the phosphorylation status of RaLP upon H_2O_2 treatment and Identifying RaLP interacting partners employing mass spectrometry. GFP-RaLP stably expressing cells (G5) were either treated with 5 mM H_2O_2 for 1 hr or left untreated. The cells were then lysed by HiLO buffer, sonicated and the clear supernatant was collected after subsequent rounds of centrifugation. The clear lysates that were obtained from treated G5, untreated G5 or untreated parental HEK 293 cells were incubated with GFP-trap for 2 hr at 4ºC. The immunoprecipitated GFP-RaLP and the associated proteins were all resolved on a 6% SDS-PAGE gel. The gel was stained with Instant Blue coomassie stain and after destaining the bands corresponding to GFP-RaLP with or without treatment were sent for trypsinization and analysed for the presence of phosphopeptide. A strip (1, 2 or 3) was taken of the gel and analysed by LCMS/MS for protein identification.

a.

Phosphopeptides identified

Untreated with H_2O_2	Treated with H_2O_2	Domain
124 DPGSSGPS**S**PETSLSR 139 (132)	124 DPGSSGP**SS**PETSLSR 139 (132)	CH2 (1-185 aa)
155 ATALTPDSCPLPGPGEPTLR 174 (156, 159)	155 A**T**AL**T**PDSCPLPGPGEPTLR 174 (156, 159)	CH2 (1-185 aa)
496 APETVQPGATAQPA**SS**HSLPHIK 518 (510/511)	496 APETVQPGATAQPA**SS**HSLPHIK 518 (510/511)	CH1 (370-525 aa)

b. **i. Untreated with H_2O_2**

Sequence coverage 67%

```
  1 MRERGQDSLA GLVLYVGLFG HPGMLHRAKY SRFRNESITS LDEGSSGGSV
 51 GNKGSPQPPH PALAPHLPTE DATLPSQESP TPLCTLIPRM ASMKLANPAT
101 LLSLKNFCLG TKEVPRLKLQ ESRDPGSSGP SSPETSLSRS GTAPPPQQDL
151 VGHRATALTP DSCPLPGPGE PTLRSRQDRH FLQHLLGMGM NYCVRYMGCV
201 EVLQSMRSLD FGMRTQVTRE AISRLCEAVP GANGAIKRRK PPVKFLSTVL
251 GKSNLQFSGM NIKLTISTCS LTLMNLDNQQ IIANHHMQSI SFASGGDPDT
301 TDYVAYVAKD PVNQRACHIL ECHNGMAQDV ISTIGQAFEL RFKQYLKNPS
351 LNTSCESEEV HIDSHAEERE DHEYYNEIPG KQPPVGGVSD MRIKVQATEQ
401 MAYCPIQCEK LCYLPGNSKC SSVYENCLEQ SRAIGNVHPR GVQSQRDTSL
451 LKHTCRVDLF DDPCYINTQA LQSTPGSAGN QRSAQPLGSP WHCGKAPETV
501 QPGATAQPAS SHSLPHIKQQ LWSEECYHGK LSRKAAESLL VKDGDFLVRE
551 SATSPGQYVL SGLQGGQAKH LLLVDPEGKV RTKDHVFDNV GHLIRYHMDN
601 SLPIISSGSE VSLKQPVRKD NNPALLHSNK
```

ii.Treated with H_2O_2

Sequence coverage 67%

```
  1 MRERGQDSLA GLVLYVGLFG HPGMLHRAKY SRFRNESITS LDEGSSGGSV
 51 GNKGSPQPPH PALAPHLPTE DATLPSQESP TPLCTLIPRM ASMKLANPAT
101 LLSLKNFCLG TKEVPRLKLQ ESRDPGSSGP SSPETSLSRS GTAPPPQQDL
151 VGHRATALTP DSCPLPGPGE PTLRSRQDRH FLQHLLGMGM NYCVRYMGCV
201 EVLQSMRSLD FGMRTQVTRE AISRLCEAVP GANGAIKRRK PPVKFLSTVL
251 GKSNLQFSGM NIKLTISTCS LTLMNLDNQQ IIANHHMQSI SFASGGDPDT
301 TDYVAYVAKD PVNQRACHIL ECHNGMAQDV ISTIGQAFEL RFKQYLKNPS
351 LNTSCESEEV HIDSHAEERE DHEYYNEIPG KQPPVGGVSD MRIKVQATEQ
401 MAYCPIQCEK LCYLPGNSKC SSVYENCLEQ SRAIGNVHPR GVQSQRDTSL
451 LKHTCRVDLF DDPCYINTQA LQSTPGSAGN QRSAQPLGSP WHCGKAPETV
501 QPGATAQPAS SHSLPHIKQQ LWSEECYHGK LSRKAAESLL VKDGDFLVRE
551 SATSPGQYVL SGLQGGQAKH LLLVDPEGKV RTKDHVFDNV GHLIRYHMDN
601 SLPIISSGSE VSLKQPVRKD NNPALLHSNK
```

Table 5.1 Summary of the result of the phosphopeptide analysis by LTQ-Orbitrap mass spectrometry. GFP-RaLP stably expressing cells (G5) were either treated with 5 mM H_2O_2 for 1 hr or left untreated. The immunoprecipitated GFP-RaLP from the two cell populations was resolved on a 6% SDS-PAGE gel that was then coomassie stained. GFP-RaLP bands were then excised from the gel and trypsinized. (a) Phosphopeptide analysis was conducted using LTQ-Orbitrap mass spectrometry. The same result was obtained from three independent experiments. aa: amino acids. Residues in red indicate phosphorylated residues. (b) The coverage sequence for GFP-RaLP obtained from untreated (i) and treated (ii) samples is in red. The underlined sequence (1-185 aa) represents the CH2 domain, while (370-525 aa) represents the CH1 region.

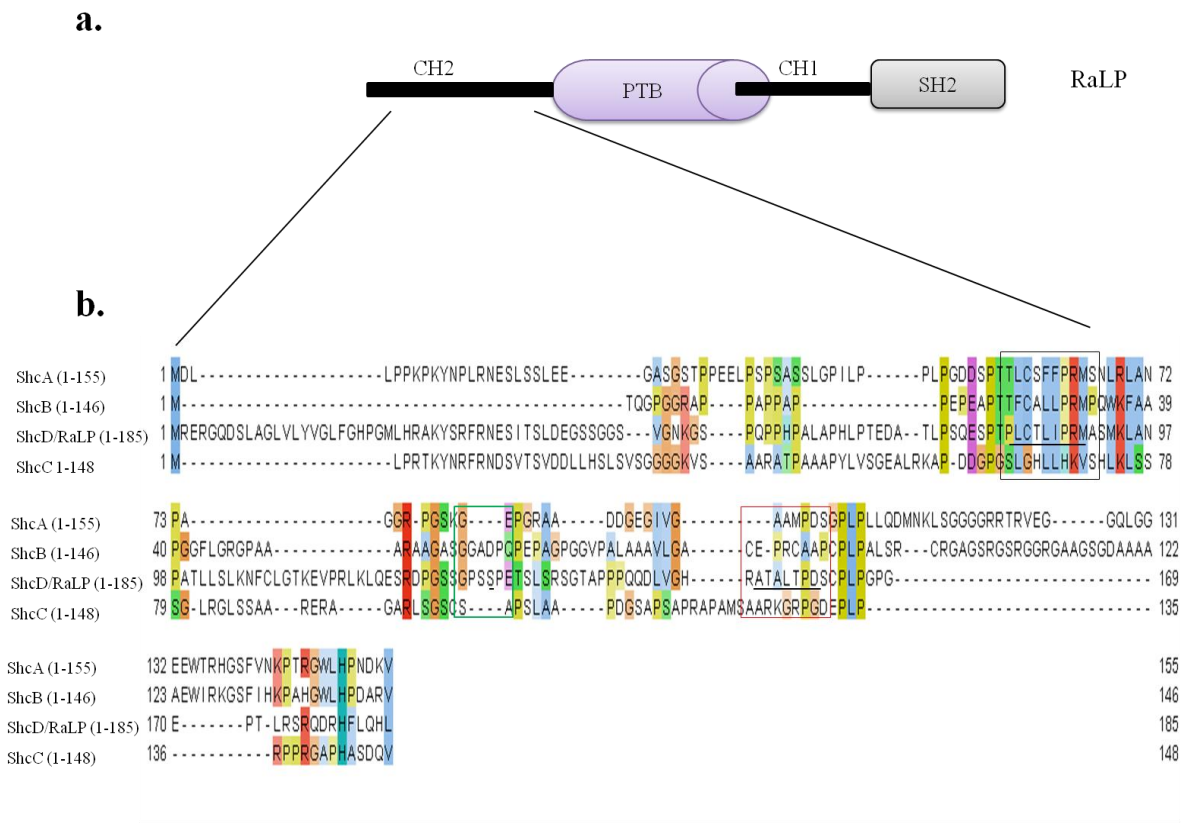

Figure 5.3 The phosphorylated residues on RaLP are not conserved among Shc proteins. (a) Schematic illustration of RaLP domains. (b) The CH2 domain of RaLP was aligned with the amino-terminal region of other Shc proteins (ShcA, ShcB and ShcC). The alignment was performed using T-coffee multiple alignment programme and Jalview software. The uniprot identifiers for the aligned proteins are as defined earlier. The red square shows the non conserved ATALTPD motif. The green square indicated GPSSP motif and the black square indicates the RaLP identified nuclear export signal (LCTLIPRM).

Each lane on the coomassie stained gel was excised separately and trypsinized to identify the GFP-RaLP associated proteins using an LTQ-Orbitrap mass spectrometer. Mass spectrometry is a sensitive technique; therefore, we needed to set inclusion criteria by which certain proteins can be considered as RaLP interacting partners. The protein should not be present in the negative control, a specific protein should be identified in at least two independent experiments, and the protein should be represented by at least 2 peptides with a significant score ($p<0.05$). After following these criteria it was possible to draw a table of all the proteins that followed the criteria with their cellular distribution and brief description to their function (Table 5.2).

In summary, employing GFP-RaLP stably expressing cells, GFP-trap and the mass spectrometry technique it was possible to identify phosphorylation sites on RaLP induced upon oxidative stress, and also to identify possible interacting partners for RaLP.

5.2.1.2 Confirmation of some of the possible RaLP interacting partners using coimmunoprecipitation and western blotting:

In order to confirm some of the potential interacting partners of RaLP, coimmunoprecipitation experiments were employed. Anti-GFP antibody was able to immunoprecipitate GFP-RaLP from G5 lysates (Figure 5.4). GFP-RaLP was found to associate with general vesicular factor p115 (p115), nuclear pore complex protein (p107) and transcription intermediary factor-1β (TIF-1β) (Figure 5.4). The immunoprecipitation was repeated three times but a faint band was always present in the negative control (IgG) (Figure 5.4), which was a concern. Immunoprecipitations were performed the opposite way round using anti-TIF-1β or anti-p115 antibodies to further confirm RaLP association with the endogenous TIF-1β and p115. TIF-1β and p115 proteins were successfully immunoprecipitated with their antibodies (Figure 5.5a, b). In the TIF-1β immunoprecipitates, a band corresponding to GFP-RaLP was observed but a band of a similar intensity was detected in the negative control (Figure 5.5a), which made us sceptical about the certainty of the RaLP and TIF-1β association. While in p115 immunoprecipitates, GFP-RaLP was detected but no band was seen in the negative control (Figure 5.5b).

Name of the protein	Localisation	Function
Nuclear pore complex protein Nup107	Nuclear pore and kinetochore during mitosis	Required for the assembly of peripheral proteins into the nuclear pore complex and phosphorylated upon DNA damage
Melanoma associated antigen D2	Nucleus and cytoplasm	Tumour antigen and phosphorylated upon DNA damage
Calcium-binding mitochondrial carrier protein Aralar2/1	Mitochondria	Present in the mitochondrial inner membrane and have a role in calcium metabolism
Mono functional C1-tetrahydrofolate synthase	Mitochondria	ATP metabolism
CCR4-NOT transcription complex subunit 1	Nucleus, cytoplasm and P-bodies	Transcriptional repressor
Tubulin beta 4/6 chain	Cytoskeleton and cytoplasm	Microtubule structure and phosphorylated upon DNA damage
Trifunctional enzyme subunit alpha	Mitochondria	Fatty acid metabolism
DnaJ homologue subfamily C/A	Cell membrane	May have an important role in presynaptic function
General vesicular transport factor p115	Cytoplasm and golgi appratus	Golgi assembly and biogenesis
Transcription intermediary factor 1-beta	Nucleus	Nuclear corepressor for KRAB domain-containing zinc finger proteins
Apoptosis inducing factor 1	Mitochondria	Translocated from the mitochondria to the nucleus to function as a proapoptotic factor in a caspase-independent pathway, while in normal mitochondria, it functions as an antiapoptotic

Table 5.2 RaLP potential interacting partners. Summary of the proteins that were found to associate with GFP-RaLP following certain inclusion criteria; 2 peptides that each have a $p<0.05$, not present in the negative control, and the protein was identified in two or more independent experiments out of three independent experiments.

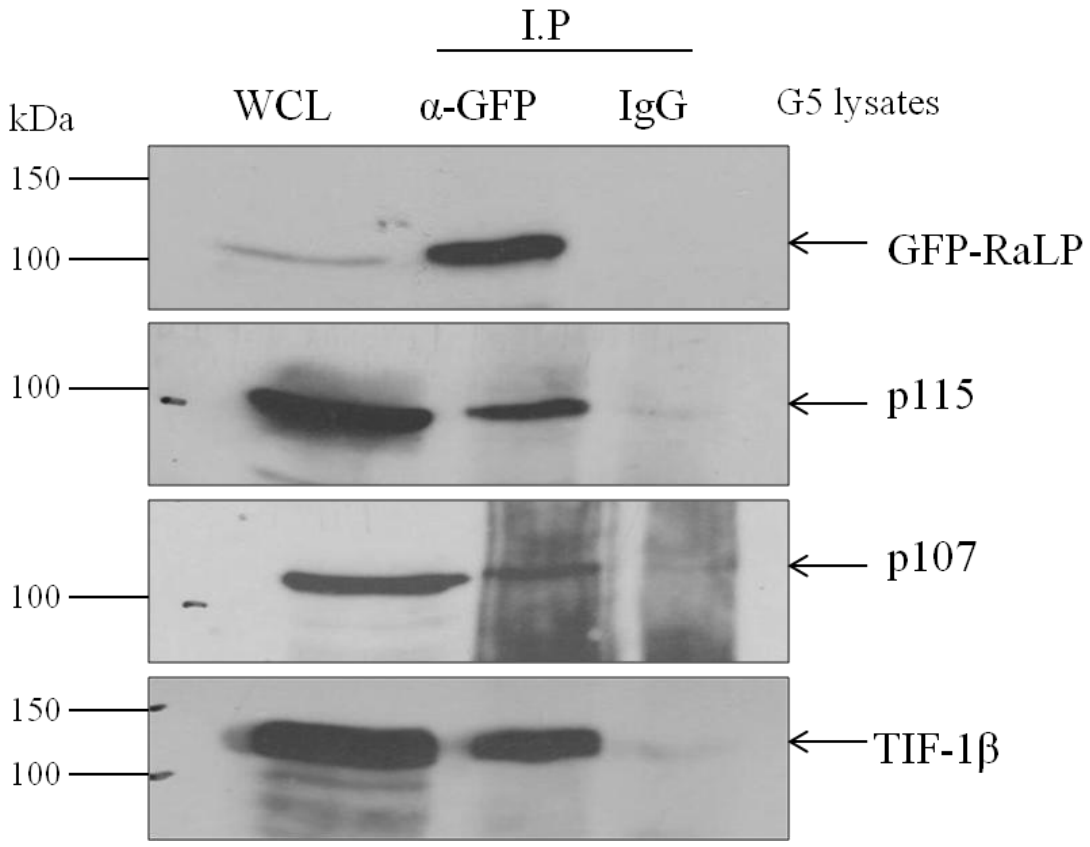

Figure 5.4 Testing some of the potential RaLP interacting partners using coimmunoprecipitation. A 10 cm dish of GFP-RaLP expressing cells (G5) was lysed with HiLO buffer. After sonication, the clear cell extract was incubated with either 3 µg of immobilised anti-GFP antibody or mouse IgG with tumbling overnight at 4°C. The immunoprecipitated proteins along with 1/10 of the whole cell lysates (WCL) were resolved on a 6% SDS-PAGE gel. Western blotting was then performed using anti-GFP, anti-p115 (General vesicular transport factor p115), anti-p107 (Nuclear pore complex protein Nup107) or anti-TIF-1β (Transcription intermediary factor 1-beta) antibodies, all at 1:1000 dilution.

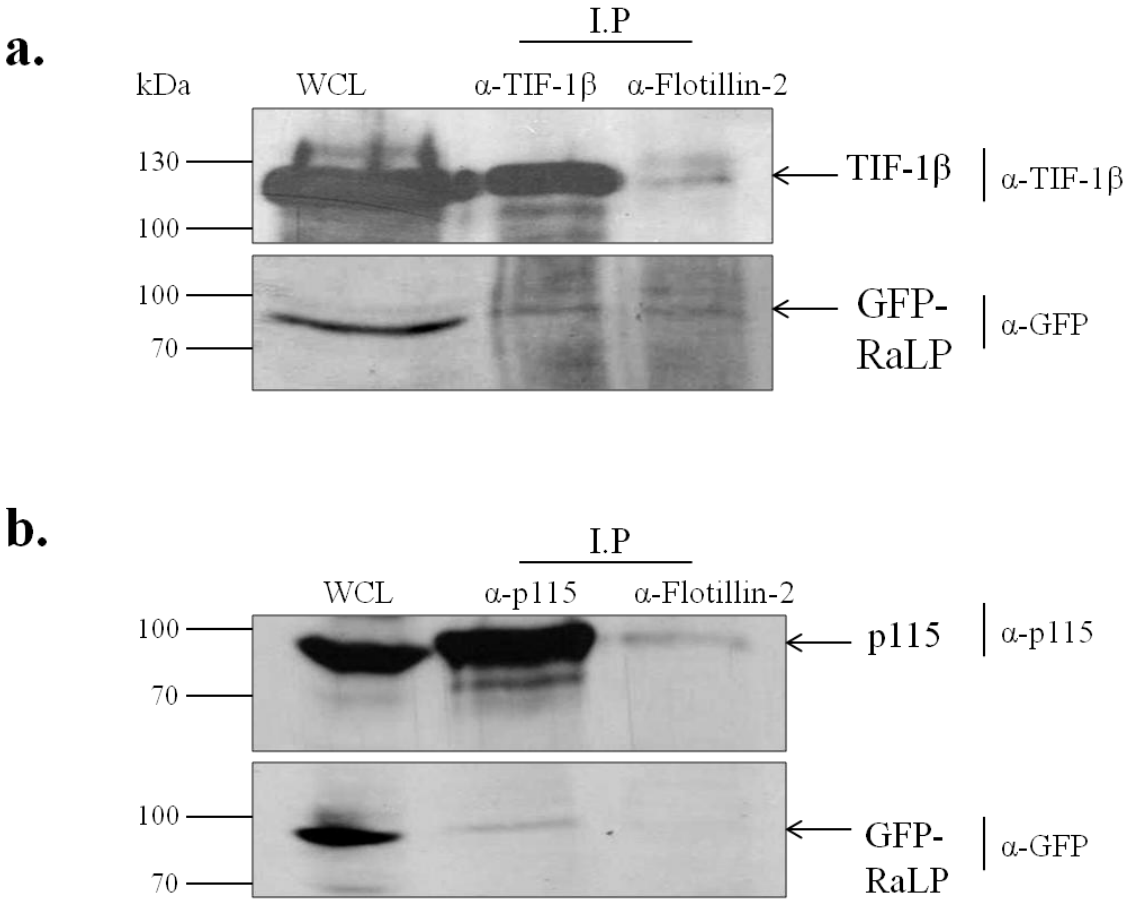

Figure 5.5 Coimmunoprecipitation to further test the association of RaLP with its potential interacting partners. Cell lysates obtained from GFP-RaLP expressing cells (G5) were incubated with 3 µg of either immobilised anti-TIF-1β (a) or anti-p115 (b) or with control antibody (α-Flotillin-2) (a, b). The immunoprecipitates along with 1/10 of the whole cell lysates were then resolved on a 6% SDS-PAGE gel. Immunoblotting analysis using anti-TIF-1β (a), anti-p115 (b) or anti-GFP (a, b) antibodies was performed.

These findings suggest that general vesicular factor p115 (p115) and nuclear pore complex (p107) might be potential interacting partners for RaLP, although these observations need more confirmation by testing whether endogenous RaLP interacts with these proteins in untransfected cells. Because we had a shortage of anti-p107 antibody, it was not possible to perform the reciprocal immunoprecipitation. Therefore, in the future reciprocal immunoprecipitation with anti-p107 needs to be conducted to confirm whether RaLP can associate with p107.

5.2.2 Properties of FLAG-RaLP stably expressing cells compared to their parental counterparts:

5.2.2.1 FLAG- RaLP expressing cells differ in cell cycle profile from their parental counterparts:

The cells that stably express FLAG-RaLP (F4) and their parental counterparts HEK 293 cells were collected and fixed followed by DNA staining using propidium iodide. The cell cycle profiles were analysed using flow cytometry. The cell cycle has four defined phases; two are gap phases (G1 and G2) in which cells grow and check on the perfection of all the steps required for successful cell division. DNA synthesis occurs during the S-phase, which is interlinked by the two gap phases. Eventually, the production of two daughter cells happens in mitosis (M-phase) (Kastan and Bartek, 2004). F4 cells demonstrated higher percentages of cells in G1 phase ($p=0.009<0.05$) as well as in G2 ($p=0.019<0.05$) when compared with HEK 293 cells. A drop in the percentage of S phase cells was observed in F4 ($p=0.01<0.05$) in contrast to HEK 293 cells (Figure 5.6a and b). From this experiment, a conclusion was drawn that FLAG-RaLP stably expressing cells exhibited G1 and G2 arrest when compared with their parental counterparts.

5.2.2.2 The reason behind G1 and G2 arrest in FLAG-RaLP expressing cells:

To gain further understanding into the molecular alterations in FLAG-RaLP expressing cells that resulted in the G1 and G2 arrest, p21/cip level, which is a known marker for G1 and G2 arrest, was compared in F4s and HEK 293 cells. Cell lysates that were obtained from subconfluent F4 and HEK 293 cells were resolved on an SDS-PAGE gel.

a.

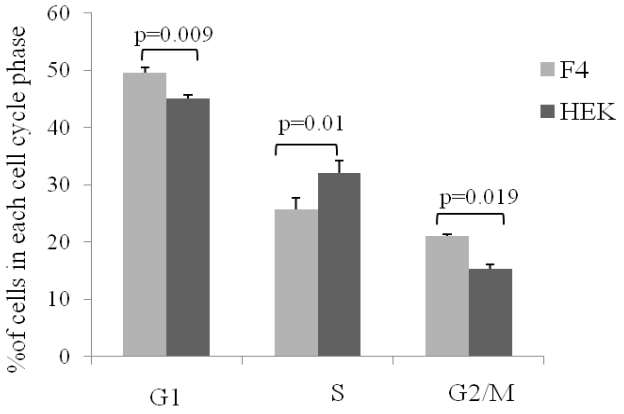

b.

(i) Parental cell line

Experiment Name:	19-7
Specimen Name:	Specimen_001
Tube Name:	-RX HEK
Record Date:	Jul 19, 2011 9:37:41 AM
$OP:	Samrein
GUID:	ff2fa07a-2f42-4d8c-a1b9-e34f5402e814

Population	#Events	%Parent	PE-A Min	PE-A Max	PE-A Mean
P1	5,671	56.7	11,876	116,159	66,965
P2	175	3.1	11,876	46,079	39,662
P3	2,520	44.4	46,785	58,247	52,130
P4	2,070	36.5	58,275	92,800	74,475
P5	859	15.1	92,871	116,159	99,070

(ii) FLAG-RaLP expressing cells

Experiment Name:	19-7 f4
Specimen Name:	Specimen_001
Tube Name:	-f4
Record Date:	Jul 19, 2011 9:29:28 AM
$OP:	Samrein
GUID:	f8a79a9c-9a10-4bd3-a116-aa4cd4a11a4a

Population	#Events	%Parent	PE-A Min	PE-A Max	PE-A Mean
P1	5,775	57.8	7,724	126,428	70,799
P2	245	4.2	7,724	48,105	38,956
P3	2,773	48.0	47,444	63,670	54,710
P4	1,684	29.2	63,023	94,152	78,982
P5	1,184	20.5	94,191	126,428	101,919

Figure 5.6 The cells that stably express FLAG-RaLP showed a slightly higher percentage of cells in G1 and G2/M than the wt counterparts using flow cytometry. (a) Parental HEK 293 cells and FLAG-RaLP expressing cells (F4) were grown until they were ~ 50% confluent. The cells were then collected and fixed followed by DNA staining with propidium iodide (PI). The cell cycle profile of the two cell lines was checked using flow cytometry employing a BD FACS Canto™ II machine. The bar chart represents a pool of three experiments and shows the percentage distribution of the cells in the different cell cycle phases (G1, S and G2/M). Error bars represent standard error of means. (b) The tables show data from one experiment for each cell line parental HEK 293 cells (i) and F4 (ii). P3: % of cells in G1; P4: % of cells in S-phase; P5: % of cell in G2/M.

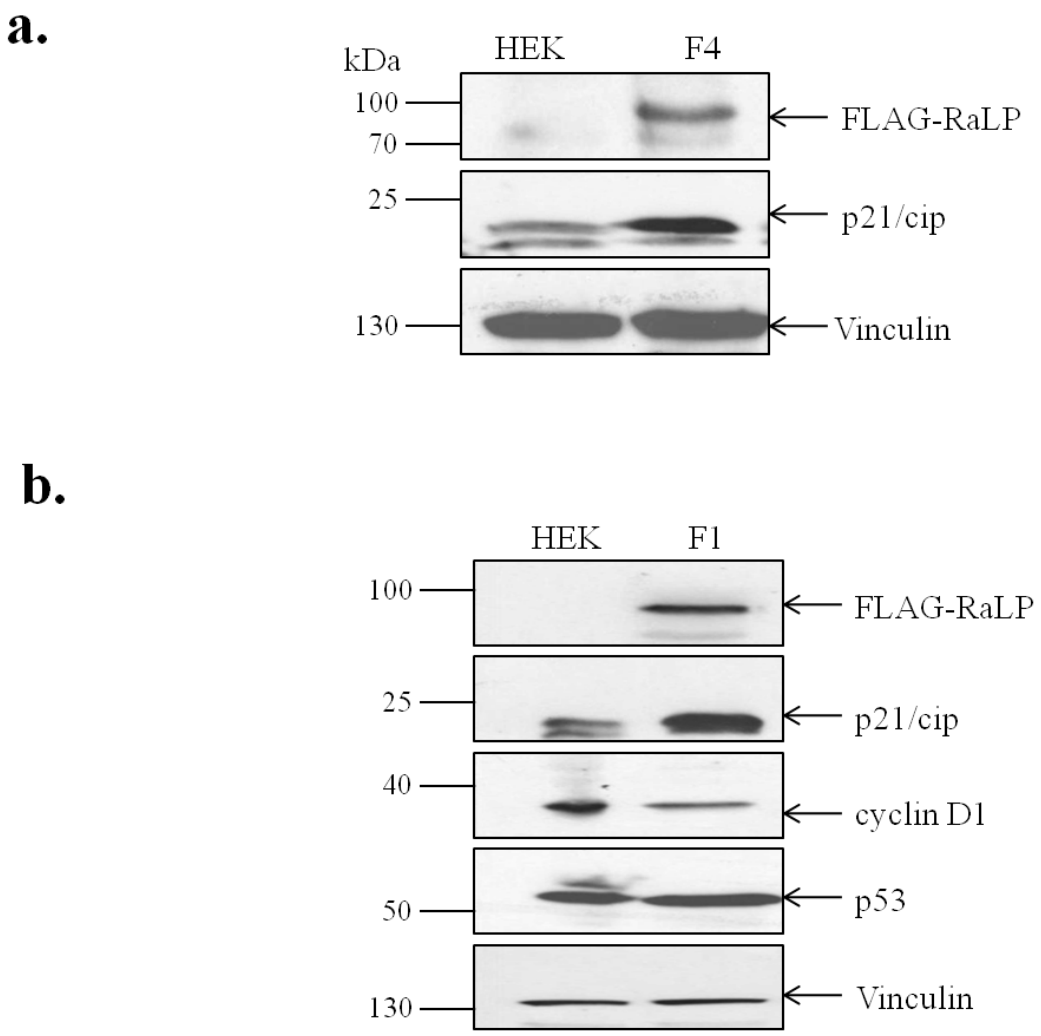

Figure 5.7 FLAG-RaLP expressing cells showed higher levels of p21 than their parental counterparts. (a) HEK 293 cells (HEK) and FLAG-RaLP expressing cells (F4) were seeded and grown to subconfluence and then lysed. Western blotting was then performed using anti-FLAG, anti-p21/cip or anti-vinculin antibodies at 1:1000 dilution. (b) A second clone (F1) was analysed similarly. FLAG-RaLP expressing cells (F1) along with their parental counterparts (HEK) were grown until they reached 60-70% confluence. The cells were then lysed followed by western blot analysis using anti-FLAG, anti-p21/cip, anti-cyclin D1, anti-p53 or anti-Vinculin antibodies.

Immunoblotting with p21/cip antibody revealed an upreglation of p21/cip in FLAG-RaLP expressing cells (F4) in comparison to HEK 293 cells (Figure 5.7a).
To exclude the possibility that the F4 had undergone additional mutations that are resulted in elevated p21 levels, the same experiment was repeated three times using another clone that expresses FLAG-RaLP (F1), which displayed the same increase in p21 expression (Figure 5.7b). In addition cyclin D1 level was determined to be downregulated in F1 cells when compared to HEK 293 cells. Accordingly, it was deduced that the upregulation of p21/cip is due to FLAG-RaLP expression rather than a mutation unique to any of the clones. p21/cip induction that was mediated by FLAG-RaLP might explain the G1 and G2 arrest observed in FLAG-RaLP expressing cells.

5.2.2.3 Transient transfected HEK 293 cells behave in a similar manner to stable cell lines:

To further rule out that the elevation in p21 levels in stable cell lines was an artefact due to clonal selection, transient transfections were performed. The cell lysate that was obtained from transiently transfected HEK 293 cells with FLAG-RaLP was compared against untransfected HEK 293 cells lysate. The cells that overexpressed FLAG-RaLP exhibited a higher level of p21/cip and lower level of cyclin D1 than their untransfected counterparts (Figure 5.8). This finding is consistent to what has been demonstrated by the stable cell lines.

5.2.2.4 RaLP full length but not RaLP that lacks the CH2 domain upregulates p21:

It was intriguing to observe that p21 expression was upregulated in cells overexpressing RaLP either stable cell lines or in transient transfectants, however we had not ruled out that this could be a stress response due to protein overexpression. Therefore, a control protein overexpression was considered to test whether the p21 upregulation is a specific observation due to RaLP protein expression. Since we believe that the least conserved CH2 domain of RaLP provides RaLP with unique function in the intracellular compartment, RaLP that lacks the CH2 domain was chosen to be our control (Figure 5.9a). HEK 293 cells this time were either left untransfected or transfected with FLAG-RaLP or FLAG-RaLPΔCH2 followed by western blot analysis.

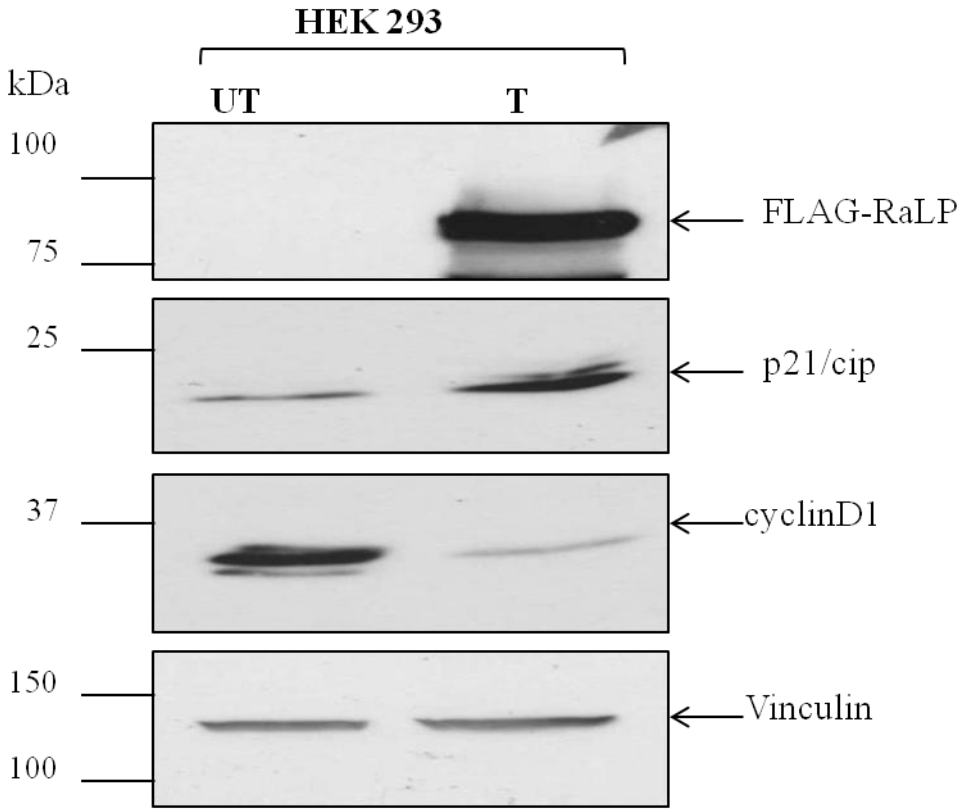

Figure 5.8 FLAG-RaLP transient transfection resulted in p21 upregulation. (a) HEK 293 cells were transiently transfected with FLAG-RaLP (T) or left untrasfected (UT). The cell lysates were then analysed by western botting using anti-FLAG, anti-p21/cip, anti-cyclinD1 or anti-Vinculin antibodies at 1:1000 dilution.

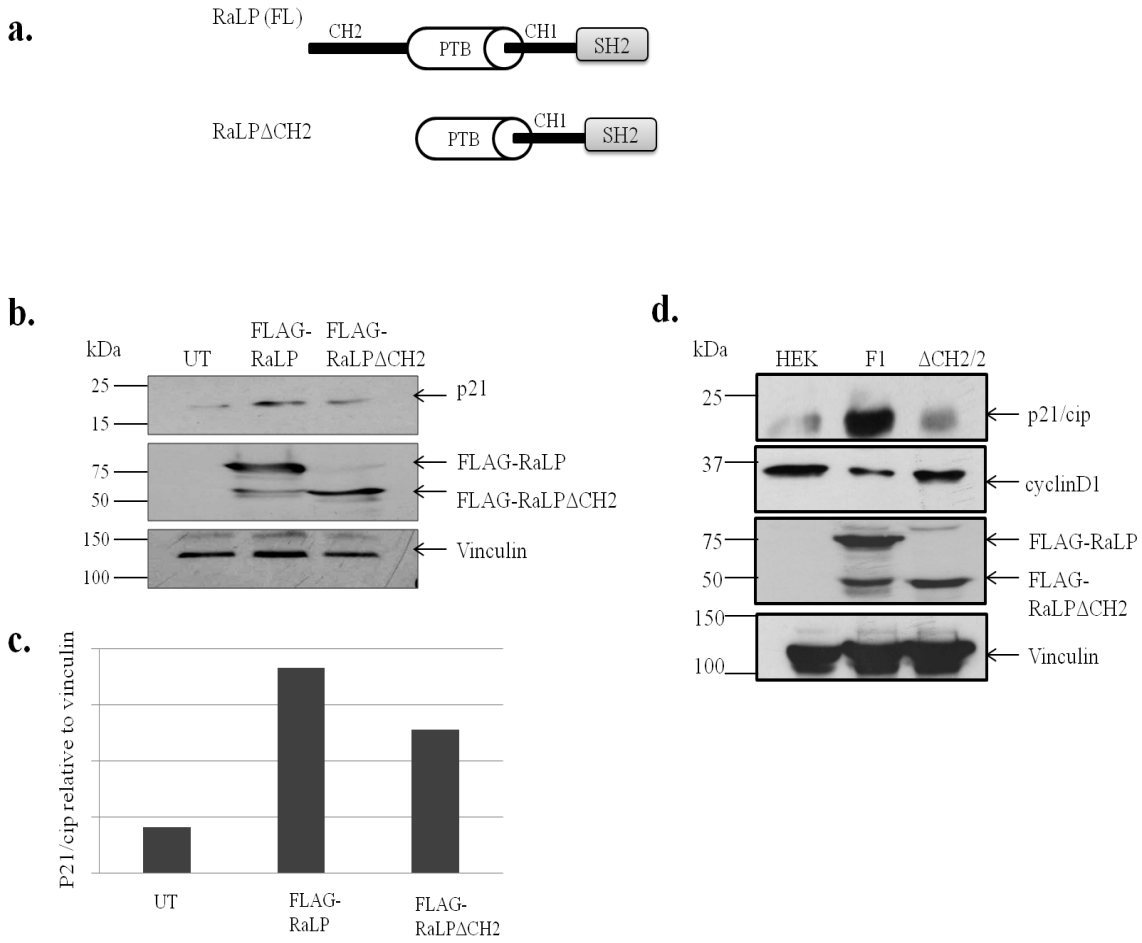

Figure 5.9 RaLP full length but not RaLP that lacks the CH2 domain upregulates p21. (a) Diagrammatic illustration of full length RaLP (FL) and RaLP that lacks the amino-terminal CH2 domain (RaLPΔCH2). (b) HEK 293 cells were either transfected with FLAG-RaLP or FLAG-RaLPΔCH2. The cells were lysed along with the untransfected HEK 293 (UT). The expression of FLAG-tagged proteins and p21/cip protein level were assessed by western blotting using anti-FLAG and anti-p21/cip antibodies respectively. Vinculin was used as a loading control. (c) The bar chart depicts p21/cip levels in relation to Vinculin. (d) FLAG-RaLP (F1) or FLAG-RaLPΔCH2 (ΔCH2/2) stably expressing cells with their parental counterparts were grown until they reached ~60-70% confluence. The cells were then lysed and resolved on a 10% SDS-PAGE gel. Immunoblotting analysis was performed using antibodies against p21/cip, cyclinD1, FLAG tag or Vinculin at 1:1000 dilutions.

The cells that over expressed FLAG-RaLP showed upregulation of p21/cip; however, the difference was not pronounced when compared with FLAG-RaLPΔCH2 expressing cells (Figure 5.9b and c). This could be related to the fact that only a subset of cells out of the whole population was transfected and expressing the protein. Consequently, it was decided to compare the stable cell line that expresses FLAG-RaLPΔCH2 (ΔCH2/2) with the stable cell line that expresses the full length protein (F1) to ensure that we are comparing cell populations where all cells express the desired protein. p21/cip level again showed upregulation in FLAG-RaLP expressing cells but not with the FLAG-RaLPΔCH2, while in contrast cyclin D1 level was downregulated by F1 cells (Figure 5.9d). Thus it was inferred that full length RaLP is responsible for the upregulation of p21/cip and downregulation of cyckin D1 in HEK 293 cells but not RaLP that lacks the CH2 domain. These data may highlight a role of the CH2 domain in this novel function of RaLP, although whether this is a result of specific protein interaction with this domain, or due to the fact that the CH2 domain confers upon the protein its cytoplasmic localisation is not clear.

5.2.2.5 GFP-RaLP expressing cells demonstrated more cytoplasmic p21/cip than GFP expressing cells:

p21/cip achieves its role as a cell cycle inhibitor mainly through its nuclear distribution; however, p21/cip role in cell differentiation, apoptosis or oncogenicity is related to its cytoplasmic distribution (Abbas and Dutta, 2009). Accordingly, this prompted us to investigate whether RaLP-mediated p21/cip upregulation is due to protein stabilisation that results in cytoplasmic sequestration of p21/cip. Cytoplasmic p21/cip regulates neurite formation in N1E-115 neuroblastoma cells (Tanaka et al., 2002). For this reason, the N1E-115 neuroblastoma cell line was chosen to study the effect of RaLP in the cytoplasmic distribution of p21/cip. N1E-115 were either made to coexpress GFP alone and FLAG-p21/cip or GFP-RaLP and FLAG-p21/cip. The fixed cells were then scanned and analysed by the assistance of a fluorescence microscope and Scanˆ R software. The cytoplasmic to nuclear ratio of FLAG-p21/cip for the two cell populations was calculated for about 150 cells for each sample. GFP-RaLP expressing cells showed a 10% elevation in the cytoplasmic FLAG-p21/cip compared to the GFP expressing cells (Figure 5.10).

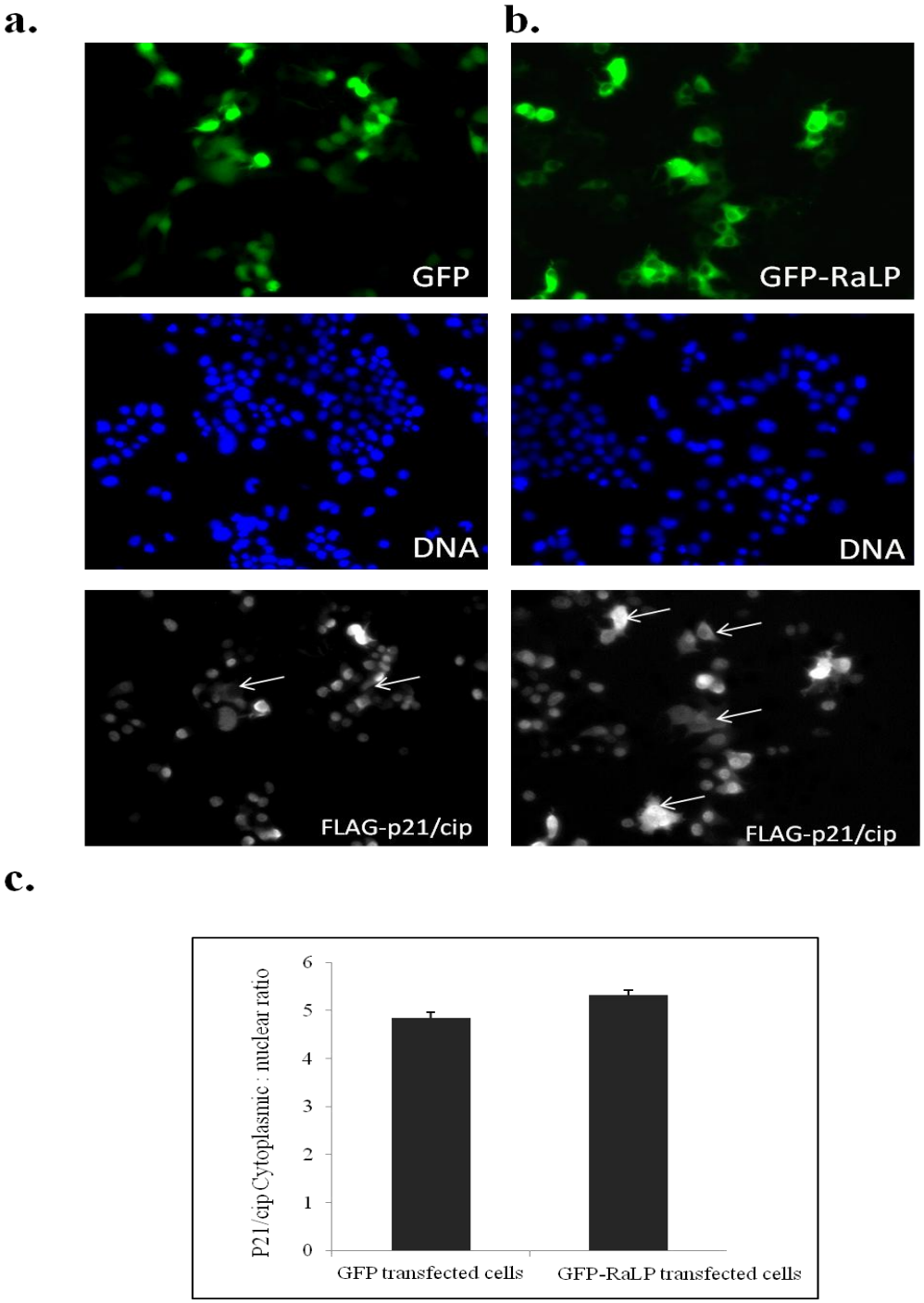

Figure 5.10: Cytoplasmic/ nuclear ration of p21/cip in cells expressing GFP-RaLP or GFP. GFP-RaLP expressing neuroblastoma cells have more p21/cip in the cytoplasm than GFP expressing cells. Neuroblastoma cells (N1E-115) were seeded on coverslips and then transfected with FLAG-p21/cip and either with GFP (a) or GFP-RaLP (b). The cells were then fixed and immunostained with anti-FLAG antibody followed by their mounting and sealing. The cells were visualised using Olympus fluorescence microscope using a 10x objective. (c) 100 fields were imaged by acquisition and screening software ScanR and Hamamatsu ORCA-AG CCD camera.
The cytoplasmic to nuclear ratio for the Texas-Red (grey channel) that represents FLAG-p21/cip was calculated by Scanˆ R analysis software.

This experiment was performed once and it provided promising evidence for RaLP's role in p21/cip upregulation in the cytoplasm via its stabilisation; however, it needs repetition, and it may be that using different conditions may yield more significant difference.

5.2.2.6 RaLP might function as an anti-apopototic candidate through p21/cip upregulation:

Based on the fact that cytoplasmic p21/cip contributes to transduction of anti-apoptotic signals, it was aimed to test whether RaLP overexpression provides the cells with resistance against apoptosis. It was initially thought to test this hypothesis using the HEK 293 parental cell line and FLAG-RaLP expressing cells (F1). The cells were treated with different H_2O_2 concentrations, as it has been reported previously that concentrations up to 1 mM induce apoptosis, while higher concentrations of H_2O_2 might induce necrosis. After applying oxidative stress for 6 hrs, apoptosis was assessed by measuring cleaved and non-cleaved caspase-3 levels. No increase in cleaved caspase-3 levels was observed in the two cell lines (HEK 293 and F1) upon H_2O_2 treatment; in contrast a general decrease in cleaved caspase-3 was seen. Interestingly, FLAG-RaLP expressing cells (F1) demonstrated lower levels of both cleaved and non-cleaved caspase-3 than parental HEK 293 (Figure 5.11a). Although this observation was seen in three independent experiments, it indeed needs to be confirmed using the other clone that expresses FLAG-RaLP. The Hela cell line was chosen to test the role of RaLP in survival, because previous studies have shown clear induction of apoptosis upon staurosporine treatment, unlike HEK 293 cells that showed no change in cleaved caspase-3 (Figure 5.11b). Staurosporine is a therapeutic agent that was shown to induce apoptosis by caspase-3 dependent and independent mechanisms (Antonsson and Persson, 2009).

Hela cells transfected with FLAG-RaLP were either unstressed or stressed using 1 µM staurosporine for 2 hrs. Apoptosis was assessed in FLAG-RaLP transfected and untransfected cells by M30 antibody, which detects caspase-cleaved cyto-keratin 18. FLAG-RaLP expressing Hela cells exhibited two fold less M30 staining than the untransfected cells (Figure 5.12). This experiment was achieved twice and it requires further repetition; however, it suggests a role for RaLP as an anti-apoptotic candidate.

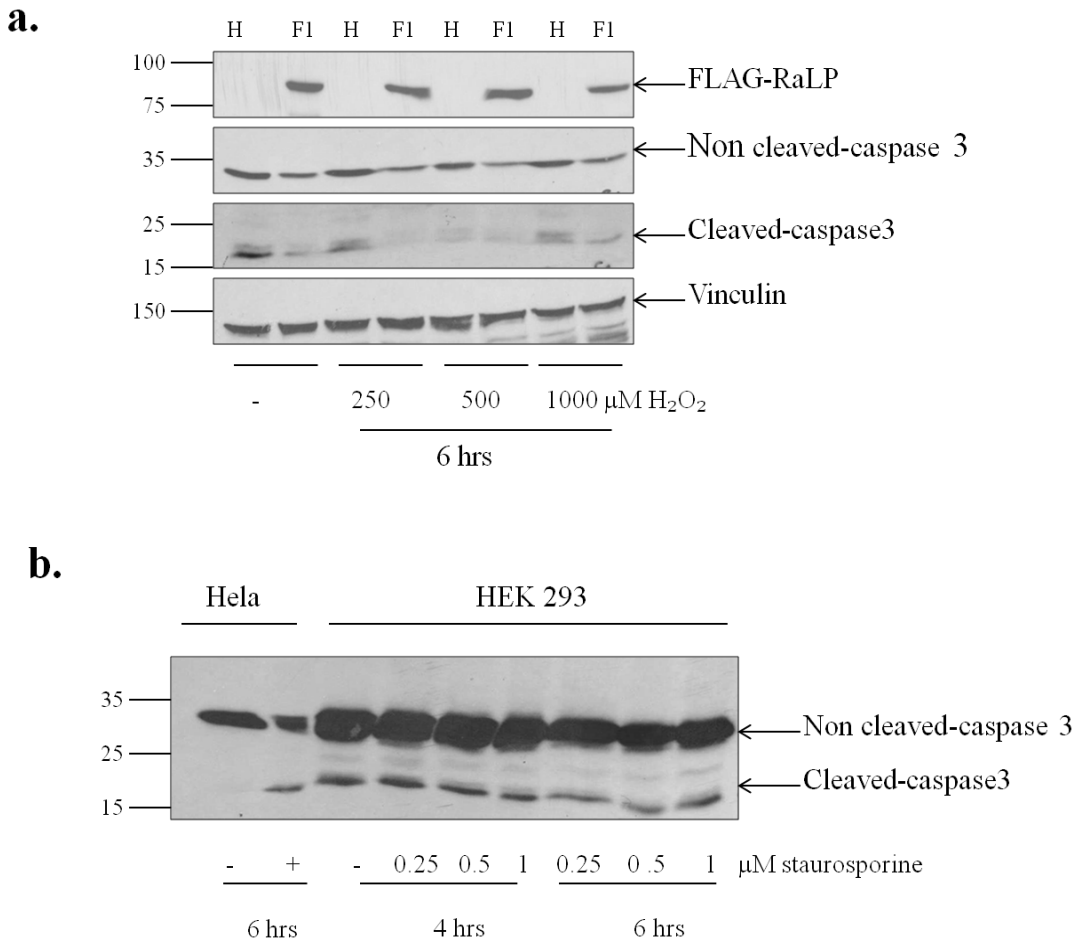

Figure 5.11 Activation of caspase-3 in HEK 293, F1 and Hela cell lines upon different stress inducing treatments. (a) FLAG-RaLP expressing cells (F1) and HEK 293 parental cells (H) were left unstressed or stressed with different H_2O_2 concentrations (250, 500 and 1000 µM) for 6 hrs. The cleaved and non-cleaved caspase-3 levels were then assessed. The blot was then reprobed with Vinculin as a loading control and anti-FLAG antibody was used to confirm the correct loading order. (b) Hela cells were left untreated or treated with 1 µM staurosporine for 6 hrs. While HEK 293 cells were unstressed or stressed with staurosporine at different concentrations (0.25, 0.5 and 1 µM) for either 4 hrs or 6 hrs. Hela and HEK 293 lysates were resolved on a 10% SDS-PAGE gel and immunoblotting analysis was performed to assess cleaved and non-cleaved caspase-3 proteins levels.

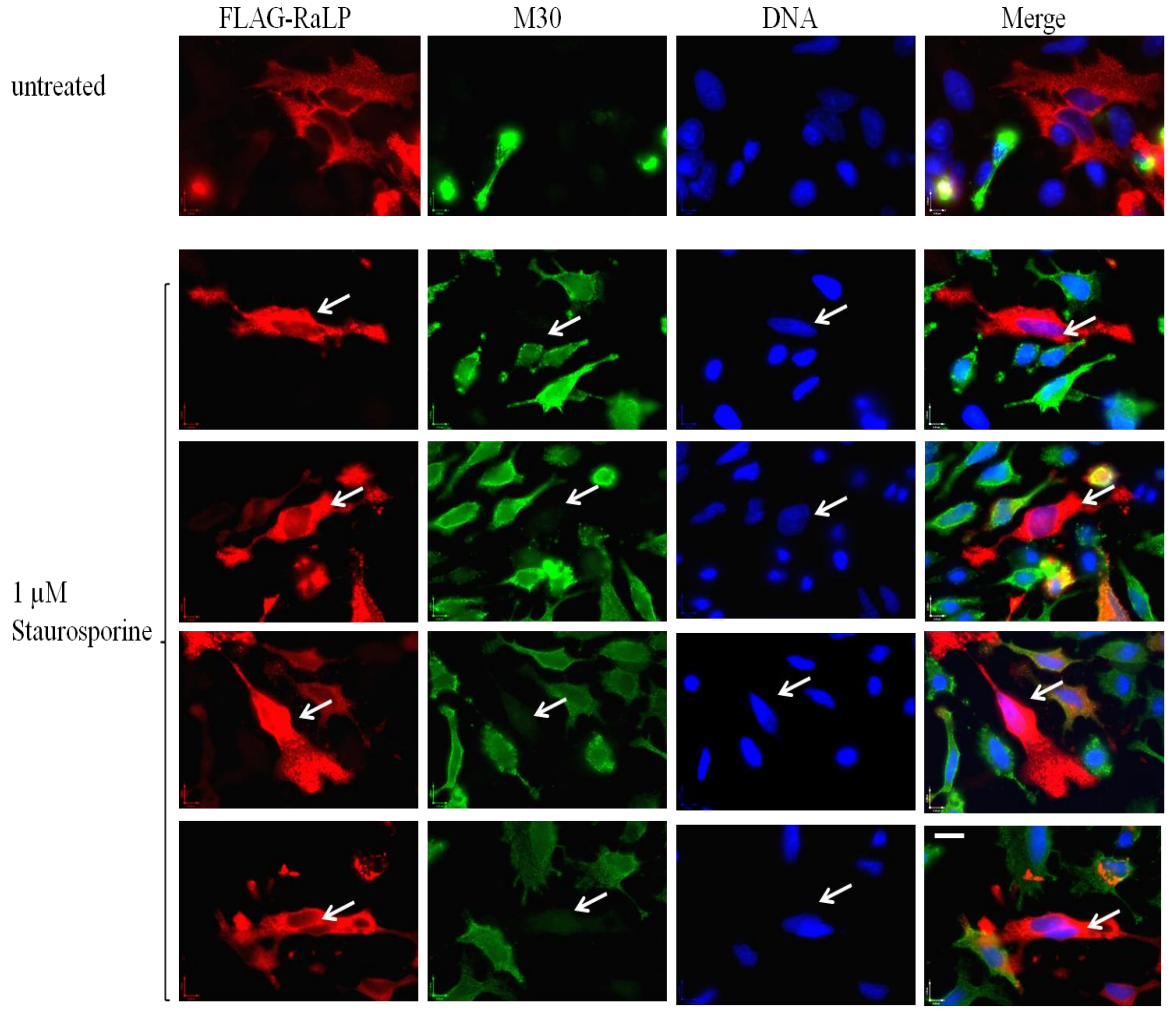

Figure 5.12 Induction of M30 staining in response to staurosporine in Hela cells expressing FLAG-RaLP or untransfected. Hela cells were seeded on coverslips overnight. The cells were then transfected with FLAG-RaLP for 24 hrs. One set of the transfected cells was incubated with 1 µM Staurosporine for 2 hrs while the other set was left unstressed. The cells were then fixed and permeabilised with methanol. Immunostaining was performed using rabbit anti-FLAG (red) and mouse M30 (green) antibodies. The cells were visualised using a Nikon fluorescence microscope and 100x 1.4 N.A oil immersion objective. Arrows indicate representative FLAG-RaLP expressing cells that show less green signal.

5.3 Discussion

The recently identified protein, RaLP; was found to induce melanoma cell invasion and tumourgenesis (Fagiani et al., 2007). In addition, its association with neurotrophin-growth factor receptors suggested a crucial role in neuronal signalling cascades (Wills et al., 2008; You et al., 2010). In an attempt to identify the function of RaLP in the intracellular compartment, HEK 293 stable cell lines that express FLAG-RaLP or GFP-RaLP were generated.

5.3.1 RaLP phosphorylation upon oxidative stress:

RaLP possesses a unique amino-terminal CH2 domain that houses potential serine and threonine phosphorylation sites according to the GPS 2.1 phosphorylation prediction programme, and it has been shown to contain a functional nuclear export signal (NES). It is also known that RaLP translocates into the nucleus in response to oxidative stress (Chapter 4). Based on these observations, it was hypothesised that the phosphorylation of any of these potential phosphorylation sites might influence RaLP nuclear translocation or RaLP's role in the nucleus. By adopting Orbitrap mass spectrometry, RaLP was shown to be phosphorylated at Thr156/Thr159 in the CH2 domain upon oxidative stress; however, it was not possible to differentiate which of the threonine residues was phosphorylated. Consistent with these data, a previous student has shown that the CH2 domain of RaLP can act as JNK substrate in in vitro kinase assays. In addition the GPS programme has also predicted JNK to phosphorylate Thr159 contained in TALTPDSCP motif.

The same prediction programme provided a prediction for other kinases (e.g. ERK, p38, PKB, CDKs, etc) that might phosphorylate Thr156/Thr159 (Figure 5.1). This can be tested in the future by executing kinase assays using recombinant wild type RaLP and mutated RaLP (Thr156A and/or Thr159A) CH2 domain as substrates or a synthetic peptide including Thr156/Thr159. These kinase assays will assist in elucidating the exact phosphorylated threonine residue, and in addition it will help to determine whether RaLP is a downstream substrate for any of the predicted kinases.

Phosphorylation of the CH2 domain was speculated to affect the nuclear export of RaLP since the CH2 houses a NES, however this possibility was excluded to some extent as Thr156 and Thr159 do not lie in close proximity to the NES (Figure 5.3).

The role of these potential phosphorylated residues on RaLP nuclear localisation can be tested by mutating threonine (156/159) to alanine in the GFP-RaLP construct or to glutamic acid and looking for changes in nuclear localisation. In the paper by Chudeland et al., 2008, they showed that SPS motif when phosphorylated could act as a nuclear import signal when phosphorylated. The TPD sequence at Thr159 of RaLP or Ser132 at SPE could similarly act as an import sequence when phosphorylated. It would also of interest to determine whether these mutations could affect transcriptional activity of RaLP as described in chapter 4.

RaLP was shown to be phosphorylated at Ser132 housed in the CH2 domain as well as at Ser510/511 in the CH1 with or without H_2O_2 treatment. Since serine phosphorylation occurs at resting conditions it might possibly play role in RaLP stabilisation. p66ShcA phosphorylation at Ser54 in its CH2 domain and Thr386 in the CH1 domain were found to affect p66ShcA stabilisation by preventing its ubiquitination (Khanday et al., 2006).

5.3.2 Identifying RaLP potential interacting partners:

To gain further insight into the RaLP molecular mechanism by which RaLP regulates the intracellular cascades, coimmunoprecipitation was employed combined with mass spectrometry to identify the potential interacting partners of RaLP. Different proteins were identified that might possibly associate with RaLP, including nuclear pore complex protein Nup107, Melanoma associated antigen D2, Calcium-binding mitochondrial carrier protein Aralar2/1, Mono functional C1-tetrahydrofolate synthase, CCR4-NOT transcription complex subunit 1, Tubulin beta 4/6 chains, DnaJ homologue subfamily C/A, general vesicular transport factor p115 (p115), Transcription intermediary factor 1-beta (TIF-1β) and Apoptosis inducing factor 1. Some of the possible RaLP interacting partners share the same intracellular distribution as RaLP, which has nuclear, mitochondrial and cytoplasmic localisations.

Based on the antibody availability, we were able to further study RaLP association with TIF-1β, p115 and Nup107. Although it was possible to coimmunoprecipitate p115 and p107 with RaLP more confirmation is required. According to our finding, TIF-1β has not proved to be a specific interacting protein with RaLP. There are still other proteins that might represent potential interacting partners for RaLP that need further testing.

p115 is shown to be required for Golgi assembly and biogenesis (Puthenveedu et al., 2001). Moreover, p115 was reported to interact with macrophage migration inhibitory factor (MIF) promoting secretion of the latter (Merk et al., 2009), which is important for the macrophage's immune response (Calandra and Roger, 2003) as well as having a role in tumour angiogenesis (Girad et al., 2012). RaLP interaction with p115 might interfere with MIF secretion, as MIF was identified in one of the mass spectrometry experiments. Such interaction might either alter the macrophage's immune response or influence the role of MIF in tumour vascularisation. Expression of RaLP in macrophage has yet to be determined.

The C-terminus of the p115 was found to possess a caspase-cleavage site which is cleaved at the onset of apoptosis. Interestingly, the p115 cleaved C-terminus was found to translocate to the nucleus to enhance the apoptotic signal that was initiated by the active caspases (Mukherjee and Shields, 2008; How and Shields, 2010). It was shown earlier that RaLP translocates to the nucleus upon oxidative stress, and RaLP may mediate an anti-apoptotic signal. Accordingly, it may be speculated that RaLP interacts with p115 preventing its cleavage and hence impeding its apoptotic action. All these hypotheses need to be studied carefully which might lead to an identification of the exact function of RaLP in cells.

In addition to the role of nuclear pore complex 107 in nucleocytoplasmic trafficking in the interphase cell (Boehmer et al., 2002), it was also shown to translocate to the kinetochore and play a role in spindle assembly during mitosis (Orjalo et al., 2006). RaLP and Nup107 association can be attributed to the fact that RaLP shuttles between the cytoplasm and the nucleus, and at some point it needs to either directly or indirectly dock at the nuclear pore complex, which has Nup107 as one of its components.

5.3.3 RaLP-mediated p21/cip upregulation:

The stable cell lines that express FLAG-RaLP demonstrated a higher percentage of cells in G1 and G2/M, and a lower percentage of cells in the S phase than the parental cell line. This interesting phenomenon was shown later to be due to the fact that FLAG-RaLP expressing cells upregulate p21/cip when compared with the parental HEK 293 cells.

p21/cip has been considered previously as a tumour suppressor protein since it functions as a negative regulator to the cell cycle; however, recently its role in mediating an anti-apoptotic signal suggested its oncogenicity (Wendt et al., 2006). p21/cip is upregulated when the cells are arrested by contact adhesion, serum starvation (Macleod et al.,1995), senescence (Westin et al., 2011) or differentiation (Tanaka et al., 2002). Adding to that, p21/cip is induced by p53 in response to DNA damage (Dulic et al., 1994).

The role of p21/cip in cell cycle regulation is related mainly to its nuclear localisation (Abbas and Dutta, 2009), while its cytoplasmic existence was shown to be associated with aggressive breast cancer (Winter et al., 2003). Furthermore, the cytoplasmic localisation of p21 is responsible for neurite formation in N1E-115 neuroblastoma cells (Tanaka et al., 2002).

Indeed, it is of interest to investigate the mechanism by which RaLP induces upregulation of p21/cip. RaLP might regulate p21 expression at the mRNA level either via mediating its transcription, or influence the mRNA stabilisation. In order to study this, quantitative RT-PCR can be performed employing the parental HEK 293 and FLAG-RaLP, or FLAG-RaLPΔCH2 expressing cell lines. Furthermore, the role of RaLP in gene transcription was shown, which might suggest that RaLP's role in regulating p21/cip expression is at the transcriptional level. This could be studied by performing chromatin immunoprecipitation assays (ChIP), looking for the CDKN1A gene, which encodes p21/cip, in RaLP-associated chromatin. Alternatively, RaLP might affect p21/cip stability by suppressing p21 ubiquitination or inducing its phosphorylation. JNK1 activation upon oxidative stress mediates growth arrest by elevating p21 protein level by inhibiting its ubiquitination (Fan et al., 2007). Independent of the p53 pathway, p21/cip is upregulated by PI3K/Akt pathway activation via its phosphorylation that renders p21 protein more stable (Li et al., 2002). On the other hand, Notch receptor activation promotes keratinocyte differentiation through induction of p21/cip (Rangarajan et al., 2001). In unpublished work by Aladowicz, 2011, RaLP was found to play a role in regulation of Notch signalling, which might explain the p21/cip upregulation by RaLP (PhD abstract).

Since RaLP prompts cells to upregulate p21/cip, the role of RaLP in cell survival was assumed. FLAG-RaLP expressing Hela cells showed a two fold reduced pro-apoptotic signal upon staurosporine treatment in comparison to their untransfected controls. This has provided a possible mechanism for RaLP in cell survival, which might be through inducing p21/cip.

To test this further p21/cip could be knocked down in FLAG-RaLP expressing Hela cells, and the effect on apoptosis examined. In addition, it is worth testing whether RaLP-mediated p21/cip induction has a role in cell differentiation.

To summarise, it has been possible by employing a GFP-RaLP stably expressing cell line and mass spectrometry to identify phosphorylated residues on RaLP in response to oxidative stress, as well as determining potential RaLP interacting partners. By exploiting FLAG-RaLP stably expressing cells, a possible role for RaLP in upregulating p21/cip has been uncovered, which might provide a mechanism through which RaLP promotes cell survival and differentiation.

Chapter 6

RaLP & Nischarin

6.1 Introduction:

A mouse embryonic yeast two hybrid cDNA library was screened to identify proteins that interact with RaLP facilitating its role in cell migration (unpublished work by Wong and Prigent). A novel protein Nischarin was found to interact with the RaLP-CH2 domain. Additionally a previous experiment (carried out in this laboratory) showed that amino acids 541 to 666 of mouse Nischarin are required for RaLP interaction (Figure 6.1).

6.1.1 Nischarin structure:

Nischarin is a large protein whose mRNA encodes a 1504 amino acid protein (Piletz et al., 2000); it is highly conserved among mammalian species (Piletz et al., 2003). Mouse Nischarin shares about 80% sequence identity with human Nischarin. The human protein is referred to as imidazoline receptor anti-sera selected (IRAS) (Alahari et al., 2000). The mouse version is considered a truncated form of the human protein that possesses an additional amino terminal Phox (PX) domain (Piletz et al., 2003; Alahari et al., 2000). On an SDS PAGE gel, Nischarin was found to run at different sizes; 85, 167,190 and 210 kDa, which were all considered to be different forms of the protein depending on the cellular context (Alahri et al., 2000; Piletz et al., 2003). The PX domain is known to bind phosphatidyl inositol-3 phosphate (PI3P) that is abundantly present in the plasma membrane, endosomal and lysosomal membranes (Lim and Hong, 2004). Therefore, the PX domain facilitates human IRAS binding to the cytoplasmic part of the plasma membrane as well as to endosomes (Lim and Hong, 2004). Nischarin also contains five leucine rich repeats downstream of the PX domain (Sun et al., 2007). A coiled-coiled region was also identified on Niscahrin using the SMART motif prediction programme, which was suggested to mediate protein-protein interaction (Lim and Hong, 2004). Moreover, the amino terminal region of the protein contains an α5 integrin interacting domain (Alahari et al., 2000). The carboxy terminal region of the protein has been shown to bind insulin receptor substrate 4 (IRS4) (Sano et al., 2002). In addition, the COOH terminal region contains proline rich motifs that possibly mediate protein complexes formation (Musgrave et al., 2003) (Figure 6.1). In this report I will refer to the mouse version of the protein as Nischarin and the human protein will be designated as human Nischarin/IRAS, as defined.

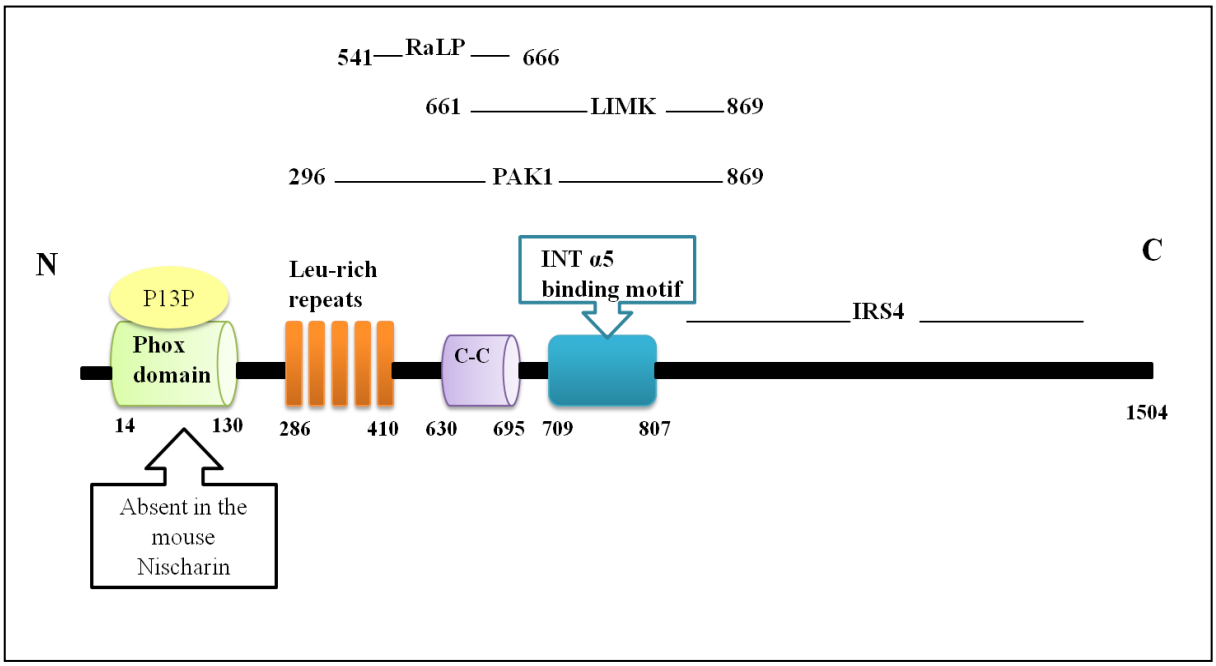

Figure 6.1 Diagrammatic representation of Nischarin/IRAS domains and protein interaction sites. The regions of Nischarin which have been shown experimentally to interact with various proteins are indicated. Amino acid numbering is based on the human Nisharin/IRAS sequence (accession number Q80TM9). N: amino terminus and C: carboxy terminus of the protein. PI3P: Phosphotidyl inositol 3 phosphate, Leu: leucine, INT: integrin, PAK1: p21-activated kinase 1, IRS4: insulin receptor substrate 4, C-C: coiled-coiled. Adapted from (Lim et al., 2004; Sun et al., 2007).

6.1.2 The role of Nischarin in signalling pathways:

6.1.2.1 Role in Migration:

Cell migration plays an indispensible role in various biological responses including wound healing, angiogenesis, early embryonic development, tumour invasion and metastasis. Intracellular cascades need to be tightly controlled to maintain the normal biological processes. Nischarin was determined to play a role as a negative regulator of cell motility through its association with α5 integrin, the receptor for fibronectin (Alahari et al., 2000). Nischarin was reported to interact with the active p21-activated kinase 1 (PAK1) and suppress its ability to bind to its downstream substrates (Figure 6.2), resulting in inactivation of LIM Kinase and myosin light chain kinase (MLCK) (Alahari et al., 2004). Active LIMK suppresses the actin severing agent cofilin by phosphorylation, and this results in formation of lamellipodia and membrane ruffles (Yang et al., 1998). Nischarin was also shown to associate with LIM kinase directly yielding less invasive and migratory breast cancer cells, via minimising the ability of LIM kinase to inhibit cofilin (Ding et al., 2008) (Figure 6.2) .

Rac GTPase is an important molecule in cell signalling and regulates cell motility, protein trafficking, cell cycle progression and cellular transformation (Edwards et al., 1999; Parri et al., 2010; Sun et al., 2012). Rac is upstream of PAK1 and promotes cell migration through PAK1 activation. Nischarin was reported also to associate with Rac abrogating its ability to activate PAK1 dependent and independent pathways (Reddig et al., 2005) (Figure 6.2).

Recently, a report using mass spectrometry to identify interacting partners for Ephrin B receptor (Eph B) in ephrin B1-Fc-stimulated NG108 neurobastoma cells revealed Nischarin as a candidate in Eph B receptor signalling (Darie et al., 2011). Eph B receptors were described before to be responsible for neural crest migration (Santiago et al., 2002), therefore Nischarin may contribute to Eph B-mediated migration in neuronal cells (Figure 6.2).

6.1.2.2 IRAS has a role in protein trafficking:

Sorting nexin proteins have a well-defined role in receptor trafficking through their PX domain, and since IRAS possesses a PX domain its role in receptor trafficking was suggested. IRAS association with early sorting and recycling endosomes was studied through its colocalisation with EEA1 and SNX2 markers for early endosomes. In addition, IRAS localisation to endosomes was proved to be through an integrated action of both the PX domain and the coiled-coiled motif. Upregulation of IRAS resulted in translocation of α5 integrin from the membrane to the endosomes and this might be the mechanism that IRAS exploits to interfere with cell migration through α5 integrin signalling (Sano et al., 2002) (Figure 6.2).

6.1.2.3 Nischarin functions as an anti-apoptotic candidate:

Upregulation of Nischarin in insulin treated pheochromocytoma cells (PC12) induced cell survival upon exposing the cells to cytotoxic conditions. This appeared to be through the PI3-kinase pathway, which resulted in a reduction in fragmented nuclei, phosphatidylserine translocation and caspase-3 activity (Dontenwill et al., 2003). In support for a role of IRAS in the insulin signalling pathway, ion trap mass spectrometry revealed IRAS as an interacting partner for insulin receptor substrate (IRS4), which is a key component in transducing the signalling from the insulin receptor (Sano et al., 2002) (Figure 6.2). Upon insulin stimulation of human embryonic kidney cells (HEK 293) overexpressing IRAS, IRAS interacts with phosphorylated IRS4 resulting in elevation of active ERK (Sano et al., 2002) which might contribute to the anti-apoptotic effect of IRAS (Kang et al., 2003).

6.1.2.4 The tumour-suppressive function of Nischarin:

The Nischarin gene is located on chromosome 3p21.1 and this segment of DNA was found to be lost in various types of cancers (Baranwal et al., 2011). Based on that, the role of Nischarin as a tumour suppressor was suggested. The mRNA expression levels were discovered to be reduced in breast cancer tissues when compared to the normal breast tissue.

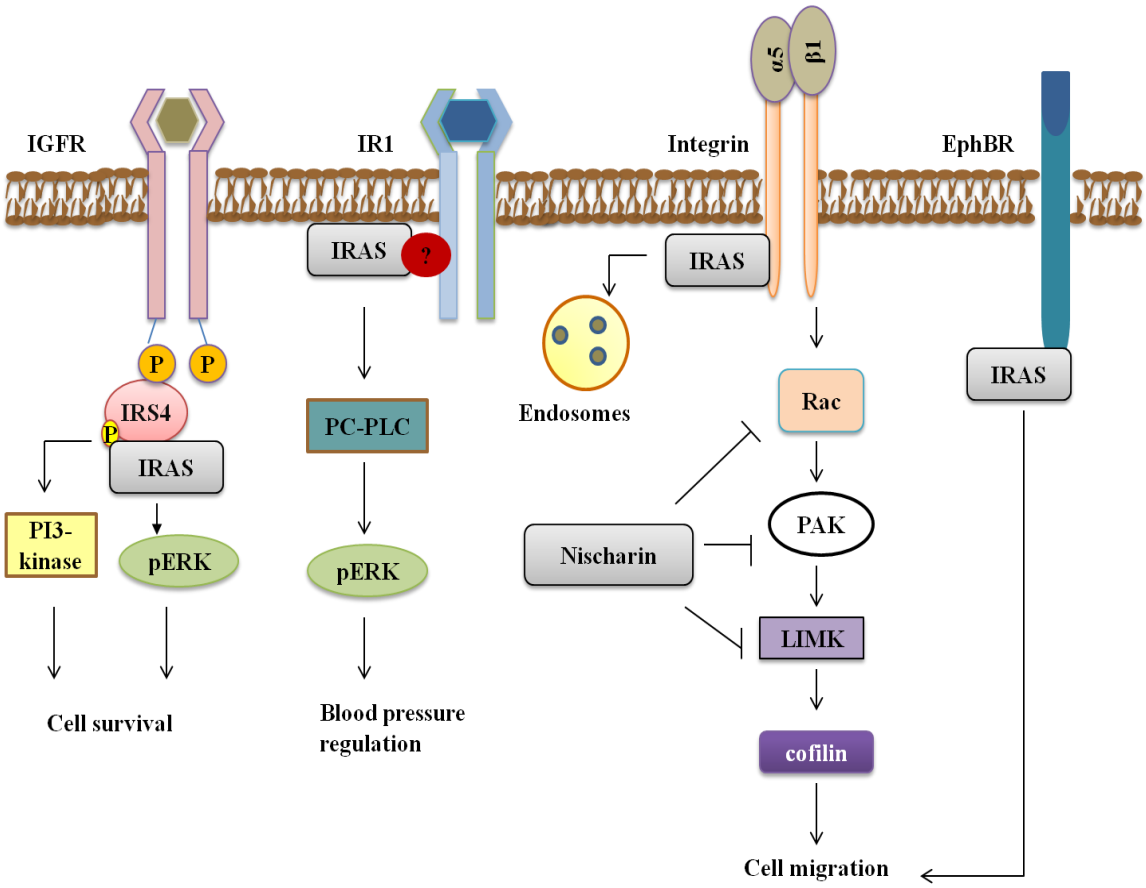

Figure 6.2 Diagrammatic illustration indicating the role of Nischarin/IRAS in signal transduction pathways. Nischarin and its human homologue IRAS have been reported to be involved in cell migration, blood pressure control, cell survival and protein trafficking. IGFR: insulin like growth factor receptor, IR1 imidazoline receptor 1, (IRAS) imidazoline receptor anti-sera selected, IRS4: insulin receptor substrate 4, pERK: phosphorylated extracellular regulated kinase, PAK1: P21-activated kinase1, EphBR: Ephrin B receptor, PC-PLC: phosphatidylcholine-selective phospholipase.

Interestingly, patients with high levels of Nischarin showed a significant elevation in recurrence-free survival when compared with patients with low levels of Nischarin. To study this further, in vivo experiments were carried out in mice. Cells that overexpressed Nischarin failed to form significant lung metastases when injected into mice in comparison to cells containing a control vector.
Moreover, Nischarin upregulation resulted in reduction in the levels of α5 integrin, phospho-ERK and phosphorylated focal adhesion kinase (FAK) (Baranwal et al., 2011).

6.1.2.5 IRAS acts in the nervous system as a candidate Imidazoline receptor:

An in vivo study was carried out in the rostral ventrolateral medulla (RVLM), an area in the brain stem that controls blood pressure, to determine the impact of IRAS/ Nischarin on the imidazoline agonist Rilmenidine-mediated hypotension. Knocking down Nischarin/IRAS in RVLM by means of anti-sense oligodeoxynucleotide (ODN) hampered the ability of Rilmenidine to evoke hypotension. Furthermore, downregulation of Nischarin/IRAS resulted in reduction in ERK1/2 activation. The study concluded that Nischarin is crucial for maintaining the Rilmenidine-induced hypotension reflex via activating ERK1/2 (Zhang et al., 2008). The impact of IRAS on activation of ERK in the imidazoline pathway was found to be through phosphatidylcholine-selective phospholipase (PC-PLC) and diacylglycerol (DAG) accumulation (Li et al., 2006) (Figure 6.2). Although some reports suggest that Nischarin/IRAS belongs to the imidazoline receptor (IR) family since it partly shares the same distribution and function as IR, no defined evidence has been found to prove the stated hypothesis (Piletz et al., 2000). In contrary to the role of IRAS in activating ERK, it was determined that Nischarin results in suppression of ERK in nerve growth factor (NGF) stimulated PC12 cells during neuronal development (Piletz et al., 2003). Interestingly in a preclinical study, Nischarin was determined to be a therapeutic target in treating morphine dependence phenomenon (Li et al., 2011).

6.1.3 Investigating RaLP and Nischarin interaction:

To explore RaLP and Nischarin interaction, we employed the immunoprecipitation technique to study their association. An imaging approach was used to determine the colocalisation of the two proteins in the intracellular compartment, which also enabled

us to determine the individual localisation of RaLP and Nischarin. Moreover, the functional consequences of RaLP and Nischarin interaction were studied by stimulating HEK 293 and then exploring the downstream changes in LIMK/cofilin or ERK pathways by performing western blotting. Finally, wound migration assays were executed to test the effect of RaLP and Nischarin interaction on cell migration.

6.2 Results:

6.2.1 Nischarin interacts with RaLP in mammalian cells:

Previously it was shown that the CH2 domain of RaLP interacts with Nischarin using Yeast two hybrid assays. To confirm the existence of this interaction in mammalian cells, coimmunoprecipitation experiments were performed. HEK 293 lysates were obtained from cells that were cotransfected with GFP-Nischarin and either FLAG-RaLP or FLAG-RaLPΔCH2 that lacks the amino-terminal CH2 domain. FLAG tagged proteins were immunoprecipitated with anti-FLAG antibody and the associated proteins were identified by performing immunoblot analysis with anti- Nischarin antibody (Figure 6.3a). Nischarin was able to coimmunoprecipitate with FLAG-RaLP but not with FLAG-RaLPΔCH2 (Figure 6.3a). The specificity of the interaction was confirmed by the fact that the control antibody (PK-TAG) failed to immunoprecipitate any FLAG tagged proteins as well as GFP-Nischarin (Figure 6.3a). Thus it was deduced that RaLP and Nischarin interaction occurs in mammalian cells as well as the CH2 domain of RaLP is indispensible for its interaction with Nischarin.

6.2.2 Human IRAS binds RaLP:

IRAS possesses an additional PX domain, therefore; it was of interest to investigate whether the PX domain interferes with RaLP interaction. HEK 293 cells were co transfected with Myc-IRAS and FLAG-RaLP and the cells were lysed. Immunoprecipitation was performed with anti-FLAG antibody and coprecipitated IRAS was detected with anti-Nischarin antibody. The immunoprecipitated FLAG-RaLP was capable of precipitating Myc-IRAS (Figure 6.3b). These findings clearly showed that the interaction between RaLP and IRAS is not affected by the amino terminal PX domain of IRAS.

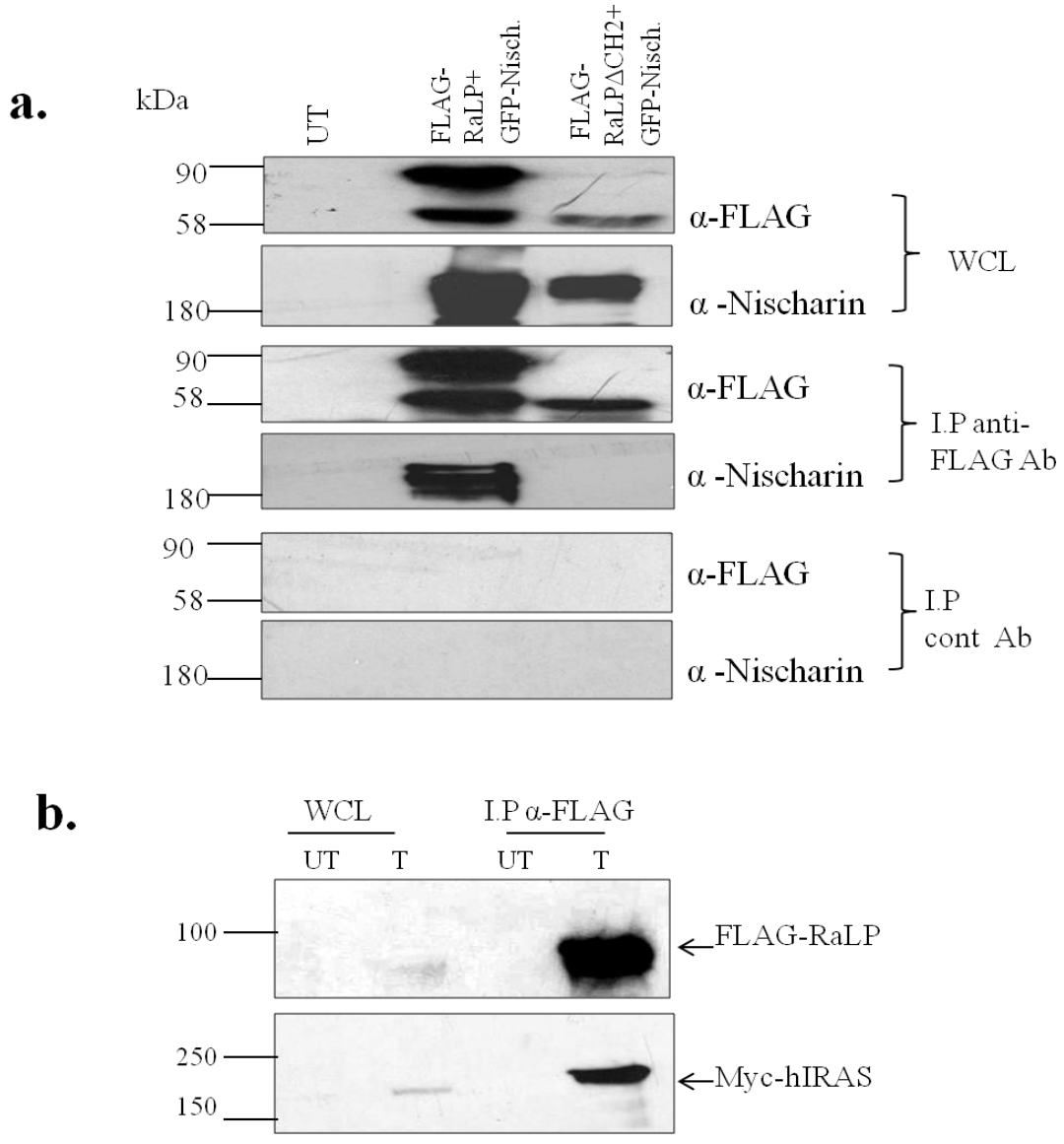

Figure 6.3 FLAG-RaLP interacts with GFP-Nischarin as well as Myc-IRAS. HEK 293 cells were cotransfected with GFP-Nischarin and either FLAG-RaLP or FLAG-RaLPΔCH2. Immunoprecipitation was performed O/N at 4˚C with anti-FLAG antibody bound to protein G-sepharose beads. Immunoprecipitated proteins along with 1/10 of the whole cell lysates (WCL) were resolved on an 8% SDS-PAGE gel and transferred to nitrocellulose membrane, followed by immunoblotting with either anti-FLAG antibody or anti-Nischarin antibody. PK-TAG antibody was used as a control. (b) HEK 293 cells were transiently cotransfected with Myc-IRAS and FLAG-RALP. The transfected cells along with the untransfected cells were lysed. 1/10 of the WCL along with FLAG-RaLP immunopreciptates were tested for the presence of Myc-IRAS by immunoblotting with anti-Nischarin antibody.

6.2.3 RaLP and Nischarin interaction occurs at the physiological levels:

RaLP and Nischarin are both abundantly expressed in neuronal tissues and cells (Jones et al., 2007; Zhang et al., 2006), therefore cell extracts were obtained from N1E-115 cells (mouse neuroblastoma cells) or SY5Y cells (human neuroblastoma cells) and coimmunoprecipitation was performed. Endogenous RaLP was immunoprecipitated with anti-RaLP antibody (abcam) and the associated endogenous Nischarin was detected by performing immunoblotting with anti-Nischarin antibody (Figure 6.4). Nischarin was present in the immunoprecipitate of the anti-RaLP antibody but not in the control immunoprecipitate. The anti-RaLP antibody from abcam recognised two bands of approximately 70 and 80 kDa in the N1E-115 cells. To confirm which of the two bands corresponded to RaLP the blot was stripped and re-probed with anti-RaLP antibody (TB2/4443). This antibody also detected two bands however the band of about 70 kDa corresponded to the bottom band recognised by abcam antibody, indicating that the the 70 kDa band is RaLP (Figure 6.4). Interestingly, only one band of about 80 kDa was observed by anti-RaLP antibody (abcam) in human neuroblastoma cells, which might need further investigations. These data revealed that RaLP and Nischarin interaction takes place when proteins are expressed at physiological level in neuroblastoma cells.

Having shown that Nischarin and RaLP can coimmunoprecipitate from both transfected and untransfected cells, we sought to determine whether we could identify other proteins with which RaLP can form a complex in N1E-115 cells, by mass spectrometry. It was hoped that if Nischarin is a significant binding partner it would also be identified by this approach. Five 10 cm dishes of N1E-115 cells were transfected with GFP-RaLP for 36 hrs. The lysates that were obtained from GFP-RaLP expressing N1E-115 or untransfected N1E-115 cells were incubated with GFP-trap. The immunoprecipitated proteins were then separated by SDS-PAGE gel electrophoresis (Figure 6.5a). The identity of the proteins (>100 kDa) was revealed by employing Orbitrap mass spectrometry. GFP-RaLP-associated proteins of a molecular weight more than 100 kDa, with a score ≥ 90, which did not exist in the negative control, are summarised in figure 6.5b. Different cytoplasmic proteins were proved to associate with RaLP for instance; Cytospin, Plectin, Tubulin, Neurobeachin and importantly Nischarin. Moreover, RaLP was found to bind TrkC and Ret receptors as well as nuclear transport components like Importin subunit β-1 and Transportin.

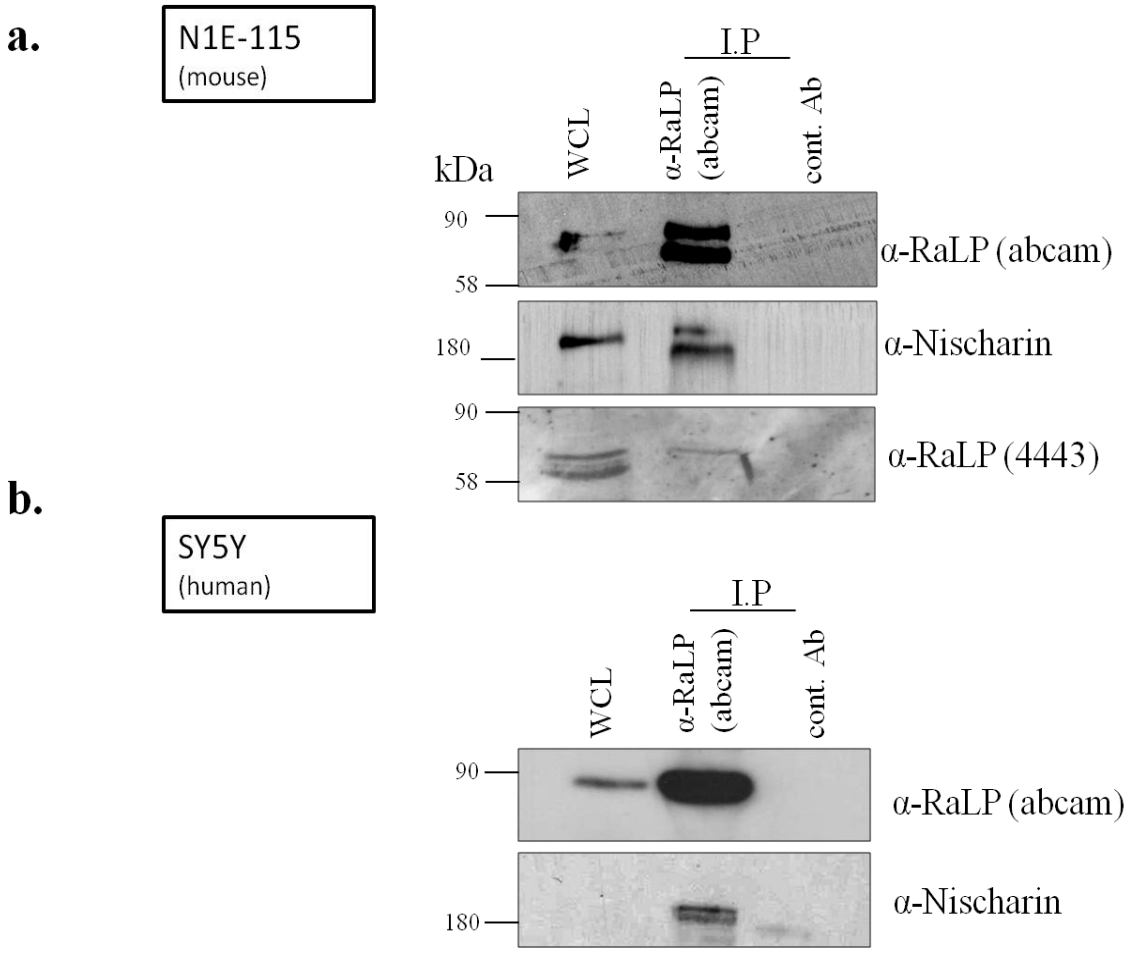

Figure 6.4 RaLP binds Nischarin in Neuroblastoma cells. Cell lysates were obtained from neuroblastoma cells from mouse N1E-115 (a) as well as from human SY5Y (b) followed by their incubation with immobilised anti-RaLP antibody (abcam) or with control antibody (cont.Ab). The immunoprecipitated proteins along with 1/10 of the whole cell lysates (WCL) were then separated on an 8% SDS-PAGE gel then western blotting was performed. The blots were probed with anti-Nischarin antibody and then reprobed with anti-RaLP antibody (abcam) and in (a) reprobed additionally with TB2/4443.

a.

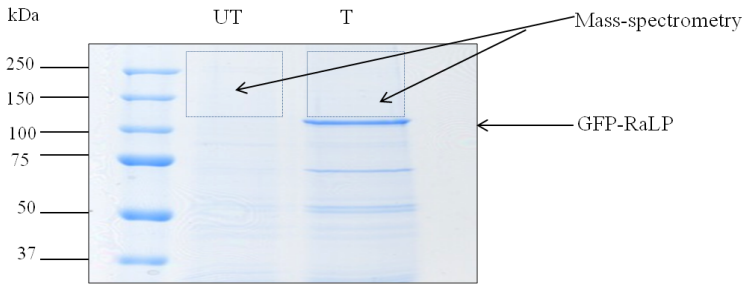

b.

Name of the protein	Score	Function
Cytospin-A	469	Microtubule associated protein
Nischarin	366	Acts either as the functional imidazoline-1 receptor (I1R) candidate or as a membrane-associated mediator of the I1R signalling. It inhibits cell migration by suppressing Rac/PAK/LIMK migratory pathway.
Plectin	322	Interlinks intermediate filaments with microtubules and microfilaments and anchors intermediate filaments to desmosomes or hemidesmosomes
Importin subunit β-1	197	Functions in nuclear protein import, either in association with an adapter protein, like an importin-alpha subunit, which binds to nuclear localization signals (NLS) in cargo substrates, or by acting as autonomous nuclear transport receptor.
Tubulin-β 5 chain	180	Tubulin is the major constituent of microtubules
Neurobeachin	179	Has essential role in synaptic transmission at the neuromuscular junction. May anchor the kinase to cytoskeletal and/or organelle-associated proteins. May have a role in membrane trafficking
NT-3 receptor (TrkC)	160	This is a tyrosine-protein kinase receptor. Known substrates for the Trk receptors are SHC1, PI 3-kinase, and PLC-gamma-1
Tubulin β-4B	141	Tubulin is the major constituent of microtubules
Transportin	97	Functions in nuclear protein import as nuclear transport receptor. Serves as receptor for nuclear localization signals (NLS) in cargo substrates.
Tubulin α-1B chain	96	Tubulin is the major constituent of microtubules
Ret	90	Receptor tyrosine-protein kinase involved in numerous cellular mechanisms including cell proliferation, neuronal navigation, cell migration, and cell differentiation upon binding with glial cell derived neurotrophic factor family ligands. Phosphorylates PTK2/FAK1. Regulates both cell death/survival balance and positional information

Figure 6.5 Investigating RaLP and Nischarin association employing mass spectrometry and N1E-115 cell lysates. (a) 5 (10 cm) dishes of N1E115 cells were transiently transfected with GFP-RaLP for 36 hrs. Along with untransfected N1E-115 cells, the cells were lysed in HiLO buffer. The lysates that were obtained from both untransfected and transfected N1E-115 cells were incubated with GFP-trap for 2 hrs. The immunoprecipitated proteins were resolved on an 8% SDS-PAGE gel. The gel was then stained with commercial instant blue coomassie for 1 hr and destained with water. (b) GFP-RaLP associated proteins in N1E1-115 cells. The indicated regions in the gel were excised and digested with trypsin followed by analysis using OrbiTrap mass-spectrometry. The identified GFP-RaLP associated proteins are indicated in (b). The proteins in the table were not present in the sample obtained from untransfected cells and the score indicates a statistical score for how well the experimental data match the database sequence. The proteins' functions were obtained from uniprot 2012.

6.2.4 Mapping the Nischarin interacting region on the CH2 domain of RaLP:

To identify which region on the CH2 domain of RaLP is required to interact with Nischarin, FLAG-RaLP constructs that lack different lengths of the amino terminal region were generated, FLAG-RaLPΔ1-24 and FLAG-RaLPΔ1-93 (Figure 6.6a). These correspond to the previously reported p69, p59 versions of RaLP (Jones et al., 2007). Each of the truncated versions and the full length FLAG-RaLP was coexpressed with GFP-Nischarin in HEK 293 cells. Anti-FLAG immunoprecipitates from the cell extracts were examined for the presence of Nischarin. Loss of the first 24 amino acids reduced RaLP and Nischarin association by about 70%, while loss of the first 93 amino acids resulted in abrogation of RaLP and Nischarin interaction (Figure 6.6b). These data indicated that the Nischarin interaction region is within the first 93 amino acids at the extreme amino terminus of RaLP, and the first 24 amino acids contribute significantly to the interaction.

6.2.5 Nischarin interacts with RaLP but not with ShcA:

The collagen homology domains are the least conserved between Shc proteins. The percentage amino acid sequence identity between RaLP-CH2 domain and p66ShcA-CH2 domain is 23% using the Uniprot alignment programme 2012, while it is 21% for ShcC and 14% for ShcB. Inorder to confirm the interaction between Nischarin and RaLP is unique among Shc proteins, mCherry-RaLP or mCherry-p66Shc were coexpressed along with GFP-Nischarin. Cell extracts were obtained followed by coimmunoprecipitation using anti-GFP antibody. Nischarin was only able to pull down RaLP but not p66ShcA (Figure 6.7). This result indicated that Nischarin specifically interacts with RaLP and not other Shc members. Additionally, these data showed that coimmunoprecipitation can occur the opposite way i.e. RaLP was also able to coimmunoprecipitate Nischarin, which confirms the specificity of the interaction.

6.2.6 RaLP and Nischarin subcellular localisation:

Having shown that RaLP and Nischarin can be precipitated as a complex from cell extracts, it was decided to study their colocalisation using confocal laser microscopy.

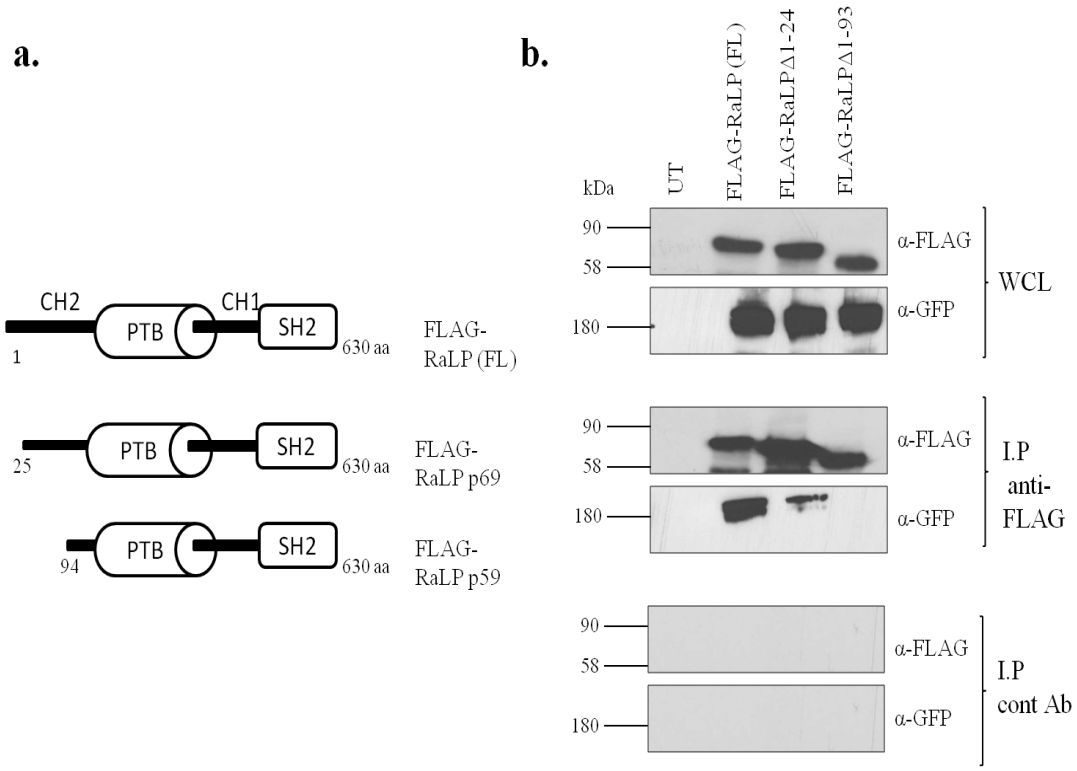

Figure 6.6 Mapping RaLP-CH2 for Nischarin interacting region. (a) HEK 293 cells were transiently cotransfected with GFP-Nischarin and either FLAG-RaLP 1-630 (FL), FLAG-RaLPΔ1-24 (p69.2 RaLP) or FLAG-RaLPΔ1-93 (p59 RaLP). The cells were lysed and incubated with 3 µg of immobilised anti-FLAG antibody or anti-PK-TAG antibody (cont Ab) O/N at 4˚C. The immunoprecipitated proteins were resolved on an 8% SDS-PAGE gel along with the 1/10 whole cell lysates (WCL). Immunoblotting was performed with anti-FLAG antibody and anti-GFP antibody.

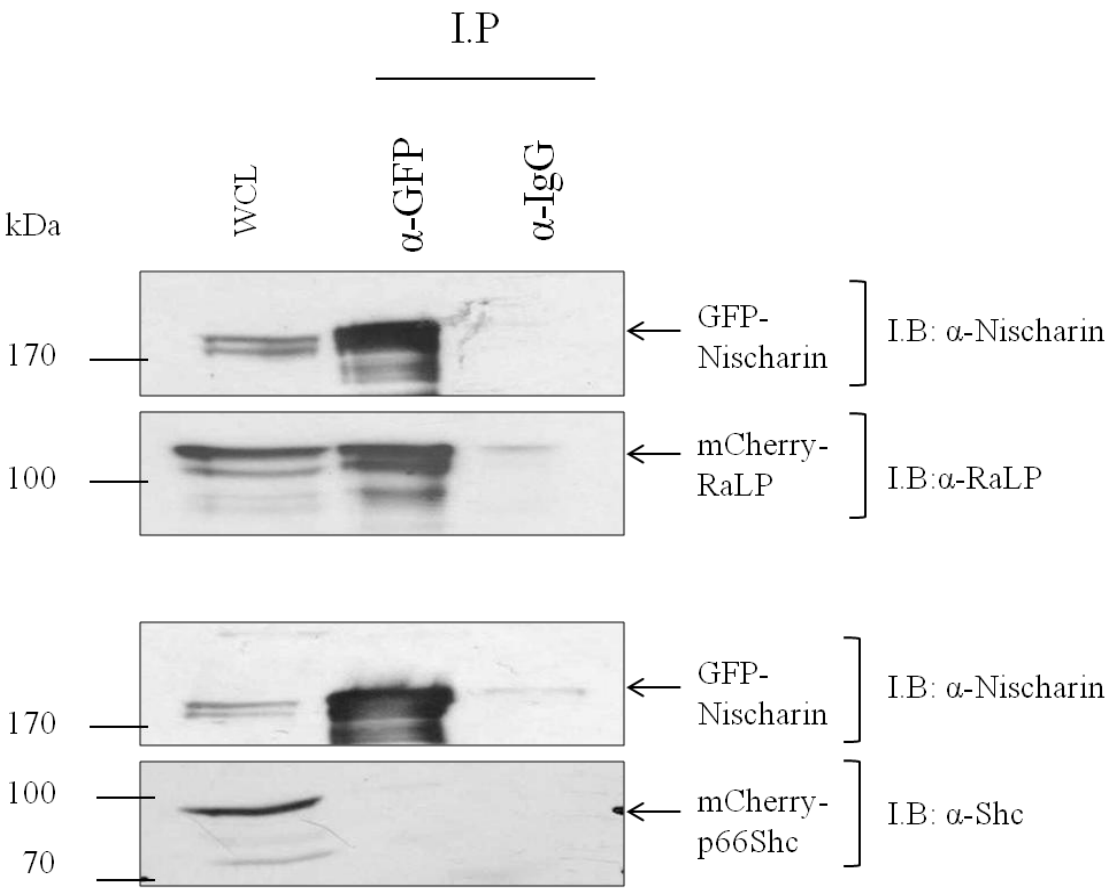

Figure 6.7 Nischarin binds RaLP but not p66Shc. HEK 293 cells were transfected with GFP-Nischarin and either mCherry-RaLP or mCherry-p66Shc. The cells were lysed and the GFP-Nischarin was immunoprecipitated by 3 µg anti-GFP antibody. The whole cell lysates (WCL) represent 1/20 of the total cell lysates. Immunopreciptates were tested for the existence of mCherry-RaLP or mCherry-p66Shc using anti-RaLP (4443) or anti-ShcA antibodies; respectively. IgG (3 µg) was used as control for the immunoprecipitation (I.P).

Initially, it was of interest to identify the localisation of each protein individually, 518.A2 melanoma cells were transfected with FLAG-RaLP or GFP-Nischarin. FLAG-RaLP was detected using a secondary anti-mouse antibody coupled to Alexafluor 594. Although, both RaLP and Nisharin showed a predominant cytoplasmic distribution (Figure 6.8a), a fraction of RaLP was observed at the membrane region. To study RaLP and Nischarin colocalisation, GFP-Nischarin and FLAG-RaLP were coexpressed in 518.A2 melanoma cells. Nischarin and RaLP displayed colocalisation in the cytoplasm particularly at the perinuclear region as well as at cell motility structures, membrane ruffles and lamellipodia (Figure 6.8b). Thus RaLP and Nischarin have a similar pattern of distribution, which might indicate their association.

6.2.7 RaLP interaction with the human version of Nischarin (IRAS):

The subcellular localisation of a signalling protein is important for its cellular function. It has been suggested that IRAS interferes with cell motility via trafficking α5 integrin to the endosomes (Lim and Hong, 2004). DAUV melanoma cells were transfected with Myc-IRAS or GFP-RaLP or with Myc-IRAS and GFP-RaLP together. Cells expressing IRAS alone demonstrated predominant cytoplasmic staining and also exhibited a vesicular-like pattern especially at the perinuclear region (Figure 6.9i). In addition staining at the membrane region was observed in a subset of cells (Figure 6.9i). RaLP expressing cells displayed staining in the nuclear compartment in a proportion of cells, diffuse cytoplasmic distribution and in a vesicle-like structure at the perinuclear region (Figure 6.9ii). RaLP was also present at the membrane ruffles (Figure 6.9ii). The cells that coexpressed both IRAS and RaLP showed a unique vesicular colocalisation at the perinuclear region and in the cytoplasm (Figure 6.9iii). Moreover, IRAS and RaLP colocalisation has extended to the plasma membrane. Interestingly, a proportion of cells demonstrated colocalisation at a structure similar to focal adhesions (Figure 6.9iii). This result confirmed the association of RaLP and IRAS in vesicle-like structures at the perinuclear region, in the cytoplasm especially around the nucleus and occasionally at the membrane region.

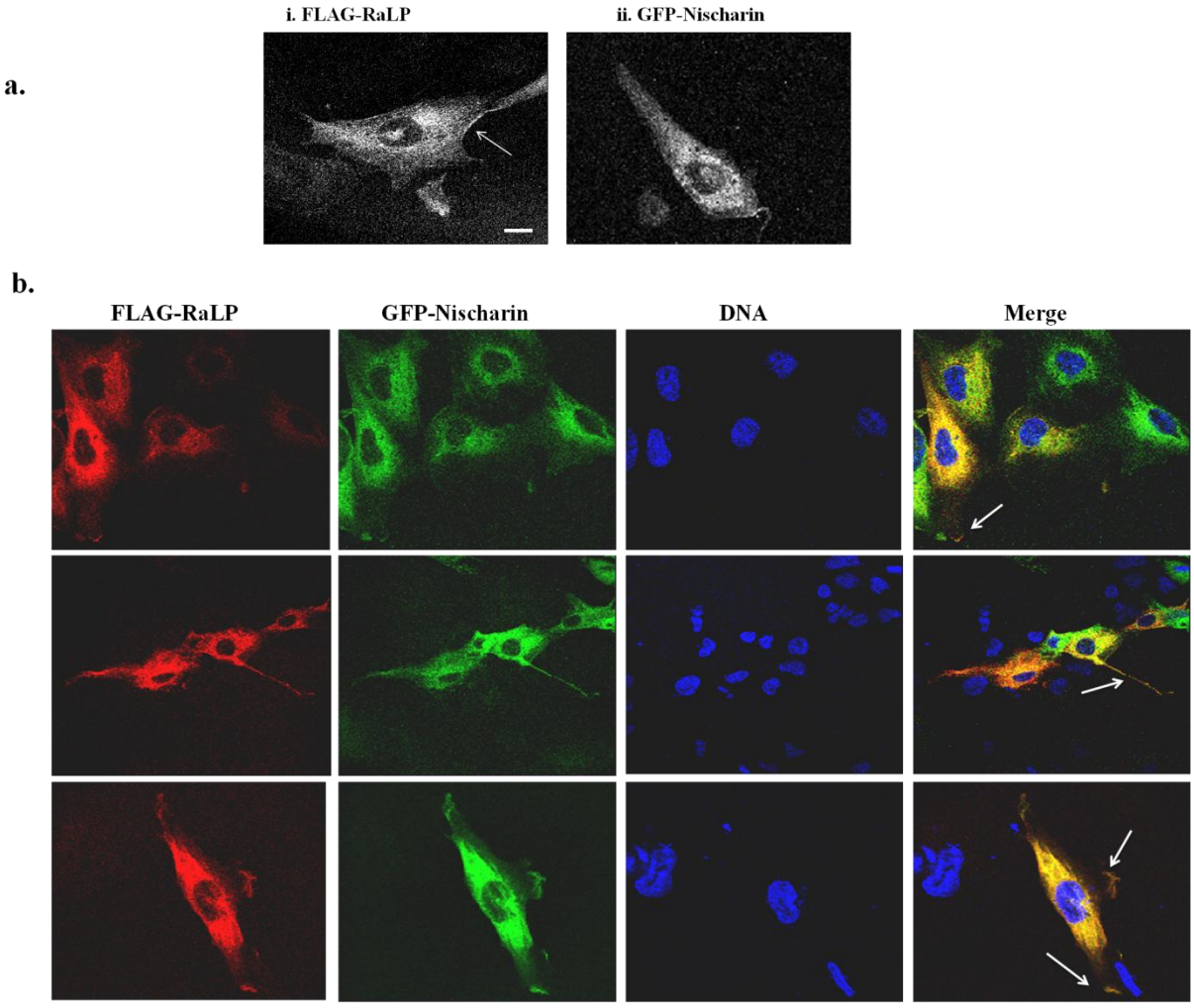

Figure 6.8 Subcellular localisation of RaLP and Nischarin. (a) 518.A2 melanoma cells were seeded on coverslips and transfected with FLAG-RaLP or GFP-Nischarin and the cells were fixed, stained and visualised as in (b). (b) 518.A2 cells were cotransfected with FLAG-RaLP and GFP-Nischarin. The cells were fixed with 3.7% formaldehyde and permeabilised by 0.1% Triton-x100, followed by staining with anti-FLAG antibody (1:500) and anti-mouse Alexafluor 594 (red) to visualise FLAG-RaLP. The DNA was stained with Hoechst (1 µg/ml) and appears in blue. The cells were visualised by Laser Confocal Microscopy using a 63 x 1.4 N.A oil immersion objective. The merge represents the overlay of red, green and blue channels. The overlay was performed by ImageJ or Leica software. The arrows indicate membrane regions where RaLP and Nischarin may colocalise. Arrows indicate the areas of interest; scale bar represents 8 µM.

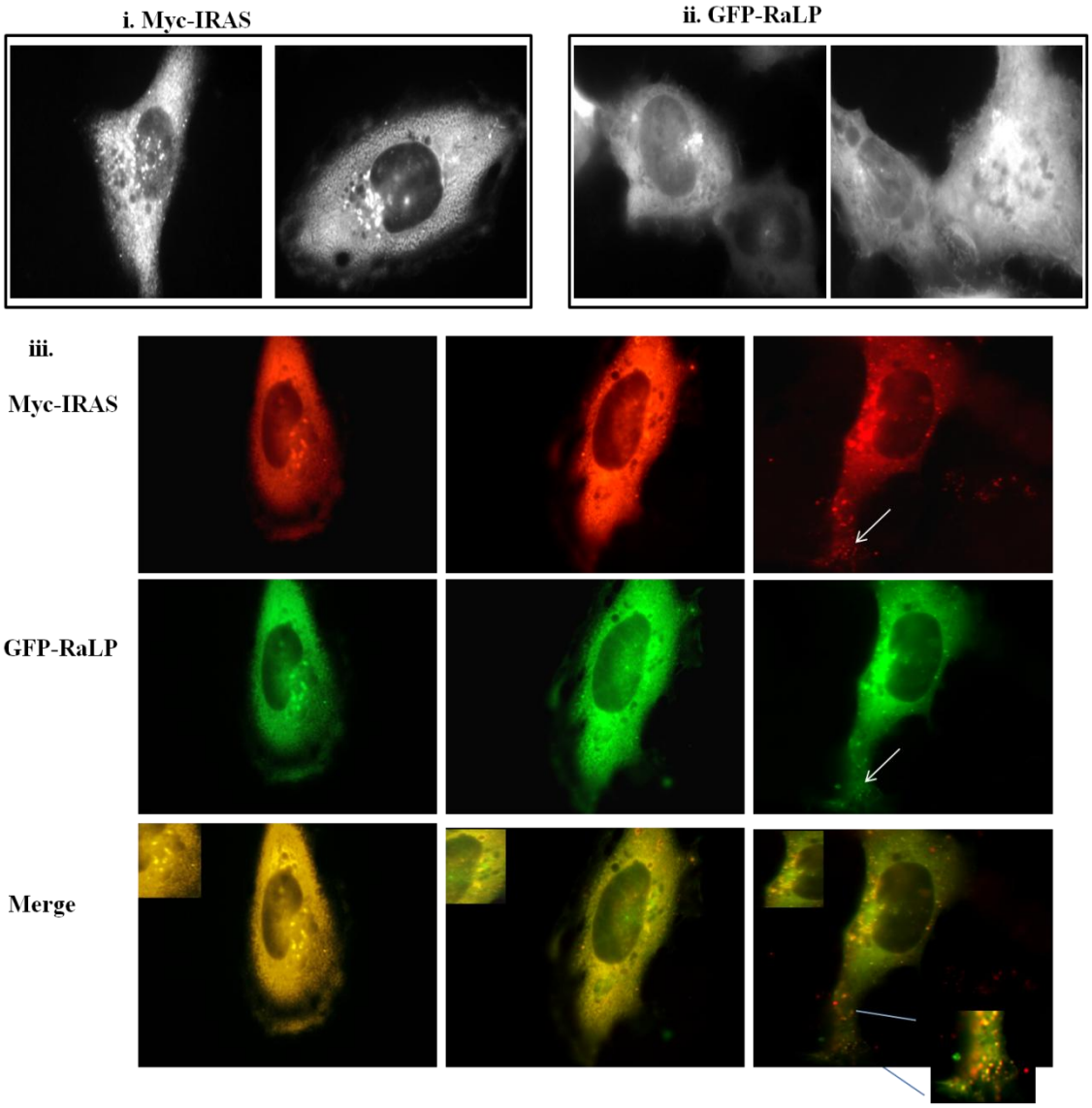

Figure 6.9 Localisation of RaLP and IRAS in DAUV melanoma cells. DAUV melanoma cells were seeded on coverslips and then were transfected with Myc-IRAS (i) or GFP-RaLP (ii) or with Myc-IRAS and GFP Nischarin (iii). After 24 hrs the cells were all fixed and the ones that were transfected with Myc-IRAS (i and iii) were permeabilised, and immunostaining with anti-Myc antibody was performed. The cells were visualised using a Nikon fluorescence microscope and 100x N.A 1.4 oil objective. In (iii) both green and red channels were merged using ImageJ software. Arrows indicate intracellular structures look like focal adhesions.

6.2.8 LIMK exists in one complex with RaLP and Nischarin:

Nischarin has previously been shown to bind LIMK; thereby inhibiting its activity and ability to promote cell migration (Ding et al., 2008). It was therefore hypothesised that RaLP might be present in the same complex with LIMK. N1E115 neuroblastoma cells were transfected with HA-LIMK and either with FLAG-RaLP or FLAG-RaLPΔCH2 and their extracts were employed for coimmunoprecipitation with anti-FLAG antibody. FLAG-RaLP was able to immunoprecipitate LIMK, whereas FLAG-RaLP that lacks the amino terminal CH2 failed to pull down LIMK. Immunoblotting for endogenous Nischarin showed a modest association of Nischarin in the LIMK/RaLP complex (Figure 6.10). Unexpectedly a faint band (less intense than in FLAG-RaLP precipitates) corresponding to Nischarin was observed in FLAG-RaLPΔCH2 precipitates, this might indicate an alternative indirect way for Nischarin to associate with RaLP. These data suggest that RaLP might associate directly or indirectly with LIMK.

6.2.9 The presence of LIMK in the complex has not interfered with RaLP and Nischarin association:

Since LIMK was found to coprecipitate with RaLP, it was of interest to examine whether LIMK has any effect on the association of RaLP and Nischarin. FLAG-RaLP stably expressing HEK 293 cells were either transfected with HA-LIMK or GFP-Nischarin or HA-LIMK and GFP-Nischarin together. FLAG-RaLP in the cells extracts was immunoprecipitated by anti-FLAG antibody and the associated proteins were then examined by western blotting (Figure 6.11a). The presence or absence of LIMK had no significant effect on RaLP and Nischarin association ($p=0.55 > 0.05$) (Figure 6.11b). FLAG-RaLP immunoprecipitated HA-LIMK successfully, although in the presence of Nischarin it does seem that RaLP/LIMK association was reduced suggesting that Nischarin might compete for LIMK binding to RaLP.

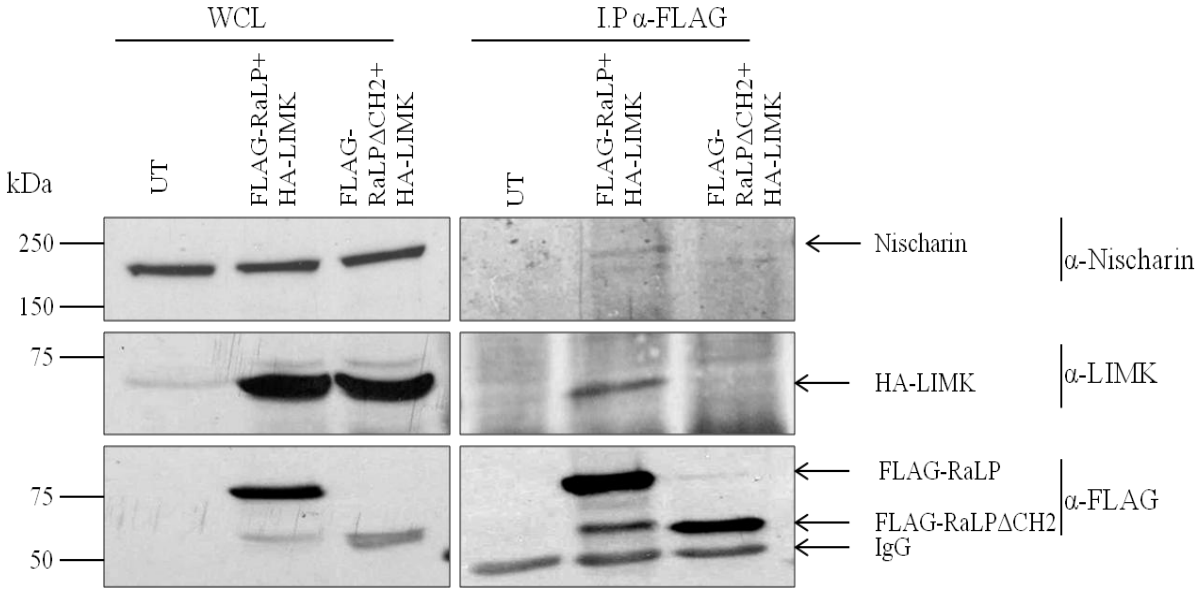

Figure 6.10 Investigating whether RaLP and LIMK are present in the same complex. N1E115 neuroblastoma cells were cotransfected with HA-LIMK and either with FLAG-RaLP or FLAG-RaLPΔCH2. Along with untransfected cells, the cells were lysed and FLAG tagged proteins were immunoprecipitated with anti-FLAG antibody. The associated proteins were tested by immunoblotting with anti-Nischarin, anti-LIMK or anti-FLAG antibodies.

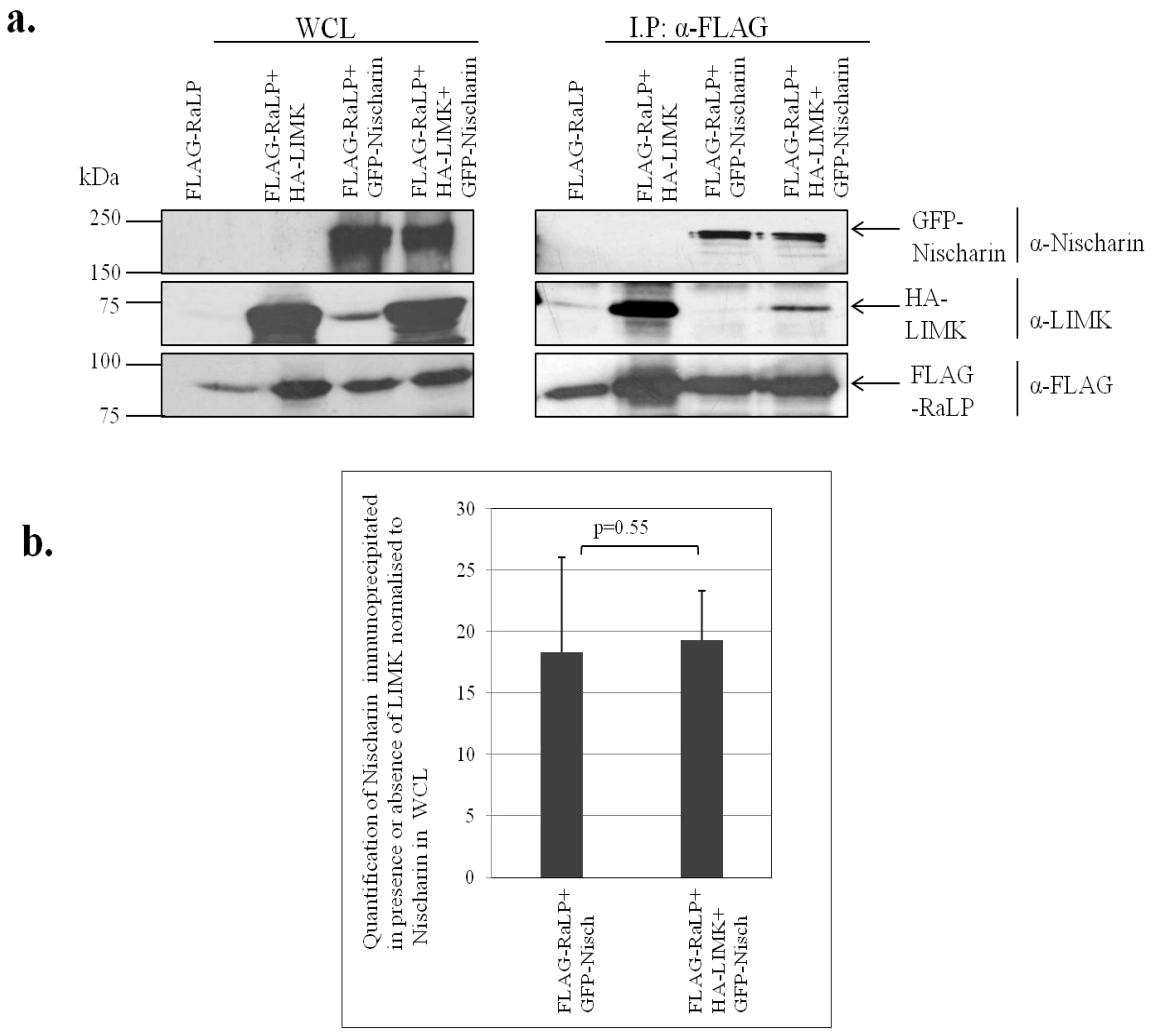

Figure 6.11 Effect of LIMK expression on the association between RaLP and Nischarin. FLAG-RaLP stably expressing HEK 293 cells were transfected with HA-LIMK, GFP-Nischarin, or HA-LIMK and GFP-Nischarin together. The cells lysates obtained from each set of the transfected cells along with untransfected FLAG-RaLP expression cells were incubated with immobilised anti-FLAG antibody. The immunoprecipitates were tested by performing immunoblotting with anti-Nischarin or anti-LIMK or anti-FLAG antibodies. (b) a bar chart represents the amount of GFP-Nischarin coimmunoprecipitated with FLAG-RaLP in the presence, or absence of HA-LIMK. The normalisation to Nischarin was achieved using imageJ and Excel software. The bar chart is a pool of three independent experiments; error bars represent standard error of mean.

6.2.10 RaLP and Nischarin interaction has no significant role in the LIMK/cofilin pathway:

In order to have a further insight into the functional consequences of the RaLP/Nischarin interaction, it was aimed to investigate the effect of this interaction on LIMK phosphorylation. The negative regulation of active LIMK by Nischarin has been reported previously, and it was found that this suppression results in the inability of active LIMK to phosphorylate its substrate cofilin (Ding et al., 2008). RaLP was suggested to induce cell migration via a MAPK independent pathway (Fagiani et al., 2007). In accordance, it was speculated that RaLP may sequester Nischarin relieving its inhibitory effect on LIMK. Several transfections were performed using HEK 293 cells, which are known to transfect very readily. The cells were transfected either with HA-LIMK, HA-LIMK plus GFP-Nischarin or with HA-LIMK, GFP-Nischarin and FLAG-RaLP; the amounts of the transfected DNA were equalised by transfecting control vectors. After 24 hrs, the cells were serum starved for 6 hrs, then treated with 20% serum after serum starvation or stimulated with 1 µg/ml EGF for 5 min.

Both serum and EGF treatments promoted an increase in phosphorylated LIMK in the presence or absence of Nischarin. Additionally, Nischarin did not have any significant effect on the level of phosphorylated LIMK (Figure 6.12). The presence of RaLP resulted in an increased level of phosphorylated LIMK, but this did not correlate with the level of phosphorylated cofilin. In fact no consistent pattern in phosphorylated cofilin (pcofilin) levels was observed; although there was more pcofilin present in all cells transfected with LIMK than in the untransfected cells (Figure 6.12). Both EGF and serum promoted cofilin phosphorylation in cells expressing LIMK without addition of Nischarin or RaLP. In the presence of serum, Nischarin appears to decrease pcofilin levels whereas EGF had no effect. The presence of RaLP together with Nischarin appeared to promote cofilin phosphorylation in the serum starved cells, inhibit phosphorylation in the presence of serum and had no effect in the presence of EGF. This experiment was repeated using the same or different conditions, but we did not get any conclusive data to suggest an effect of the Nischarin/RaLP interaction on phosphorylation of cofilin. In addition, N1E115 cells were used as they express both LIMK and Nischarin endogenously. The cells were transfected with either FLAG-RaLP or FLAG-RaLPΔCH2 to explore whether cofilin phosphorylation is affected or not.

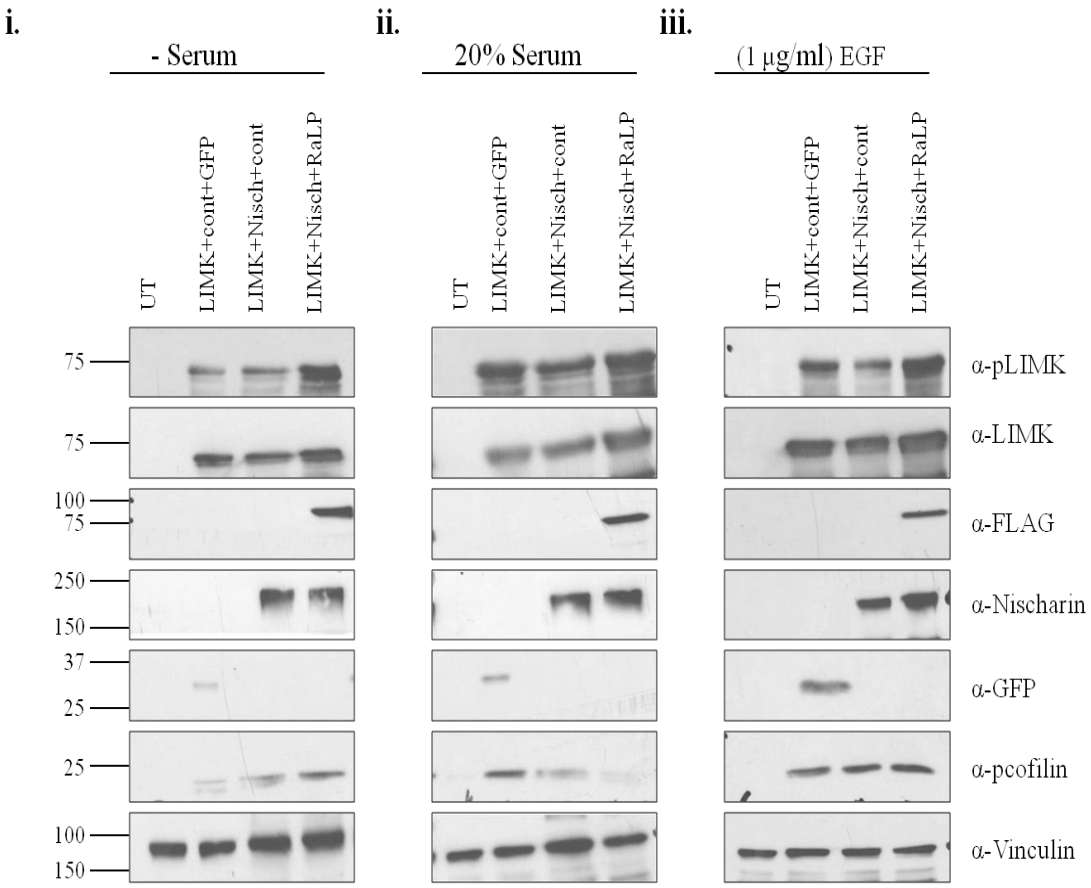

Figure 6.12 The effect of RaLP/Nischarin association on cofilin phosphorylation. HEK 293 cells were either untransfected (UT) or transfected with HA-LIMK together with control vector (cont), GFP, GFP-Nischarin (Nisch) or FLAG- RaLP (RaLP) in various combinations as indicated. After 24 hrs, the transfected cells along with the untransfected cells were either left serum starved for 6 hrs (i), or after serum starvation the cells were stimulated with 20% serum for 30 min (ii), or after serum starvation the cells were treated with 1 µg/ml EGF for 5min (iii). The cells were lysed and the extracts were immunoblotted with the indicated antibodies.

An elevation in pcofilin was observed in both RaLP and RaLPΔCH2 overexpressing cells (data not shown). Since RaLPΔCH2 cannot bind Nischarin this suggests that RaLP could be involved in activation of the LIMK/pcofilin pathway, and this must be independent of its ability to interact with Nischarin. Based on these data, it was deduced that the RaLP/Nischarin interaction has no obvious role in the LIMK/pcofilin pathway although RaLP is able to associate with LIMK. Moreover, RaLP might have an impact on this pathway independent of its interaction with Nischarin.

6.2.11 RaLP and IRAS association might affect ERK regulation:

IRAS was reported to regulate various signalling pathways via regulating extracellular regulated kinase (ERK) (Sano et al., 2002; Zhang et al., 2008). We therefore sought to determine whether RaLP interaction with IRAS has any impact on ERK activation. HEK 293 cells were transiently transfected with pCMV-vector plus GFP, Myc- IRAS plus GFP, or Myc-IRAS plus FLAG-RaLP (Figure 6.13a). IRAS overexpression negatively affected ERK activation ($p=0.02<0.05$) (Figure 6.13a and b), while its association with RaLP rescued ERK phosphoryation ($p=0.023<0.05$) (Figure 6.13a and b). RaLP expression alone presented higher levels of pERK than when it was associated with IRAS (Figure 6.13). These data suggested that IRAS impinges on ERK phosphorylation, while its coexpression with RaLP results in rescuing ERK activation in HEK 293 cells growing under normal conditions in medium containing 10% serum.

6.2.12 Effect of Nischarin overexpression on cell migration in FLAG-RaLP expressing HEK 293 cells:

To study the effect of the RaLP/Nischarin interaction on cell migration, wound assays were performed. HEK 293 cells and FLAG-RaLP stably expressing cells (F1) were either transfected with GFP or GFP-Nischarin. The closure of the wound through the monolayer cells was followed up for 24 hrs with images taken every 20 minutes and three positions were selected for each well (Figure 6.14a). For each position, the regression in wound area was calculated by subtracting the wound area at the selected time point from the initial wound area (0 time point).

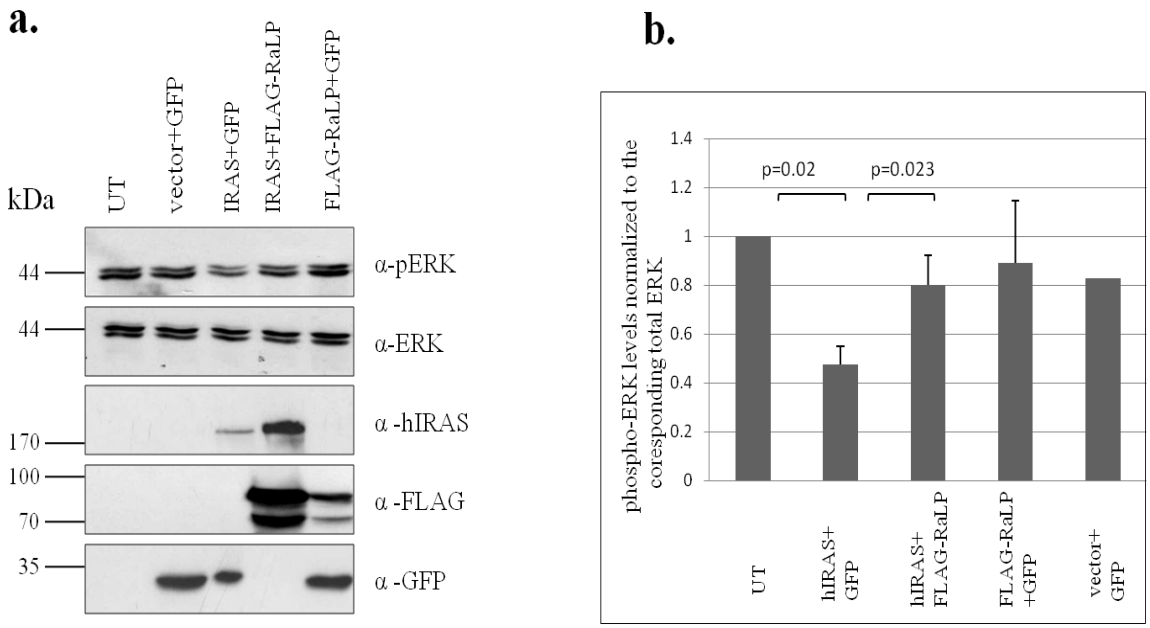

Figure 6.13 Effect of RaLP and IRAS interaction on ERK phosphorylation. (a) HEK 293 cells were transfected with empty pCMV vector plus GFP or Myc-IRAS plus GFP or Myc-IRAS plus FLAG-RaLP or with FLAG-RaLP plus GFP. The cells that grew under normal conditions were lysed. The cell extracts obtained from the transfected cells along with the untransfected cells were resolved on a 10% SDS-PAGE gel. Immunoblotting was performed with the indicated antibodies. (b) a bar chart representing p-ERK levels normalized to total ERK in the cell lysates. N=3, $P<0.05$ and error bars represent standard error of mean.

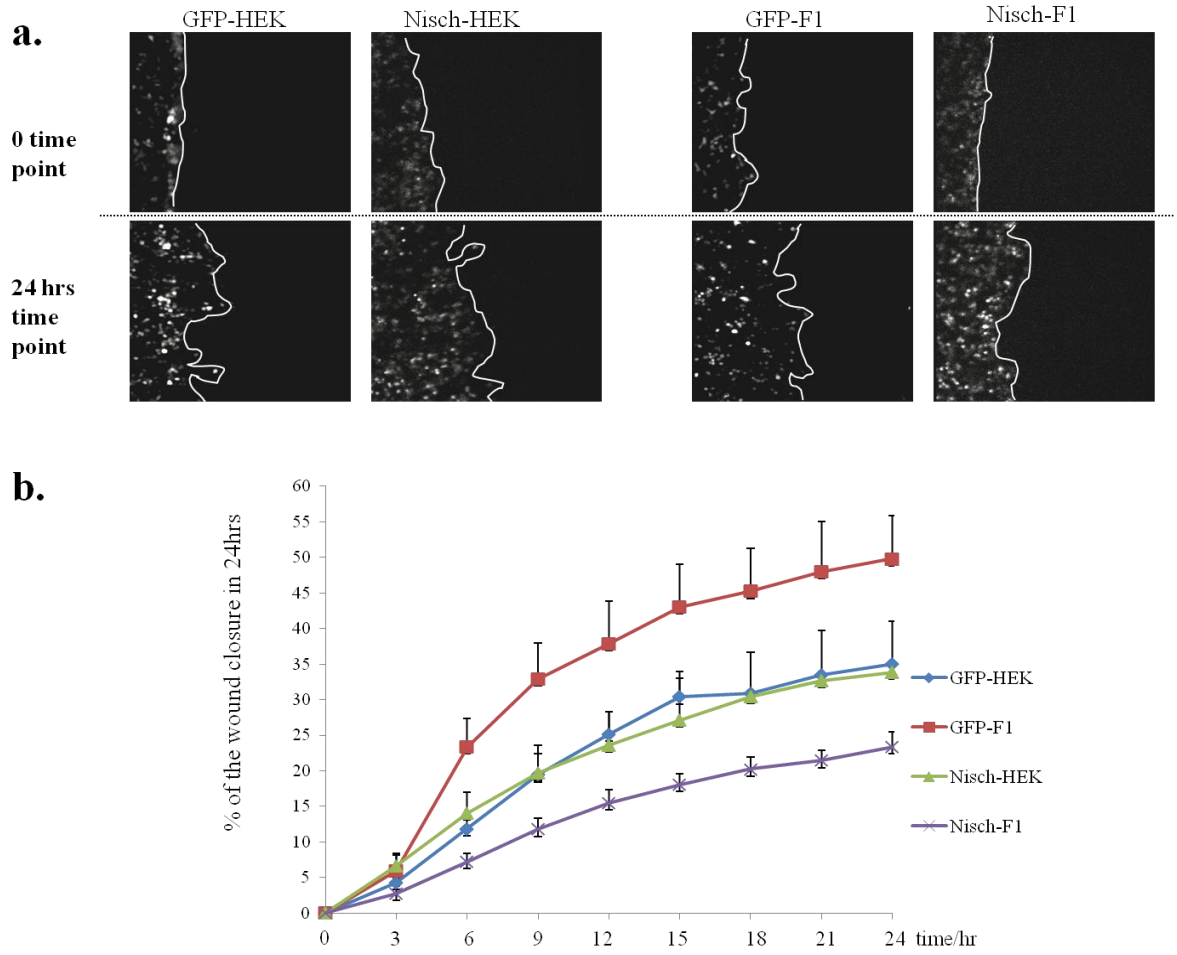

Figure 6.14 The effect of Nischarin upregulation on cell migration. (a) HEK 293 and FLAG-RaLP stably expressing cells (F1) were seeded into a 6 well plate overnight. The cells were either transfected with GFP (GFP-HEK and GFP-F1) or GFP-Nischarin (Nisch-HEK and Nisch-F1) for 24 hrs. A straight scratch was made in the middle of each well generating a wound through the confluent cells. The migration of cells was recorded for 24 hrs using a Nikon fluorescence microscope, Nikon-NIS-elements software and 10x 0.3 N.A objective. (a) illustrates representatives snap shots for one position out of 3 at 0 and 24 hrs time points, for the transfected HEK and F1 cell lines. (b) a graph shows the percentage of wound closure that was calculated at 8 time points. The average of 3 positions was plotted and error bars represent standard error of the mean.

This was then expressed as a percentage of initial wound area (0 time point), to give % of wound closure. The comparison was made based on the average obtained from three calculated % wound closure (3 positions) for the same selected time point.

The GFP-Nischarin expressing F1 cells showed low migratory rate in comparison to the transfected F1 cells expressing GFP alone. HEK 293 cells that were transfected with Nischarin demonstrated no difference in cell migration when compared with GFP control vector transfected HEK cells. Moreover, GFP expressing F1 cells migrated faster than the HEK 293 cells that were expressing GFP (Figure 6.14b). Although this experiment was performed only once, it helped us to infer that RaLP induced migration in HEK 293 cells, and this enhanced migration might be impeded by Nischarin overexpression.

6.3 Discussion

Although RaLP has been reported to play a role in melanoma cell migration (Fagiani et al., 2007) the molecular basis for this observation remains obscure. To unmask RaLP's role in migration, a yeast two hybrid library screen was conducted to identify RaLP binding partners that might facilitate its role in migration. A novel protein, Nischarin, that functions as a negative regulator of cell motility was found to interact with the CH2 domain of RaLP. It was of importance to study this interaction further in mammalian cells to provide us with an understanding of how RaLP might induce cell migration. Coimmunoprecipitation experiments using transfected HEK 293 cells provided clear evidence that RaLP and Nischarin can interact in mammalian cells. Our data also showed that RaLP can also bind to the human homologue of Nischarin (IRAS), which contains an additional PX domain capable of binding PI3P. Accordingly, this indicates that the RaLP interacting region is conserved in both mouse and human versions of Nischarin.

RaLP that lacked the amino-terminal CH2 domain failed to immunoprecipitate Nischarin; therefore, RaLP-CH2 domain is a prerequisite for its interaction with Nischarin. The CH2 domain was mapped further to find out the minimum region required for the complete interaction. A region from amino acid 1 to 93 was determined to be indispensible for the interaction to occur, notably, this deletion mutation results in RaLP nuclear translocation. This might indicate the cytoplasmic presence of RaLP is crucial for this interaction to occur. Deletion of amino acids 1 to 24 reduced the interaction by 70%, which might pinpoint the importance of these residues in the stabilisation of the interaction. For the first time, it was shown that the CH2 domain of RaLP is involved in protein-protein interaction. Association with Nischarin is unique to RaLP among the Shc proteins. Although p66ShcA possesses a CH2 domain, Nischarin was not able to coimmunoprecipitate with p66ShcA. Consequently, this might indicate that RaLP association with Nischarin has a distinct role either in the neuronal cells which express both proteins or possibly in melanoma cell migration.

RaLP and Nischarin were proved to associate when expressed at physiological levels in neuroblastoma cells, suggesting a role for this interaction in mouse and human neuronal cells. Investigations on the pattern of RaLP expression exhibited a predominant

expression in the mouse nervous system as well as in neural crest derived human melanocytes (Jones et al., 2007; Fagiani et al., 2007). Moreover, RaLP association with nerve growth factor receptors was determined and its role in neuronal development and differentiation was suggested (You et al., 2010). In support of a role for RaLP function in neuronal cells, our proteomics data revealed the neurotrophin receptor (TrkC) and Ret as binding partners for RaLP, which both have been proven to play a role in neuronal cell survival and differentiation, respectively. Equally important, a role for IRAS in imidazoline signalling has been described in neuronal cells, and it has been reported to be an anti-apoptotic candidate and in neuronal differentiation (Minichiello and Klein, 1996; Takaku et al., 2013). Further studies are needed to investigate the impact of the RaLP/Nischarin interaction in neuronal growth, differentiation and survival.

Since Nischarin is a known inhibitor of LIMK, this prompted us to investigate the functional consequences of RaLP and Nischarin interaction on the LIMK/cofilin migratory pathway. It was assumed that RaLP might sequester Nischarin or block Nischarin/ LIMK association relieving the inhibitory effect on LIMK allowing the cells to acquire an invasive phenotype. Despite the presence of LIMK in RaLP immunoprecipitates, we could not delineate any significant impact on phosphorylation of cofilin, the downstream LIMK substrate. In contrast to LIMK's role in actin assembly through deactivating actin severing factor cofilin, it has also been shown to coordinate microtubules in endothelial cells through its interaction with Tubulin (Gorovoy et al., 2005). Based on this observation, it is worth exploring whether LIMK and RaLP association interferes with microtubules dynamics, especially since the proteomic data identified Tubulin α and β as interacting proteins for RaLP.

Despite Nischarin's reported role in inhibiting the LIMK/cofilin pathway, our experiments did not show a consistent effect of Nischarin on pLIMK or pcofilin. This might be explained by the fact that in the previous published work (Ding et al., 2008), the researchers used kinase assays to test the effect of Nischarin's inhibitory action on LIM Kinase activity, and different cell systems and experimental conditions were employed. Alternatively, the role of phosphorylation of cofilin in cell migration is controversial since the switch of cofilin between phosphorylated and unphosphorylated states is proved to be crucial for active cell motility (Nishita et al., 2005).

As a consequence, it worth considering the above mentioned points in the future experiments to investigate the exact impact of the RaLP/Nischarin interaction on the LIMK/pcofilin migratory pathway.

Based on mass spectrometry data, different cytoskeletal-associated proteins including Tubulin α/β and Plectin were revealed to associate with RaLP. It will be important to investigate whether any of these proteins interact with the RaLP/Nischarin complex as well as to test the effect of this complex formation on the cytoskeleton. Indeed, this might provide compelling evidence for the molecular events resulting from RaLP and Nischarin interaction.

In v-ErbB-transformed fibroblasts, Shc was found to form a multi phospho-protein complex with Grb2, Nck, actomyosin associated protein; caldesmon, PAK1 and MLCK (McManus et al., 2000). This complex was suggested to permit the EGFR oncoprotein to modify the cytoskeleton and block the proapoptotic cascade through PAK1 regulation of MLCK, LIMK and inactivation of proapototic factor Bad (McManus et al., 2000). Subsequently, RaLP might be involved in a similar complex including PAK and LIMK which might explain the presence of LIMK in FLAG-RaLP immunoprecipitates.

HEK 293 cells overexpressing IRAS showed a decline in p-ERK levels and this was moderately rescued when RaLP was coexpressed with IRAS. The cells were grown in the presence of 10% serum, which might explain the difficulty in highlighting the exact upstream initiators for this effect. RaLP and IRAS association might be needed for transducing insulin-like growth factor receptor (IGFR) signal by forming a complex with insulin receptor substrates offering the cells protection against apoptosis via activating the ERK pathway. A recent study found that ShcA associates with IRS1 and 4 upon activation of insulin-like growth factor receptor (Kulahin et al., 2012). RaLP like ShcA isoforms is reported to act as a substrate for IGFR (Smith et al., 2006; Fagiani et al., 2007). IRAS upregulation in insulin treated PC12 cells resulted in suppression of caspase-3 activity due to serum deprivation (Dontewill et al., 2003) and in addition to the reported IRAS/IRS4 association (Sano et al., 2002), provides compelling evidence that IRAS acts in the IGF pathway. To elicit a dramatic effect on ERK activation due to the RaLP/IRAS interaction, we might need to use a different cell line and different

conditions to gain further insight into the circumstances and the resulting biological response of RaLP/IRAS interaction.

ShcA was determined to translocate into early endosomes with EGFR after EGF stimulation (Oksvold et al., 2000). A report by Lim and Hong showed that IRAS might exert an inhibitory effect on cell migration via trafficking α5 integrin into early endosomes. The vesicular pattern of distribution IRAS and RaLP at the perinuclear region might suggest the translocation of RaLP with α5 integrin into the endosomes. Therefore in our preliminary wound assay experiment, Nischarin could abrogate RaLP's effect on migration via its sequestration into the endosomes at the perinuclear region (Figure 6.14).

Different reports have addressed the significance of the Shc and α5β1 integrin association. In an epithelial cell model, Shc was demonstrated to play a role in MAPK and α5β1 integrin cross talks through its phosphorylation by integrin-associated tyrosine kinases (Kuwada and Li, 2000). IRAS was found to be responsible for α5 integrin trafficking (Sano et al., 2002), and in agreement with this, Nischarin was reported recently to downregulate α5 integrin at the protein level (Branwal et al., 2011). Therefore, RaLP and Nischarin/IRAS association might affect α5 integrin trafficking, or interfere with the cross talks between α5β1 integrin and MAPK. The focal adhesion pattern of distribution that was demonstrated by RaLP and IRAS might indicate the coexistence of these proteins with integrins.

In summary, RaLP was found to consistently interact with Nischarin and human IRAS. Preliminary experiments showed the possible role of this interaction in ERK activation, while no significant data were obtained to elucidate the impact of the RaLP/Nischarin interaction on the LIMK/pcofilin migratory pathway.

Chapter 7

Discussion & Conclusions

7. Discussion

Melanoma is one of the most life-threatening cancers**,** because of its ability to metastasise early once it reaches a certain progression stage. Therefore, nowadays a lot of research is focusing on investigating the transition phase of melanoma to a more aggressive phenotype. Interestingly, RaLP was found to be upregulated in vertical growth phase and metastatic melanomas, therefore RaLP characterisation is crucial to understand its exact role in melanoma cell invasion and progression.

The newly identified protein, RaLP, belongs to the Shc family of adaptor proteins that is responsible for propagating extracellular signals to the internal environment of the cell. RaLP has the same structural hallmark of the Shc proteins (CH2-PTB-CH1-SH2). Our background knowledge about the Shc family represented a platform to study the melanoma associated Shc adaptor, RaLP.

7.1 The intracellular distribution of RaLP:

According to our data, the intracellular distribution of RaLP was found to be at the membrane region, cytosol, mitochondria, vesicle-like structures and a small fraction in the nucleus. Shc proteins were shown previously to exist in the cytosol and to be recruited to the membrane region upon exposure to certain stimuli (Sato et al., 2000). In addition, the mitochondrial localisation of p46ShcA isoform is dependent on a mitochondrial target sequence (MTS) (Ventura et al., 2004), and interestingly the same MTS is conserved in RaLP. Although RaLP possesses the same MTS as p46ShcA, it might translocate to the mitochondria through an alternative mechanism, as p66ShcA was shown to translocate to the mitochondria independent of the MTS (Giorgio et al., 2005).

Using mass spectrometry, some mitochondrial proteins (e.g. Trifunctional enzyme subunit alpha, Apoptosis inducing factor 1 and Mono functional C1-tetrahydrofolate synthase) were identified in GFP-RaLP co-precipitates, which might support the presence of both GFP-tagged RaLP, and the endogenous protein in the mitochondrial fraction (Table 5.2). Surprisingly, the mitochondrial staining that was detected by the anti-RaLP antibody (4443), was not observed in cells transfected with GFP-RaLP. This discrepancy might be attributed to the interference of the tag with the efficient mitochondrial import, or alternatively RaLP overexpression may mask the fact that a

small proportion is retained in the mitochondria. It will be important to show the specificity of the anti-RaLP antibody mitochondrial staining by knocking down endogenous RaLP. As it was difficult to knock down RaLP, it might be worth trying to generate a RaLP-/- cell line by introducing a plasmid expressing an antisense RNA or shRNA transcript. It will also be of interest to explore the mechanism by which RaLP translocates to the mitochondria, as well as the possible function of RaLP in the mitochondria.

7.2 RaLP shuttles between the cytoplasm and the nucleus:

Interestingly, although RaLP was mainly present in the cytoplasm, a proportion of both the transfected and endogenous RaLP exists in the nuclear compartment. This is in contrast to a previous report that revealed no evidence for its presence in the nuclear compartment (Fagiani et al., 2007). Nuclear presence is not a novel phenomenon for Shc proteins, since ShcA has previously been shown to translocate to the nucleus, although the exact nuclear function has not yet been described (Yoshida et al., 2004; Yukimasa et al., 2005; George et al., 2009). Other adaptors like downstream of tyrosine kinase1 (DOK1), which is mainly a cytoplasmic protein, was found to shuttle between the cytoplasm and the nucleus (Niu et al., 2006).

Introducing point mutations into the ^{83}LCTLIPRM^{90} motif in the CH2 domain revealed a functional RaLP nuclear export signal that allows RaLP to export from the nucleus via the CRM export system. It was also of importance to understand the mechanism by which RaLP translocated into the nucleus. A close observation of the RaLP sequence revealed amino acids 237-240 (KKRK) that might represent a functional nuclear localisation signal. Mutation of the KKRK motif in p59RaLP had no pronounced impact on p59RaLP nuclear localisation, which suggests that RaLP depends on other mechanisms to be imported into the nucleus.

RaLP was found to form a complex with Importin-beta, which represents a key component of nuclear transport machinery (Jakel and Gorlich, 1998), as well as to Nup107, that regulates the nucleocytoplasmic shuttling of proteins (Boehmer et al., 2002). Taken together, it was speculated that RaLP might form a complex with other proteins facilitating its nuclear translocation.

Subsequently, it was sought to gain insight into the conditions that might trigger RaLP nuclear translocation. Notably in previous studies, stimulating cells with agents that induce DNA damage e.g. IR, UV, cisplatin and H_2O_2, resulted in EGFR translocation to the nucleus (Xu et al., 2009; Liccarddi et al., 2011). As RaLP is a known downstream substrate of the EGFR (Fagiani et al., 2007), and the related protein p66ShcA has been shown to play a role in the oxidative stress response (Migliaccio et al., 1999) we investigated RaLP nuclear localisation following H_2O_2 treatment. Our studies revealed that a proportion of RaLP accumulates in the nucleus when the cells are exposed to H_2O_2. RaLP nuclear translocation might be promoted by its phosphorylation by EGFR, or RaLP could possibly form a complex with EGFR, which in turn facilitates RaLP translocation to the nucleus (Figure 7.1a). Alternatively, RaLP nuclear translocation might be facilitated by forming a complex with another protein (Figure 7.1a). RaLP and EGFR association in the nuclear fraction after hydrogen peroxide treatment needs to be determined. Although phosphorylation was shown previously to play a role in protein nuclear translocation of some proteins (Chuderland et al., 2008), this is not always the case as Stat2 nuclear import was induced by EGF treatment without any effect on its phosphorylation (Johnson et al., 1999). According to these observations, RaLP nuclear translocation might possibly be independent of its phosphorylation status (Figure 7.1a).

In an attempt to determine the role of RaLP in the nucleus, we sought to investigate whether RaLP associates with DNA. Preliminary experiments showed that there is a possible RaLP and DNA association. The RaLP-CH1 domain consists of cysteine and histidine residues that are unconserved in other Shc proteins, that may represent a possible Zinc finger-like motif that facilitates protein-DNA interaction (Molkentin, 2000; Filion et al., 2006). Moreover, the CH2 domain of RaLP is rich in proline residues that might mediate RaLP-DNA interaction, as it has been shown previously that proline rich motifs initiate protein-DNA association (Gerber et al., 1994; Alevizopoulos et al., 1995). Accordingly, RaLP could possibly associate with the DNA directly through RaLP via a possible Zinc-finger like domain, or the proline rich motifs in the CH2 domain. Alternatively, RaLP might associate with the DNA indirectly by being involved in a transcriptional complex (Figure 7.1b). The association of RaLP with CCR4-NOT transcription complex (Table 5.2) has also provided additional evidence for a contribution of RaLP to gene transcription.

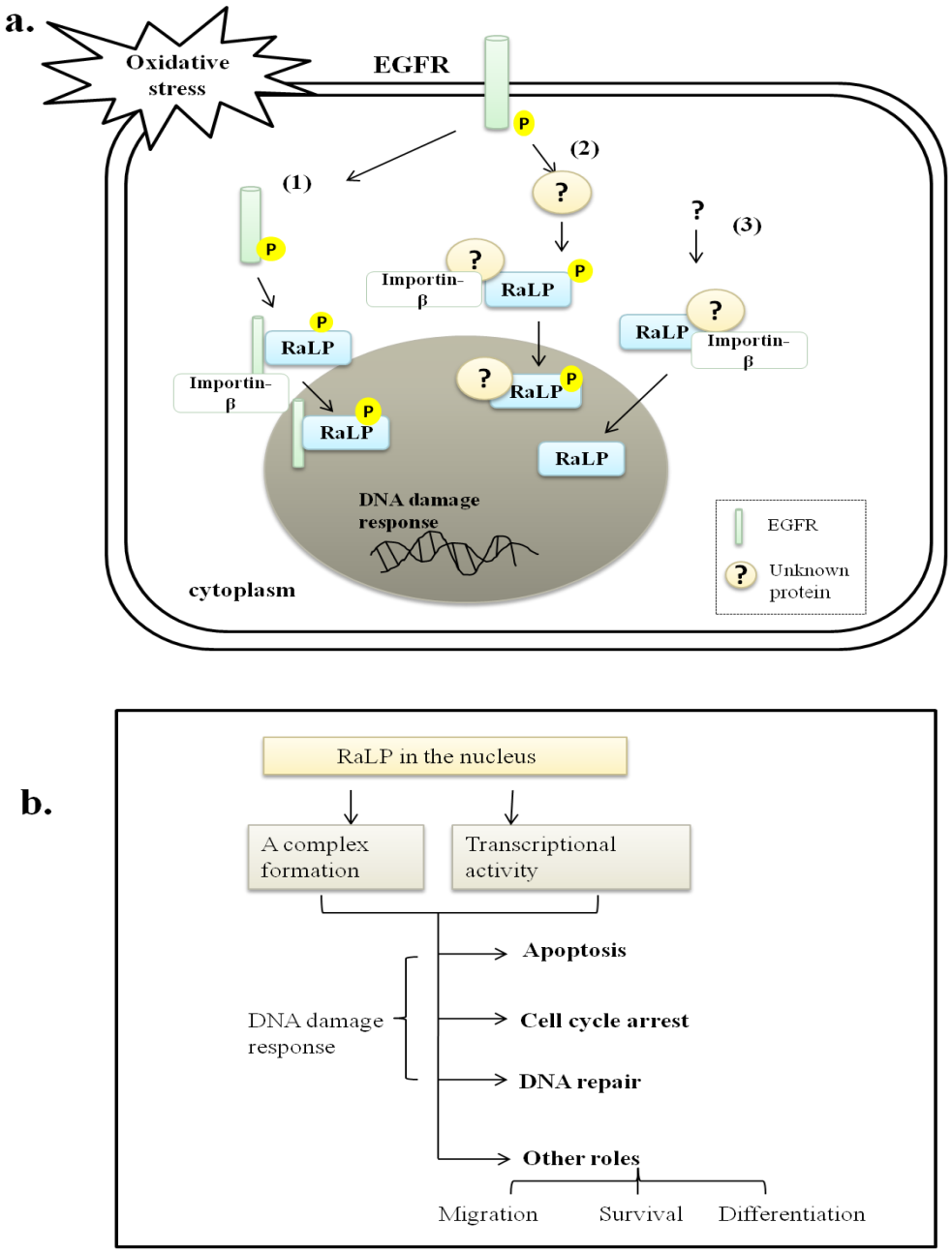

Figure 7.1 RaLP in the nucleus: (a) Mechanisms for RaLP nuclear transport in response to the oxidative stress. (1) and (2) represent RaLP nuclear translocation through activated EGFR-dependent mechanisms, which might either require formation of a complex with phosphorylated EGFR (1), or active EGFR might phosphorylate a protein that forms a complex and phosphorylates RaLP promoting RaLP entery to the nucleus (2). (3) RaLP nuclear transport might also be through forming a complex with a protein that is independent of EGFR stimulation. RaLP phosphorylation might be required for the nuclear role of RaLP or it might only convey a cytoplasmic signal in response to oxidative stress. (b) a diagrammatic representation shows possible roles for RaLP in the nucleus. RaLP could possibly regulate gene transcription in a direct or indirect way, thereby playing a role in the DNA damage response to oxidative stress and other pathways independent of the DNA damage response.

RaLP's role in gene regulation could explain the function of RaLP either in inducing cell motility or in the response to DNA damage by oxidative stress (Figure 7.1b).
The DNA/RaLP association requires further confirmation using more advanced techniques such as the ChIP on chip assay, that might additionally help in identifying the DNA sequence associated with RaLP.
Herein for the first time we found that RaLP shuttles between the cytoplasm and the nucleus. The wide distribution of RaLP in intracellular compartments suggests diverse functional roles for RaLP, as might be expected for a signalling adaptor. More work needs to be conducted in order to explore and characterise the exact role of the novel melanoma associated adaptor RaLP/ShcD in the nucleus.

7.3 RaLP isoforms

Shc proteins were shown to exist as multiple isoforms in the intracellular compartment due to alternative initiation codons or mRNA splicing. Since RaLP contains potential alternative initiation codons in its amino-terminal region, it prompted us to assume that RaLP might have shorter isoforms. The developed anti-RaLP antibody (4443) detected other bands in addition to the 70 kDa band that may represent different translation products of RaLP. The shorter isoform, p59RaLP, was observed in DAUV melanoma cells and human embryonic kidney cells, using anti-RaLP antibody (4443), it was also noticed in the cerebellum lysates of adult mouse brain (Jones et al., 2007). Based on these observations, the existence of RaLP isoforms needs to be studied thoroughly as it may help to explain the diverse intracellular distribution of RaLP; especially as our result suggests that shorter isoforms would have a nuclear existence.

7.4 RaLP phosphorylation

In this report we were able to show for the first time that RaLP becomes phosphorylated on Thr156/159 upon oxidative stress. Similarly a fraction of RaLP was shown to translocate to the nucleus when subjecting cells to H_2O_2, which raises a question as to whether threonine phosphorylation plays a role in RaLP nuclear translocation, whether it has an impact on RaLP's nuclear role, or if it is only required for RaLP's cytoplasmic function.

Many cellular proteins are regulated at the post translational level by their ubiquitination and then subsequent degradation by the 26S proteosome (Aiken et al., 2011). Two sequences have been described that target proteins for degradation by proteosomes; a PEST sequence (Rechsteiner and Rogers, 1996) and a destruction box (Fenteany and Schreiber, 1998). PEST motifs play a role in protein ubiquitination (Rechsteiner and Rogers, 1996). It was described previously that phosphorylation or dephosphorylation of serine and or threonine residues within the PEST motif plays an important role in the stability of PEST-containg proteins (Yaglom et al., 1994; Marchal et al., 1998; Khanday et al., 2005). Under oxidative stress, p66ShcA ubiquitination was shown to be inhibited by its phosphorylation at Ser52 and Thr386 (Khanday et al., 2005).

GPS.ARM 1.0 destruction box prediction programme revealed no destruction sequence in RaLP sequence, while, computational analysis of the RaLP sequence on a PEST motif prediction programme (EmBoss) predicted RaLP amino acids 123-134 as a potential PEST sequence. Interestingly, the potential PEST sequence (^{123}DPGSSGPS<u>S</u>PE^{134}) in RaLP contains Ser132 that was identified to be phosphorylated in both H_2O_2 treated and untreated cells. The phosphorylation of Ser132 might also acts as an atypical nuclear translocation signal, as the SPS motif phosphorylation in ERK, MEK1 or SMAD3 mediates Importin7 association, which then promotes the nuclear translocation of the proteins (Chuderland et al., 2008). Using mass spectrometry it was not possible to assess the degree of phosphorylation on Ser132, whether it increases or decreases with the H_2O_2 treatment. The degree of Ser132 phosphorylation might be investigated by employing phosphoamino acid assay, or by generating a phospho-specific antibody, which can then be used to detect Ser132 phosphorylation under H_2O_2 treated or untreated conditions. Thereafter, ubiquitination assays can also be performed on RaLP and its mutant RaLP/Ser132A to test whether Ser132 phosphorylation affects protein stability.

It is evident that RaLP becomes phosphorylated on Thr156/159 in the CH2 domain under oxidative stress; Thr159 was predicted as a site for JNK phosphorylation. Using kinase assays, the CH2 domain of RaLP has been shown to be a substrate for the activated JNK (Unpublished work by Khan and Prigent). JNK activation is required for cells to respond to the oxidative stress (Lu et al., 2007); accordingly phosphorylated RaLP might be required to convey a signal downstream of active JNK, under oxidative stress conditions.

The identification of RaLP phosphorylation on Ser132 and Thr156/159 in the CH2 domain, which is one of the least conserved regions among the other Shc proteins, suggesting a relevance of Ser132 and Thr156/159 phosphorylation in the distinct intracellular functions of RaLP.

7.5 RaLP mediated-p21 upregulation:

To test the molecular changes due to RaLP overexpression, stable cell lines were generated. It appeared that RaLP expression resulted in p21/cip upregulation, which in turn caused a moderate arrest of cells at G1 and G2 phases of the cell cycle. RaLP-mediated p21/cip upregulation might also be linked to the RaLP function in an anti-apoptotic pathway as FLAG-RaLP expressing cells displayed a higher survival percentage in comparison to FLAG-RaLP nonexpressing cells. This interesting phenomenon necessitates further work to find out the mechanism by which RaLP upreguates p21/cip, as well as the effect of the RaLP induced-p21/cip upregulation on cell differentiation and survival.

p21/cip is a well known negative regulator of the cell cycle and its regulation was reported to be through p53 dependent or independent mechanisms. Independent of the p53 pathway, p21/cip is upregulated by PI3K/Akt pathway activation (Li et al., 2002) as well as chronic simulation of ERK (Tombes et al., 1998; Lee et al., 2006).

Moreover, ectopic expression of p52 or p66 ShcA, but not p46, enhanced EGFR association with c-Src contingently upon EGF stimulation. ShcA (p52/p66) co-immunoprecipitated with c-Src thereby resulted in its activation (Sato et al., 2002) . The functional impact of ShcA/Src interaction was shown to induce the phosphorylation of Stat3/5b/1 transcription factor. EGF was reported to mediate Stat phosphorylation via Src stimulation in an epidermoid carcinoma cell line (A431) (Olayioye et al., 1999). Phosphorylated Stat relocates to the nucleus and hence promotes p21/cip1 expression (Chin et al., 1996). The cells overexpressing p52/p66 ShcA exhibited elevated levels of phosphorylated Src and Stat phosphorylation regardless of EGF treatment when compared to cells overexpressing p46ShcA. Based on the findings, the mechanism underlying RaLP-mediated p21/cip upregulation might be through Src-Stat activation, or alternatively through activation of PI3K/Akt or MAPK/ERK pathways.

RaLP-mediated p21/cip upregulation is an interesting observation that might explain the suggested functions of RaLP in cell survival and differentiation; however, further experiments are required to study the molecular mechanism underlying this observation.

7.6 RaLP interacting partners:

To obtain further understanding to the cellular role of RaLP, mass spectrometry was employed to identify some potential interacting partners. Interestingly, the resulting possible interacting partners of RaLP in this report have a parallel intracellular distribution to RaLP, as some nuclear, mitochondrial, cytoplasmic and membrane proteins were identified (Table 5.2 and Figure 6.5). It will be important to verify these potential associations further by conducting co-immunoprecipitation experiments.

7.6.1 RaLP association with microtubules:

Tubulin was shown to be present in GFP-RaLP precipitates in both transfected HEK 293 and neuroblastoma cell lines. ShcA was also shown to associate with tubulin (George et al., 2009), although no detailed study has yet been carried to address the Shc/tubulin association. Tubulin was described previously to associate with SH2 containing proteins, in particular the Grb2 adaptor protein (Itoh et al., 1996) that is known to bind Shc; this might suggest a mechanism for the Shc/ tubulin association. Furthermore, RaLP association to the cytoskeleton might be through tubulin independent mechanism as other cytoskeletal-associated Plectin and SPECC1l (Cytospin-A) (Wiche, 1998; Saadi et al., 2011) were shown to precipitate with RaLP from neuronal cell lysates. To this end, the association of RaLP with the cytoskeleton as well as the functional impact of this interaction on neuronal cell motility and differentiation require more investigations.

7.6.2 RaLP as a component in neuronal/neuromuscular transmission:

DNaJ proteins comprise a family of co-chaperone proteins that assist Heat shock protein 70 and 90 in their functions involving protein folding, stability and transport (Sterrenberg et al., 2011), as well as contributing to signal transmission at the synaptic junction of the neurones (Buchner and Gundersen, 1997). Our proteomics data revealed

members of this family as interacting partners of RaLP, likewise ShcA was reported to associate with DnaJ9 (George et al., 2009). Another interesting protein was found to associate with RaLP in the neuronal cell lysate, Neurobeachin that plays a crucial role in signal transmission at the neuromuscular junction (Su et al., 2004). It is possible that the association of DnaJ or Neurobeachin with RaLP might highlight a role of RaLP in neurotransmission as the impact of RaLP in clustering of acetylcholine receptors has previously been described (Jones et al., 2007).

7.6.3 RaLP acts as a substrate to TrkC/ Ret receptor tyrosine kinases:

Intriguingly, our proteomics data identified Ret oncoprotein and TrkC as possible interacting partners for RaLP. These receptor tyrosine kinases most likely represent upstream regulators of RaLP in neuronal cells. The role of TrkC in survival and cell motility is contingent upon NT-3 stimulation (Tauszig-Delamasure and Bouzas-Rodriguez, 2011; Ivanon et al., 2012). Ret conveys survival signals via ShcC/PI3K/Akt pathway activation in neuronal cells (De Falco et al., 2005). Shc proteins are known to play a key role in the TrkC and Ret signalling pathways (Haung and Reichardt, 2003; Knauf et al., 2003; De Falco et al., 2005). Consequently in a neuronal context, RaLP might exist in the same protein complex as Ret oncoprotein and TrkC, assisting in relaying survival signals downstream the receptors (Figure 7.2).

Based on our proteomics data, we were able to identify potential interacting partners for RaLP, which might provide further understanding of the function of RaLP in the intracellular compartment.

7.7 RaLP and Nischarin:

The role of RaLP in migration was described to be via MAPK dependent and independent pathways. Yeast two hybrid screens were carried out to identify RaLP interacting partners facilitating its role in migration (unpublished work by Wong and Prigent). A negative regulator of cell motility, Nischarin was found to interact with the CH2 domain of RaLP.

To gain further understanding of the significance of the RaLP/Nischarin interaction, it was aimed to investigate their association in mammalian cells. In this report it was

possible to show that RaLP and Nischarin co-immunoprecipitate from transfected cells. In addition we were able to show that both proteins interact in neuroblastoma cells when present at physiological levels.

To further determine the association between RaLP and Nischarin, confocal microscopy was employed which revealed an interesting co-localisation of RaLP and Nischarin at the membrane ruffles and the lamellipodia. When Nischarin was overexpressed individually in melanoma cells, it did not show a significant membrane localisation, while a proportion of RaLP clearly resided at the membrane. Accordingly, it appears that RaLP causes recruitment of Nischarin to the membrane. This observation was confirmed in a different perspective using neuronal cells (unpublished work by Barnett and Prigent).

Nischarin has been shown to inhibit cell motility through suppression of the PAK/LIMK/pcofilin migratory pathway (Alahari et al., 2003). It was speculated that RaLP might sequester or inhibit Nischarin, thereby inducing the PAK/LIMK migratory pathway. Unexpectedly, in this report it was not possible to prove that the RaLP/Nischarin interaction has an effect on the LIMK/pcofilin pathway. Using mass spectrometry to identify proteins associated with the RaLP/Nischarin complex in neuronal cells, Nischarin was identified as one of RaLP interacting partners further suggesting that this interaction is significant. In the same experiment different cytoplasmic proteins (e.g. Cytospin-A, Plectin, Tubulin-β and Neurobeachin) were shown to associate with RaLP, which might be present in the RaLP/Nischarin complex; indeed this finding requires further confirmation. It will also be of interest to determine whether the RaLP/Nischarin interaction depends on the phosphorylation of either or both of the proteins.

Further experiments were performed to investigate whether RaLP binds the human version of Nischarin (hIRAS). RaLP and hIRAS were successfully co-immunoprecipitated from lysates of transfected cells; their association was confirmed further by colocalisation experiments, which revealed their colocalisation at a vesicles-like structures.

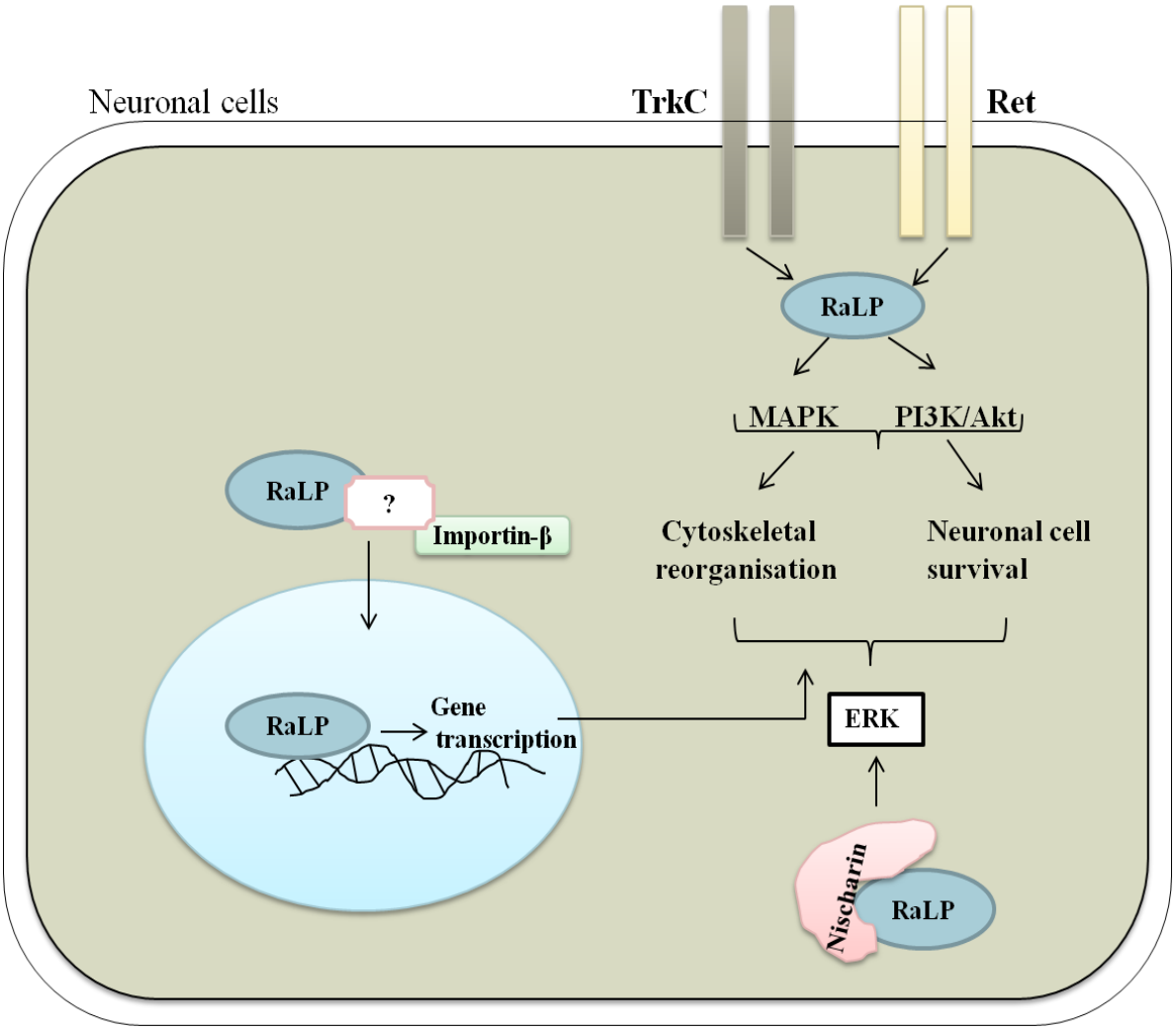

Figure 7.2 Possible underlying mechanisms by which RaLP promotes its biological functions. RaLP is abundantly expressed in neuronal cells and might form a multiprotein complex with TrkC and Ret receptors thereby inducing cell survival and cytoskeleton rearrangement. RaLP interacts with human Nischarin resulting in ERK activation that plays a key role in cell survival and cytoskeleton reorganisation. RaLP also associates with Importin-β facilitating its nuclear translocation; this enables RaLP to contribute to the transcription machinery to regulate gene expression which in turn might affect cell survival and cytoskeletal reorganisation.

Interestingly in this report, we were able to provide preliminary evidence, which highlighted a role of RaLP/hIRAS interaction in ERK activation. The functional impact of this observation requires more work to determine the molecular mechanism underlying ERK activation and the resulting biological consequence.

ShcA and hIRAS have both been shown to distribute in the endosomes (Oksvold et al., 2000; Sano et al., 2002), therefore it will be of interest to explore whether RaLP sequesters hIRAS in the endosomes preventing hIRAS-mediated α5 integrin trafficking that might induce cell motility. This hypothesis could be determined by fractionating the endosomes from cells, and subsequently examining whether RaLP and hIRAS co-immunoprecipitate with each other. Furthermore, herein it was proved that the interaction between Nischarin and RaLP requires the CH2 domain of RaLP, which is important for RaLP cytoplasmic localisation. Therefore, it was sought to determine whether Nischarin influences RaLP nuclear translocation. A preliminary experiment showed no significant difference in the percentage of cells containing FLAG-RaLP in the nucleus in the presence or absence of GFP-Nischarin. Although this might indicate that Nischarin expression does not affect RaLP nuclear translocation, the experiment should be repeated to obtain more reliable results.

7.8 Closing comment:

In this report it is clear that our understanding of the function of RaLP has improved, although further work needs to be performed to unmask the exact molecular mechanism by which RaLP achieves its effects. Further understanding of its role in invasion and migration might provide additional strategies for melanoma treatment. We employed our background knowledge about the Shc proteins, which enabled us to highlight the CH2 domain of RaLP as a key region responsible for RaLP's unique function. For the first time, the CH2 domain of RaLP was shown to house a functional NES and to promote RaLP nuclear export through the CRM receptor (Figure 7.3). Moreover, it contains potential phosporylated serine and threonine sites that might be responsible for RaLP's distinct role in conveying signals under oxidative stress conditions, or they might influence RaLP protein stability or subcellular localisation (Figure 7.3).
Unlike the full length RaLP, a truncated version lacking the CH2 domain did not affect p21/cip levels, which indicates the pivotal role of the CH2 domain in the

RaLP-mediated p21/cip upregulation. The CH2 domain also accommodates proline rich motifs, that might facilitate RaLP's ability to recruit other proteins as in the case of Nischarin, and it may also be involved in initiating RaLP/DNA association (Figure 7.3). Indeed, thorough future investigations will likely provide further insights into the CH2 domain impact on RaLP regulation, subcellular distribution and interactions with other proteins. Our combination of experimental approaches has resulted in many clues into the multifunctional role of this complex protein in different cellular compartments and processes. These observations will provide the basis for future investigations to delineate the molecular mechanisms by which RaLP regulates melanoma cell, and possibly neuroblastoma cell migration.

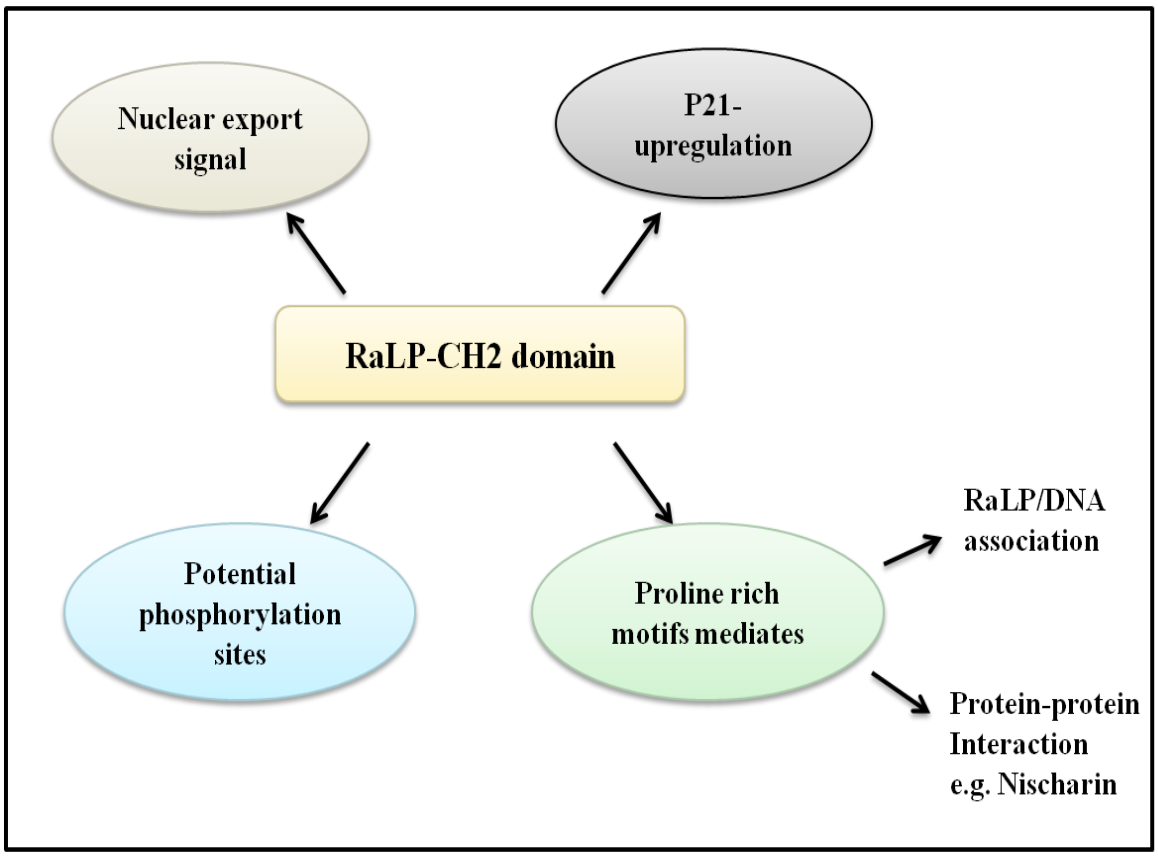

Figure 7.3 The potential roles of the RaLP-CH2 domain. RaLP shares a common structural modularity with other Shc proteins. The amino terminal CH2 domain is one of the least conserved regions on RaLP. It houses different proline rich motifs that mediate protein-protein interaction and RaLP/DNA association. The CH2 domain also accommodates potential phosphorylated serine and threonine residues that might regulate RaLP stability and/or the downstream signaling. The nuclear distribution of RaLP also relies on the NES that is contained in the CH2 domain. RaLP mediated-p21/cip upregulation is likely contingent upon the CH2 domain. Interaction with Nischarin has been shown to be mediated by the CH2 domain of RaLP.

Chapter 8
Bibliography

Abbas, T., and Dutta, A. (2009). p21 in cancer: intricate networks and multiple activities. Nat Rev Cancer 9, 400-414.

Aiken, C.T., Kaake, R.M., Wang, X., and Huang, L. (2011). Oxidative stress-mediated regulation of proteasome complexes. Mol Cell Proteomics 10, 1-11.

Alam, S.M., Rajendran, M., Ouyang, S., Veeramani, S., Zhang, L., and Lin, M.F. (2009). A novel role of Shc adaptor proteins in steroid hormone-regulated cancers. Endocr-Relat Cancer 16, 1-16.

Alahari, S., Lee, J., and Juliano, R. (2000). Nischarin, a novel protein that interacts with the integrin α5 subunit and inhibits cell migration. J Cell Biol 151, 1141-1154.

Alahari, S. (2003). Nischarin inhibits Rac induced migration and invasion of epithelial cells by affecting signaling cascades involving PAK. Exper Cell Res 288, 415-424.

Alahari, S., Reddig, P., and Juliano, R. (2004). The integrin-binding protein Nischarin regulates cell migration by inhibiting PAK. EMBO J 23, 2777-2788.

Aladowicz, E. (2011). RaLP, a novel prognostic molecular marker in melanoma, is involved in the Notch pathway. (Thsesis abstract, PhD). University of Milan. Available from: http://hdl.handle.net/2434/155518. [accessed February 2013]

Alevizopoulos, A., Dusserre, Y., Tsai-Pflugfelder, M., Von der Weid, T., Wahli, W., Mermod, N.A. (1995). Proline-rich TGF- -responsive transcriptional activator interacts with histone H3. Genes Dev 9, 3051-66.

Barberis, L., Wary, K., Fiucci, G., Liu, F., Hirsch, E., Brancaccio, M., et al. (2000). Distinct roles of the adaptor protein Shc and focal adhesion kinase in integrin signaling to ERK. J Biol Chem 275, 36532-36540.

Baranwal, S., Wang, Y., Rathinam, R., Lee, J., Jin, L., McGoey, R., Pylayeva, Y., et al. (2011). Molecular characterisation of the tumour-suppressive function of Nischarin in breast cancer. J Natl Cancer Inst 1031, 1-16.

Boehmer, T., Enninga, J., Dales S., Blobel, G., and Zhong, H. (2002). Depletion of a single nucleoporin, Nup107, prevents the assembly of a subset of nucleoporins into the nuclear pore complex. Proc Natl Acad sci 100, 981-985.

Borradori, L., and Sonnenberg, A. (1999). Structure and function of hemidesmosomes: more than simple adhesion complexes. J Invest Dermatol 112, 411-418.

Buchner, E., and Gundersen, C.B. (1997). The DnaJ-like cysteine string protein and exocytotic neurotransmitter release. Trends Neurosci 20, 223–227.

Bulyk, M.L., Huang, X., Choo, Y., and Church, G.M. (2001). Exploring the DNA-binding specficities of zinc fingers with DNA microarrays. Proc Natl Acad Sci 98, 7158-7163.

Calandra, T., and Roger, T. (2003). Macrophage migration inhibitory factor: a regulator of innate immunity. Nat review 3, 791-800.

Camici, G.G., Cosentino, F., Tanner, F.C., and Lu¨scher, T.F. (2008). The role of p66Shc deletion in age-associated arterial dysfunction and disease states. J Appl Physiol 105, 1628–1631.

Chin, Y.E., Kitagawa, M., Su, W.C., You, Z.H., Iwamoto, Y., Fu, X.Y. (1996). Cell growth arrest and induction of cyclin-dependent kinase inhibitor p21 WAF1/CIP1 mediated by STAT1. Science 272, 719-22.

Chaddi, A., and Sorokin, A. (2010). Endothelin-1 induces p66Shc activation through EGF receptor transactivation: Role of β_1Pix/Gα_{i3} interaction Cell Signal 22, 325-329.

Chambers, I., Silva, J., Colby, D., Nichols, J., Nijmeijer, B., Robertson, M., et al. (2007). Nanog safeguards pluripotency and mediates germline development. Nature 450, 1230–1234.

Chuderland, D., Konson, A., and Seger, R. (2008). Identification and characterisation of a general nuclear translocation signal in signaling proteins. Mol Cell 31, 850-861.

Collins, B.M., McCoy, A.J., Kent, H.M., Evans, P.R., and Owen, D.J. (2002). Molecular architecture and functional model of the endocytic AP2 complex. Cell 109, 523–535.

Collins, L.R., Ricketts W.A., Yeh, L., and Cheresh, D. (1999). Bifurication of cell migratory and proliferative signaling by the adaptor protein Shc. J Cell Biol 147, 1561-1568.

Conti, L., Sipione, S., Magrassi, L., Bonfanti, L., Rigamonti, D., Pettirossi, V., et al. (2001). Shc signaling in differentiating neural progenitor cells. Nat Neurosci 4, 582-586.

Darie, C., Deinhardt, K., Zhang, G., Cardasis, H., Chao, M., and Neubert, T. (2011). Identifying transient protein-protein interaction in EphB2 signaling by blue native PAGE and mass spectrometry. Proteomics 11, 4514-4528.

De Falco, V., Guarino, V., Malorni, L., Cirafici, A.M., Troglio, F., Erreni, M., et al. (2005). RAI(ShcC/N-Shc)-dependent recruitment of GAB1 to RET oncoproteins potentiates PI3-K signalling in thyroid tumors. Oncogene 24, 6303-6313.

Dekker, R.J., Boon, R. A., Rondaij, M.G., Kragt, A., Volger, O.L., Elderkamp, Y.W., et al. (2006). KLF2 provokes a gene expression pattern that establishes functional quiescent differentiation of the endothelium. Blood 107, 4354-4363.

Ding, Y., Milosavljevic, T., and Alahari, S. (2008). Nischarin inhibits LIM Kinase to regulate Cofilin phosphorylation and cell invasion. Mol Cell Biol 28, 3742-3756.

Dontenwill, M., Piletz, J.E., Chen, M., Baldwin, J., Pascal, G., Ronde, P., et al. (2003). IRAS is an Anti-Apoptotic Protein. Ann N Y Acad Sci 1009, 400-412.

Dulić V, Kaufmann W.K., Wilson S.J., Tisty T.D., Lees E., Harper J.W., et al. (1994). p53-dependent inhibition of cyclin-dependent kinase activities in human fibroblasts during radiation-induced G1 arrest. Cell 76, 1013–1023.

Edwards, D.C., Sanders, L.C., Bokoch, G.M., and Gill, G.N. (1999). Activation of LIM-kinase by PAK1 couples Rac/Cdc42 GTPase signalling to actin cytoskeletal dynamics. Nat Cell Biol 1, 253-259.

Fagiani, E., Giardina, G., Luzi, L., Cesaroni, M., Quarto, M., Capra, M., et al. (2007). RaLP, a new member of the Src Homology and Collagen family, regulates cell migration and tumour growth of metastatic melanomas. Cancer Res 67, 3064-3073.

Fagotto, F., Gluck, U., and Gumbiner, B. (1998). Nuclear localisation signal-independent and importin/karyopherin-independent nuclear import of β-catenin. Current Biol 8, 181-190.

Faisal, A., El-Shemerly, M., Hess, D., and Nagamine, Y. (2002). Serine/ Threonine phosphorylation of ShcA. J Biol Chem 277, 30144-30152.

Faisal, A., Kleiner, S., and Nagamine, Y. (2004). Non-redundant role of Shc in Erk activation by cytoskeletal reorganisation. J Biol Chem 279, 3202–3211.

Fan, Y., Chen, H., Qiao, B., Liu, Z., Luo, L., Wu, Y., et al. (2007). c-Jun NH2-terminal kinase decreases ubiquitination and promotes stabilization of $^{p21WAF1/CIP1}$ in K562 cell. Biochem Biophys Res Commun 355, 263-268.

Fenteany, G., and Schreiber, S.L. (1998). Lactacystin, proteasome function, and cell fate. J Biol Chem 273, 8545–8548.

Filion, G.J., Zhenilo, S., Salozhin, S., Yamada, D., Prokhortchouk, E., and Defossez, P.A. (2006). A Family of Human Zinc Finger Proteins That Bind Methylated DNA and Repress Transcription. Mol Cell Biol 26, 169-181.

Fixman, E., Fourniert, T., Kamikura, D., Naujokas, M., and Park, M. (1996). Pathways downstream of Shc and Grb2 are required for cell transformation by the Tpr-Met oncoprotein. J Biol Chem 271, 13116-13122.

Fornerod, M., Ohno, M., Yoshida, M., and Mattaj, I. (1997). CRM1 is an Export Receptor for Leucine-Rich Nuclear Export Signals. Cell 90, 1051-1060.

Frisch, S.M., and Francis, H. (1994). Disruption of epithelial cell-matrix interactions induces apoptosis. J Cell Biol 124, 619-626.

Galimov, E.R. (2010). The Role of p66shc in Oxidative Stress and Apoptosis. Nature Rev 2, 41-50.

George, R., Chan, H.L., Ahmed, Z., Suen, K.M., Stevens, C.N., Levitt, J.A., et al. (2009). A complex of Shc and Ran-GTPase localises to the cell nucleus. Cell Mol Life Sci 66, 711-720.

Gerber, H.P., Seipel, K., Georgiev, O., Höfferer, M., Hug, M., Rusconi, S., et al. (1994). Transcriptional Activation Modulated by Homopolymeric Glutamine and Proline Stretches. Science 263, 808-811.

Gertz, M., Fischer, F., Wolters, D., Steeghborn, C. (2008). Activation of the lifespan regulator p66Shc through reversible disulfide bond formation. Proc Natl Acad Sci 105, 5705-5709.

Giles, A.J., Bender, T.P., and Ravichandran, K.S. (2009). The adaptor protein Shc plays a key role during early B cell development. J Immunol 183, 5468-5476.

Giorgio, M., Migliaccio, E., Orsini, F., Paolucci, D., Moroni, M., Contursi, C., et al. (2005). Electron transfer between cytochrome c and p66Shc generates reactive oxygen species that trigger mitochondrial apoptosis. Cell 122, 221–233.

Girard, E., Strathdee, C., Trueblood, E., and Que´va, C. (2012). Macrophage migration inhibitory factor produced by the tumour stroma but not by tumour cells regulates angiogenesis in the B16-F10 melanoma model. Br J Cancer 107, 1498-1505.

Gorovoy, M., Niu, J., Bernard, O., Profirovic, J., Minshall, R., Neamu, R., et al. (2005). LIM Kinase 1 coordinates microtubule stability and actin polymerization in human endothelial cells. J Biol Chem 280, 26533-26542.

Gotoh, N., Toyoda, M., and Shibuya, M. (1997). Tyrosine phosphorylation sites at amino acids 239 and 240 0f Shc are involved in epidermal growth factor-induced mitogenic signaling that is distinct from Ras/Mitogen-activated protein kinase activation. Mol Cell Biol 17, 1824-1831.

Graiani, G., Lagrasta, C., Migliaccio, E., Spillmann, F., Meloni, M., Madeddu, P., et al. (2005). Genetic deletion of the $p66^{Shc}$ adaptor protein protects from angiotensin II-induced myocardial damage. Hypertension 46, 433-440.

Gu, J., Tamura, M., Pankov, R., Danen, E., Takino, T., Mastumoto, K., and Yamada, K. (1999) Shc and FAK differentially regulate cell motility and directionality modulated by PTEN. J Cell Biol 146, 389-403.

Guglielmol, G.M., Baass, P.C., Ou, W-J., Posner, B.I., and Bergeron, J.J. (1994). Compartmentalization of SHC, GRB2 and mSOS, and hyperphosphorylation of Raf-1 by EGF but not insulin in liver parenchyma. EMBO J 13, 4269-4277.

Guo, J., Cong, L., Rybin, V.O., Gertsberg, Z., and Steinberg, S.F. (2010). Protein kinase C-δ regulates the subcellular localisation of Shc in H_2O_2-treated cardiomyocytes. J Physiol Cell Physiol 299, 770 –778.

Hallberg, B., Ashcroft, M., Loeb, D.M., Kaplan, D.R., and Downward, J. (1998). Nerve growth factor induced stimulation of Ras requires Trk interaction with Shc but does not involve phosphoinositide 3-OH kinase. Oncogene 17, 691 - 697.

Hardy, W.R., Li, L., Wang, Z., Sedy, J., Fawcett, J., Frank, E., Kucera, J., Pawson, T. (2007). Combinational ShcA docking interactions support diversity in tissue morphogenesis. Science 317, 251-256.

Haung, E.J., and Louis, F., Reichardt, L.F. (2003). Trk receptors: Roles in neuronal signal transduction. Annu Rev Biochem 72, 609-642.

Hawley, S.P., Wills, M.K., Rabalski, A.J., Bendall, A.J., Jones, N. (2010). Expression patterns of ShcD and Shc family adaptor proteins during mouse embryonic development. Dev Dyn 240, 221-231.

Helton, E.S., Zhang, J., and Chen, X. (2008). The proline-rich domain in p63 is necessary for the transcriptional and apoptosis-inducing activities of Tap63. Oncogene 27, 2843-2850.

Hill, R.J., Zozulya, S., Lu, V., Hollenbach, P.W., Shaikh, B.J., Bogenberger, J., and Gishizky, M.L. (1996). Differentiation induced by the c-MpI cytokine receptor is blocked by mutant Shc adaptor protein. Cell Growth Differ 17, 1125-1134.

Hinsby, A.M., Lundfald, L., Dorte, K., Ditlevsen, D.K., Korshunova, I., Juh, L., et al. (2004). ShcA regulates neurite outgrowth stimulated by neural cell adhesion molecule but not by fibroblast growth factor 2: evidence for a distinct fibroblast growth factor receptor response to neural cell adhesion molecule activation. J Neurochem 91, 694–703.

How, P., and Shields, D. (2011). Tethering function of the caspase cleavage fragment of golgi protein p115 promotes apoptosis via a p53-dependent pathway. J Biol Chem 286, 8565-8576.

Itoh, T., Miura, K., Miki, H., and Takenawa, T. (1996). β-Tubulin binds Src homology 2 domains through a region different from the tyrosine-phosphorylated protein-recognizing Site. J Biol Chem 271, 27931–27935.

Ivanov S.V., Panaccione, A., Brown, B., Guo, Y., Moskaluk, C.A., Wick, M.J., et al. (2012).TrkC signaling is activated in adenoidcysticcarcinoma and requires NT3 to stimu late invasive behavior. Oncogene, available from doi: 10.1038/onc.2012.377.

Jackson, J.G., Yoneda, T., Clark, G.M., Yee, D. (2000). Elevated levels of p66 Shc are found in breast cancer cell lines and primary tumors with high metastatic potential. Clin Cancer Res 6, 1135-1139.

Jakel, S., and Gorlich, D. (1998). Importin b, transportin, RanBP5 and RanBP7 mediate nuclear import of ribosomal proteins in mammalian cells. EMBO J 17, 4491–4502.

Jina, H., Liaob, L., Parka, Y., and Liua, Y. (2012). Neddylation pathway regulates T-cell function by targeting an adaptor protein Shc and a protein kinase Erk signalling. Proc Natl Acad Sci 110, 624-629.

Johnson, L.R., Mccormack, S.A., Yang, C., Pfeffer, S.R., and Pfeffer, L.M. (1999). EGF induces nuclear translocation of STAT2 without tyrosine phosphorylation in intestinal epithelial cells. J Physiol Cell Physiol 276, 419-425.

Jones, J.C., Kurpakus, M.A., Cooper, H.M., and Quarantat, V. (1991). A function for the integrin α6β4 in the hemidesmosome. Cell Reg 2, 427-438.

Jones, N., Hardy, W.R., Friese, M.B., Jorgensen, C., Smith, M.J., Woody, N.M., et al. (2007). Analysis of a Shc family adaptor protein, ShcD/Shc4, that associates with muscle-Specific kinase. Mol Cell Biol 27, 4759-4773.

Kang, S., Song, J., Kang, H., Kim, S., Lee, Y., and Park, D. (2003). Insulin can block apoptosis by decreasing oxidative stress via phosphatidylinositol 3-kinase- and extracellular signal-regulated protein kinase-dependent signalling pathways in HepG2 cells. Eur J Endocrinol 148, 147–155.

Kao, A.W., Waters, S.B., Okada, S., and Pessin, J.E. (1997). Insulin stimulates the phosphorylation of the p66- and 52-kilodalton Shc isoforms by distinct pathways. Endocrinology 138, 2474-2480.

Kastan, M.B., and Bartek, J. (2004). Review article Cell-cycle checkpoints and cancer. Nature 432, 316-323.

Kasuno, K., Naqvi, A., DeRicco, J., Yamamori, T., Santhanam, L., Mattagajasingh, I., et al. (2007). Antagonism of p66shc by melanoma inhibitory activity. Cell Death Differ 14, 1414–1421.

Khanday, F.A., Yamamori, T., Mattagajasingh, I., Zhang, Z., Bugayenko, A., et al. (2006). Rac1 leads to phosphorylation-dependent increase in stability of the p66shc adaptor protein: Role in Rac1-induced oxidative stress. Mol Biol Cell 17, 122–129.

Kim, C.S., Kim, Y.R., Naqvi, A., Kumar, S., Hoffman, T.A., Jung, S.B., et al. (2011). Homocysteine promotes human endothelial cell dysfunction via site-specific epigenetic regulation of p66shc. Cardiovasc Res 92, 466–475.

Klaunig, J., Kamendulis, L., and Hocevar, B. (2010). Oxidative stress and oxidative damage in carcinogenesis. Toxicol Pathol 38, 96-109.

Knauf, J.A., Kuroda, H., Basu, S., and Fagin, J.A. (2003). RET/PTC-induced dedifferentiation of thyroid cells is mediated through Y1062 signaling through SHC-RAS-MAP kinase. Oncogene 22, 4406-4412.

Kodiha, M., Chu, A., Matusiewicz, N., and Stochaj, U. (2004). Multiple mechanisms promote the inhibition of classical nuclear import upon exposure to severe oxidative stress. Cell Death Differ 11, 862-874.

Kosugi, S., Hasebe, M., Tomita, M., Yanagawa, H. (2008). Nuclear export signal consensus sequences defined using a localisation-based yeast selection system. Traffic 9, 2053-2062.

Kosugi, S., Hasebe, M., Matsumura, N., Takashima, H., Miyamoto-Sato, E., Tomita, M., and et al. (2009). Six classes of nuclear localization signals specific to different binding grooves of importin alpha. J Biol Chem 284, 478-485.

Kudo, N., Matsumori, N., Toaka, H., Fujiwara, D., Schreiner, E., Wolf, B., et al. (1999). Leptomycin B inactivates CRM1/exportin 1 covalent modification at a cysteine residue in the central conserved region. Cell Biol 96, 9112-9117.

Kulahin, N., Sanni, S.J., Slaaby, R., Nøhr, J., Gammeltoft, S., Hansen, J.L., and Jorgensen, R.A. (2012). BRET assay for monitoring insulin receptor interactions and ligand pharmacology. J Recept Signal Transduct Res 32, 57-64.

Kumar, A., Hoffman, T., DeRicco, J., Naqvi, A., Jain, M., and Irani, K. (2009). Transcriptional repression of Kruppel like factor-2 by the adaptor protein p66shc. Fed Americ Soc Exp Biol 23, 4344-4352.

Kumar, S., Kumar S., Rajendran, M., Alam, S.M., Lin, F.F., Cheng, P.W., Lin, M.F. (2011). Steroids up-regulate p66Shc longevity protein in growth regulation by inhibiting its ubiquitination. PLoS 6, available from doi:10.1371/ journal.pone.0015942.

Kutay, U., Bischoff, R., Kostka, S., Kraft, R., and Gorlich, D. (1997). Export of Importin α from the Nucleus is mediated by a specific Nuclear Transport factor. Cell 90, 1061-1071.

Kuwada, S., and Li, X. (2000). Integrin alpha5/beta1 mediates fibronectin-dependent epithelial cell proliferation through epidermal growth factor receptor activation. Mol Biol Cell 7, 2485-2496.

Lai, K.V., and Pawson, T. 2000. The ShcA phosphotyrosine docking protein senistizes cardiovascular signalling in the mouse embryo. Genes Dev 14, 1132-1145.

Le, S., Connors, T.J., and Maroney, A.C. (2001). c-Jun N-terminal kinase specifically phosphorylates p66ShcA at serine 36 in response to ultraviolet irradiation. J Biol Chem 276, 48332–48336.

Lebiedzinska, M., Wieckowska, A., Giorgi, C., Karczmarewicz, E., Pronicka, E., Pinton, P., et al. (2010). Oxidative stress-dependent p66Shc phosphorylation in skin fibroblasts of children with mitochondrial disorders. Biochim Biophys Acta 1797, 952-960.

Lee, J.H., Lee, J.S., Kim, S.E., Moon, B.S., Kim, Y.C., Lee, S.K., et al. (2006). Tautomycetin inhibits growth of colorectal cancer cells through p21cip/WAF1 induction via the extracellular signal–regulated kinase pathway. Mol Cancer Ther 5, 32222-3231.

Lee, S.K., Chung, J.I., Park, M.S., Joo, H.K., Lee, E.J., Cho, E.J., et al. (2011). Apurinic/apyrimidinic endonuclease 1 inhibits protein kinase C-mediated p66shc phosphorylation and vasoconstriction. Cardiovasc Res 91, 502–509.

Li, F., Wu, N., Su, R.B., Chen, Y., Lu, X.Q., Liu, Y., and Li, J. (2011). Imidazoline receptor anti-sera-selected/Nischarin regulates the effect of agmatine on the development of morphine dependence. Addict Biol 17, 392-408.

Li, F., Wu, N., Su, R.B., Zheng, J.Q., Xu, B., Lu, X.Q., et al. (2006). Involvement of phosphatidylcholine-selective phospholipase C in activation of mitogen-activated protein kinase pathways in imidazoline receptor anti-sera-selected. J Cell Biochem 98, 1615-1628.

Li, Y., Dowbenko, D., and Lasky, L.A. (2002). Akt/PKB phophorylation of $p21^{cip/WAF1}$ enhances protein stability of $p21^{cip/WAF1}$ and promotes cell survival. J Biol Chem 277, 11352-11361.

Liang, S.H., Clarke, M.F. (1999). A bipartite nuclear localisation signal is required for p53 nuclear import regulated by a carboxyl-terminal domain. J Biol Chem 274, 32699-32703.

Liccardi, G., Hartley, J.A., and Hochhauser, D. (2011). EGFR Nuclear translocation modulates DNA repair following cisplatin and ionizing Radiation treatment. Cancer Res 71, 1103-1114.

Lim, K., and Hong, W. (2004). Human Nischarin/Imidazoline receptor antisera-selected protein is targeted to the endosomes by a combined action of a PX domain and a coiled-coil region. J Biol Chem 279, 54770-54782.

Lioubin, M.N., Algate, P.A., Tsai, S., Carlberg, K., Aebersold, A., and Rohrschneider L.R. (1996). $P150^{Ship}$, a signal transduction molecule with inositol polyphosphate-5-phospahatase activity. Genes Dev 10, 1084-1095.

Liu, Z., Yuan, F., Yang, Q., Cao, J., Zhou, Y., Ren, J., et al. (2011). GPS-ARM: computational analysis of APC/C-mediated degradation by predicting D-andKEN-boxsubstrates**.** PLoS one, available from: doi:10.1371/journal.pone.0034370.

Lotti, L., Lanfrancone, L., Migliaccio, E., Zompetta, C., Pelicci, G., Salcini, A., et al. (1996). Shc proteins are localized on endoplasmic reticulum membranes and are redistributed after tyrosine kinase receptor activation. Mol Cell Biol. 16, 1946-1954.

Lu, G.D., Shen, H.M., Chung, M., and Ong, C.N. (2007). Critical role of oxidative stress and sustained JNK activation in aloe-emodin-mediated apoptotic cell death in human hepatoma cells. Carcinogenesis 28, 1937–1945.

Luschnig, S., Krauss, J., Bohmann, K., Desjeux, I., and Volhard, C-N. (2000). The Drosophila SHC adaptor protein is required for signaling by a subset of receptor tyrosine kinases. Mol Cell 5, 231–241.

Ma, Z., Liu, Z., Wu, R-F., and Terada, L.S. (2010). p66Shc restrains Ras hyperactivation and suppresses metastatic behaviour. Oncogene 14, 5559–5567.

Ma, Z., Myers, D.P., Wu, R.F., Nwariaku, F.E., and Terada, L.S. (2007). p66Shc mediates anoikis through RhoA. J Cell Biol 179, 23-31.

Macleod, K., Sherry, N., Hannon, G., Beach D., Tokino, T., Kinzler K., et al. (1995). p53-dependent and independent expression of p21 during cell growth, differentiation, and DNA damage. Genes Dev 9, 935-944.

Magrassi, L., Conti, L., Lanterna, A., Zuccato, C., Marchionni, M., Cassini, P., et al. (2005). Shc3 affects human high-grade astrocytomas survival. Oncogene 24, 5198–5206.

Mainiero, F., Pepe, A., Wary, K.K., Spinardi, L., Mohammadi, M., Schlessinger, J., et al. (1995). Signal transduction by the $\alpha_6\beta_4$ integrin: distinct β_4 subunit sites mediate recruitment of Shc/Grb2 and association with the cytoskeleton of hemidesmosomes. EMBO J 14, 4470-4481.

Marchal, C., Haguenauer-Tsapis, R., and Urban-Grimal, D. (1998). A PEST-Like sequence mediates phosphorylation and efficient ubiquitination of yeast uracil permease. Mol Cell Biol 18, 314–321.

Marchetto, S., Fournier, E., Beslu, N., Aurran-Schleinitz, T., Dubreuil, P., Borg, J., et al. (1999). Shc and Ship phosphorylation and interaction in response to activation of the FLT3 receptor. Leukemia 13, 1374-1382.

Masui, S., Nakatake, Y., Toyooka, Y., Shimosato, D., Yagi, R., Takahashi, K., et al. (2007). Pluripotency governed by Sox2 via regulation of Oct3/4 expression in mouse embryonic stem cells. Nat Cell Biol 9, 625–635.

Maures, T.J., Chen, L., and Carter-Su, C. (2009). Nucleocytoplasmic shuttling of the adaptor protein SH2B1beta (SH2-B1β) is required for nerve growth factor (NGF)-dependent neurite outgrowth and enhancement of expression of a subset of NGF-responsive genes. Mol Endocrinol 23, 1077-1091.

Mauro, L., Sisci, D., Bartucci, M., Salerno, M., Kim, J., Tam, T., et al. (1999). SHC-α5β1 integrin interactions regulate breast cancer cell adhesion and motility. Exp Cell Res 252, 439-448.

McGlade, J., Cheng, A., Pelicci, G., Pelicci, P.G., and Pawson T. (1992). Shc proteins are phosphorylated and regulated by the v-Src and v-Fps protein-tyrosine kinases. Biochmeistry 89, 8869-8873.

McManus, M., Boerner, J., Danielsen A., Wang, Z., Matsumura, F., and Maihle, N. (2000). An oncogenic epidermal growth factor receptor signals via a p21-activated kinase-Cadesmon phosphotyrosine complex. J Biol Chem 275, 35328-35334.

Merk, M., Baugh, J., Zierow, S., Leng, L., Pal, U., Lee, S., et al. (2009). The Golgi-Associated Protein p115 Mediates the Secretion of Macrophage Migration Inhibitory Factor. J Immunol 182, 6896-6906.

Migliaccio, E., Giorgio, M., Mele, S., Pelicci, G., Reboldi, P., Pandolfi, P.P., et al. (1999). The p66Shc adaptor protein controls oxidative stress response and life span in mammals. Nature 402, 309-312

Mitsui, K., Matsumoto, A., Ohtsuka, S., and Yoshimura, A. (1999). Cloning and characterisation of a novel p21/cip interacting zinc finger protein, Ciz1. Biochem Biophys Res Commun 264, 457-464.

Miyake, I., Ohira, M., Nakagawara, A., and Sakai, R. (2009). Distinct role of ShcC docking protein in the differentiation of neuroblastoma. Oncogene 28, 662-673.

Molkentin J.D. (2000). The zinc finger-containing transcription factors GATA-4, -5, and -6. J Biol Chem 275, 38949–38952.

Mukerjee, S., and Shields, D. (2008). Nuclear import is required for the pro-apoptotic function of the Golgi protein p115. J Biol Chem 284, 1709-1717.

Musgrave, I., Dehle, F., and Piletz, J. (2003). Assembly of PRR-Containing Receptors on scaffolds. Ann N Y Acad Sci 1009, 413-418.

Nakamura, T., Muraoka, S., Sanokawa, R., and Mori, N. (1998). N-Shc and sck, two neuronally expressed Shc adapter homologs. J Biol Chem 273, 6960-6967.

Nan, X., Ng, H., Johnson, C.A., Laherty, C.D., Turner, B.M., Eisenman R.N., and Bird, A. (1998). Transcriptional repression by the methyl-CpG-binding protein MeCP2 involves a histone deacetylase complex. Nature 393, 387-389

Nemoto, S., Combs, C.A., French, S., Ahn B.H., Fergusso, M., Balaban, R.S., et al. (2006). The mammalian longevity-associated gene product $p66^{shc}$ regulates mitochondrial metabolism. J Biol Chem 281, 10555-10560.

Neudauer ,C.L., McCarthy, J.B. (2003). Insulin like growth factor I-stimulated melanoma cell migration requires phosphoinositide 3-kinase but not extracellular-regulated kinase activation. Exp Cell Res 286, 128-137.

Niu, Y., Roy, F., Saltel, F., Andrieu-Soler, C., Dong, W., Chantegrel, A.L., et al. (2006). A nuclear export signal and phosphorylation regulate Dok1 subcellular localisation and functions. Mol Cell Biol 26, 4288-4301.

Niwa, H., Miyazaki, J., Smith, A.G. (2000). Quantitative expression of Oct-3/4 defines differentiation, dedifferentiation or self-renewal of ES cells. Nat Genet 24, 372–376.

Northey, J.J., Chmielecki, J., Ngan, E., Russo, C., Annis, M.G., Muller, W.J., et al. (2008). Signaling through ShcA is required for transforming growth factor –β and Neu/ErbB-2-induced breast cancer cell motility and invasion. Mol Cell Biol 28, 3162-3176.

Noseda, M., Chang, L., McLean, G., Grim, J.E., Clurman, B.E., and Smith, L.L. (2004). Notch activation induces endothelial cell cycle arrest and participates in contact inhibition: Role of p21cip repression. Mol cell Biol 24, 8813-8822.

O'Bryan, J.P., Songyang, Z., Cantley, L., Der, C.J., and Pawson, T. (1996). A mammalian adaptor protein with conserved Src homology 2 and phosphotyrosine-

binding domains is related to Shc and is specifically expressed in the brain. Biochemistry 93, 2729-2734.

Obreztchikova, M., Elouardighi, H., Ho, M., Wilson, B.A., Gertsberg, Z., and Susan, F.S. (2006). Distinct signaling functions for Shc isoforms in the heart. J Biol Chem 281, 20197-20204.

Okabayashi, Y., Sugimoto, Y., Totty, N., Hsuan, J., Kido, Yoshiaki., Sakaguchi, K., et al. (1996). Interaction of Shc with adaptor protein Adaptins. J Biol Chem. 271, 5265-5296.

Okada, S., Kao, A.W., Ceresa, B.P., Blakie, P., Margolis, B., and Pessin, J.E. (1997). The 66-kDa Shc isoform is a negative regulator of the epidermal growth factor – stimulated mitogen activated protein kinase pathway. J Biol Chem 272, 28042-28049.

Oksvold, M.P., Skarpen, E., Lindeman, B., Roos, N., and Huitfeldt, H.S. (2000). Immunocytochemical localisation of Shc and activated EGF receptor in early endosomes after EGF stimulation of HeLa cells. J Histochem Cytochem 48, 21-33.

Olayioye, M.A., Beuvink, I., Horsch, K., Daly, J.M., and Hynes, N.E. (1999). ErbB receptor-induced activation of Stat transcription factors is mediated by Src tyrosine kinases. J Biol Chem 274, 17209–17218.

Ong, S.H., Dilworth, S., Hauck-Schmalenberger I., and Kiefer, T.P. (2001). ShcA and Grb2 mediate polyoma middleT antigen-induced endothelial transformation and Gab1 tyrosine phosphorylation. EMBO J 20, 6327-6336.

Orjalo, A.V., Arnaoutov, A., Shen, Z., Boyarchuk, Y., Zeitlin, S.G., Fontoura, B., et al. (2006). The Nup107-160 nucleoporin complex is required for correct bipolar spindle assembly. Mol Biol Cell 17, 3806–3818.

Orsini, F., Migliaccio, E., Moroni, M., Contursi, C., Raker, V.A., Piccini, D., et al. (2004). The life span determinant p66Shc localizes to mitochondria where it associates

with mitochondrial heat shock protein 70 and regulates trans-membrane potential. J Biol Chem 279, 25689-25695.

Oshikawa, J., Kim, S.J., Furuta, E., Caliceti, C., Chen, G., McKinney, R.D., et al. (2012). Novel role of p66Shc in ROS-dependent signaling and angiogenesis in endothelial cells. AJP- Heart Circ Physiol 302, 724-732.

Pasini, L., Turco, M.Y., Luzi, L., Aladowicz, E., Fagiani, E., and Lanfrancone, L. (2009). Melanoma: targeting signalling pathway and RaLP. Expert opin 13, 93-103.

Parri, M., Chiarugi, P. (2010). Rac and Rho GTPases in cancer cell motility control. Cell Commun Signal, available from doi: 10.1186/1478-811X-8-23

Pelicci, G., Lanfrancone, L., Grignani, F., McGlade, J., Cavallo, F., Nicoletti, I., et al. (1992). A novel transforming protein (SHC) with an SH2 Domain is implicated in mitogenic signal transduction. Cell 70, 93-104.

Pelicci, G., Troglio, F., Bodini, A., Melillo, R.M., Pettirossi, V., Coda, L., and et al. (2002). The Neuron-Specific Rai (ShcC) Adaptor protein inhibits apoptosis by coupling Ret to the phosphatidylinositol 3-kinase/Akt signaling pathway. Mol Cell Biol 22, 7351-7363.

Piletz, J., Ivanov, T.R., Sharp, J.D., Ernsberger, P., Chang, C.H., Pickard, R.T., et al. (2000). Imidazoline receptor antisera-selected (IRAS) cDNA: cloning and characterisation. DNA Cell Biol 19, 319-329.

Piletz, J., Wang, G., and Zhu, H. (2003). Cell signalling by Imidazoline-1 Receptor Candidate, IRAS and the Nischarin Homologue. Ann N Y Acad Sci 1009, 392-399.

Ptasznik, A., Kaplan, A.T., and Bokoch, G.M. (1995). G protein-coupled chemoattractant receptors regulate Lyn tyrosine kinase Shc adaptor protein signaling complexes. J Biol Chem 270, 19969-19973.

Puthenveedu, M.A. and Linstedt, A.D. (2001). Evidence that Golgi structure depends on a p115 activity that is independent of the vesicle tether components giantin and GM130. J Cell Biol 155, 227-237.

Rangarajan, A., Talora, C., Okuyama, R., Nicolas, M., Aster, J., Krishna S., et al. (2001). EMBO J. 20, 3427-3436.

Rajendran, M., Thomes, P., Zhang, L., Veeramani, S., Ming-Fong Lin, M.F. (2010). p66Shc-a longevity redox protein in human prostate cancer progression and metastasis. Cancer Met 29, 207-222.

Ratcliffe, K.E., Tao, Q., Yavuz, b., Stoletov, K.V., Spring, S.C., and Terman, B.I. (2002). Sck is expressed in endothelial cells and participates in vascular endothelial growth factor-induced signaling. Oncogene 21, 6307-6316.

Ravichandran, K.S. (2001). Signaling via Shc family adapter proteins. Oncogene 20, 6322-6330.

Ravichandran, K.S., Lorenz, U., Shoelson, S.E., and Burakoff, S.J. (1995). Interaction of Shc with Grb2 regulates association of Grb2 with mSOS. Mol Cell Biol 15, 593–600.

Ravichandran, K.S., Zhou, M., Pratt, J.C., Harlan, J.E., Walk, S.F., Fesik, S.W. (1997). Evidence for a requirement for both phospholipid and phosphotyrosine binding via the Shc phosphotyrosine-binding domain in vivo. Mol Cell Biol 17, 5540–5549.

Rechsteiner, M., and Rogers, S.W. (1996). PEST sequences and regulation by proteolysis. Trends Biochem Sci 21, 267-271.

Reddig, P., Xu, D., and Juliano, R. (2005). Regulation of p21-activated Kinase-independent Rac1 Signal Transduction by Nischarin. J Biol Chem 280, 30994-31002.

Saadi, I., Alkuraya, F.S., Gisselbrecht, S.S., Goessling, W., Cavallesco, R., Turbe-Doan, A., et al. (2011). Deficiency of the cytoskeletal protein SPECC1L leads to oblique facial clefting. Am J Hum Genet 89, 44-55.

Sakaguchi, K., Okabayashi, Y., and Kasuga, M. (2001). Shc mediates ligand-induced internalization of epidermal growth factor receptors. Biochem Biophysic Res Comm 282, 1154-1160.

Sakai, R., Henderson, J.T., O'Bryan, J.P., Elia, A.J., Saxton, T.M., Pawson, T. (2000). The mammalian ShcB and ShcC phosphotyrosine docking proteins function in the maturation of sensory and sympathetic neurons. Neuron 28, 819-833.

Sano, H., Liu, S., Lane, W., Piletz, J., and Lienhard, G. (2002). Insulin receptor substrate 4 associates with the protein IRAS. J Biol Chem 277, 19439-19447.

Santiago, A., and Erickson, C.A. (2002). Ephrin-B ligands play a dual role in the control of neural crest cell migration. Development 129, 3621-32.

Sato, K., Kmoto, M., Kakumoto, M., Horiuchi, D., Iwasaki, T., Tokmakov, A., et al. (2000). Adaptor protein Shc undergoes translocation and mediates up-regulation of the tyrosine kinase c-Src in EGF-stimulated A431 cells. Genes Cells 5, 749-764.

Sato, K., Nagao, T., Kakumoto, M., Kimoto, M., Otsuki, T., Iwasaki, T., et al. (2002). Adaptor protein Shc is an isoform-specific direct activator of the tyrosine kinase c-Src. J Biol Chem 277, 29568–29576.

Saucier, C., Papavasiliou, V., Palazzo, A., Naujokas, M. A., Kremer, R., and Park, M. (2002). Use of signal specific receptor tyrosine kinase oncoprotein reveals that pathways downstream from Grb2 or Shc are sufficient for cell transformation and metastesis. Oncogene 21, 1800-1811.

Savino, T.M., Ortensi, B., Ferro, M., Ulivieri, C., Fanigliulo, D., Paccagnini, E., et al. (2009). Rai acts as a negative regulator of autoimmunity by inhibiting antigen receptor signaling and lymphocyte activation. J Immunol 182, 301-308.

Schneider, E., Keppler, R., Prawitt, D., Steinwender, C., Roos, F., Thuroff, J., et al. (2010). Migration of renal tumor cells depends on dephosphorylation of Shc by PTEN. J Int Oncol 38, 823-831.

Smith, M., Hardy, W., Murphy, J., Jones, N., and Pawson, T. (2006). Screening for PTB domain binding parteners and ligand specificity using proteome-derived NPXY peptide arrays. Mol Cell Biol. 26, 8461-8474.

Smith, M.J., Hardy, W.R., Li, G., Goudreault, M., Hrsch, S., Metalnikov, P., et al. (2010). The PTB domain of ShcA couples receptor activation to the cytoskeletal regulator IQGAP1. EMBO J 29, 884-896.

Smith, S.M., Crowe, D.L., and Lee, M.K. (2006). β1 integrins modulates $p66^{ShcA}$ expression and EGF-induced MAP kinase activation in fetal lung cells. Biochem Biophys Res Commun 342, 909-918.

Smith, W.W., Norton, D.D., Gorospe, M., Jiang, H., Nemoto, S., Holbrook, N.J., et al. (2005). Phosphorylation of p66Shc and forkhead proteins mediates Aβ toxicity. JCB 169, 331-339.Sterrenberg, J.N., Blatch, G.L., and Edkins, A.L. (2011). Human DNAJ in cancer and stem cells. Cancer Lett 312, 129-142.

Stevenson, L.E., Ravichandran, K.S., and Frackelton, A.R. (1999). Shc dominant negative disrupts cell cycle progression in both G0-G1 and G2-M of ErbB2-positive breast cancer cells. Cell growth differ 10, 61-71.

Su, Y., Balice-Gordon, R.J., Hess, D.M., Landsman, D.S., Minarcik, J., Golden, J., et al. (2004). Neurobeachin is essential for neuromuscular synaptic transmission. J Neurosci 24, 3627-3636.

Sun, L., Liu, O., Desai, J., Karbassi, F., Sylvain, M., Shi, A., Zhou, Z., et al. (2012). CED-10/Rac1 regulates endocytic recycling through the RAB-5 GAP TBC-2. PLoS Genet, available from doi: 10.1371/journal.pgen.1002785.

Sun, Z., Chang, C., and Ernsberger, P. (2007). Identification of IRAS/Nischarin as an I1-imidazoline receptor in PC12 rat pheochromocytoma cells. J Neurochem 101, 99–108.

Tanaka, H., Yamashita, T., Asada, M., Mizutani, S., Yoshikawa, H., and Tohyama, M. (2002). Cytoplasmic p21/cip regulates neurite remodelling by inhibiting Rho-kinase activity. J Cell Biol 158, 321-329.

Tauszig-Delamasure, S., and Bouzas-Rodriguez, J. (2011). Targeting neurotrophin-3 and its dependence receptor tyrosine kinase receptor C: a new anti-tumoral strategy. Expert Opin Ther Targets 15, 847-858.

Tell, G., Quadrifoglio, F., Tiribelli, C., and Kelley, M.R. (2009). The many functions of APE1/Ref-1: Not only a DNA repair enzyme. Antioxid Redox Signaling 11, 601-619.

Thomas, D., and Bradshaw. R.A. (1997). Differential utilization of ShcA tyrosine residues and functional domains in the transduction of epidermal growth factor-induced mitogen-activated protein kinase activation in 293T Cells and nerve growth factor-induced neurite outgrowth in PC12 Cells. J Biol Chem 272, 22293-22299.

Thomas, D., Patterson, S., and Bradshaw, R. (1995) Src homologous and collagen (Shc) protein binds to F-actin and translocates to the cytoskeleton upon nerve growth factor stimulation in PC12 cells. J Biol Chem 270, 28924-28931.

Tombes, R.M., Auer, K.L., Mikkelsen, R., Valerie, K., Wymann, M.P., Marshall, C.J., et al. (1998). The mitogen-activated protein (MAP) kinase cascade can either stimulate or inhibit DNA synthesis in primary cultures of rat hepatocytes depending upon whether its activation is acute/phasic or chronic. Biochem J 330, 1451 –1460.

Trinei, M., Giorgio, M., Cicalese, A., Barozzi, S., Ventura, A., Migliaccio, E., et al. (2002). A p53-p66Shc signalling pathway controls intracellular redox status , levels of oxidation-damaged DNA and oxidative stress- induced apoptosis. Oncogene 21, 3872-3878.

Troglio, F., Echart, C., Gobbi, A., Pawson, T., Pelicci, P.G., De Simoni M.G., and Pelicci G. (2004). The Rai (Shc C) adaptor protein regulates the neuronal stress response and protects against cerebral ischemia. Proc Natl Acad Sci 101, 15476–15481.

Turco, M.Y., Furia, L., Dietze, A., Fernandez, L., Ronzoni, S., Sciullo, A., and et al. (2012). Cellular heterogeneity during embryonic stem cell differentiation to epiblast stem cells is revealed by the ShcD/RaLP adaptor protein. Stem Cells 30, 2423-2436.

Ursini, S.J., Hardy, W.R., Zuo, D., Lam, S.H., Sangulin, V., Cardiff, R.D., et al. (2008). ShcA signaling is essential fot tumour progression in mouse models of human breast cancer. EMBO J 27, 910-920.

Vanderlaan, R.A., Hardy, W.R., Golam, M., Pasculescu, A., Jones, N., P.deTombe P., et al. (2011). The ShcA phosphotyrosine docking protein uses distinct mechanisms to regulate myocyte and global heart function. Circ Res, 108:184-193.

Ventura, A., Luzi, L., Pacini, S., Baldari, C.T., and Pelicci, P.G. (2002). The p66Shc longevity gene is silenced through epigenetic modifications of an alternative promoter. J Biol Chem 277, 22370–22376.

Ventura, A., Maccarana, M., Raker, V.A., and Pelicci, P.G. (2004). A Cryptic targeting signal induces isoform-specific localisation of p46Shc to mitochondria. J Biol Chem 279, 2299-2306.

Wang, P., and Jin, T. (2010). Hydrogen peroxide stimulates nuclear import of the POU homeodomain protein Oct-1 and its repressive effect on the expression of Cdx-2. BMC Cell Biol, available from doi: 10.1186/1471-2121-11-56.

Wary, k., Mainiero, F., Isakoff, S., Marcantonio, E., and Giancotti, F. (1996). The Adaptor protein Shc couples a class of integrins to the control of cell cycle progression. Cell 87, 733-743.

Wendt, J., Haefen, C.V., Hemmati, P.G., Guner, D., Schulze-Osthoff, K., Dorken, B. et al. (2006). Induction of $p21^{CIP/WAF-1}$ and G2 arrest by ionizing irradiation impedes caspase-3-mediated apoptosis in human carcinoma cells. Oncogene 25, 972-980.

Wiche, G. (1998). Role of plectin in cytoskeleton organization and dynamics. J Cell Sci 111, 2477-2486.

Wills, M., and Jones, N. (2008). The ShcD phosphotyrosine adaptor protein exhibits novel binding characteristic with the TrkA neurotrophin receptor. Studies by Undergraduate Researchers at Guelph 2, 59-70.

Wills, M. and Jones, N. (2012). Teaching an old dogma new tricks: twenty years of Shc adaptor signalling. Biochem J 447, 1-16.

Winters, Z.E., Leek, R.D., Bradburn, M.J., Norbury, C.J., and Harris, A.L. (2003). Cytoplasmic $p21^{WAF1/CIP1}$ expression is correlated with HER-2/neu in breast cancer and is an independent predictor of prognosis. Breast Cancer Res 5, 242-249.

Westin, E.R., Aykin-Burns, N., Buckingham, E.M., Spitz, D.R., Goldman, F.D., and Klingelhutz, A.J. (2011). The p53-$p21^{WAF/CIP}$ pathway mediates oxidative stress and senescence in dyskeratosis congenita cells with telomerase insufficiency. Antioxid Redox Signal 14, 985-997.

Xia, F., Lee, C.W., and Altieri, D.C. (2008). Tumor Cell Dependence on Ran-GTP–Directed Mitosis. Cancer Res 68, 1826-1833.

Xue, Y., Ren J, Gao, X., Jin, C., Wen, L., and Yao, X. (2008). GPS 2.0, a Tool to Predict Kinase-specific Phosphorylation Sites in Hierarchy. Mol Cell Proteomics. 7, 1598-1608.

Xu, Y., Shao, Y., Zhou, J., Voorhees, J., and Fisher, G. (2009). Ultraviolet Irradiation-Induces Epidermal Growth Factor Receptor (EGFR) Nuclear Translocation in Human Keratinocytes. J Cell Biochem 107, 873-880.

Yaglom, J., Linskens, M.H., Sadis, S., Rubin, D.M., Futcher, B., and Finley, D. (1994). p34Cdc28-mediated control of Cln3 cyclin degradation. Mol Cell Biol 15, 731-741.

Yang, C.H., and Horwitz, S.B. (2000). Taxol Mediates Serine Phosphorylation of the 66-kDa Shc Isoform. Cancer Res 60, 5171–5178.

Yang, N., Higuchi, O., Ohashi, K., Nagata, K., Wada, A., Kangawa, K., Nishida, E., and Mizuno, K. (1998). Cofilin phosphorylation by LIM-kinase 1 and its role in Rac-mediated actin reorganisation. Nature 393, 809-812.

Yoshida, S., Masaki, T., Feng, H., Yuji, J., Miyauchi, Y., Funaki, T., et al. (2004). Enhanced expression of adaptor molecule p46Shc in the nuclei of hepatocellular carcinoma cells: Study of LEC rats. Int J Oncol 25, 1089-1096.

You, Y., Li, W., Gong, Y., Yin, B., Qiang, B., Yuan, J., et al. (2010). ShcD interacts with TrkB via its PTB and SH2 domains and regulates BDNF-induced MAPK activation. Biochem Mol Biol Rep 43, 485-490.

Yukimasa, S., Masaki, T., Yoshida, S., Ushida, N., Watanabe, S., Usuki, H., et al. (2005). Enhanced expression of p46Shc in the nucleus and p52Shc in the cytoplasm of human gastric cancer. Int J Oncol 26, 905-911.

Zhu, L., and Parada, L.F. (2002).The molecular and genetic basis of neurological tumours. Nat Rev 2, 616-626.

Zhang, J., and Abdel-Rahman, A. (2006). Nischarin as a functional imidazoline (I_1) receptor. FEBS Lett 580, 3070-3074.

Zhang, J., and Abdel-Rahman, A. (2008). Inhibition of Nischarin expression attenuates rilemidine-evoked hypotension and phosphorylated extracellular signal-regulated kinase 1/2 production in the rostral ventrolateral medulla of rats. J Pharmacol Exp Ther 324, 72-78.

Zhou, M.M., Ravichandran, K.S., Olejniczak, E.F., Petros, A.M., Meadows, R.P., Sattler, M., et al. (1995). Structure and ligand recognition of the phosphotyrosine binding domain of Shc. Nature 378, 584-592.